Applications and Industry®

September 1960

Transactions Papers

General Applications Division

Industry Division

NUMBER 50

Published Bimonthly by

AMERICAN INSTITUTE OF ELECTRICAL ENGINEERS

(See inside back cover)

Note to Librarians. The six bimonthly issues of "Applications and Industry," March 1960–January 1961, will also be available in a single volume (no. 79) entitled "AIEE Transactions—Part II. Applications and Industry," which includes all technical papers on that subject presented during 1960. Bibliographic references to Applications and Industry and to Part II of the Transactions are therefore equivalent.

Applications and Industry. Published bimonthly by the American Institute of Electrical Engineers, from 20th and Northampton Streets, Easton, Pa. AIEE Headquarters: 33 West 39th Street, New York 18, N. Y. Address changes must be received at AIEE Headquarters by the first of the month to be effective with the succeeding issue. Copies undelivered because of incorrect address cannot be replaced without charge. Editorial and Advertising offices: 33 West 39th Street, New York 18, N. Y. Nonmember subscription $8.00 per year (plus 50 cents extra for foreign postage payable in advance in New York exchange). Member subscriptions: one subscription at $2.50 per year (balance of $5.00 subscription price to be paid by application of annual dues) to any one of three divisional publications: Communication and Electronics, Applications and Industry, or Power Apparatus and Systems: additional annual subscriptions $5.00 each. Single copies when available $1.50 each. Second-class mail privileges authorized at Easton, Pa. This publication is authorized to be mailed at the special rates of postage prescribed by Section 132.122.

Printed in United States of America

Number of copies of this issue 5,100

Electric-Locomotive-Maintenance Cost Equation

J. W. HORINE
MEMBER AIEE

HAS generally been recognized that comotive maintenance costs increase age. However, the impact of y's inflationary economy has materi- compounded these cost increases, some measure of them is vital to ve power replacement studies since re to evaluate such increases properly have serious future consequences. unately, statistical methods are avail- which can provide reasonably rate forecasts by means of analyzing costs, and then projecting the loped trend into the future.

Problem

he solution, however, is not an easy . First, that railroad which has iled accurate locomotive maintenance s over a period of years on a given vidual group of units is doubly sed since not only are the needed a available, but also that road's nings must have been excellent because expense of compiling such detailed a would otherwise have been prohibi-

econd, maintenance costs are not nly distributed in time. Major over- ls, variously known as "class repair," ileage overhauls," or "scheduled heavy airs," are generally made on the ipment at intervals of 3 or more years, l distort annual figures.

A third group of distorting factors ses from fluctuations in the business lth of the nation. Income is reduced car loadings drop, and expenses cluding locomotive maintenance) must trimmed to help net revenue. "De- red maintenance," which must some y be picked up, then enters the picture. ncurrently, locomotive mileage drops, wer may be stored, further distortions the data occur, and this, in turn, is ain aggravated by the fact that while some maintenance costs vary with mile- age, others are a function of time.

Finally, inflation wields an overriding power on all of the foregoing variants, and labor and material costs intermit- tently and nonconcurrently spurt ahead or hold level for short periods.

Out of this confusion of figures it is desired to isolate the trend of rising costs which can be attributed to age. Of first consideration is the manner in which the costs are to be expressed. Three such measures, each with its advantages and disadvantages, are in general use: dollars per unit per year, cents per unit-mile, and cents per (rated) 1,000 rail horse- power-miles. The first cost expression needs no explanation, the second is obtained by dividing the dollars per unit per year by the annual unit-miles for that year and changing to cents, and the third cost expression is obtained by dividing the second (cents per unit-mile) by the rated rail horsepower of the unit expressed in thousands (i.e., 4.4 for a 4,400-horsepower unit).

This last measure will be used herein, primarily because it facilitates comparison between power units of different horse- power and reflects the decreased use due to greater shoppings with age.

The Data

A major railroad had recognized for some time that rising maintenance costs combined with obsolescence dictated the replacement of a certain class of electric locomotive, 2 of which were placed in service in 1931, 62 in 1934, and 28 in 1935. In November 1959, their retire- ment over the next 4 years was an- nounced. This group, which can be said to have practically run out its life, has therefore been selected to illustrate the cost versus age relationship desired.

Admittedly, the available maintenance cost data are not exact in that they are costs for a pool of power containing a few electric locomotives of other classes. However, the class in question produced 87% of the horsepower-miles of the pool, and hence the figures are reasonably representative for that class and, for the sake of simplicity, the maintenance cost data used will hereinafter be deemed to be for that class. Further, the ages of the three groups of 2, 62, and 28 units have been averaged and centered, and this average figure has been taken as the unit age.

On the foregoing basis, in Table I, columns 1 and 2 show the reported maintenance cost versus age for these 92 locomotive units. These are the reported figures with no adjustments of any character, and are the basic data plotted in Fig. 1.

The Solution

It is self-evident that the costs for each year must be comparable in terms

Table I. Maintenance Costs in Cents Per 1,000 (Rated) Horsepower-Miles as Reported and as Adjusted to Year 1958 Base

Maintenance Cost as Reported	Locomotive Age, Years	Multiplier Factor to 1958 Base	Maintenance Cost Adjusted to 1958 Base
2.75	3	3.133	8.616
2.89	4	3.133	9.054
3.34	5	3.133	10.464
4.00	6	3.133	12.532
4.22	7	3.155	13.314
4.22	8	3.144	13.267
5.32	9	3.019	16.061
4.43	10	2.782	12.324
5.83	11	2.596	15.135
9.74	12	2.488	24.233
9.47	13	2.467	23.362
8.40	14	2.116	17.774
11.74	15	1.948	22.869
10.06	16	1.714	17.242
10.27	17	1.599	16.422
13.19	18	1.500	19.785
14.53	19	1.349	19.601
16.88	20	1.297	21.893
17.20	21	1.267	21.792
16.90	22	1.234	20.854
18.15	23	1.219	22.130
19.52	24	1.132	22.100
22.15	25	1.056	23.390
20.42	26	1.000	20.420

per 60-600, recommended by the AIEE Land ansportation Committee and approved by the EE Technical Operations Department for pres- ation at the ASME-AIEE Railroad Confer- e, Pittsburgh, Pa., April 20–21, 1960. Manu- ipt submitted January 15, 1960; made available printing March 11, 1960.

W. HORINE is with The Pennsylvania Railroad mpany, Philadelphia, Pa.

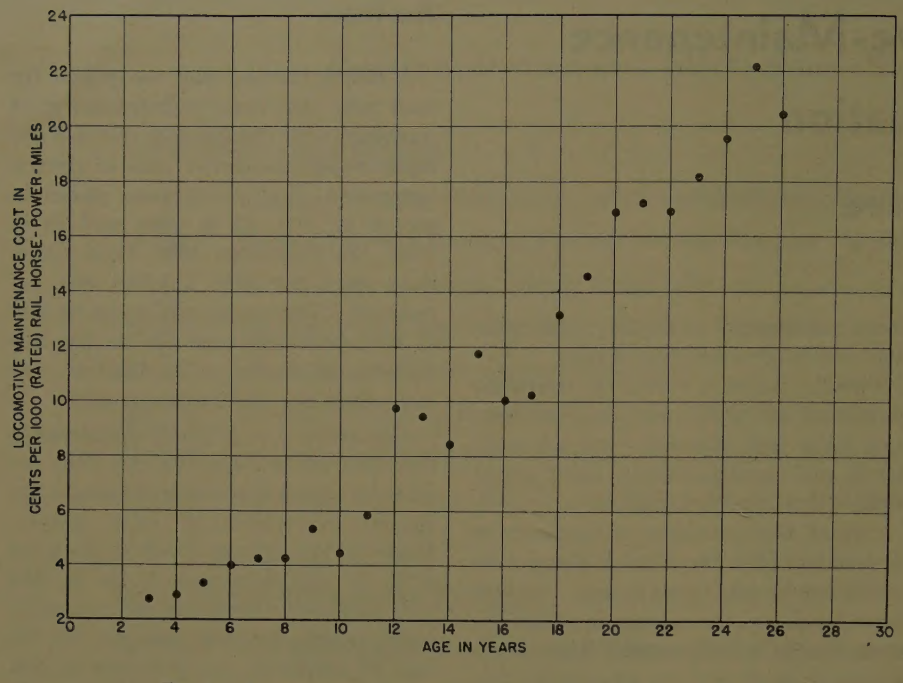

Fig. 1. Locomotive maintenance cost versus age, as reported

of the same dollar value, i.e., adjusted for inflation. This is readily done by calculating an appropriate multiplier for each year from published indexes of material prices and wage rates.[1] For the case in point, adjustment to base year 1958 was selected. The yearly multipliers and corresponding adjusted annual maintenance costs are shown in columns 3 and 4 of Table I, with these costs plotted in Fig. 2.

The problem now becomes one of determining the trend of a statistical time series, a relatively simple form of correlation between an independent variable (X, or age) and a dependent variable (Y, or cost). Generally, the proposed use of the trend, when found, dictates the degree of exactness and the form of solution used. If interpolation (i.e., determination of Y at some specific point within the range of the known data) is intended, then a fitted trend of maximum accuracy is needed. If extrapolation (i.e., projection of the calculated trend to determine the value of Y at some point outside the range of known data) is intended, then the simplest trend curve that reasonably fits the data should be used to minimize distortion and error. Extrapolation is, of course, the intended use, since the problem, in its simplest terms, could be stated as: "At what future age will the cost of maintenance plus fixed charges of these locomotives become greater than the cost of maintenance plus fixed charges of a new, modern locomotive?"

Inspection of Figs. 1 and 2 immediately reveals an outstanding dissimilarity; the costs of Fig. 1 show an increase with age accelerating at an alarming rate, whereas the increases in costs of Fig. 2 appear to be decelerating with age. Since a straight-line trend (first-degree curve) would neither accelerate nor decelerate the cost change, the simplest curve that would represent the true condition conceivably could be a second-degree or parabolic trend.

This, then, has been calculated from the cost and age data of Fig. 2, details of the calculation being shown in Appendix I. Fig. 3 reproduces Fig. 2 with the calculated line of trend shown heavy solid line within the data limits with light dashed projection beyond data limits.

The question immediately arises as the validity of these projections, and as the degree of confidence that can placed on their use. This must be kno before such fitted curves can be used rather important decisions. The soluti fortunately, is simple.

A measure of the degree of "goodne of fit, known as the Index of Correlati can be determined from the calculati made in determining the trend. T index ranges in value from 0.0 for correlation whatsoever to 1.0 for perf correlation, i.e., the calculated curve wo pass through every point of the da This index has been calculated for line of trend and has the value of 0. Details of the calculation are shown Appendix II.

This value of 0.97 is unusually high this type of statistic, and indicates tha high degree of confidence may be plac on the fitted trend, still bearing in mi that the projection presupposes no ma changes in maintenance and operati practices from those which were in effe during the data period. Further, t curve could not be used to forecast ma tenance costs of units of different physi characteristics, such as a rectifier-ty locomotive with axle-hung motors a improved modern insulations as compar with a straight electric locomotive wi

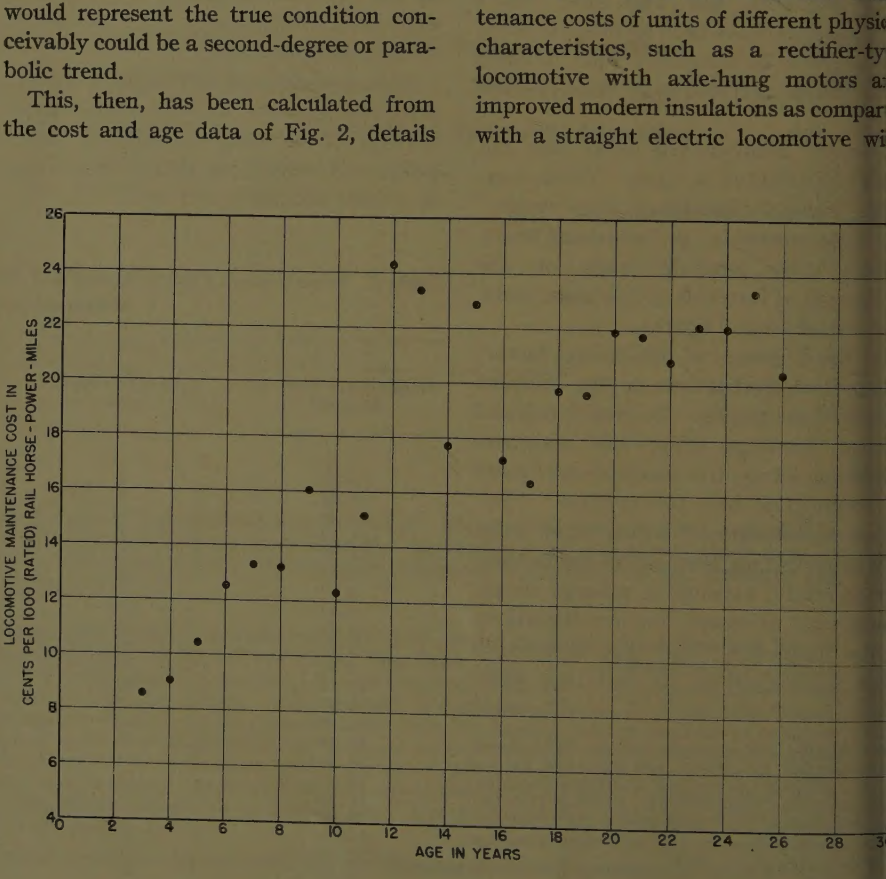

Fig. 2. Locomotive maintenance cost versus age, adjusted to 1958 base

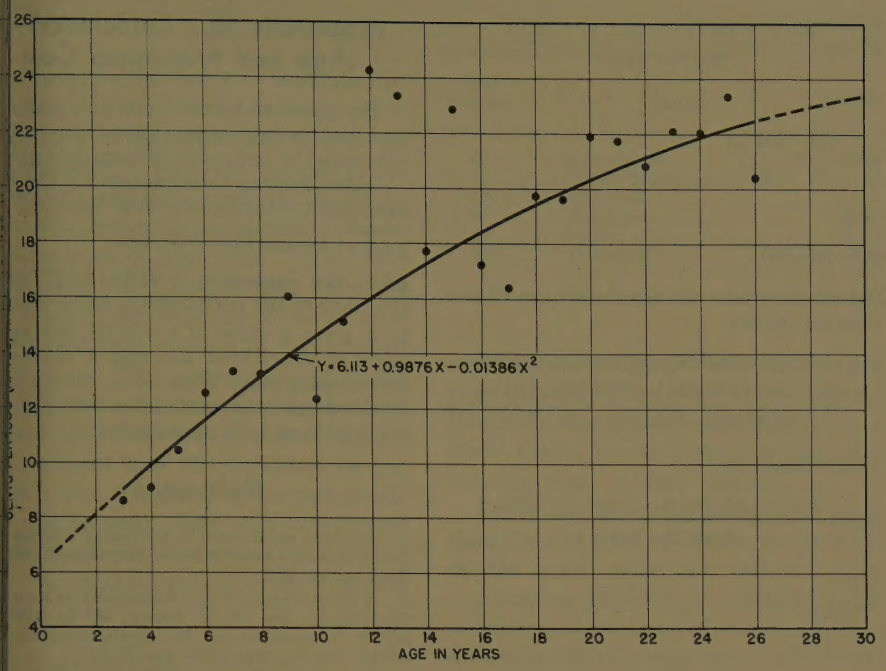

Fig. 3. Line of trend of locomotive maintenance cost versus age

me-mounted motors and the insulations mmonly in use for the past several cades.

ie Application

It is evident from the shape of the line trend, that it will eventually reach a ximum. The rate of growth is the st derivative of Y with respect to X d the maximum value of Y occurs nen the rate of growth becomes zero. nis occurs at 35.6 years with a maximum st of 23.71 cents per 1,000 (rated) rail rsepower-miles. Details of the calcula- n are in Appendix III.

If continued on beyond that age, the ojected curve would, of course, turn wnward, a condition for which there is apparent justification. Instead, if ojected values beyond that age are quired, it can only be assumed that aintenance costs have leveled off at iat maximum value.

onclusions

1. There is a definite relationship etween age and electric locomotive aintenance costs which can be evaluated hen reasonably accurate cost data are vailable.

2. The calculated trends obtained ust be used with caution, and must not e assumed to apply to electric loco- otives of different designs.

3. When a calculated cost trend easonably fits the base data, projections of the trend to forecast future costs for either power replacement studies or budgeting purposes and to determine the amount and age at which maintenance cost will be a maximum are of considerable value.

4. The chief value of these data in connection with consideration of new units lies in the fact that it can undoubtedly be assumed that new units will give a better performance.

Appendix I. Calculation of Line of Trend

The age in years X and the maintenance cost adjusted to 1958 base Y are tabulated and values of X^2, XY and X^2Y are calculated in Table II. It will be noted that costs and ages of 12, 13, and 15 years have been omitted. This has been done on the basis that the costs for those ages are badly out of line with other years, since these ages fell within the latter part of World War II when abnormal conditions prevailed and the accuracy of the reported data is questionable.

The method of least squares was used to derive a second-degree equation which expresses line of trend. The preliminary equation is shown in the following standard form:

$$\Sigma y = na + \Sigma xb + \Sigma x^2 c$$

$$\Sigma xy = \Sigma xa + \Sigma x^2 b + \Sigma x^3 c$$

$$\Sigma x^2 y = \Sigma x^2 a + \Sigma x^3 b + \Sigma x^4 c$$

Substitution in this formula and subsequent solution gives:

$$354.13 = 21a + 308b + 5{,}658c \quad (1)$$

$$5{,}864.96 = 308a + 5{,}658b + 115{,}892c \quad (2)$$

$$114{,}254.05 = 5{,}658a + 115{,}892b + 2{,}510{,}682c \quad (3)$$

$$7{,}253.64 = 430a + 6{,}309b + 115{,}892c \quad (1)$$

$$5{,}864.96 = 308a + 5{,}658b + 115{,}892c \quad (2)$$

$$1{,}388.68 = 122a + 651b \quad (10)$$

(The values of Σx^3 and Σx^4 can be obtained from statistical tables.)

$$127{,}058 = 6{,}673a + 122{,}575b + 2{,}510{,}682c \quad (2)$$

$$114{,}251 = 5{,}658a + 115{,}892b + 2{,}510{,}682c \quad (3)$$

$$12{,}897 = 1{,}015a + 6{,}683b \quad (11)$$

$$14{,}256 = 1{,}252a + 6{,}683b \quad (10)$$

$$12{,}897 = 1{,}015a + 6{,}683b \quad (11)$$

$$1{,}449 = 237a$$

$$6.113 = a$$

$$1{,}388.68 = 745.78 + 651b \quad (10)$$

Table II. Calculation for Appendix I

X	Y	X^2	XY	X^2Y
3	8.616	9	25.848	77.544
4	9.054	16	36.216	144.864
5	10.464	25	52.320	261.600
6	12.532	36	75.192	451.152
7	13.314	49	93.198	652.386
8	13.267	64	106.136	849.088
9	16.061	81	144.549	1,300.941
10	12.324	100	123.240	1,232.40
11	15.135	121	166.485	1,831.33
(12)	(24.232)	(144)		
(13)	(23.362)	(169)		
14	17.774	196	248.836	3,483.70
(15)	(22.869)	(225)		
16	17.242	256	275.872	4,413.95
17	16.422	289	279.174	4,745.96
18	19.785	324	356.130	6,410.34
19	19.601	361	372.419	7,075.96
20	21.893	400	437.860	8,757.20
21	21.792	441	457.632	9,610.27
22	20.854	484	458.788	10,093.34
23	22.13	529	508.990	11,706.77
24	22.10	576	530.400	12.729.60
25	23.39	625	584.750	14,618.75
26	20.42	676	530.920	13,803.92
308	354.13	5,658	5,864.955	114,251.05

$642.90 = 651b$

$0.9876 = b$

$354.13 = 128.37 + 304.18 + 5{,}658c \quad (1)$

$78.42 = -5{,}658c$

$-0.01386 = c$

These results are then used as the constants in the standard form equation:

$$y = a + bx + cx^2$$

and substituting gives the line-of-trend equation:

$$y = 6.113 + 0.9876x - 0.01386x^2$$

Appendix II. Calculation of Index of Correlation

In standard form, the equation of Index of Correlation is as follows:

$$i^2yx = \frac{a\Sigma(y) + b\Sigma(xy) + c\Sigma(x^2y) - Nc^2y}{\Sigma(y)^2 - Nc^2y}$$

where

$$cy = \frac{\Sigma y}{N} = \frac{354.13}{21}$$

and

$$cy^2 = 284.361$$

Substitution into the standard form of the equation gives:

$$i^2yx = \frac{(6.113 \times 354.13) + (0.988 \times 5{,}864.99) - (0.0139)(114.251) - (284.361)(21)}{(6{,}405.3) - (284.361)(21)}$$

This reduces to

$$i^2yx = \frac{2{,}164.8 + 5{,}794.6 - 1{,}588.1 - 5{,}971.6}{6{,}405.3 - 5{,}971.6}$$

$$= \frac{399.7}{433.7} = 0.92$$

$$iyx = 0.97$$

Appendix III. Calculation of Age and Maximum Cost

The age at which cost reaches a maximu and the corresponding figure for cost a calculated by use of the differential calculu

Differentiating the equation for the bas age–cost-per-horsepower-mile relation,

$$y = 6.113 + 0.9876x - 0.01386x^2$$

gives the expression $0.9876 - 0.02772x$ f the slope of the curve which, being equate to 0, gives a value of $x = 35.63$, the age years at which cost becomes a maximur Substituting this value of x in the bas equation gives a value of $y = 23.71$ cen per 1,000 rail horsepower-miles.

References

1. INDEXES OF RAILROAD MATERIAL PRICES A WAGE RATES. Association of American Railroa Washington, D.C.

2. A REAPPRAISAL OF THE ECONOMICS OF RAILW ELECTRIFICATION, H. F. Brown, R. L. Kimba *AIEE Transactions*, pt. II (*Applications and I dustry*), vol. 73. Mar. 1954, pp. 35–51.

A Digital Computer Simulation of Single-Track Railroad Operation

R. T. COUPAL
NONMEMBER AIEE

L. L. GARVER
NONMEMBER AIEE

W. R. SMITH
NONMEMBER AIEE

IMPROVED SIGNAL SYSTEMS such as Centralized Traffic Control (CTC) have enabled railroads to move train traffic on a single main track with passing sidings that formerly required two tracks or the general use of train orders and time-table authority. A digital computer program has been designed to aid railroad management in selecting the proper siding locations and signal spacing when considering a CTC system. Using an IBM (International Business Machines Corporation) *650* computer the traffic pattern of up to ten trains operating at one time on a 100–150-mile division of a railroad may be predicted. Initial information stored in the computer memory describes the grades, curve speed restrictions, signal locations, and track layout of the railroad. Also, data for each train are available to the computer. This information includes the number, weight, and type of cars, the power of the locomotive, the origin and destination, and the time of departure.

The program to be described in this paper directs the computer to determine the time of arrival and departure of each train at each siding or station along the railroad, taking into account the conflicting route requirements. It is also the function of the computer to provide the location of train meets or passes.

As one train reaches its destination the data for another train may be read into the computer so that many trains, representing days of railroad operation, may be studied. Data describing the trains or track layout may be changed easily. This allows the study of railroad operation under the conditions of varying train departure times on a given railroad, or fixed departure times and varying siding locations and signal spacings.

The Digital Computer

For those not familiar with the elements of an IBM *650* computer the following brief description will aid in understanding the terms used in this paper. The electronic digital computer may be visualized as three functional units: a magnetic drum memory, arithmetic unit, and the program register. The magnetic drum memory has a capacity of storing 20,000 digits (numbers 0 9) in groups of 10. Each group with sign is considered a word, making a tot of 2,000 words. A word is located on th drum by a 4-digit address. The arit metic unit performs multiplication, div sion, addition, and subtraction. This un can locate and use information stored o the memory drum without destroying th information. Further, it is capable placing the results of its computations the memory. The program register co trols the sequence of operations perform by the arithmetic unit. The progra register can recognize when the result any operation is zero or nonzero, plus minus, and can also examine any digi of a word for an *8* or *9*. With the features, logic may be programmed in the computer. The transferring of i formation from punched cards into th memory and the punching of informatio from the memory into blank cards is al controlled by the program register. T sequence of instructions interpreted by th program register is called the program.

Paper 60-47, recommended by the AIEE Lan Transportation Committee and approved by t AIEE Technical Operations Department f presentation at the AIEE Winter General Meetin New York, N. Y., January 31–February 5, 196 Manuscript submitted February 4, 1959; mad available for printing November 20, 1959.

R. T. COUPAL, L. L. GARVER, and W. R. SMITH a with the General Railway Signal Compan Rochester, N. Y.

The authors wish to acknowledge the assistance i obtaining actual railroad drawings and tra graphs given by the signal department of t Canadian Pacific Railroad. They have also giv counsel on actual railroad operating practices an possible means of simulation.

Program

ıe program necessary to simulate the ation of many trains running on a e track is separated into two parts. calculation program provides the ructions and data necessary to mathtically predict the speed-time-distance acteristics of any train. With this rmation the computer may calculate much time will elapse as a train els from one portion of the railroad another. The route logic program vides the computer with a numerical hod of visualizing the track layout a railroad and the positions of the ns. The computer must have avail- the necessary data and instructions hat when two trains conflict, one train y be recalculated into an available ng.

E Calculation Program

The calculation program provides the ed-time-distance characteristic for each in to be moved over the railroad. is is accomplished by solving the ce equation for train acceleration

$$\text{celeration} = \frac{\text{Locomotive Tractive Effort} - \text{Train Resistance}}{\text{Mass of the Train}}$$

For diesel-electric operation, which has en assumed in this development, the ctive effort is related by a constant to locomotive horsepower divided by in speed. The train resistance is a nction of train speed, car weights, and ner factors. For this program the vis formula and constants are used.[1] e appendix contains a development of actual formula used. The train istance is related to the types of cars d their weights, the speed of the train, d the grade and curvature of the track. erefore data for both the train and the ck characteristics are stored in the mputer memory. The storage of the in data will be covered later in this per. The track data contain one try for each change in grade or rvature, and there are approximately ır of these changes per mile to be excted on an average railroad. The data these track sections are stored seentially in the computer memory with e location necessary for each section constant grade and curve.

In the 10-digit track data number, three gits represent the acceleration per ton cause of the grade in this section, two gits represent the acceleration per ton cause of curvature (always negative), d three digits give the length of the ction in tens-of-feet. The remaining two digits give a speed limit in miles per hour that may be imposed by the railroad timetable because of such things as a sharp curve, tracks through a city, or a crossing with another railroad.

Using the foregoing train and track data the computer calculates the progress of the train along the railroad. The acceleration available is computed and if a change in velocity is indicated, it is solved by the following formulas

$$V_2 = V_1 + at \qquad X = \frac{V_1 + V_2}{2}\, t$$

where

a = acceleration available at speed V_1
V_1 = initial speed
t = 6-second constant acceleration period
V_2 = speed after the acceleration
X = distance traveled

No change in velocity is indicated either by zero acceleration available or when the speed is greater than a speed limit but not greater than the speed limit plus 5 miles per hour. The time to travel the next distance is then calculated by dividing the distance by the speed. Thus the time to travel from one portion of the railroad to another may be calculated for any train.

The Route Logic Program

The route logic program directs the computer in determining points of train conflicts and sidings where the trains may pass. The signal system on an actual railroad divides the track into sections called signal blocks which may be occupied by only one train. Therefore these signal blocks, actual or proposed, were chosen to be the sections used by the computer to visualize the railroad. Each signal block was assigned one memory location for its data and the sequence of signal blocks determined the sequence of memory locations.

Of the ten digits in each memory location representing a signal block, four digits represent the length of the section in tens-of-feet, four digits indicate the

Table I. Types of Signal Section Considered

Code Number	Name	Represents
00	Intermediate	single mainline track with no entrance to sidings
02	Double Track Intermediate	double mainline tracks with no entrances to siding
10	Approach	single mainline track with a switch to a siding at one end
20	Mainline	single mainline track adjacent to a siding
30	Siding	single track siding
50	Transition	double mainline tracks at the transition from a single mainline track

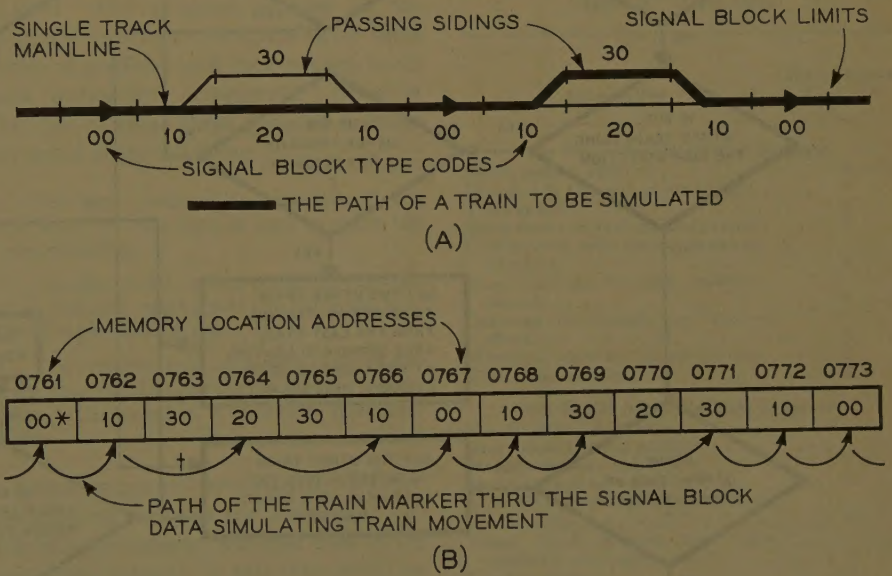

Fig. 1. Method used to simulate train movement

A—Railroad track and signal diagram
B—Computer memory drum representation
* Only the first two of ten digits are shown in each memory location.
† Sections not used by the train are skipped in the memory.
Two 30 sections are used to allow two trains to use the same siding when direction and length permit

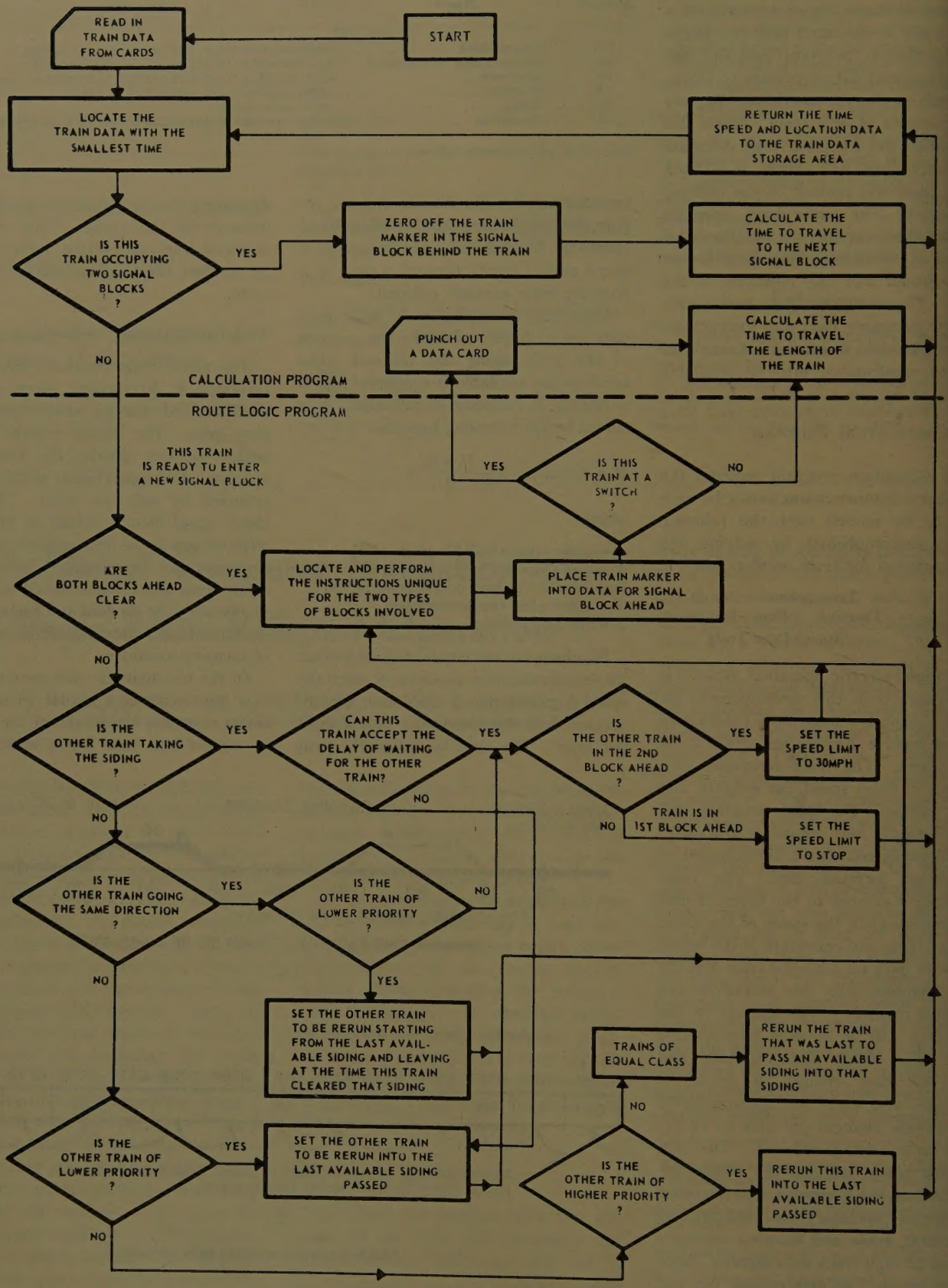

Fig. 2. Flow diagram of computer program for predicting railroad operation

nce of a train in the block, and the ining two digits indicate the type of l section. The types of signal sec- considered in this program and their numbers are given in Table I.

rtain operations have to be performed he train is calculated from one l block to another. Many of the ations are unique to the two types of ks involved. In order to locate the ram for these operations, the com- r is directed to take the first digit of ype code of the block occupied and the 2-digit-type code for the block d of the train. This forms a 2- number unique for the two signal ks involved and the direction of travel. number is added to a master 4- number to form the address of the instruction in a subroutine. As an nple when the computer calculates a train is preparing to enter an proach" block from an "intermediate" k the number *0* and *10* are added to *10* and then combined with the ter number *1300* to give *1310*. This ne address of the first instruction in subroutine.

s previously mentioned four digits he signal block data are used to in- te the presence of a train in that k. This 4-digit number, termed a in marker," is the address of the word of data for the train. The ts are zeros when no train is in the k. The data address of a train in signal data forms one half of a cross rence so that when given a train ker the entire data for the train may ocated. The other half of the cross rence is formed by storing with the n data the address of the signal section upied. Therefore, given the train data, signal data for the section occupied those around it may be located.

o simulate the movment of the train ng the railroad the train markers are ved from signal block to signal block. e computer calculates the time at which rain will enter the next signal block stores it with the train data. When time is earlier than the times stored h the other trains, the train marker placed into the signal block ahead. e computer then calculates the time en the last car of the train will clear block behind. Time, speed, and grade tion location are stored back with the in data. When the other trains have n moved in a similar manner and the e for this particular train is again the liest, its train marker in the block ind is replaced by zeros. Fig. 1 tches the path of a train marker in resenting a train movement. The sequence of this cycle is repeated as follows:

1. Enter the train marker in the block and calculate the time when the block behind will be cleared.
2. Move the other trains as required.
3. Zero the block behind and calculate the time to enter the next signal block.
4. Move the other trains and return to 1.

A conflict occurs when two trains try to occupy the same signal block. Railway signals, however, will also detect the presence of a train in the second block ahead and on a following move will indicate a 30-mph speed limit for a train entering the section. This also will constitute a train conflict, especially when a fast passenger train overtakes a slow freight train. Therefore the route logic program directs the computer to test both the first and second signal blocks ahead of a train for occupancy. If no train marker is found, the program continues as described in the previous paragraph. The largest portion of the route logic program is devoted to instructions directing the computations when a train marker is located. The pattern of these instructions becomes very involved but the general form may be understood by referring to Fig. 2.

The important information for this program was contained in numbers, called "markers," that could be zero or nonzero, *8* or *9*, and positive or negative. The train marker used in the signal block data is one example of a zero or nonzero marker. The program register of the computer is able to recognize these three types of qualities and then branch to its next instruction accordingly. Some of the uses of these three types of markers are listed in the following.

1. The sign, positive or negative, of the first word of train data is used to mark the train direction.
2. Another word in the train data group, when nonzero, marks that the train has conflicted with another train.
3. The number *8* in a specific digit of the train data marks the train as being a freight train. The number *9* marks a passenger train.

Other important information conveyed by markers includes the answers to the following questions: Was this train in the last siding passed? Is this train being rerun after conflicting with another train? Is the train in an "Approach" signal block and preparing to take the siding? These markers with two allowable states direct the computer to follow the particular instructions necessary for any train conflict and rerunning involved.

Scheduled Delays

The program just described has assumed that all trains would be operated to travel the railroad in a minimum amount of time as allowed by locomotive power and route conflicts. In actual practice however many trains are required to stop somewhere along the railroad. A local freight train will make many stops to set off and pick up cars. A passenger train makes scheduled stops and at other points has scheduled passing times. A subprogram is included to allow the simulation of three types of delays: a stop for a definite period of time, a stop for a definite period of time but the train may not depart until a scheduled time has passed, and a scheduled entry time where the train need not stop but it cannot enter the next block until the scheduled time has passed. This program requires the use of a memory location for each train and the data must be stored in the computer memory before the calculation begins.

Train Data

The train data include information for use in both the calculation program and route logic program. Ten groups of 20 words each have been reserved in the memory for train data. This allows ten trains to be operating on the simulated railroad at one time. Additional train

Table II. Train Data

Information	No. of Digits Required
For Use in the Calculation Program	
Grade section address	4
Distance to the next grade change	4
Train speed	3
Speed limits (maximum and present)	4
Braking rate with normal brake application	4
Three constants for train resistance formula	10
Constant for locomotive tractive effort	6
Minimum speed for full horsepower	3
Next delay location	8
For Use in the Route Logic Program	
The direction of travel	sign
Train identification number	3
Priority number and type	2
Train marker for this train	4
Time for next change in signal block occupancy	4
Signal block address that train marker is occupying	8
Conflict marker	10
Length of the train in feet	4
The address and time of clearing past the last siding	8
The grade section and distance to go at the last siding	8
The same information for the 2nd to last siding passed	16
Train being rerun marker	1
In approach taking siding	1
Been in siding	1

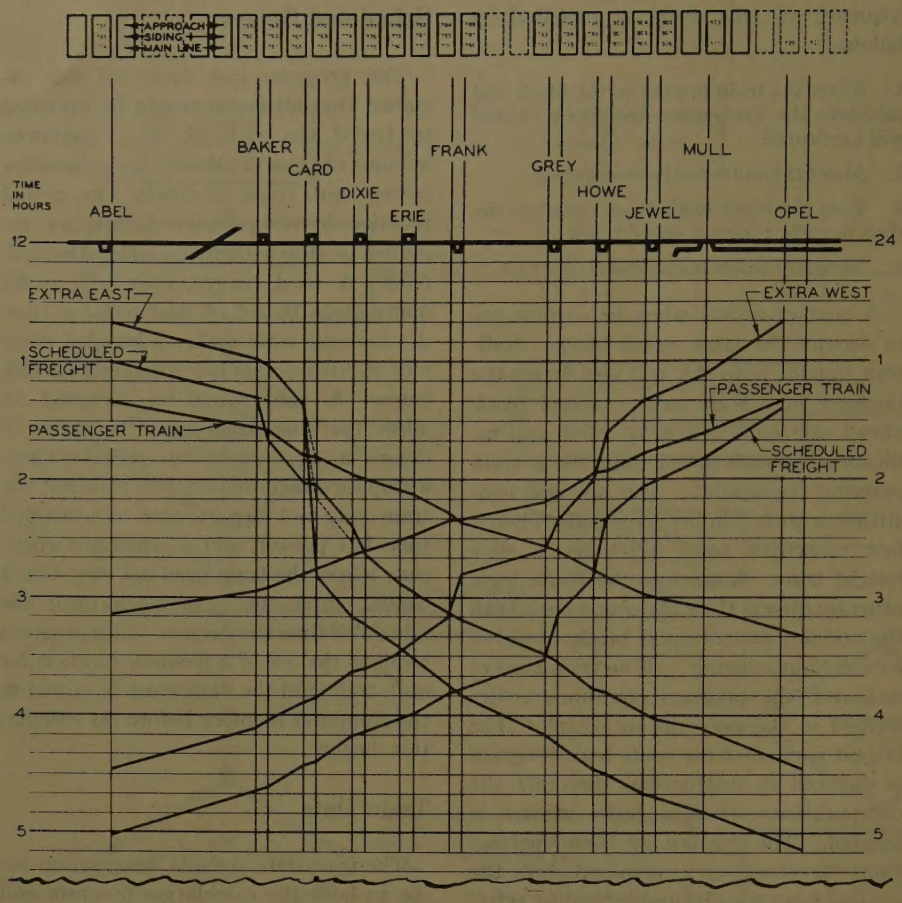

Fig. 3. Train graph predicted for the Trenton Division, Canadian Pacific Railroad

——— Predicted traffic pattern
– – – Calculations made but superseded by a rerun because of train conflicts

data may be read from cards into an area made available when a train completes its run. This allows days of operation to be studied without continually stopping the computer. Table II is a list of the information contained in the train data area and the number of digits required.

Answer Cards

Answer cards are punched by the computer each time it calculates a train passed the entrance or exit to a siding. These cards contain the train identification number as originally assigned in the input data, the addresses of the two signal blocks the train marker is occupying, the time the front end of train passes the switch, and the conflict marker which is normally zero but will contain a train marker when the train is being rerun into a siding for a meet or pass.

The information on these answer cards may be plotted to give the time-distance graph, called a train graph, of the simulated railroad operation. It is these train graphs, such as shown in Fig. 3, which aid railroad management in choosing the siding locations best suited to their traffic needs or show the effect of rescheduling trains on an existing track layout.

Conclusions

This program is offered as an aid to railroad management for evaluating the effects of possible changes in right-of-way, signal equipment or train schedules. The major advantage of the computer is its ability to locate the points of conflict before having to make a routing decision. This allows the horsepower per ton, grade and curve, and speed restrictions to have full effect in determining where meets will be made.

New data for a complete change in track and signal layout may be prepared from blueprints in one-half day. Train data such as departing time may be changed in a few minutes. Using the IBM *650* computer approximately 8 minutes are required to calculate one of many trains over 100 miles of railroad. The program offers a relatively easy method to evaluate many proposed changes in either the right-of-way or the operating schedule without the expense and difficulty involved in actual field tests.

Appendix

The Davis formula for railroad frei car rolling resistance is:

$$R = 1.3 + \frac{29}{W} + kV + \frac{CAV^2}{Wn}$$

where

R = resistance, pounds/ton
W = average weight per axle, tons
k = constant depending upon equipment
V = speed, miles/hour
C = constant depending upon equipment
A = effective cross-sectional area, square f
n = total number of axles

The actual values for the constants m tioned may be found in reference 1, page

Combining this equation in the fo equation

$$F = 100Wa + RW + 20PW + 0.8DW$$

and solving for acceleration

$$a = \frac{F}{100W} - \frac{R}{100} - 0.2P - 0.008D$$

where

a = acceleration, miles/hour/second
F = force of the locomotive, pounds
100 W = effective mass including inei effect of rotating wheels
R = train resistance as given by the Da formula
P = per-cent grade of the track
D = degrees curvature of the track

The force of the locomotive may solved for by the equation

$$F = \frac{375(HP)0.8}{V^*}$$

where

F = force of the locomotive available overcoming train resistance in pou
HP = rated horsepower of the locomotive
V^* = train speed or minimum speed for maximum horsepower, whichever larger

The minimum speed for maximum hor power is considered to be the speed at wh the locomotive tractive effort is equal 25% of the weight of the locomotive on driving axles.

Reference

1. Train Resistance of Freight Trains un Various Conditions of Loading and Spe *Proceedings*, American Railway Engineering A ciation, Chicago, Ill., vol. 42, 1941, pp. 69–86.

Discussion

I. H. Cole (Canadian National Railwa Montreal, Que., Canada): The Canad National Railways (CNR) are implement a program of siding extensions and cent ized traffic control on about 4,500 mile their transcontinental single-track l The requirement is to do it economica A computer program has been written

650 data processing equipment to ate train dispatching by CTC on e track and it provides a very conven- method for comparing various alterna- iding combinations and for deciding on h is most suitable for the job.

le logic in the computer program has developed from a detailed analysis of dispatching in CTC territory; major asis has been laid on simulating ately train dispatchers' decisions. In respect, there is a radical difference een the simulation of train dispatching loped by the General Railway Signal pany and that developed by the CNR. example, in the General Railway Signal pany's simulation, opposing trains are ed to progress to the point where a ion between them is inevitable. Then, st-mortem analysis is held to decide on t should have been done in the first nce to have avoided the situation and, result of the post-mortem one of the s is moved back while the other is ed to proceed. But the logic associ- with moving a train back is very diffi- to formulate when the move entangles with other trains that were following it. In the CNR's logic, on the other hand, the imminence of conflicts between trains are foreseen and steps are taken to resolve them consistent with the aim of moving the traffic safely and expeditiously; in fact, this is as it happens in practice and the results of our simulation approximate very closely to train dispatching by human operators.

The basis of the CNR's method of analyzing the traffic capacity of a single track on an IBM *650* digital computer, is, first the computer is programmed to prepare the ideal train time-lines for a typical week's traffic (a train's ideal time-line is its distance travelled versus elapsed time when the train occupies its own track): this is how the traffic would move when, in the ideal case there is no interference between trains. The running times of the trains involved are obtained from the results of their on-line performance or from performance calculations with a high-speed digital computer. Next, the computer is programmed to resolve the conflicts between the ideal time-lines for the sidings combination under test, in accordance with agreed rules for the movement of traffic. These rules take account of the relative train priorities as well as the time-in-hand of trains relative to their published schedules. Lastly, a supplemental program compares the "resolved" time lines with their ideal counterparts and calculates the amount of interference that resulted from moving the prevailing traffic with the particular sidings combination under test.

The program previously referred to occupies about 3,000 locations of a 4,000-word magnetic drum. It is quite fast and takes about 90 minutes of computer time to process a week's traffic, consisting of 150 trains, over a single track with 20 sidings.

R. T. Coupal, L. L. Garver, and W. R. Smith: Mr. Cole's discussion of the program which has been developed by CNR shows another method of analysis of the problem. Since we know very little about the actual operation of their program we cannot intelligently compare the two programs.

rench Technical Advances in the Field of Railroad Electrification

F. NOUVION
NONMEMBER AIEE

HE FRENCH NATIONAL Rail- roads network, of standard gage ck, comprises more than 39,500 kilom- s (km) or almost 25,000 miles of route. French Railroad Companies were ionalized on January 1938, and im- diately thereafter efforts were made nodernize them.

Regarding the "traffic unit" as a com- ation on an equivalent basis of pas- gers-km and tons-km, from 1949 to 8 freight and passenger traffic in- sed 70 billion to 85 billion traffic units. ring the same period the number of road employees decreased from 465,- to 360,000, bringing the traffic units man hour from 60 to 100.

The modernization of the French Rail- ds embodies mainly the electrifica- of certain lines and the conversion of ers to diesel operations. Table I gives parative figures for the years 1939 and 8.

r 60-602, recommended by the AIEE Land sportation Committee and approved by the E Technical Operations Department for ntation at the AIEE-ASME Railroad Con- ce, Pittsburgh, Pa., April 20–21, 1960. Manu- t submitted January 19, 1960; made available rinting March 25, 1960.

OUVION is with the French National Railroads, York, N. Y.

At present, on the Société Nationale des Chemins de Fer Français (SNCF), there are 4,000 miles of electrified route, representing 16% of the total route mileage and 50% of the total traffic. At the end of 1963, 4,700 route-miles or 18% of the total route-mileage should be electrified and 63% of the total traffic will then be handled by electricity. From the standpoint of energy, the advantages of electrification are considerable: high efficiency, possibility of using power derived from domestic sources, particularly from power stations employing hydraulic energy or blast furnace gases.

Fig. 1 shows that the railroad consumption is steady during the day. In 1958, 34% of our energy was consumed during off-peak hours; on a national basis the traction energy to total energy ratio remains low and practically constant despite electrification.

Fig. 2 summarizes the relative efficiencies for the various types of motive power. Today, electric traction leads and will continue to do so increasingly. Energy consumption per ton hauled is low. The following figures, recorded on our North-Eastern lines, show the average consumption per gross ton-km hauled:

1955—19.6 watt-hours
1956—20.9 watt-hours
1957—22.3 watt-hours
1958—21.5 watt-hours

In 1945, 2,200 route-miles had been electrified at 1,500-volts direct current, the standard system in France since 1923. The SNCF has improved this system to a high degree, as evidenced by the railroad world speed record established on March 28 and 29, 1955, during which a speed of 204 mph (miles per hour) was attained. These d-c passenger locomotives are given class repair every 750,000 miles.

From a technical point of view, one could have been satisfied with the results of the 1,500-volt d-c electrification, but this solution appeared to be too expensive, therefore a more economical system was sought. There were two other very well known solutions in the world: the 3,000-volt d-c and the low-frequency a-c systems—$16^2/_3$ and 25 cps (cycles per second).

The low-frequency current could not be considered because it requires special frequency high-voltage lines which are

Table I. Performances of the Different Forms of Traction

	Millions Train-Miles	
	1939	1958
Steam	230	130
Electric	43	110
Diesel rail car	23	78
Total	296	318

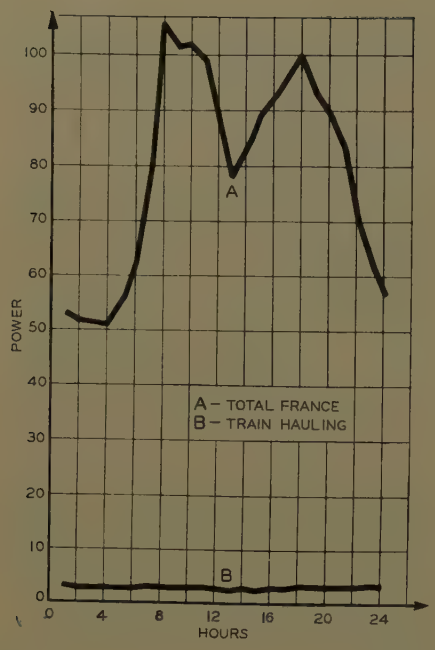

Fig. 1. Hourly variation of power consumption

not justified in any event; therefore only the 3,000-volt d-c system or some other new system remained.

The 3,000-volt d-c electrification was studied carefully and was given up since, in this system, the locomotives had proved to be much inferior to our 1,500-volt d-c locomotives. Fig. 3 shows the comparative speed–tractive-effort curves of two CC locomotives from the same manufacturer.

One point will be sufficient to indicate why we could not consider using 3,000-volt direct current to haul, for instance, the Mistral train: instead of one BB of 80 tons, we would have required two CC 3,000-volt d-c locomotives.

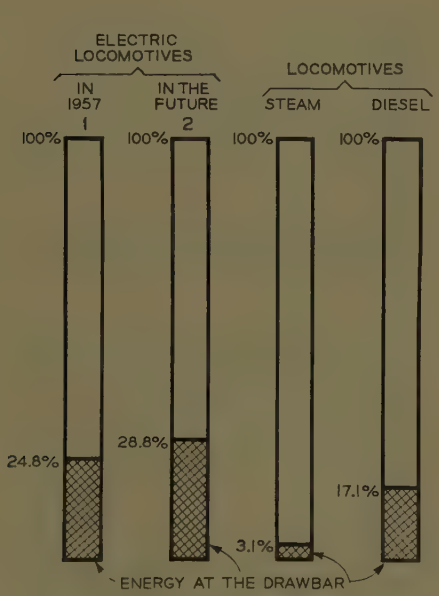

Fig. 2. Relative efficiencies

Since we could not be satisfied with any of the existing systems of electrification, we turned to the study of the 50-cps single-phase system, and all the calculations that were made in 1955 have proved that the single-phase traction at industrial frequency was producing a saving of 25% in first costs, and 7% on yearly expenses, over the 3,000-volt d-c system.

Since then, single-phase traction has been much improved while d-c traction has undergone only minor improvements.

Fixed Facilities

High-Voltage Lines

With the d-c system two transmission lines usually run parallel to the railroad tracks in order to feed the substations, i.e., the length of the high-voltage lines is twice that of the track.

With single-phase 25 kv, the distance between substations is such that they can be installed either at the existing high-voltage distribution substation locations, or close to these locations.

For instance, on the Valenciennes-Thionville line, out of 220 route-miles, less than 5 miles of high-voltage feeder have been installed.

Substations

Although we have considerably reduced the size of our d-c substations, they still remain much more complex than the a-c substations.

Moreover, since the a-c substations are less numerous, the advantage of the single-phase system is obvious. The ratio of costs can be evaluated at better than 3 to 1 in favor of single-phase alternating current. The distance between these single-phase substations ranges from 25 to 50 miles.

Catenary

Here again, the catenaries are provided with less copper, about half of what is needed with 3,000-volt direct current. Therefore the single-phase catenary is less costly than the direct current to the extent of approximately 20% in first cost.

Our a-c catenary is made of a bronze tin bearing messenger of 0.10075 in. (inch)^2 and a hard copper contact wire of 0.1658 in.^{2}; see Fig. 4. The total cross sectional area is equivalent to 0.2265 in.^{2} of copper.

Fig. 5 shows overhead line feeders. Only one circuit breaker per direction is provided, the sectionalizing being carried out by remotely controlled switches located in wayside switching stations.

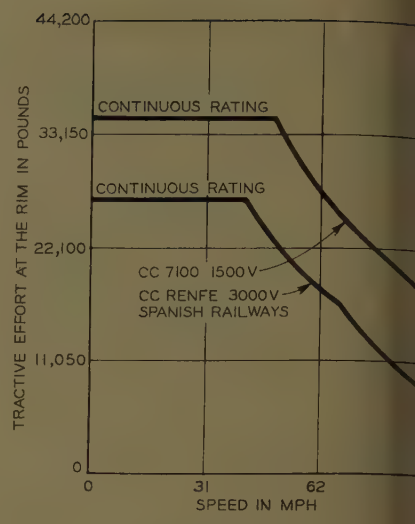

Fig. 3. 1,500-volt and 3,000-volt locomotives

Harmonics and Unbalanced Loads

It should be pointed out that, from t beginning, the problem of harmonics d not give us any difficulty, although rec fier locomotives are operated on all o newly electrified lines.

Experience has proved that curre harmonics do not aggravate the curre unbalance by more than 10%; as f voltage harmonics, experience has prov them not to be a trouble on the Fren high-voltage networks. Furthermore, t measured harmonics are almost of t same value in a-c and d-c syste equipped with rectifier substations (s Fig. 6). The unbalance must be e amined for each substation. The curre unbalance is generally of no importan because of the number of generators co nected to the network. The acceptal voltage unbalance should be no more th 3% for a permanent unbalance, or 5 for a temporary unbalance. After stu of this unbalance, the single-phase co nection or, if necessary, the Scott co nection can be chosen, because the pow of the feeding network is always i creasing.

At the beginning of the single-pha electrification, we were always fearful some unbalances; therefore, we provid numerous substations with Scott conn tions. Now, on the completed, or unc completion, North-Eastern network, shall have only five substations with Sco connection, out of a total of 43.

Vertical and Horizontal Clearanc

Electrification requires the provision clearances between structures (tunn arch, glass roof, iron fittings, etc.) a live electrical parts.

The clearances required for 25

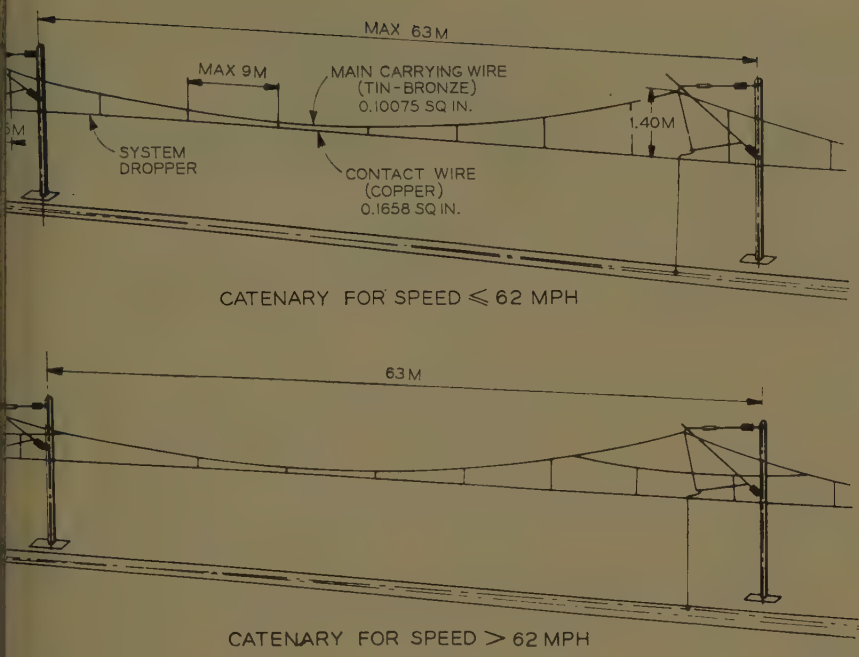

Fig. 4. 25-kv single-phase catenary

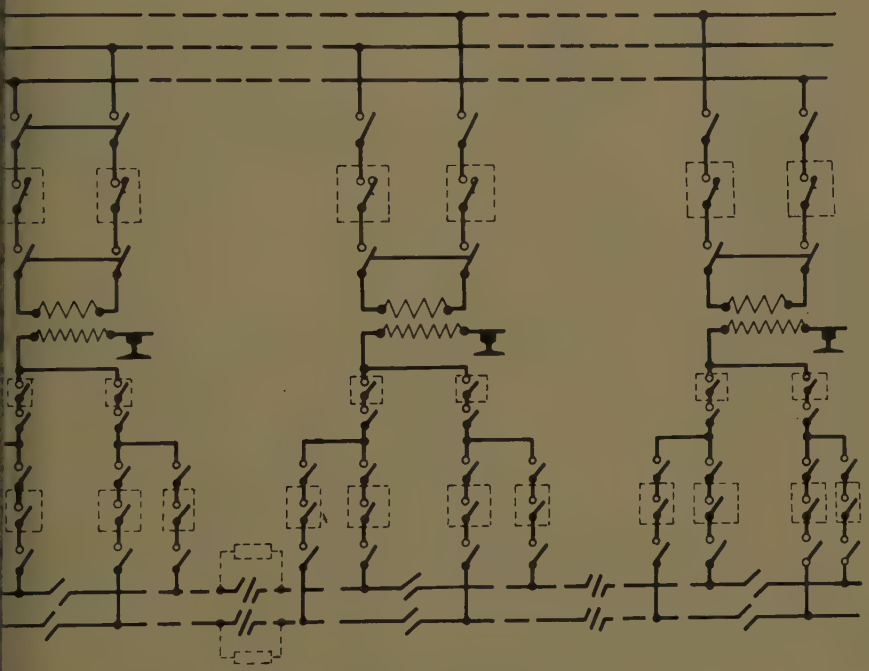

Fig. 5. Single-phase substation

	SINGLE PHASE RECTIFIER				SIX PHASE RECTIFIER	
RMONICS UMBER	1 THEORETICAL CASE OF SQUARE WAVE PRIMARY CURRENT	2 ACTUAL CASE WITH WELL SMOOTHED CURRENT	3 ACTUAL CASE WITH NORMAL PULSATION (FROM TEST BENCH)	4 BRITISH RAILWAYS TESTS (ON PRIMARY SIDE OF SUBSTATION)	5 THEORETICAL CASE	6 ACTUAL VALUES FOR AN INDUCTIVE VOLTAGE DROP OF 3 TO 45% (COMMITTEE NO. 22 OF THE C.M.I.)
3	33.3	FROM 26 TO 28.5	FROM 21.7 TO 22.5	20	0	
5	20	FROM 12.5 TO 15.5	FROM 10.4 TO 10.7	8.55	20	FROM 16.6 TO 18.66
7	14.3	FROM 8 TO 9.6	FROM 5.6 TO 6.6	5.25	14.3	FROM 11.2 TO 12.1
9	11	FROM 7 TO 6.6	FROM 3.4 TO 4.5	3.20	0	
11	9.1	FROM 3.3 TO 4.4	FROM 2.2 TO 2.9	2.20	9	FROM 4.7 TO 6.37
13	7.7	FROM 2 TO 2.9	FROM 1.6 TO 1.9	1.85	7.7	FROM 3.1 TO 4.23
15	6.7	FROM 1 TO 2	FROM 1.1 TO 1.07	1	0	
17	5.9	FROM 0.5 TO 1.4	FROM 0.9 TO 0.66	0.65	5.9	FROM 1.4 TO 2.12
MS VALUE THE FIRST HARMONICS	45.5%	FROM 31% TO 35%	FROM 25% TO 26%	23%	28%	FROM 21% TO 23.5%

Fig. 6. Harmonics

and 3 kv according to International Union of Railway specifications are as follows:

	25 Kv, In.	3 Kv, In.
Between catenary and loads	11.417	8.661
Between live electrical parts (catenary or pantograph) and earth		
Vertically	8.661*	10.630† 5.906
Horizontally	6.693*	10.630† 3.937

* Short period.

† During extended period.

On open track, it is always easy to comply with the clearance requirements, but this is not the case under bridges and in tunnels. Generally, the central part of the tunnel arch is well suited for installation of insulator attachments.

As shown in Fig. 7, it is necessary sometimes to widen the arch of the tunnel at the height of the pantograph "horns," but it is at this point that the additional insulation required between 25 kv and 3 kv is the smallest ($2^3/_4$ in. for short periods).

The insulated pantograph horns minimize, and in some instances may avoid, the necessity of widening the arch. Fig. 8 shows the schematic arrangement applied on all 25-kv pantograph bows of the SNCF and the increase in clearance allowed by utilization of insulated horns. It seems certain that the use of new insulating materials will permit a further reduction in the clearance requirements.

Telecommunications

In France, whether we electrify or not, telecommunication circuits are put in cables in order to improve the quality of telephone communications.

Rolling Stock

Are industrial frequency locomotives inferior to d-c locomotives? At first we thought so, but in fact we encountered pleasant surprises: the locomotives with static current convention outclass the conventional d-c locomotives.

Experiments have been made with all types of locomotives: with the synchronous d-c converter, the single-phase 3-phase converter, and the single-phase commutator motors. None of them can compete with the overwhelming superiority of the mercury-arc rectifier locomotive. Therefore, I shall speak only of the latter, of which there are three types in France:

Series BB *12000* (1954), of which 113 are in service and 35 on order

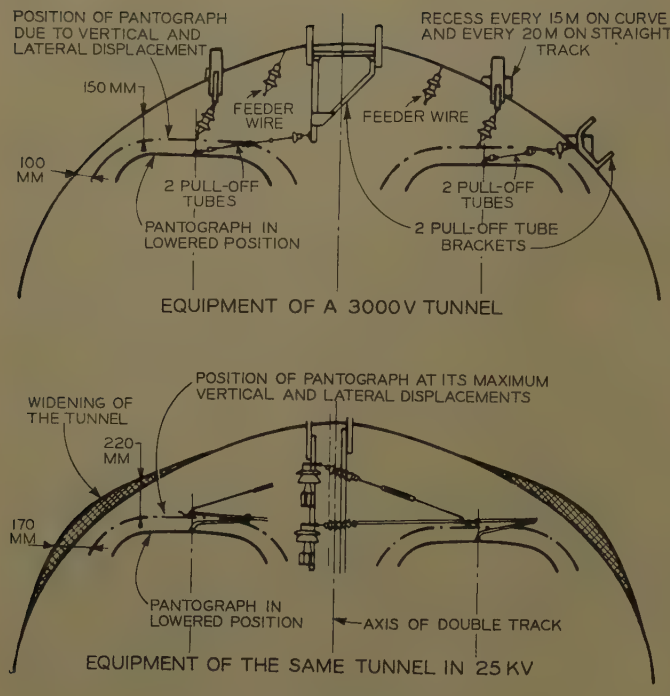

Fig. 7. Tunnel clearances

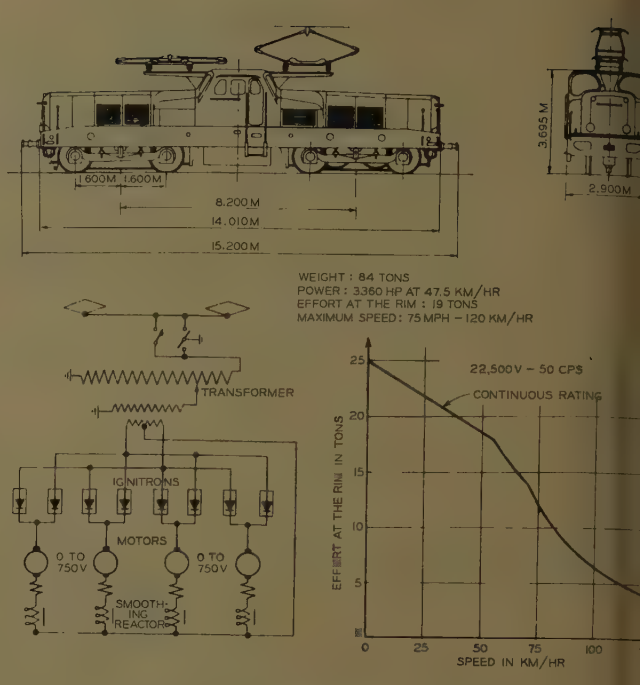

Fig. 9. BB 12000 ignitron locomotives

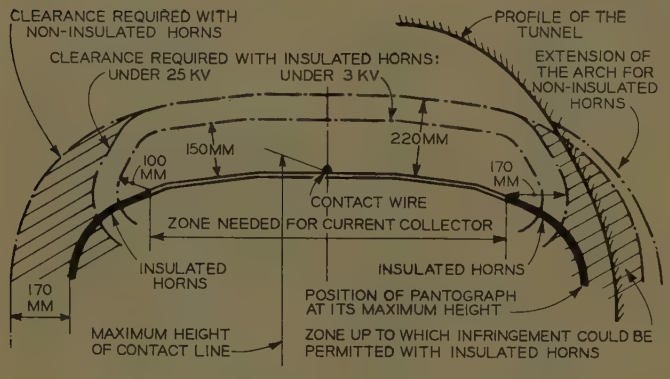

Fig. 8. Insulation of the pantograph horns

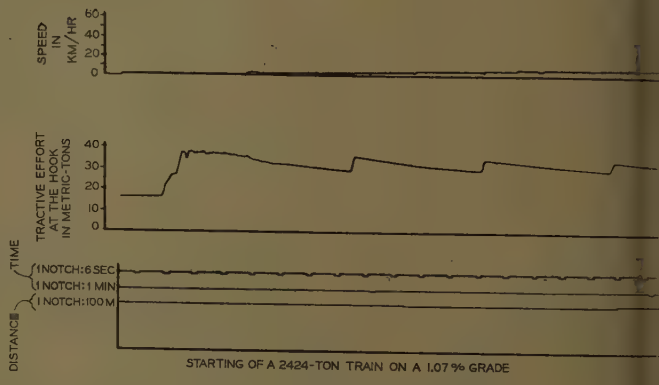

Fig. 10. Locomotive BB 12006

Series BB *16000* (1958), of which 37 are in service and 14 on order

Series BB *16500* (1958), of which 43 are in service and 162 on order

BB 12000 Ignitron Locomotives

These locomotives weigh 185,000 lb (pound) and deliver 3,360 hp (horsepower) in continuous rating; see Fig. 9. They are capable of hauling 1,656 metric tons on a 1.08% grade and 2,800 metric tons on a 0.5% grade.

In 1956 and 1957, we carried out a series of systematic adhesion tests on a BB *12000* and obtained a starting coefficient of adhesion of 47.5%.

On a single-phase locomotive, with all traction motors connected in parallel, the speed variation of one of them does not affect the others in case of slipping. As for the slipping axle, with motor fed under constant voltage, its normal tractive-effort–speed characteristics is kept, while slipping. Whether slipping is caused by insufficient adhesion or by a sudden increase of tractive effort, the slipping will cease when the tractive effort and the rail-wheel friction balance each other.

On the contrary, when an axle begins to slip on a d-c locomotive where, in starting position, all motors are connected in series, once the slipping has started the difference between tractive and resistive effort increases, the slipping speed steadily accelerates, and, very quickly, the motor starts to race.

We went very far in heavy load starting tests. Fig. 10 shows the starting effort curve of a 2,424-metric-ton train, which the BB *12006* locomotive started twice on a 1.07% grade.

Furthermore, it is quite certain that the electric part is not the only one concerned in the remarkable results obtained with our ignitron locomotives, as the low traction arrangement on these locomotives reduces the weight transfer to a minimu see Fig. 11.

BB 16000 Ignitron Locomotives

These locomotives haul fast hea passenger trains over the Paris-Lille li and will do it later on the Paris-Strasbo line. They deliver 4,920 hp, in co tinuous rating, and weigh 185,000 Their maximum speed is 100 mph; Fig. 12.

Their characteristics enable them haul, at 74.5 mph, a 1,000-metric-ton tra on a 0.5% grade. Besides, these loc

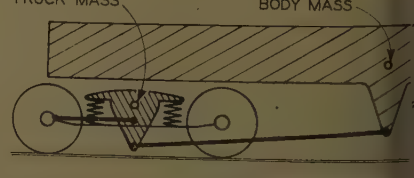

Fig. 11. Low-traction arrangement

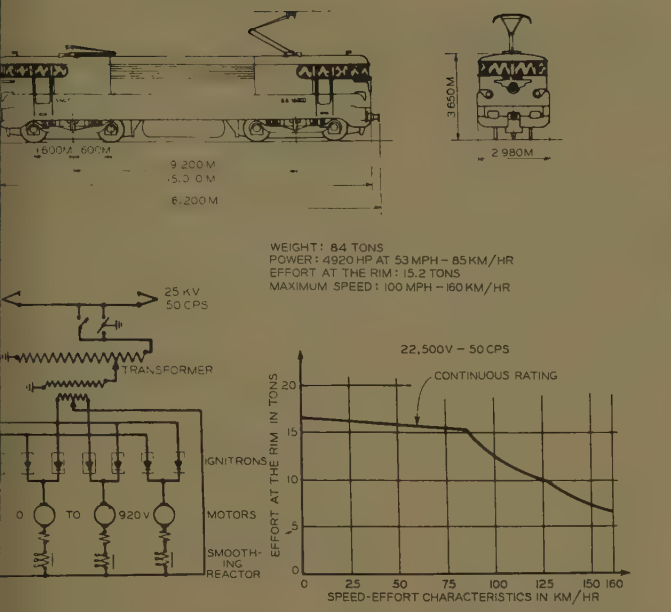

Fig. 12. BB 16000 ignitron locomotives

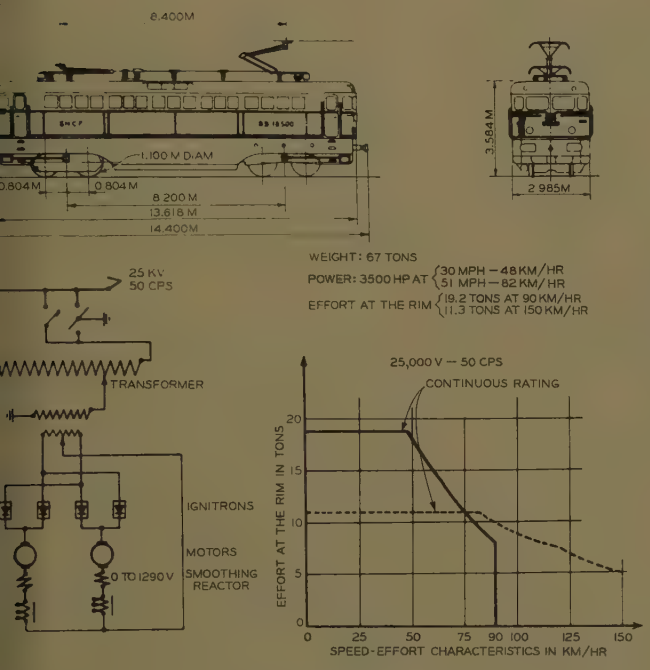

Fig. 13. BB 16500 ignitron locomotives

otives maintain a speed of 100 mph on vel tangent track with an 800-ton train; ey haul the fastest trains in France at .5 mph between Arras and Longueau.

B 16500 Ignitron Locomotives

These locomotives weigh 147,700 lb and ve a continuous rating of 3,500 hp; e Fig. 13.

They are the most economical among e general purpose electric locomotives, anks to the development of technical novations which produce a remarkable comotive, using a new formula.

Our ideas led:

1. For the first time, to the realization of mass-produced trucks with only one traction motor.

2. Also, for the first time, to the utilization of a gear shift (Fig. 14), permitting a change over—within a few minutes—from a freight into a passenger locomotive. For freight traffic the maximum speed is 56 mph and for passenger traffic, it is 93.5 mph.

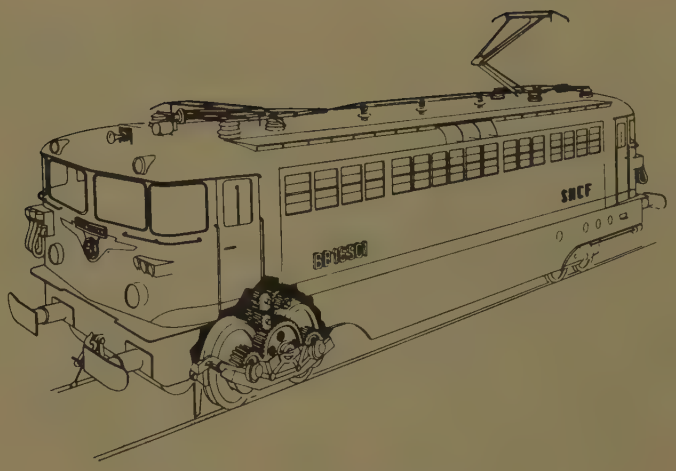

Fig. 14. BB 16500 gear shifting

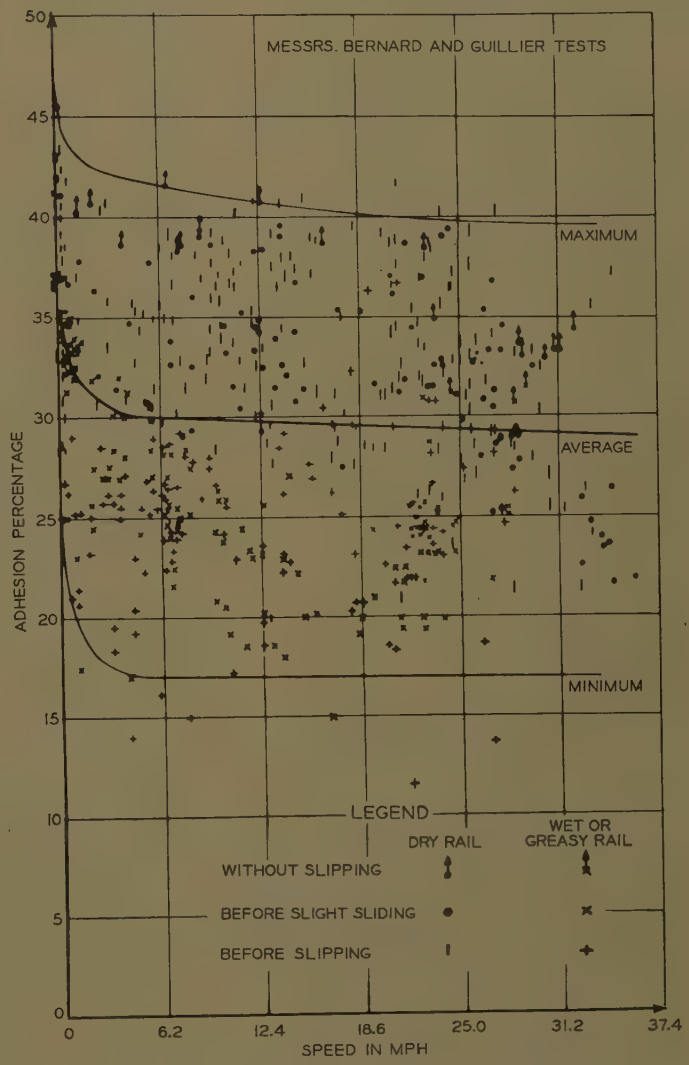

Fig. 15. BB 16500 adhesion tests without sanding

The over-all results obtained by Messrs. Bernard and Guillier during the adhesion tests carried out on several BB *16500* locomotives, without sanding, on straight and curved tracks, on dry, wet, and greasy rails, are shown in Fig. 15.

It is seen that the average curve starts from about 36% adhesion at speed zero,

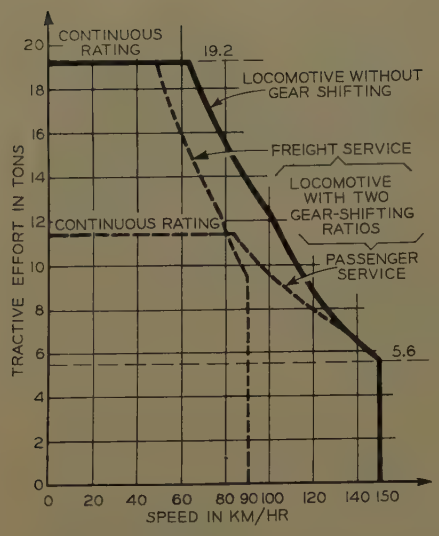

Fig. 16. Advantage of gear shifting

decreases to 30% at a speed of 6 mph, and still remains at 29% at a speed of 31 mph. The top curve shows that the best values are about 40% at a speed of 25 mph.

The results with BB *16500* locomotives equipped with single-motor trucks seem to be 20% better than those obtained with VB *12000* locomotives, particularly at high speeds.

A proof of the exceptional adhesion qualities found by the SNCF for single-phase locomotives with current conversion is that the weight of the locomotives built has steadily decreased each succeeding year, as shown here:

1952—256.000 lb
1953—243.000 lb
1954—185.000 lb
1955—174.000 lb
1957—161.000 lb
1958—161.000 lb
1959—143.000 lb

Practically, for the BB *16500*, we have taken a coefficient of adhesion of 36%, at starting.

To build a conventional locomotive with the same performances, we would have had to install equipment of 4,500 hp; see Fig. 16. The single motor per truck and the gear shift enable us to save 960 hp and 13 tons of weight, and in addition, to improve the electrical efficiency of the locomotive.

The tonnage rating of the BB *16500* locomotives is as follows:

Freight.....2,490 metric tons on a 0.5% grade
(Common rolling stock).....1,830 metric tons on a 0.8% grade
1,525 metric tons on a 1.0% grade
Passenger.....900 metric tons on level track at 86 mph

As to passenger trains hauled with the BB *16500* locomotives, let me just point out that the trip Paris-Lille is made with a 606-ton train, composed of 13 cars, at an average speed of 79 mph.

Maintenance

Our locomotives are available 90% of the time. Experience enables us to state that, for 1,500-volt d-c and a-c locomotives, maintenance expenses per mile are practically the same. Table II presents the maintenance expenses of the single-phase BB *12000* and the d-c BB *8100* locomotives in 1957, both engines used for freight and passenger traffic.

Adhesion

Research in different directions is being carried on further to improve the adhesion and take advantage of the lightening of our locomotives. For instance, instead of sanding, our studies are aimed at eliminating foreign materials between rail and wheel (water, oil film, greasy material, etc...), which cause losses of adhesion.

These results may be obtained by different means: 1. cleaning of the rail by mechanical processes and 2. electrical sparking. Besides, this latter process removes the gases absorbed by the metals on the surface, which is an important cause for the reduction of the metal-to-metal adhesion. The coefficients of adhesion obtained in the laboratory by this means are remarkably high and promise good results for experimental operation.

We know now how to improve the adhesion of d-c locomotives, which has been poor, due mostly to:

The starting rheostat which flattens the tractive-effort-speed characteristics.

The series-coupling of motors at starting, hence the uncertainty of the voltage at the terminals of each motor.

Nowadays, in all instances, we install the starting rheostat at the head of the circuit and provide parallel starting.

In addition, our work is directed towards two objectives: 1. Research on a device which detects slipping. We have fitted each axle with a tachometer-alternator. The sensitiveness of this device, equipped

Table II. Comparative Maintenance Expenses

	BB 12000 25 Kv 50 Cps	BB 8100 1,500-Volt D-C
Inspection and daily maintenance		
Labor in hours/1,000 miles	13.3	13.1
Labor and material new francs/mile	0.22	0.223
Inspection, daily maintenance, and class repair		
Labor and material new francs/mile	0.44	0.436

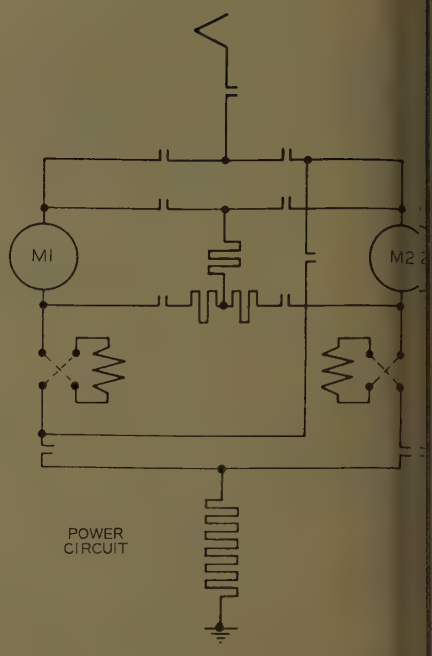

Fig. 17. BB 9401 1,500-volt d-c locomotiv

with an electronic amplifier, reaches differential speed of 1.5 mph. 2. Researc on antislip electric circuits using physic means of spontaneous action, in order t oppose slipping.

In accordance with the locomotiv wiring, the devices developed interven either permanently, or momentarily. W tried with success:

1. To prevent slipping by shunting th traction motor armature. In case on motor slips during series-coupling, a resist ance is automatically connected in parallel with the armature. Therefore, the curren of the faulty motor is diverted and it torque decreases, while it is stabilized on th other motors. The shunted motor work practically on separate excitation and th absorption of the slipping is fast.

2. To initiate an antislip action with balancing resistive bar, which has the effec of maintaining the voltage at the terminal of the slipping armature and of reinforcing its field.

Our 1,500-volt d-c lightweight BB *9400* locomotives, the first unit of which was put into service during the summer of 1959, benefit from those improvements; 116 locomotives of this type have been ordered. They weigh 132,000 lb and deliver 2,900 hp in continuous rating, with a maximum speed of 80 mph. They are equipped with single-motor trucks; the starting rheostat is eliminated, not by using multiple contactors as in conventional solutions, but by providing a tap-changer of only 4 contactors in air. Fig. 17 gives the basic layout of the locomotive; the armature-shunt resistance used in series coupling and the balancing resistive bar used in parallel coupling are shown.

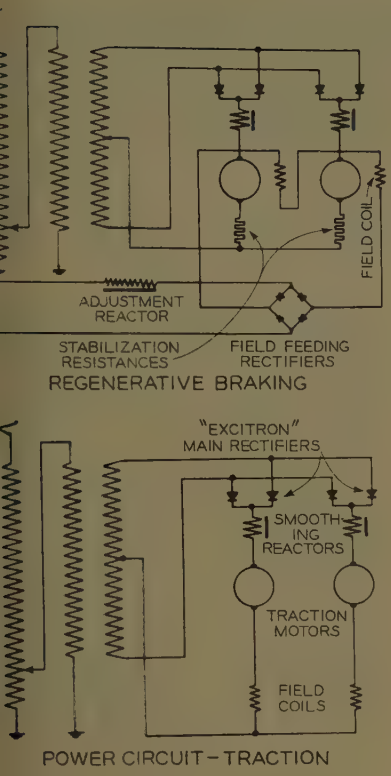

Fig. 18 (left). BB 16500 excitron locomotives

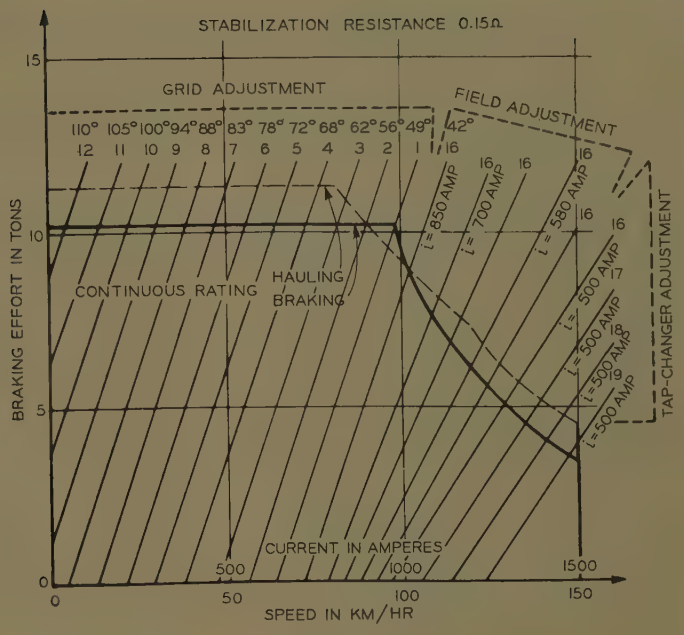

Fig. 19 (right). BB 16500 excitron locomotives

Ve are modifying our present 1,500-volt locomotives in accordance with these ndards because our tests showed that 80-ton locomotive is able to perform service of a 107-ton CC with con-tional diagram.

AR SHIFTING

We have shown the advantages of cks equipped with gear shifting. ould the gear shifting be made while ning, or should the locomotive be uired to stop?

The gear shifting in a running position ds to complicated and expensive me-anical devices. The small number of ditional advantages procured do not tify, for the time being its adoption in ss production. However, it might be eresting to test a prototype.

NITRONS, EXCITRONS, GERMANIUM, SILICON

There are in service, or on order, 318 comotives equipped with *2070* ignitron bes of 8, 10, and 12 inches diameter. Also on order are 50 BB *16500* loco-otives equipped with excitrons fitted for regenerative braking. Fig. 18 gives the schematic diagram of these locomotives in running and regenerative braking conditions. Fig. 19 shows the tractive-effort–speed characteristics in regenerative braking position.

Of course, we are interested in semiconductors, and our 5,000-hp BB *20103*, equipped with silicon power rectifiers, is by far the most spectacular application on rolling stock. But if the simplicity, safety of operation, and maintenance are considered, we believe mercury arc rectifiers are technically more advisable than semiconductors at this time. Semiconductors have the reputation of outclassing the mercury arc rectifiers. It is hoped that this appreciation will hold true in the future. But for us, semiconductors have not yet been perfected for mass applications, even if the purchasing price is not taken into consideration. Of course our opinion, which reflects the present situation, will change when technical progress has overcome our objections.

World Fame of French Electric Traction Technique

The efforts, the research, and the bold achievements of France in industrial frequency electrification have had great repercussions, and the SNCF is proud to have played a leading part in the development of the 50-cps system.

Industrial frequency electric traction has been adopted by many countries where all kinds of traffic, all kinds of tracks (narrow, standard, broad gage), and furthermore all types of climates are encountered. According to the specifications, the same equipment has to work under temperatures ranging from −58 to +113 degrees Fahrenheit. Having seen our achievements, Great Britain, India, Japan, Luxemburg, Portugal, Turkey, and Russia, have undertaken industrial frequency electrifications. China and Russia have ordered French locomotives.

In India, the SNCF had the honor of being chosen as technical associate to the railroads of this large country, for the first stage of a huge electrification program.

The SNCF is proud of its achievements and is certain that it can continue its good performance and maintain its good reputation. As always, new ideas will be welcomed from every quarter, as long as they seem to us to advance the electrification program, because we believe above all in an impartial approach in improving the technique.

Discussion

. G. McClean (General Motors Corporation, La Grange Park, Ill.): Mr. Nouvion's teresting paper is a valuable contribution our knowledge of railway electrification, id its report of the locomotive develop-ents is particularly stimulating.

The term traffic unit as used is the sum of freight ton kilometers and passenger kilometers. Is there a factor which could be used to convert passenger kilometers to ton kilometers? The statistics would then be of greater international comparative value if expressed as total ton kilometers to permit the derivations of traffic densities.

Assuming one passenger kilometer equals one passenger ton kilometer (which is a normal figure) then the traffic unit would, of course, in fact become ton kilometers. On this basis the 1958 traffic would total 85 billion ton kilometers. Since the term billion is ambiguous internationally, would Mr. Nouvion confirm that this is 85×10^9?

Could Mr. Nouvion also confirm the traffic density on the lines so far electrified and to be electrified in the period 1959 to 1963 and give the approximate total cost figures for the fixed installation for the 700

miles to be electrified 1958 to 1963, and the number and cost of locomotives and multiple units cars?

Presumably 13% traffic (63% minus 50%) is 12,750 million, and the 2% route (18% minus 16%) equals 800 kilometers. This would be a density of 15 million ton kilometers per kilometer of single track. But on electrification prior to 1959, 50% of traffic on 16% route, or say 6,000 kilometers of single track excluding sidings, would indicate a density of 7 million ton miles. This would imply that the lines to be electrified in 1959–1963 have denser traffic than those previously electrified.

Mr. Nouvion indicates a relative efficiency for the diesel locomotive measured at the drawbar of 17.1% against 24.8% in 1957 and 28.8% in the future for electric locomotives. A typical United States railroad operation of a diesel-electric locomotive is represented by a 1,500-hp locomotive operating in multiple unit in freight service.

A typical over-all load factor of 60% is derived, of course, from operation for various periods of time at various throttle positions. Efficiency of the Diesel electric locomotive is primarily of concern for the purpose of estimating fuel consumption. The time spent operating on higher throttle positions is of greatest importance for such a calculation. We may typically take three quarters of full load with a locomotive weighing 108 metric tons running at 40 mph, pulling a trailing load of 906 metric tons (1,000 United States tons). At this operating condition the rolling resistance of the locomotive is approximately 1,000 pounds and of the train 9,000 pounds.

Over a wide range of load operations, the efficiency of the diesel engine is conservatively 34% and of the over-all transmission 83%. The 1,500-hp rating of the diesel engine is measured as the net input into the generator for traction, and at 3/4 load the additional horsepower (neglecting train heating) is approximately 80 hp. Thus, in a typical United States operating condition, the over-all efficiency is 24.1%.

F. H. Brown (Commonwealth Edison Company, Joliet, Ill.): The AIEE is most fortunate in having this informative paper for its *Transactions* and reference records.

The discusser has seen at first hand some of the developments of the application of electric power at industrial frequency to the French Railways. In Paris, in 1948, discussion with some of the French electrical manufacturers disclosed the interest of the railway engineers in the development of 50-cycle traction motors. American electrical manufacturers had also been asked to participate in this development. There was no domestic demand for motors of this frequency in the United States, but one American manufacturer was of the opinion that the solution of the problem could be found by applying rectified single-phase alternating current at 50 cycles (or any other commercial frequency) to standard d-c traction motors by means of ignitron rectifiers and suitable smoothing reactors. The name of L. J. Hibbard will always be associated with this development.

In 1951, at the Railway Conference at Annecy, in the French Alps, the discusser was afforded the opportunity to witness the performance of various types of motive power at the 75-km test line electrified with 50-cycle single-phase power at 25 kv. At that test the only motive power operated by ignitron-rectifier equipment was a 600-volt d-c motor car taken from the Paris suburban electrification, similar to the test car operated by the Pennsylvania Railroad in the Philadelphia area between 1948 and 1955. The various test locomotives were operated by single-phase commutator-type motors or by d-c motors supplied from a 50-cycle single-phase motor-generator set. There was one locomotive equipped with a multianode-type mercury-arch rectifier. At that conference, the discusser had the temerity to predict that ignitron rectifier locomotive would become an important competitor with locomotives having the a-c commutator-type motors, as well as those having d-c motors supplied from a motor-generator set, although the weight of engineering opinion at that time leaned heavily toward the latter type.

Phase unbalancing and low power factor were still being visualized by the power supply engineers as serious problems yet to be solved, with harmonic disturbances from rectifiers as an added problem of unknown magnitude.

The Annecy Conference and tests were a prelude to the electrification, with 50 cycles at 25 kv, of the important freight line between Valenciennes and Thionville, along the Belgian border, which was placed in service early in 1955. Only 5 out of the 105 locomotives built for the initial operation of this line were of the ignitron-rectifier type. The performance of these locomotives was so outstanding that all of the locomotives ordered since 1955 for the extensions of the 25-kv 50-cycle system have been of the rectifier type, as pointed out in Mr. Nouvion's paper.

Without detracting from the remarkable achievements of the engineers of the French National Railways in their successful development of railway electrification at industrial frequency, the American manufacturers who developed the ignitron-rectifier locomotive should feel proud of their contribution to this type of railway electrification.

The problems of phase unbalancing, low power factor, and harmonic disturbances visualized by the French power engineers in 1951 were found to be of less severity than anticipated after operation started in 1955, and quite capable of solution without expensive additional equipment.

Attention is called to the fact that since the first five substations were installed, using Scott-connected transformers to aid in phase balancing, all later substations have been equipped with standard single-phase transformers. Attention is also directed to the very low mileage of additional power transmission line required to serve this new system of railway electrification, as compared with former systems of electrification, because of the ability to take the power supply directly from the existing network.

These factors are, or should be, of interest to the American electric power engineers. It is becoming increasingly evident that within the forseeable future, the American railways having dense traffic must turn from the expensive maintenance of a multiplicity of small-capacity mobile power plants to the more economic use of purchased electric power for their locomotive units and operations.

Mr. Nouvion's paper points out the most economical solution that has been found over more than a half century of progress in railway electrification—a solution which is being applied with increasing usage on railways throughout the world.

F. Nouvion: According to the 1958 traffic handled by the French National Railroads the conversion factor can be expressed as follows:

One passenger-km is equivalent to 1.5 passenger train gross ton-km. The billion figure is understood as 10^9.

Some main lines so far electrified have the following traffic density:

Paris–Lyons, 512 km	45×10^6 gross ton hauled/km/year
Paris–Orleans, 120 km	45×10^6 gross ton hauled/km/year
Valenciennes–Thionville, 270 km	24×10^6 gross ton hauled/km/year
Paris–Arras, 193 km	28×10^6 gross ton hauled/km/year

Other lines electrified earlier have less traffic density than those just cited, but features more pressing than traffic density such as grades, tunnels, operating conditions etc., were ruling at that time.

On lines to be electrified in the period from 1959–1963 the traffic density will be, according to present conditions, an average of 26×10^6 gross ton hauled/km/year.

For the foregoing projected lines, which include Tarascon–Marseille in 1,500 volts direct current, an evaluation made under the 1959 economic conditions shows, for the entire 1959–1963 project, an average cost of 600,000 new francs per km of route, for fixed facilities.

These routes are mainly double-track and even four-track routes out of Paris Ea Station.

Besides work strictly related to electrification, the previously quoted figure comprises modifications of signaling and telecommunication systems, modernization work, etc., which amounts to about 50% of the total cost.

It may be worthwhile to know that a survey made in the event of electrification of industrial-frequency single-phase, 25-kv current of the Marseille-Vintimille line, which takes into account the sole work related directly to electrification, showed an average cost of 293,000 new francs/km double-track route.

According to traffic we evaluate:

The cost of motive power: from 14.1 10^6 new francs to 55.5×10^6 new francs per 100 km of route.

The number of locomotives: from 15 to 58 units per 100 km of route.

The 17.1% efficiency given for diesel locomotives, is an average annual efficiency figure for locomotives, taking into account light runnings, no-load runs, etc., which should not be too different in the United States and in France, whereas Mr. McClean's figure is related to the efficiency at nominal rating, or to conditions somewhat similar.

Transformation Method for the Study of Nonlinear Components

C. LAKSHMI-BAI
ASSOCIATE MEMBER AIEE

ɔpsis: A simple transformation is ınced for correlating the characteristic nonlinear element with the harmonic ent in its frequency response to sinu-al inputs. By a process of curve fitting characteristic is represented by a nomial. The frequency response to soidal inputs is represented as a Fourier es. The polynomial and the Fourier es are related by means of the simple sformation $x=\sin\theta$. The method is lied to some of the common non-arities encountered in control system ponents. Its use in the determination the describing function, as well as the monic response function, is discussed. tails in the case of an experimental ification are included.

IS well known that Fourier series is used to determine the harmonic content the response of linear or nonlinear ele-nts to periodic driving functions. r calculating the Fourier coefficients is necessary to have the response ıction defined over a cycle. However, ite often the nonlinear characteristic is own only graphically. Making use of is characteristic, Lewis has described a ethod of calculating the Fourier coeffi-nts by graphical integration.[1] This ts quite involved due to the presence of ıbounded functions in the interval of tegration. Booton uses the principle effective gain to correlate mathe-atically the output and input of a non-ıear element.[2]

The method presented in this paper is lieved to be rigorous in its approach and ractical in application yet simple and rect. It makes use of two well-known ıd powerful analytical tools. One is the mple transformation

$$=\sin\theta,\ -1\leq x\leq +1 \qquad (1)$$

ıd the other is the process of curve tting.[3] The nonlinear characteristic represented as a polynomial in x (and ierefore in $\sin\theta$) by virtue of equation 1. ow it is a matter of simple trigono-ietric identities to calculate the harmonic ontent in the response of the nonlinear lement. The method is limited only to inusoidal inputs. However, this class is f practical interest in control systems. Conversely, when the harmonic content ı the response to sinusoidal inputs is determined by experiment, the method is useful in presenting a polynomial representation for the nonlinear characteristic even without going through the process of curve fitting.

The most important use lies in determining the harmonic response function of the nonlinear element as the ratio of Laplace transforms of the polynomial in x and the input sine function, both taken in the time domain. By considering the fundamental component only, it leads to the describing function of the element. However, in this technique the true nonlinear characteristic is made use of instead of the equivalent linearized one. By a further change of variable, the method can be extended to inputs of linear combinations of sine components with different amplitudes and frequencies. This leads to the application in determining the dual-input describing function after West and others.[4] Several illustrative examples have been worked out. The analysis has been verified experimentally in case of a lightning arrester disk which has a double-valued nonlinear characteristic. The calculated values of the harmonic components agree very well with those experimentally found with the aid of a wave analyzer.

Nomenclature

a_n, b_n = Fourier coefficients
$P_n(x)=\cos n\theta$
$Q_n(x)=\sin n\theta$
$F(x)$ = response of the nonlinear element in the x domain
$G(\theta)$ = response of the nonlinear element in the θ domain

Basic Theory

Let

$$y=F(x) \qquad (2)$$

be the characteristic of a nonlinear element. If

$$x=\sin\theta,\ -1\leq x\leq 1 \qquad (3)$$

is the input, then

$$y=F(\sin\theta), \qquad (4)$$

or

$$F(\sin\theta)=G(\theta+2\pi) \qquad (5)$$

From equations 4 and 5 $F(\sin\theta)$ is also a periodic function with period 2π. As θ varies over any range, the transformation 3 shows that the interval for x is limited to $-1\leq x\leq +1$. Further, the function G in the θ domain corresponds to the function F in the x domain. It is to be observed that the direct transformation 3 is essentially single-valued and thus is unique. The inverse transformation which is multivalued is not required in the analysis.

Consider Fig. 1. $F(x)$ is a single-valued function and varies from -1 to $+1$, for all values of θ. As $\sin\theta$ goes from -1 to $+1$, $F(x)$ traces the curve between $-1\leq x\leq +1$ and as $\sin\theta$ goes from $+1$ to -1, being single-valued, $F(x)$ retraces its path in $+1\geq x\geq -1$. Equation 4 being periodic can be represented by a Fourier series

$$F(\sin\theta)=\frac{a_0}{2}+\Sigma_n(a_n\cos n\theta+b_n\sin n\theta) \qquad (6)$$

where a_n and b_n are given by the usual integral representations for Fourier coefficients. Let two polynomials $P_n(x)$ and $Q_n(x)$ be defined by

$$P_n(x)=\cos n\theta \qquad (7)$$

$$Q_n(x)=\sin n\theta \qquad (8)$$

for $n=0, 1, 2, 3, \ldots$

Consider the following trigonometric identities:

$$\cos^2 n\theta+\sin^2 n\theta=1 \qquad (9)$$

$$2\sin\theta\sin n\theta=-\cos(n+1)\theta+\cos(n-1)\theta \qquad (10)$$

$$2\sin\theta\cos n\theta=\sin(n+1)\theta-\sin(n-1)\theta \qquad (11)$$

The transformation equation as given by equation 3 is $x=\sin\theta$.

From equations 3, 9, 10, and 11 the polynomials P_n and Q_n of equations 7 and 8 satisfy the following recurrence relations:

$$2xQ_n=-P_{n+1}+P_{n-1} \qquad (12)$$

$$2xP_n=+Q_{n+1}-Q_{n-1} \qquad (13)$$

Also, from equations 3 and 9

Paper 60-865, recommended by the AIEE Feedback Control Systems Committee and approved by the AIEE Technical Operations Department for presentation at the AIEE Summer General Meeting, Atlantic City, N. J., June 19-24, 1960. Manuscript submitted January 13, 1960; made available for printing May 26, 1960.

C. Lakshmi-Bai is with the Indian Institute of Science, Bangalore, India.

The author takes pleasure in expressing her gratitude to Dr. P. Venkata Rao for his valuable guidance in the preparation of this paper. The author is also thankful to Dr. H. V. Gopalakrishna for supplying the lightning arrester, and to Professor H. N. Ramachandra Rao for guidance and encouragement, and to the authorities of the Indian Institute of Science for providing the facilities for carrying out this work.

$P_0=1$; $Q_0=0$; and $Q_1=x$ (14)

Equations 12, 13, and 14 are sufficient for evaluating $P_n(x)$ and $Q_n(x)$ for positive integral values of n. The values are shown in Table I.

Making use of the tabulated values for P_n and Q_n it is possible to represent equation 6 as a polynomial in x, defined in the interval $-1\leq x\leq+1$,

$$F(x)=\frac{a_0}{2}+\sum_n [a_nP_n(x)+b_nQ_n(x)] \qquad (15)$$

Since the Fourier expansion constitutes an expression over a cycle (or half cycle in case of symmetric functions), it utilizes information on all parts of the characteristic, as does the polynomial representation in x. This is directly and linearly connected with the Fourier expansion by means of transformation 3. It is to be observed that $P_n(x)$ and $Q_n(x)$ are orthogonal in the x domain, just as cos $n\theta$ and sin $n\theta$ are in the θ domain.

Having known the characteristic of the nonlinear element, it can be expressed as a polynomial in x by the process of curve fitting. Expressions for $P_n(x)$ and $Q_n(x)$ from Table I are substituted in equation 15, and rearranged as polynomial in x, with coefficients which are linear combinations of a_n and b_n. Starting with the highest degree term in equation 15 the coefficients are compared with those of the polynomial obtained by curve fitting. This process determines the values of a_n and b_n for all relevant values of n; and equation 15 is uniquely known for the given nonlinear element.

Now $P_n(x)$ and $Q_n(x)$ of equation 15 are simply replaced by cos $n\theta$ and sin $n\theta$ to obtain the Fourier series as in equation 6. It is to be observed that the coefficient of the highest degree term in x of equation 15 is solely related to the coefficient of the highest frequency component in the Fourier representation for $F(x)$ as in equation 6.

Further it may be observed that $P_n(x)$ and $Q_n(x)$ are related to the Chebychev polynomials,[5] where x stands for cos θ instead of sin θ. However, there is no particular advantage in using these Chebychev polynomials in the present case, as the recurrence relations given by equations 10 and 11 enables one readily to calculate the necessary polynomials.

The process of curve fitting itself may briefly be described as follows. From the given characteristic curve a set of m points is taken. Assume that this set of points is related by some function $y=F(x)$. This function, in general, can be taken as a polynomial in x of degree n, $(n<m)$. Then one follows the principle of least squares which states that the best representation of the data is that which makes the sum of the squares of the residuals a minimum. This process finally leads to $n+1$ linear equations to evaluate for $n+1$ undetermined coefficients. Thus, the required polynomial is uniquely determined. However, the common nonlinearities encountered in servosystem practice are generally simple and are symmetric about the origin. In such cases the process of curve fitting is much more simplified than the general case previously described.

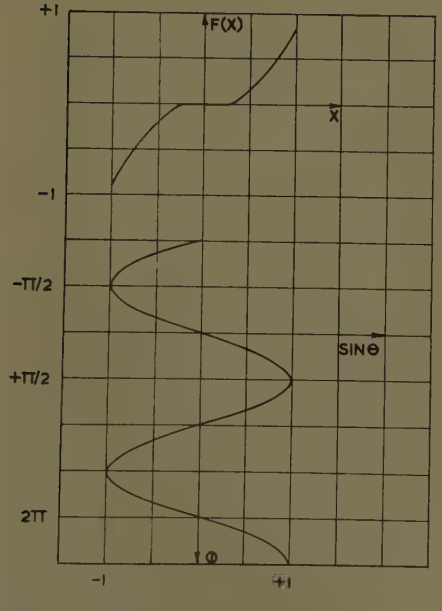

Fig. 1. A representative nonlinear characteristic and a sine input of unity amplitude

Table I. Table of Characteristic Functions from Equations 7 and 8

n	$P_n=\cos n\theta$	$Q_n=\sin n\theta$
0	1	0
1	$\sqrt{1-x^2}$*	x
2	$1-2x^2$	$2x\sqrt{1-x^2}$*
3	$(1-4x^2)\sqrt{1-x^2}$*	$3x-4x^3$
4	$1-8x^2+8x^4$	$(4x-8x^3)\sqrt{1-x^2}$*
5	$(1-12x^2+16x^4)\sqrt{1-x^2}$*	$5x-20x^3+16x^5$
6	$1-18x^2+48x^4-32x^6$	$(6x-32x^3+32x^5)\sqrt{1-x^2}$*
7	$(1-24x^2+80x^4-64x^6)\sqrt{1-x^2}$*	$7x-56x^3+112x^5-64x^7$

* When $F(x)$ is double-valued, marked functions are to be used for $F_B(x)$, and unmarked functions for $F_A(x)$ with reference to Fig. 7. When $F(x)$ is single-valued, only unmarked functions are to be used.

Examples

Example 1

Fig. 2 shows the characteristic of dead space. One fits the curve,

$$F(x)=0.8x^3, \text{ in } -1\leq x\leq+1 \qquad (16)$$

Equation 16 will be compared with equation 15 after substituting for the polynomials P_n and Q_n from Table I. It is to be observed that since $F(x)$ is a single-valued symmetric function $a_0=a_{2n+1}$ $b_{2n}=0$ for all values of n.

Now substituting for $Q_1(x)$ and $Q_3(x)$,

$$F(x)=b_1x+b_3(3x-4x^3)+\ldots \qquad (1$$

Since equation 16 does not conta terms higher than the cubic, b_5, b_7, etc., a zero.

Comparing equations 16 and 17,

$$b_3=-0.2, \text{ and } b_1=+0.6 \qquad (1$$

Thus, $F(x)$ can be written as

$$F(x)=0.6x-0.2(3x-4x^3) \qquad (1$$

Therefore

$$F(\sin\theta)=0.6\sin\theta-0.2\sin 3\theta \qquad (2$$

Equation 20 is the Fourier series fo

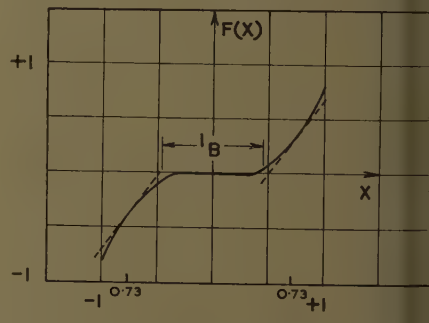

Fig. 2. Output versus input characteristi for an element with dead space

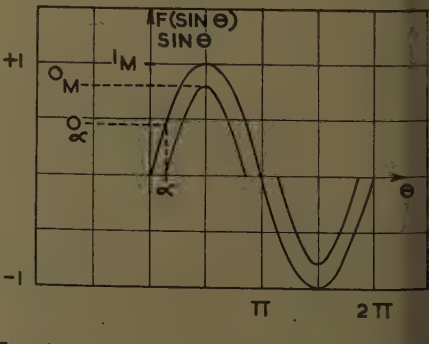

Fig. 3. Output O(t) as a function of time for input $i(t)=I_M \sin t$ to an element with dead space, shown for $I_M\times I_B/2$

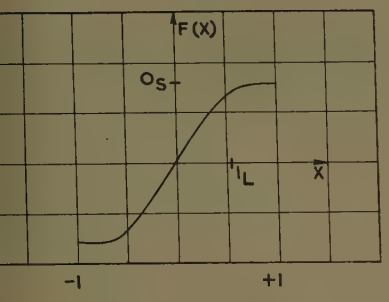

4. Output versus input characteristic
n element whose output is limited by
saturation

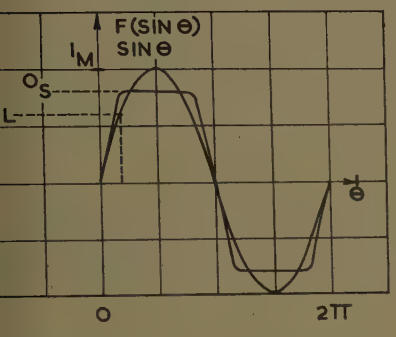

5. Output O(t) as function of time for
t i(t)=I_M sin t, to a saturated element
$I_M > I_L$, the limiting value of input

in θ). Fig. 3 shows the response of the
ment with dead space to sine input
ction.
et

$$I_M \sin t \qquad (21)$$

input function has a maximum ampli-
e 1, so that $I_M=1$. α, the angle up to
ch there is zero response, is given from
. 2, by

$$\sin^{-1}\frac{I_B}{2I_M}=\sin^{-1}\frac{0.46}{1}=28° \qquad (22)$$

ere I_B is the width of the dead band.
ximum amplitude of output is given
$K(I_M-I_B/2)$ where K is the average
e between $x=I_B/2$ and $x=1$.
Thus

$$\frac{d}{dx}(0.8x^3)=1.27;\ \text{at } x=0.73 \qquad (23)$$

erefore, maximum amplitude of out-
wave=1.27(1−0.46)=0.81, whereas
calculated peak value from the
urier representation, equation 20, is

From Fig. 3, it will be noted that α is
ependent of the frequency of the input
usoid, and that the fundamental of the
put is in phase with that of the input.
e magnitude of the output is a function
the ratio $I_B/2I_M$ only, and is independ-
of frequency.
The output wave as arrived at by this method conforms with that arrived at by standard methods.[6]

EXAMPLE 2

Consider the case of voltage saturation in electronic amplifiers. Fig. 4 shows the saturation characteristic. O_s stands for the saturated value of the output for large positive values of the input $i(t)$. Assuming symmetry, $-O_s$ stands for the saturated value of output for large negative values of the input. Let I_L be the limiting value of the input, for which saturation just occurs, either in the positive or the negative direction depending on the sign of the input.

If to an amplifier having the input-output characteristic of Fig. 4, a sinusoidal input $i(t)=I_M \sin t$ is applied in which I_M I_L, the output $O(t)$ is given by the sum of a number of harmonics. The amplitudes of these harmonics are calculated by the transformation method. $\alpha=\sin^{-1} I_L/I_M$ corresponds to the value of input for which saturation just occurs.

Let the input be given by

$$x=I_M \sin t \qquad (24)$$

From Fig. 4

$I_M=1$ ampere

$I_L=0.6$ ampere

$O_s=0.80$

$\alpha=37$ degrees (25)

By a method of curve fitting, one gets the characteristic of Fig. 4, to be

$$F(x)=1.53x-0.9x^3+0.1x^5, \text{ in } -1\leq x\leq +1 \qquad (26)$$

It is emphasized that equation 26 represents the actual harmonic curve, and not the linearized approximate curve as in other methods. Equation 26 is compared with

$$b_1Q_1(x)+b_3Q_3(x)+b_5Q_5(x)+\ldots \qquad (27)$$

It is to be noted that for exactly the same reasons as in example 1, $a_0=0$, $a_n=0$ for all n, and $b_{2n}=0$; coefficients higher than b_5 are zero, since the polynomial has no terms higher than x^5 in equation 26. Substituting for Q_1, Q_3, Q_5 from Table I, in equation 27

$$F(x)=b_1x+b_3(3x-4x^3)+ b_5(5x-20x^3+16x^5)+\ldots \qquad (28)$$

Comparing coefficients of like terms in equations 28 and 26 starting with the highest degree terms

$$b_5=+0.006,\ b_3=+0.194 \text{ and } b_1=0.917 \qquad (29)$$

From equations 26, 28, and 29 the harmonic content in the response to sinusoidal inputs is given by

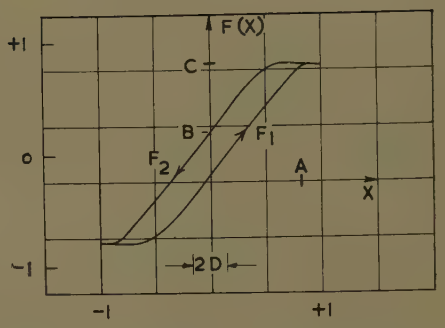

Fig. 6. A double-valued nonlinear characteristic (ideal hysterisis loop of constant width and saturation)

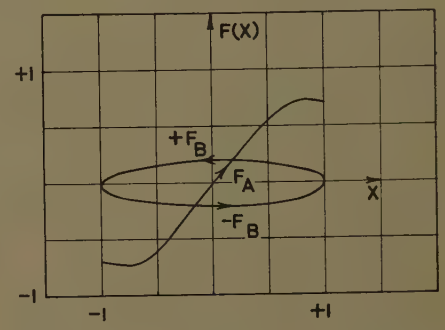

Fig. 7. Two new functions, whose sum and difference together represent the double-valued nonlinear characteristic of Fig. 6

$$F(\sin)=0.917 \sin\theta+ 0.194 \sin 3\theta+0.006 \sin 5\theta \qquad (30)$$

Fig. 5 gives the input and output curves as a function of θ.

It should be noted that for an electronic amplifier the form of the curves in Fig. 5 and the value of α are independent of the frequency of the input sinusoid for the range of frequencies that are of interest. For such sinusoidal inputs the fundamental of the output $O(t)$ is in phase with the fundamental of the input I_M and the ratio between them is a number that is a function of the magnitude of α. Thus

$$\frac{O_s}{I_M}=G(\alpha) \qquad (31)$$

when $G(\alpha)$ gives the describing function of the saturated amplifier. The response curve as derived and shown in Fig. 5 agrees well with those obtained by standard methods.[6]

EXAMPLE 3

Consider the hysteresis curve as shown in Fig. 6. Let $F(x)=F_1(x)$, while x is increasing and $F(x)=F_2(x)$, while x is decreasing. Let two new functions be defined as follows:

$$F_A(x)=\frac{1}{2}\{F_2(x)+F_1(x)\} \qquad (32)$$

$$F_B(x)=\frac{1}{2}\{F_2(x)-F_1(x)\} \qquad (33)$$

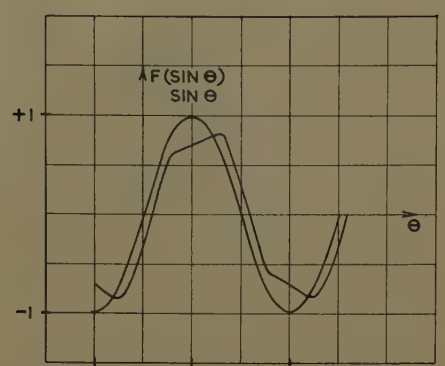

Fig. 8 (left). Output $F(\sin\theta)$ as function of time for input $i(t)=I_M \sin t$, in case of the hysteresis characteristic of Fig. 6, when evaluated as in Fig. 7

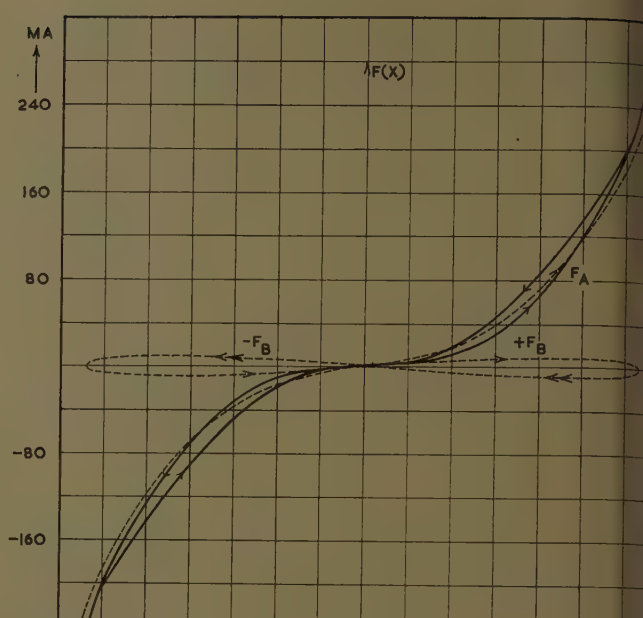

Fig. 9 (right). Solid line represents double-valued characteristic of the lightning arrester disk, determined by experiment. Dashed line represents two new functions F_A, F_B (obtained from curve fitting) whose sum and difference approximate the two branches of the experimental characteristic

so that

$$F_2(x)=F_A(x)+F_B(x) \quad (34)$$

$$F_1(x)=F_A(x)-F_B(x) \quad (35)$$

where $F_A(x)$ is a single-valued function, and $F_B(x)$ is a double-valued function in $-1\leq x\leq +1$, as shown in Fig. 7.

Taking the following numerical values for A, B, C, and D of Fig. 6, one can fit a curve to F_A and F_B of Fig. 7.

$$A=0.8,\ B=0.2,\ C=0.8, \text{ and } 2D=0.3 \quad (36)$$

$$F_A(x)=1.3x-0.6x^3 \quad (37)$$

$$F_B(x)=\pm 0.2\sqrt{1-x^2} \quad (38)$$

Consider the equation

$$F_A(x)=b_1Q_1(x)+b_3Q_3(x)+\ldots \quad (39)$$

Substituting for Q_1 and Q_3 in equation 39 one gets

$$F_A(x)=b_1x+b_3(3x-4x^3)+\ldots \quad (40)$$

Comparing coefficients in equation 37 with those in equation 40, starting with the highest degree term, one gets

$$b_3=+0.15 \text{ and } b_1=+0.85 \quad (41)$$

In equation 39 $a_n=b_{2n}=0$, since $F_A(x)$ is a single-valued function of x.

$F_B(x)$ is a double-valued function. On comparing equation 38 with equation 15, one gets $a_1=0.2$. Thus,

$$F_B(x)=\pm 0.2\cos\theta \quad (42)$$

From equations 37, 40, and 41, one gets

$$F_A(\sin\theta)=0.85\sin\theta+0.15\sin 3\theta \quad (43)$$

Making use of the definition of $F(x)$, along with equations 34, 35, 42, and 43 one gets

$$F(\sin\theta)=0.85\sin\theta+0.15\sin 3\theta-0.2\cos\theta \quad (44)$$

Equation 44 holds good for both the branches of curve in Fig. 5, and for all values of θ. Fig. 8 shows the response curve in comparison with the input sinusoid of unity amplitude.

EXAMPLE 4

Evaluation of the describing function in case of nonsinusoidal inputs: In particular, consider an input which is the sum of a first harmonic and a third harmonic, each of them with different amplitudes. Thus, let:

$$x=a\sin\theta+c\sin 3\theta \quad (45)$$

Let the nonlinear characteristic of interest be

$$F(x)=x^3 \quad (46)$$

Consider a change of variable

$$y=\sin\theta \quad (47)$$

so that from equations 45, 46, and 47, one gets

$$F(x)=(ay+3cy-4cy^3)^3 \quad (48)$$

Expanding equation 48 and denoting it by $H(y)$, one gets

$$F(x)=H(y)=(a+3c)^3y^3-12c(a+3c)^2y^5+48c^2(a+3c)y^7-64c^3y^9 \quad (49)$$

It is important to observed that the harmonic content in the response of the element with characteristic $F(x)$, to an input $a\sin\theta+c\sin 3\theta$ is essentially the same as the harmonic content in the response of the element with characteristic $H(y)$ to an unity-amplitude sinusoidal input. Equation 49 is compared with

$$\frac{a_0}{2}+b_1Q_1(y)+b_3Q_3(y)+b_5Q_5(y)+b_7Q_7(y)+b_9Q_9(7)+\ldots \quad (50)$$

$F(x)$ being a single-valued function has its $a_0=a_n=b_{2n}=0$ for all values of n. E pressions for the various Q's in equati 50 are substituted for, from Table and the b-coefficients evaluated give t following values:

$$b_9=-\frac{1}{4}c^3,\ b_7=\frac{-3ac^2}{4},\ b_5=\frac{3}{4}ac(c-a)$$

$$b_3=\frac{1}{4}(3c^3+6a^2c-a^3), \text{ and}$$

$$b_1=\frac{3a}{4}(2c^2-ac+a^2)$$

Equations 6 and 51 together give t Fourier series for $H(\sin\theta)$, which is esse tially the same for $F(a\sin\theta+c\sin 3\theta)$.

From equation 51, the coefficient the fundamental component is given b $3a/4(2c^2-ac-a^2)$. The input comp nent of this frequency is a $\sin\theta$, hence t apparent gain is $3/4(2c^2-ac+a^2)$, a there is no phase change. When $c=0$, th is for a single frequency input, the ga reduces to $3a^2/4$, which is the conve tional describing function for a cubic cha acteristic. Thus, the dual input descri ing function[4] for this case is given by 3 $(2c^2-ac+a^2)$.

EXAMPLE 5

Nonunity amplitude for the input si function: Let $f(x)$ be the nonlinear cha acteristic and let the input under conside tion be

$$x=A\sin\theta \quad (5$$

Now, the Fourier coefficients for $f($ with input as in equation 52 are esse

II. Harmonic Content at Different itudes for the Input Sine-Voltage at ycles, and the Calculated Values at 450 Volts Rms

ment .	Rms Applied Voltage in Volts	Harmonic Percentage 2nd	3rd	4th	5th
.....	174	5.65	23.8	0	0
.....	252	7.85	28.6	0.8	2.35
.....	356	7.5	27.1	0	2.35
.....	450	7.3	27.1	0	3.85
ated ues.....	450	7.0	27.0	0	3.0

Table III

Example	Values as per Grief: Describing Function	Values as per Grief: Phase Shift in Degrees	Values as per This Method: Describing* Function	Values as per This Method: Phase Shift in Degrees
1 Dead space	0.415	0	$\frac{0.6}{1.27}=0.47$	0
2 Saturation	0.675	0	$\frac{1.53}{2.167}=0.705$	0
3 Hysteresis	0.9	8	$\frac{0.85}{1}=0.85$	13

* The describing function is calculated as (1/average slope) × (describing function calculated for nonunity gain). The average slope in example 1 is taken at $x=0.73$, and in example 2 at $x=0.5$.

r the same as those for $f(A.x/A)$ with t

$$\sin\theta \qquad (53)$$

ch means that x is to be replaced by in the recurrence relations given by ations 10 and 11, and x/A to be treated new variable.

AMPLE 6

lightning arrester disk[7] has been en as the sample under consideration. 9 shows the experimental character- as a continuous curve and the fitted ves as dotted ones. The peak value of lied voltage is 636 volts, and is con- ted to a scale of one unit on the x-axis. e corresponding current is 248 milli- peres, and is also converted to a scale of nit on the y-axis. This scaling is neces- y to study the nonunity amplitude of sine-input in the interval $-1\leq x\leq+1$ in example 5.

The fitted curve has the equation

$$3x+0.75x^3+0.035x^5+0.005(2x\sqrt{1-x^2}) \qquad (54)$$

The last term in equation 54 takes e of the double-valued nature of the aracteristic. On comparing equation with equation 15 and evaluating the b's e gets

$$=0.066;\ b_2=\frac{7}{100}\,b_1;\ b_3=\frac{27}{100}b_1;$$

$$\text{and } b_5=\frac{3}{100}\,b_1 \qquad (55)$$

In equation 55, b_2, b_3, and b_5, respec- rely, stand for the second, third, and th harmonic components in the re- onse. These are expressed as percent- ges of the fundamental. Thus, the ourier series for its response is given by

$$(\sin\theta)=0.066\left(\sin\theta+\frac{7}{100}\sin 2\theta+\frac{27}{100}\sin 3\theta+\frac{3}{100}\sin 5\theta\right) \qquad (56)$$

Different amplitudes of sine-input are applied to the specimen at 50 cycles per second frequency. In each of these cases the harmonic content is measured on a wave analyzer. The calculated values are for an applied rms voltage of 450 volts. Table II compares the calculated values with the experimental ones, and also gives the harmonic content at various amplitudes for the input.

Discussion

Grief[8] has given the values of the describing function under the assumptions that the nonlinearity must be symmetric about the zero-point, and that the gain of the nonlinear element is unity. However, when the gain is different from one, a scalar multiplier can be introduced.

In the present paper, these assumptions are relaxed. In the process of curve fitting it is immaterial whether the curve is symmetric or not as borne out in example 6. The gain of the nonlinear element is the same as the slope of its characteristic curve; and this need not be unity.

To compare the values obtained by the present method with those of Grief, average slope in the interval 0 to 1 is taken out as an equivalent scalar multiplier. Since the method on hand relaxes the two assumptions the difference in values as compared with Grief's should be in favor of the present method.

In case of double-valued functions, the original curve is represented as the sum or difference of a single-valued and a new double-valued function. The term introduced by the latter should be treated as a correction term, rather than as part of the polynominal; this is so, because, in general it is an irrational term and therefore cannot make up the polynomial.

In Fig. 8, around $\theta=\pi/2$, there is a slight upward slope for the response curve. Strictly speaking, this slope should be the same as the slope of that part of the hysteresis curve which is horizontal (Fig. 6). This is due to the fact that in fitting the curve as in Fig. 7, the ellipse F_B introduces a certain error towards the saturation point. It is this error that is carried over to the response curve. In view of this, an asteroid may give a better fit rather than an ellipse in certain cases. However, the example worked out is for an ideal loop with constant width.

The experimental and the fitted curve are shown in Fig. 9, in case of the lightning arrester disk. The characteristic is a double-valued function and also has a slight dissymmetry. Both these are taken care of by the term $2x\sqrt{1-x^2}$, which corresponds to a second-harmonic component. Its presence has been found in the experimental wave analysis also.

Example 4 is only a brief attempt at showing the application of the method to the generalized describing functions. For a correct understanding and appreciation of the advantages of the method it would be helpful if a specific problem is taken up for detailed study.

A table, showing the output-input responses of nonlinear devices, where all of the quantities have been normalized, is under preparation and will be presented in due course.

Conclusions

As stated in the discussion, the only limitation on the accuracy of the method is set by the degree of accuracy with which the curve fitting is carried out.

Minor dissymmetries and nonunity gain of the nonlinear element can be duly taken care of.

The most important use is in determining the harmonic response function of the nonlinear element as $L\{F(x)\}/L(x)$, both the Laplace transforms being taken in the time domain; for $-1\leq x\leq+1$.

Considering only the fundamental component of the response leads to the conventional describing functions.

One of the striking features of the method is that it can be readily ex-

tended to multiple sine inputs as shown in example 4. This is useful in evaluating the multiple-input describing function.

References

1. Harmonic Analysis for Nonlinear Characteristics, L. J. Lewis. *AIEE Transactions*, pt. I (*Communication and Electronics*), vol. 73, 1954 (Jan. 1955 section), pp. 693–700.

2. The Measurements and Representation of Nonlinear Systems, R. C. Booton. *Transactions*, Professional Group on Circuit Theory, Institute of Radio Engineers, New York, N. Y., vol. PGCT-1, no. 4, Dec. 1954, pp. 32–34.

3. Methods in Numerical Analysis (book), K. L. Nielsen. The Macmillan Company, New York, N. Y., 1956, p. 260.

4. The Dual Input Describing Function and Its Use in the Analysis of Nonlinear Feedback Systems, J. C. West, J. L. Douce, R. K. Livesley. *Proceedings*, Institution of Electrical Engineers, London, England, vol. 103, pt. B, 1956, p. 463.

5. Tables of Chebychev Polynomials (book). National Bureau of Standards, Washington, D. C. 1952.

6. Frequency Response (book), R. Oldenburger editor. "Approximate Frequency Response Methods for Representing Saturation and Deadband," H. Chestnut. The Macmillan Company, 1956, p. 269.

7. Lightning Arrester Development, H. Gopalakrishna. *Thesis*, University of Mysore, India, 1957.

8. Describing Function Method of Servomechanism Analysis Applied to Most Commonly Encountered Nonlinearities, H. Grief. *AIEE Transactions*, pt. II (*Applications and Industry*), vol. 72, Sept. 1953, pp. 243–48.

Adjustable Frequency Drives with Rotating Machine Power Supply

A. T. BACHELER
ASSOCIATE MEMBER AIEE

C. G. HELMICK
MEMBER AIEE

THE squirrel-cage induction motor so well known to manufacturers and users of machinery of all kinds is usually considered to be a constant-speed drive because the power available for energizing the motors nearly always has a fixed frequency. This is the frequency of the available power supply from a utility company or local power plant. If an adjustable frequency power supply with the proper characteristics is provided, these motors will operate over a wide speed range with essentially constant torque capability. The rugged, simple construction of the squirrel-cage motor or the similar reluctance synchronous motor can thus be combined with the flexibility of an adjustable speed drive. Fig. 1 shows the basic elements of an adjustable frequency drive consisting of a synchronous generator, its adjustable speed drive, starting equipment, and the drive motors.

The adjustable frequency drive system has come into general and widespread use in the synthetic textile yarn industry in the last 10 years. It has been used in the sugar-cane milling and steel industries for many years and in a few specialized applications such as testing machines, nuclear power-plant coolant pumps, and film-forming machines. But the surface has just been scratched and there are certainly many more instances where the adjustable frequency drive can be used advantageously. The purpose of this paper is to describe the special characteristics of adjustable frequency drives including torque characteristics of induction and synchronous motors, starting methods, and draw control methods, and to illustrate these features with typical applications. Greater familiarity with this system of power transmission may stimulate new ideas and new uses on existing and new process machinery.

The investment in the adjustable frequency power supply may be justified by one or more of the following considerations, where applicable:

1. The mechanical simplicity of the a-c squirrel-cage induction motor and the similar reluctance-type synchronous motor makes them desirable as driving means at the point of use of power on a machine. Power is delivered to the motor through a fixed or flexible electric cable in contrast to gear trains, chains, line shafts, bevel gears or other mechanical means of delivering mechanical power at the same place.

2. The shaft, bearings, and frame of the motor may be used as part of the driven machine and carry part or all of the drive member.

3. Extremely high shaft speeds are obtainable with direct-connected squirrel-cage motors operating at high frequency. Flat belt drives may approach the speeds thus obtainable but present problems in wear and replacement.

4. Squirrel-cage induction motors and reluctance motors have only stationary electric connections and are readily obtainable with sealed prelubricated ball bearings requiring no attention for several years. These motors can be put in places that would be too hazardous or inaccessible for the maintenance required for other types of adjustable speed drives.

5. The electrical characteristics of an a-c motor permit abrupt or cushioned starting of a driven member, replacing a clutch with a simple switch or starter for the motor. A motor driving a part of a machine may be removed from the power supply by a relay in the event of an overload and leave the remainder of the machine in production. A mechanical line-shaft drive, on the other hand, may be shut down completely, or may continue running and damage the machine.

Basic Features of Adjustable Frequency Systems

A basic feature of the adjustable frequency drive is that all induction or syn-

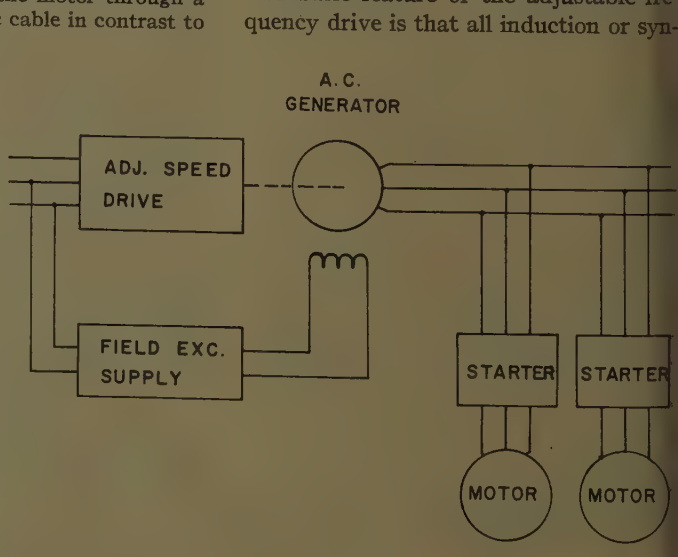

Fig. 1. Basic elements of adjustable frequency drive system

Paper 57-714, recommended by the AIEE General Industry Applications Committee and approved by the AIEE Technical Operations Department for presentation at the AIEE Summer General Meeting, Montreal, Que., Canada, June 24–28, 1957. Manuscript submitted March 29, 1957; made available for printing March 1, 1960.

A. T. Bacheler is with Westinghouse Electric Corporation, Buffalo, N. Y., and C. G. Helmick is with Westinghouse Electric Corporation, East Pittsburgh, Pa.

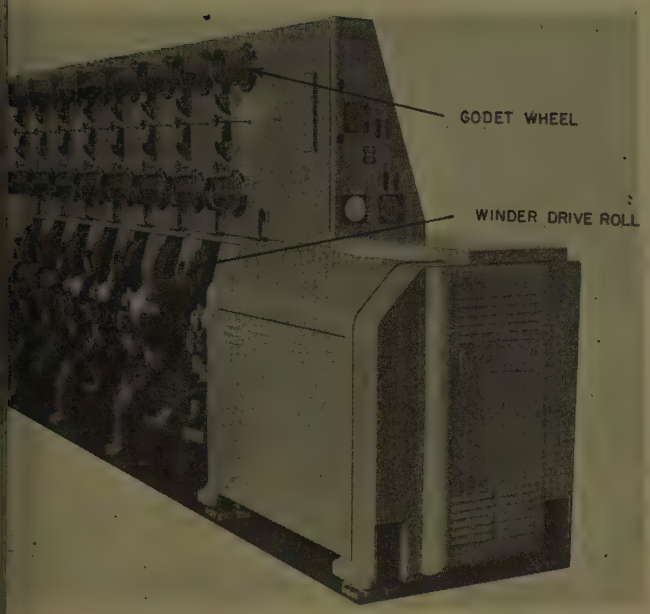

Fig. 2. Portion of synthetic textile fiber spinning machine

Fig. 3. Rod mill run-out table with adjustable frequency roll motors

onous motors connected to a given a-c wer supply will have the same syn- onous speed if they all have the same mber of poles.

When the sections of a machine driven a multiple-motor adjustable frequency ve must run at exactly the same speed, nchronous motors must be used. der steady-state conditions there is no eed error between machine sections or tween an individual machine section d the power-supply generator. An gular error will appear if there is a ad change, but this load-angle change n be made small by selecting a motor sufficient size.

The exact relationship between the nchronous speeds of motor and power- pply generator permits precise speed ntrol of the load by regulating the sup- y frequency.

A prime example of the use of syn- ronous motors on an adjustable fre- uency power supply is the modern syn- hetic fiber spinning machine. Individual umps for extruding the spinning solution re driven by synchronous motors ener- ized from a common adjustable fre- uency power supply. Godet wheels, as hown in Fig. 2, are driven by individual ynchronous motors energized from an djustable frequency power supply in- ependent of that for the pumps. The urface-drive rolls for the winder are also riven by synchronous motors operating ither from the same power supply as Godet motors or from a power supply perating at a slightly different frequency.

Induction motors have a slip which is lependent upon load, representing an rror in speed regardless of how well the power-supply frequency is controlled. If the normal slip is not objectionable, or if the motor can be selected large enough so that it will have an acceptably low value of slip, the induction motor should be used. In the example of the spinning machine, the light friction load of winder rolls might be driven by a low-slip induction motor of the same physical size as the synchronous motor required to synchronize the WK^2 of the rolls. An extremely low slip on the order of 0.2% or less could be obtained.

The slip of the induction motor can be put to good use in some applications. The rod-mill run-out table illustrated in Fig. 3 is an example in the steel industry. Rolls for transporting the hot rod are individually driven by squirrel-cage motors having substantial slip. All are energized from an adjustable frequency generator. As the rod runs down the table and each roll picks up its share of the load, traction between the rod and the rolls tends to keep all rolls running at the same speed. Since the motor speed torque characteristics are similar, each motor carries its own share of the load within the limits established by variation in full-load slip from one motor to the next. The higher the average slip, the less effect variations in roll diameter will have upon load division.

Motor Performance

Requirements for an adjustable frequency power supply depend upon the particular characteristics of the motors when operated on an adjustable frequency system. Most electric machines, including induction motors, synchronous motors, and generators, are capable of operating at a fixed value of flux density in the iron. The voltage generated in the windings of a specific machine operated over a speed range as a generator is proportional to the flux density and the speed. Similarly, the motor is capable of supporting a voltage that is proportional to the frequency.

It follows, therefore, that it is a basic fundamental of adjustable frequency drives that the machines can operate at essentially constant volts per cycle. Since motors so energized have nearly constant flux the torque is proportional to the in-phase component of load current. The ability of motors to carry constant-load current, and therefore, constant torque, over a wide frequency range depends on several factors, of which the most important are the relationship of copper and iron loss and the type of ventilation system. These factors must be taken into consideration when applying motors to a variable frequency system. Many adjustable frequency drives can make use of standard 60-cycle open, or even enclosed, fan-cooled motor designs. This is not intended to imply that any squirrel cage or synchronous motor meeting National Electrical Manufacturers Association Standards for voltage and frequency variation can be operated at its rated torque over a wide speed range. Each application should be considered in the light of its special requirements. It is frequently practical to select standard 60-cycle motors of the next higher horsepower(hp) rating, especially in the case of fractional hp motors.

The use of standard motor designs makes it desirable to standardize on motors having the same voltage rating at 60 cycles, such as 220 or 440 volts. This practice benefits both manufacturer and user in reducing the amount of design work and the delivery time. The emergency replacement of motors becomes easier when a standard 60-cycle machine has been selected.

The speed-torque curves of Fig. 4 are typical of an induction motor operated at various frequencies from 50 to 20 cycles at constant volts per cycle. At the lower frequencies there appears a reduction in maximum torque. It is caused by *IR* drop in the primary winding of the motor which reduces the internal voltage and the motor flux. The rated torque would also be reduced slightly for the same reason. In the case of a variable torque load such as a centrifugal pump, a slight reduction in available torque would be acceptable. On the other hand, a constant torque load such as a conveyor, may require as much continuous and peak torque capacity at low speed as at high speed. This can be provided by a 10 to 15% increase in applied voltage at the lower frequencies. The starting torque of the motor is also increased by the same means.

Effect of Line-Voltage Drop on Pull-In Torque of Synchronous Motors

Reluctance synchronous motors are subject to a similar reduction in maximum torque at low frequency when operated at constant volts per cycle. They are, furthermore, subject to reduction in pull-in torque and pull-out torque at the low frequencies. When synchronizing the reluctance synchronous motor, or excited synchronous motor, high current and power input are required during the acceleration of the rotor into synchronism with the rotating magnetic field. The reluctance motor in particular is subject to reduction in torque when the applied voltage is reduced. At low frequency with the corresponding value of low voltage available, line drop as well as impedance drop in the power supply and in the motor itself all combine to reduce the voltage.

Fig. 5 shows oscillograms taken on a 1-hp 3,900-rpm 4-pole 130-cycle reluctance motor driving a set of rolls having a WK^2 of 10 pounds-feet squared. These oscillograms were taken at 17 cycles and demonstrate the high pull-in current required, as well as the reduction of line voltage due to line drop. The tests were taken for the purpose of establishing corrective measures for low pull-in torque.

The oscillograms have traces of applied voltage at the motor terminals and motor current. In the trace of the terminal voltage, the envelope of voltage decreased in magnitude simultaneously with an increase in current magnitude. This is indicative of the regulation of the power supply and the line to the motor. The motor was started by gradually raising the applied voltage from zero to rated line voltage by means of a motor-operated adjustable autotransformer. Pull-in did not occur until the applied voltage was high enough to develop the required pull-in torque for the rolls running at light load. The oscillograms show the fini acceleration and pull-in as the volta approached 100%.

In test no. 1 the a-c generator volta was set at 41 volts and the motor co nected to the generator with about 1 feet per conductor of no. *12* wire. T current pulsations are due to slipping pol and the voltage pulsations are caused b line-voltage drop. At pull-in, the pea current was 23.6 amperes rms and t motor terminal voltage was reduced to 2 volts. After the motor pulled into sy chronism the voltage at the motor ro to 37 volts at a motor current of 13. amperes.

In test no. 2 the no. *12* wire was re placed with no. *6* wire and the generat voltage set at 34 volts. The motor agai pulled into step at about 29 volts and 2 amperes. After the motor pulled int synchronism the voltage at the moto terminals rose to 33 volts, at a load cur rent of 11.2 amperes, demonstrating tha with reduced line impedance the power supply kva requirements can be reduced

These two tests illustrate the im portance of line-impedance drop at th low frequencies in determining the re quirements of the power supply. While the use of heavier wire improved the syn chronizing conditions, the final solution to the problem of synchronizing at low frequency was to use a higher voltage system having lower current requirements The line drop in the normal size wire then became small and the required percentage of voltage increase at low frequency was materially reduced.

In the case illustrated no appreciable gain could have been made by the use of

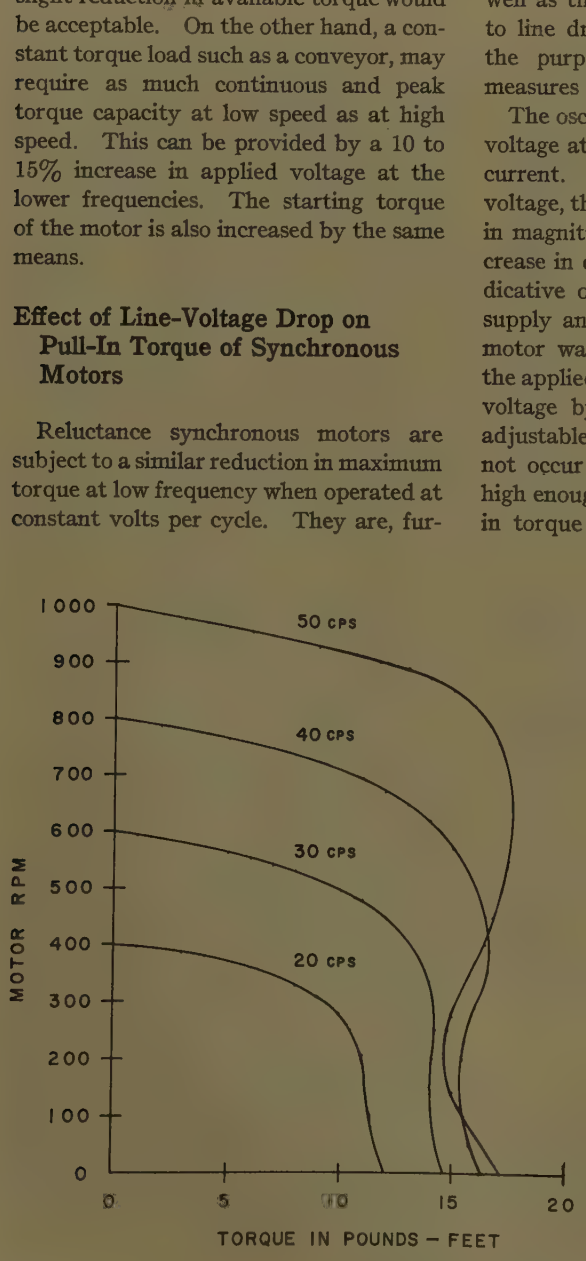

Fig. 4 (left). Induction motor speed-torque curves for various frequencies at constant volts per cycle

Fig. 5 (below). Oscillograms of pull-in tests on reluctance synchronous motor at 17 cycles

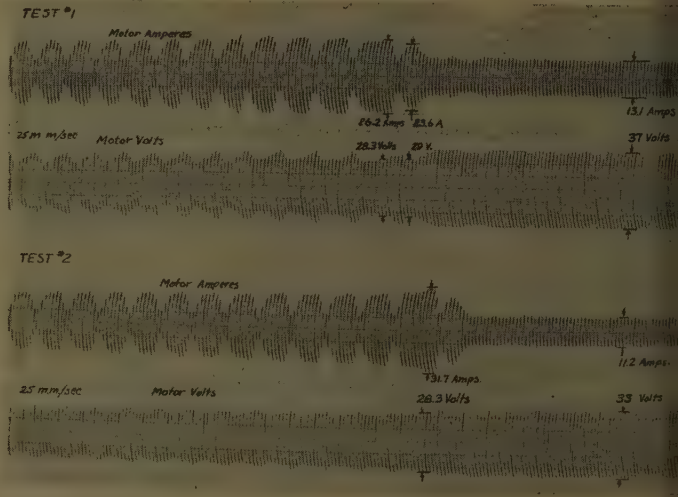

enerator of lower impedance since ly all the voltage drop was in the ng, the generator being very large pared to a single motor.

synchronous motor for driving a high tia load must be selected to have quate pull-in torque under the re- ed voltage condition that occurs at -in. The pull-in current may exceed e times the rated current. The gen- or and distribution system should be cted to minimize the voltage drop dur- pull-in. Since the pull-in torque of a ctance synchronous motor varies as ower between the square and cube of lied voltage, a 10% reduction in tage can result in a reduction in pull-in que greater than 20%.

wer-Supply Characteristics

This paper is limited to adjustable fre- ency drives having rotating machines the means of obtaining adjustable fre- ency power. In all but very special plications either a synchronous genera- or a wound-rotor induction-frequency anger is used.

A synchronous generator produces a fre- ency exactly proportional to its speed. hen the generator is separately excited a fixed excitation, the generated no-load ltage is directly proportional to speed d therefore constant volts per cycle is tained. Voltage regulation of the nchronous generator is relatively great, pecially with low power-factor loads. nless deliberately made oversized, the nerator may have a regulation of the der of 50% or greater. With definite otor loads, however, a generator voltage gulator is almost never required to pro- de satisfactory control of generator volt- ge. If the load drops off, or some of the otors are disconnected, the generator oltage rises and the exciting current to ne remaining motors also rises. This lim- s the rise in generator voltage. When ne generator load varies to such an extent nat occasional manual adjustment of the eld current is objectionable, a load-com- ensation circuit can be used, wherein the oad current is fed back through current ansformers and rectifiers to augment the enerator excitation.

All of the power input to the generator nust be delivered as mechanical power at ne shaft (except for the separate field- xcitation power). The size of the driv- ng equipment for the generator is there- ore determined by the required output nd the efficiency, not counting the excita- ion losses.

Due to its separate excitation the syn- hronous generator provides the most suit- able way of obtaining increased volts per cycle for increasing the pull-in or pull-out torques of reluctance motors. An increase in excitation at the low-frequency end of the range can be obtained with generators of essentially standard design. Generator field heating is a limitation in operating over a speed range since ventilation is reduced at low speeds and greater losses are produced in the field due to the increased excitation. A boost in volts per cycle up to about 15% is usually all that is required. Forced ventilation is generally required for cooling the generator at speeds below about 600 rpm.

Selection of a synchronous-generator rating for an adjustable frequency drive must take into account the starting methods and the size of motor to be started. Adjustable frequency starting of all motors of a drive from low frequency requires no increase in size of generator over that required to supply the running load. Momentary overexcitation of the generator field may be required for breakaway.

In the case of motors that are started across the line or at reduced voltage at operating frequency the generator should be large enough to permit starting the largest motor without causing other motors to pull out of step or stall. This usually requires that the voltage be held to 85% or greater during starting. Field forcing during the starting interval is easily obtainable and may permit using a generator of normal size. If the largest motor to be started represents a substantial percentage of the generator load consideration should be given to load compensation.

Power requirements during synchronizing of motors also affect the selection of generator size or method of excitation. A synchronous motor may draw two to three times rated current during pull-in, and the generator must maintain sufficient voltage at this time to develop the required pull-in torque at the motor.

The requirements vary so widely from one adjustable frequency application to another that no specific data are presented suggesting generator sizes. The generator rating should be determined in each case from the particular requirements including characteristics of the motors to be energized.

Wound-rotor induction - frequency changers offer another means of obtaining the adjustable frequency supply. The primary winding of the wound-rotor machine is excited from the constant frequency power supply. The rotor is driven by an adjustable speed drive. Adjustable frequency power is obtained at the secondary terminals. The output frequency is stated by the following relationship:

$$\text{Frequency in cps} = \text{line frequency} \pm \frac{\text{no. of poles} \times \text{rpm}}{120}$$

In this statement the sign is plus if the primary is on the stator and the rotor is turned opposite to the direction of rotation of stator magnetic field, or minus if the rotor is turned in the direction of the field. Energizing the rotor as the primary reverses the sign.

The frequency changer acts as a transformer. Part of the power input comes from the constant-frequency line, and the rest from the shaft, as shown in the following formula which neglects all losses and assumes a 60-cycle power supply:

$$100\% \text{ power output} = \frac{60}{F} \times 100\% \text{ electric-power input} + \left(\frac{F-60}{F}\right) \times 100\% \text{ mechanical-power input}$$

where F = output frequency. If the output frequency is less than 60 cycles the sign of the second term becomes negative and mechanical-power output must be absorbed.

The reactive kva is all delivered by transformer action and its magnitude on the primary side is in proportion to the ratio of primary to secondary frequencies. In determining the input kva requirements of the frequency changer, its own exciting current must also be added.

For output frequencies greater than one half of primary frequency, the drive power requirements of the frequency changer are less than that of the synchronous generator.

The output voltage at no load is proportional to the output frequency and to the primary voltage. Inherent voltage regulation should be not greater than 15% for most applications since the control of output voltage is not accomplished without resorting to sizeable transformers, induction or step-type regulators, etc.

Since a wound-rotor induction-frequency changer has an output frequency at zero speed equal to primary frequency it is not as suitable as the synchronous generator for starting drives by adjustable frequency control. The induction frequency changer is generally suitable for drives operating above one half of the line frequency and where the motors can be started at the operating frequency. The inability to change the volts-per-cycle ratio easily is a limitation in applying frequency changers and makes the

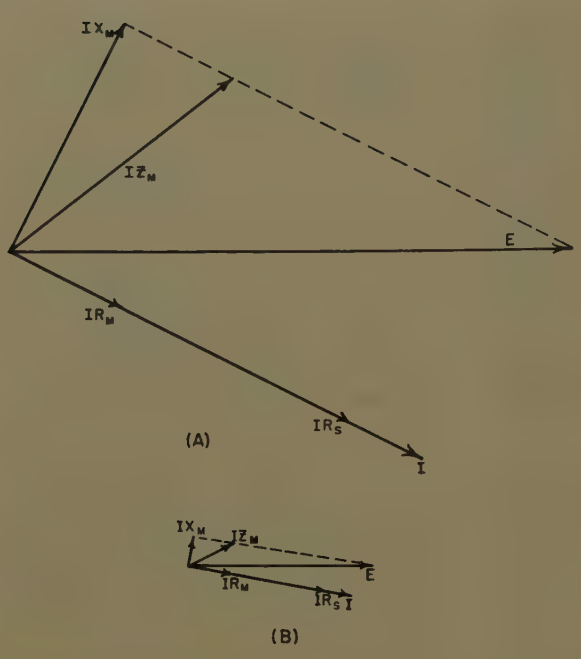

Fig. 6 (left). Vector diagram for resistance starting of motor at 50% voltage at 90 cycles (A), and with same starting resistors at 30 cycles (B), at constant volts per cycle

E = phase voltage
I = line current
X_m = motor reactance per phase, locked
R_m = motor resistance per phase, locked
R_s = starting resistance per phase

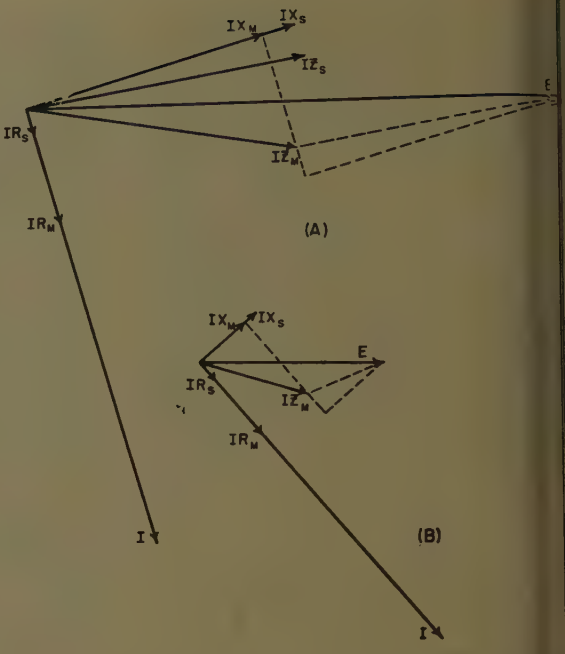

Fig. 7. See Fig. 6 for caption and identification, except:

X_s = starting reactance, per phase
R_s = resistance of reactor per phase

synchronous generator a better choice at low frequencies. The wound-rotor frequency changer is seldom used where the output frequency may for continuous periods of time equal the line frequency. Burning of the slip rings can occur. But the frequency changer can be used at frequencies near the input frequencies as described later.

A substantial number of induction frequency changers have been installed in rayon plants in various parts of the world where the available power supply is 50 or 60 cycles and the desired operating frequency is in the range of 100 to 150 cycles or higher. Generally economics will determine whether an induction frequency changer or a synchronous generator should be used. For frequencies of 30 cycles or lower, the synchronous generator is usually more economical and provides easy adjustment of the volts-per-cycle ratio.

The means of obtaining the adjustable frequency from either a synchronous generator or an induction frequency changer requires an adjustable speed drive. It is not within the scope of this paper to discuss such adjustable speed drives other than to mention that they may be electric drives such as a d-c adjustable voltage system, a motor and eddy-current coupling, a-c adjustable speed motor, or hydraulic or mechanical transmission.

Starting Methods

Starting methods for adjustable frequency drives are just as varied and versatile as those for use on commercial a-c power systems. The simplest and least costly method of starting the motors of an adjustable frequency system is to start them with the generator and bring them up to speed by raising the frequency. The motors can be solidly connected to the generator without switches but with suitable overcurrent protective means. This method of starting does not require an increase in generator size.

Sometimes a single motor of a group must be started while the others are running. The simplest and most economical method of starting an individual motor is to start it across the line. Since adjustable frequency power supplies are usually of limited capacity, this may impose problems in voltage regulation of the a-c generator or speed regulation of the driving equipment, and lead to the use of reduced-voltage starters. Reduced-voltage starting methods may be classified under the resistance type, reactance type, adjustable autotransformer type, and fixed tap autotransformer type.

The resistance starter can be used as on constant frequency systems, but its application to adjustable frequency systems is best limited to those having a very narrow frequency range. Furthermore, the loss in the resistance will reflect as an impact load on the adjustable speed drive and cause excessive speed deviation. When used on a wide-range adjustable frequency system, a single-step resistance starter with enough resistance to obtain the desired starting current at high frequency may not permit a loaded motor to start at the low frequency. A preferred starter is one whose impedance varies directly with the frequency.

A starting reactor has a small fixed component of resistance of the winding, and a reactance directly proportional to frequency. Thus a reactance starte presents an impedance that tends t match the locked impedance of a moto at various frequencies.

The vector diagrams in Figs. 6 and illustrate the advantages of a fixed re actance starter over a fixed resistanc starter at 90 cycles and 30 cycles whe used with identical motors and constan volts-per-cycle power supply. A start ing current of 50% of full-voltage startin current is available at 90 cycles in eac case. The reactance-type starter pro vides an approximation to constant start ing current and torque over a wide fre quency range, while the resistance starte does not.

Saturable core reactors can be used fo starting motors when even the reduce kva increments of a multiple-step impe ance starter are too great for either th generator or its drive.

An adjustable autotransformer-typ starter provides smooth characteristi on starting due to the uniform increase i applied voltage. It also has the grea advantage of reducing the reflected kv at the generator, in comparison with series-impedance starter.

The expense of an autotransformer typ of starter of the variable type is justifie on high precision regulated adjustable fr quency systems when the size of th motor to be started is a substantial po tion of the available generating capaci and where other methods of starti

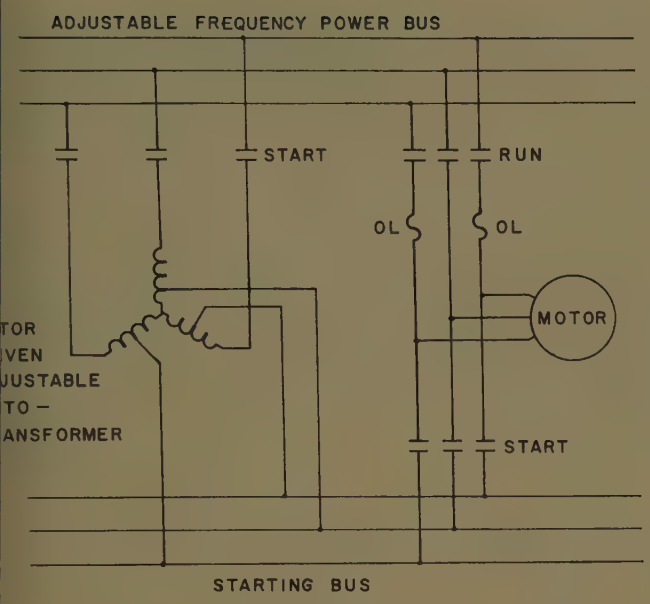

Fig. 8. Adjustable autotransformer starter

uld not provide a sufficiently smooth rt to limit the speed deviation to ac- btable values. This method of starting used to considerable extent on synthetic er spinning machines for the starting of mp motors, windup motors, and other xiliary motors of substantial size. A nple diagram of this starter is shown in g. 8.

Intermediate between the reactance arter and the adjustable autotrans- rmer starter is the fixed-tap autotrans- rmer starter. This starter is suitable r adjustable frequency drives because it ovides the same percentage of voltage duction at all frequencies. It also has e advantage of reducing the kva drawn om the generator for a given voltage duction in comparison with the reduc- nce-type starter. It does have the mitation that the load is applied in sub- antial steps to the adjustable frequency ower supply.

raw Control Methods

Frequently the application requires that ertain sections of a driven machine have eir speeds adjustable with respect to ther sections. Some small synthetic ber spinning machines used for research r development purposes require rel- tive speed adjustment or draw be- ween the Godet wheels and the winder olls (see Fig. 2). It is desirable to hold he speed ratio, once set, within the same ccuracy as the speed accuracy of the ain drive. A range of 5 to 10% rela- ive speed control can be obtained with ccuracy of the order of 0.1% by the use f an induction frequency changer. The requency changer is energized from the djustable frequency power supply and the electrical output feeds the motors whose speed is to be varied. Fig. 9 illustrates a typical draw frequency changer for two motors. The shaft of the induction frequency changer is driven by a motor energized from the adjustable frequency power supply. To vary the speed relationship a mechanical adjustable-ratio transmission is interposed between the induction frequency changer and its driving motor.

As an example, consider that a draw of 0 to +10% is required. The frequency changer must be driven over a speed range to obtain the draw range and it must increase the line frequency in order to obtain positive draw. It is not feasible to operate the frequency changer at zero speed, so a minimum speed is selected in order to produce about 3% increase in frequency. The gear ratio between the motors and their load is selected to make up for this 3% gain in motor speed so that the actual draw will now be equal to zero. The maximum draw of 10% requires that the motors themselves run at 110% of 103% speed, or 113.3% speed. The frequency changer, therefore, must run at a speed such as to raise the generator frequency by 13.3% at maximum draw.

The frequency increase can be obtained by driving the frequency changer either with or against the rotation of the magnetic field. It is far more economical to drive the frequency changer against rotation of the field since the horsepower required is so much less.

The change in frequency through the draw frequency changer is low and its speed is low. From the power relationships previously stated, it will be recognized that the horsepower to drive the draw frequency changer is low.

The frequency changer and its driving motor magnetizing and reactive kva, as well as the losses, must be supplied from the adjustable frequency power supply and must be included with the load when calculating the generator rating.

This method of draw control tends to be expensive but it may be the only practical solution if many motors are involved or if space at the machinery does not permit the mounting of any drive equipment other than the motors. When space requirements permit, various types of mechanical speed-adjusting transmissions should be considered from the standpoints of performance, accuracy, maintenance, and economics. But mechanical transmissions that are subject to slip may introduce difficulties when a precise synchronized operation between machines is required.

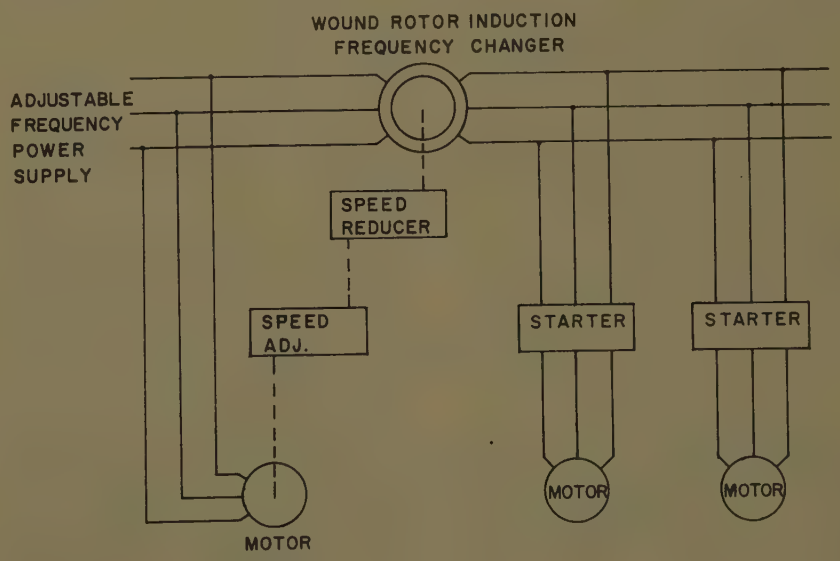

Fig. 9. Draw control frequency changer

Typical Applications

A partial list of typical applications will indicate the widely different fields in which use has been made of the adjustable frequency drive. All of the machines listed below operate or have the ability to operate at several different speeds or over a continuous range of speeds:

1. Film-forming machines.
2. Steel mill run-out tables.
3. Textile bobbin winders.
4. Yarn twisters.
5. Yarn winder traverse motions.
6. Synthetic-yarn spinning machines.
7. Carpet looms.
8. Rayon bucket spinning machines.
9. Rayon extractors.
10. Sealed pumps for nuclear-power plants.
11. Internal grinders.
12. Spin-testing machines.
13. Model test stands.
14. Dynamometers.
15. Conveyors.
16. Sugar-mill tandem drives.

The cost of an adjustable frequency power supply is normally justifiable only when there are a large number of duplicate or similar motors driving numerous sections of a machine. This is of special interest to textile machinery builders and users since the textile industry is characterized by multiple-station machinery having many identical spindles, rolls, or bobbins operating at the same speed. The predominance of textile applications in this list is therefore not surprising.

It is the hope of the authors that this paper will stimulate further consideration of the effective use of adjustable frequency drive systems on multiple-station machinery, or where exact synchronism is required between a number of drive units.

Equations for Evaluating Short-Circuit Forces on Multiple-Strap Single-Phase and Polyphase Busses for Supplying Low-Frequency Induction Furnaces

T. H. CHIN
ASSOCIATE MEMBER AIEE

THOMAS J. HIGGINS
FELLOW AIEE

THE PURPOSE of this paper is threefold: to advance general equations for calculating the short-circuit forces associated with each subconductor, conductor, and bus support of a multiple-conductor rectangular-strap single-phase or polyphase bus; to illustrate application of these equations in actual design by numerical analyses of several busses typical of the different major types encountered in practice; and to determine the efficiency and relative accuracy of several approximate procedures advanced for reducing the total numerical labor incident to application for a specified bus.

The essential values of the general equations may be summarized as follows. General equations underlying calculation of the short-circuit forces associated with the individual phases of multiply subdivided conductor busses comprised of conductors of structural shape are available in the literature.[1] However, exhaustive survey[2] reveals that explicit expressions for the forces associated with the individual subconductors, conductors, and individual bus supports are not available, except for the special case of the bus comprised of coplanar phases, each phase conductor comprised of two channels placed flange to flange, a geometry detailed by Siegel and Higgins.[3] But under the heavy loads typical of modern central station, electric furnace, electric welder, and other industrial plant-distribution systems, there has occurred an increasing use of busses comprised of multiple-conductor phases. Accordingly, as stressed by Schurig,[4] Jones (in a private letter to the second author), and other designers of such busses, there is a pressing need of equations enabling calculation in design of the essential electrical quantities determining performance of the bus in practice. Such equations have been advanced in a recent paper[5] for calculation of the inductances, reactances, impedances, current distribution, and voltage drops. In addition to these parameters which determine the electrical performance of the bus, it is obviously most desirable (especially in the design of busses to carry the very large currents associated with modern electric induction-furnace operations), to have equations for calculating the mutual electromagnetic forces which determine the mechanical performance of the bus under normal or short-circuit conditions. Precisely such equations are advanced in this paper.

Paper 60-651, recommended by the AIEE Industrial and Commercial Power Systems Committee and approved by the AIEE Technical Operations Department for presentation at the AIEE North Eastern District Meeting, Providence, R. I., May 2–4, 1960. Manuscript submitted April 4, 1957; made available for printing March 21, 1960.

T. H. CHIN is with Westinghouse Electric Corporation, Pittsburgh, Pa.; and THOMAS J. HIGGINS is with the University of Wisconsin, Madison, Wis.

Scope of Paper

By use of well-established basic theory, specific general equations for the short-circuit forces associated with the individual subconductors, conductors, and bus supports of a rectangular-strap multiple-conductor bus are effected through use of geometric mean distance theory. Subsequently, equations enabling a more rapid and less laborious numerical calculation are effected by obtaining the limiting forms assumed by the general equations as the width of the rectangular strap conductors is decreased to zero.

With these equations available, application is illustrated by specific calculation of the short-circuit forces on the subconductors, conductors, and bus supports of three specifically dimensioned busses typical of the designs encountered in induction-furnace practice.

Confirmative of the correctness of both the general equations and of the numerical calculation, corresponding values ca

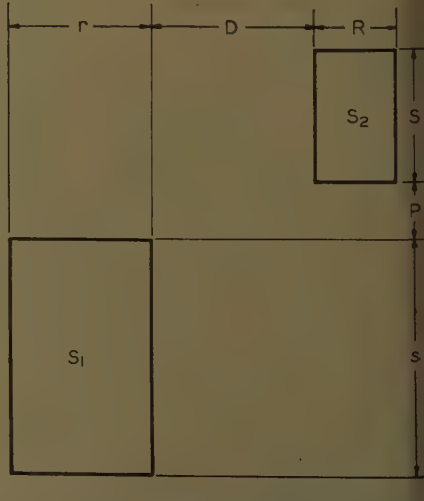

Fig. 1. Two arbitrarily located parallel-side rectangular areas

ed for both the full cross sections and line-segment approximations are d to be in good agreement. Similarly, e sequence is found to have little t on the magnitude of the total force conductor or bus support. Acngly, it is to be concluded that the sponding approximate methods of lation, as detailed in the paper, d sufficient accuracy for most design oses. Finally, a concise summary he essential values enfolded in the ysis concludes the paper.

ivation of Basic Equations for hort-Circuit Forces

GLE-PHASE SUBDIVIDED-CONDUCTOR US

y well-established theory, the induct- L of a bus comprised of two conduc- with rectangular cross-sections S_1 and rranged as in Fig. 1 is

$$2 \log (D_{12}^2/D_{11}D_{22})$$

$$= -(2/I^2)\sum_{i=1}^{2}\sum_{j=1}^{2} w_i w_j S_i S_j \log D_{ij} \quad (1)$$

ere I is the magnitude of the circuit rent; w_i and w_j are, respectively, the rent densities in S_i and S_j, taken itive for current in one direction and ative for current in the other direction; l D_{ij} is the geometric mean distance ween S_i and S_j. The energy in the gnetic field associated with the current is $W=LI^2/2$; whence equation 1 lds

$$= -\sum_{i=1}^{2}\sum_{j=1}^{2} w_i w_j S_i S_j \log D_{ij} \quad (2)$$

The rectangular components of the tual electromagnetic force exerted beeen the two conductors are

$$= f_D = \partial W/\partial D;\ f_y = f_P = \partial W/\partial P \quad (3)$$

bstituting from equation 2 in equation ields

$$= -\sum_{i=1}^{2}\sum_{j=1}^{2} w_i w_j S_i S_j \partial(\log D_{ij})/\partial D \quad (4)$$

d

$$= -\sum_{i=1}^{2}\sum_{j=1}^{2} w_i w_j S_i S_j \partial(\log D_{ij})/\partial P \quad (5)$$

In practice it commonly happens that ch of the two conductors is comprised of veral subconductors connected in parel; say one comprised of m subconducrs numbered from 1 to m and the other n subconductors numbered from $m+1$ $m+n$. The pertinent generalizations equations 4 and 5 are

$$f_D = -\sum_{i=1}^{m+n}\sum_{j=1}^{m+n} w_i w_j S_i S_j \partial(\log D_{ij})/\partial D \quad (6)$$

and

$$f_P = -\sum_{i=1}^{m+n}\sum_{j=1}^{m+n} w_i w_j S_i S_j \partial(\log D_{ij})/\partial P \quad (7)$$

In general, f_D and f_P are the component forces on a specified conductor or a specified subconductor according as D and P are parameters locating the specified conductor with respect to the other; or are parameters locating the specified subconductor with respect to the other $(m+n-1)$ subconductors.

POLYPHASE SUBDIVIDED-CONDUCTOR BUS

If an n-phase system is comprised of n distinct conductors, one conductor, say a, can be considered as carrying current I_a (the currents being expressed as complex quantities) and the remaining $(n-1)$ conductors can be considered as connected in parallel and carrying the return current. Hence, the bus can be "interpreted" as a single-phase bus comprised of two conductors, one full, the other subdivided; whence it follows from equations 6 and 7 that the component forces on conductor a are

$$f_D = -I_a\sum_{i=b}^{n} I_i \partial(\log D_{ai})/\partial D \quad (8)$$

and

$$f_P = -I_a\sum_{i=b}^{n} I_i \partial(\log D_{ai})/\partial P \quad (9)$$

If the individual conductors are subdivided, a comprised of a' subconductors numbered from 1 to a', b of b' subconductors numbered from $a'+1$ to $a'+b'$, and correspondingly for the others, equations 6 and 7 give

$$f_D = -\sum_{i=1}^{a'}\sum_{j=1}^{a'+\ldots+n'} w_i w_j S_i S_j \times \partial(\log D_{ij})/\partial D \quad (10)$$

and

$$f_P = -\sum_{i=1}^{a'}\sum_{j=1}^{a'+\ldots+n'} w_i w_j S_i S_j \times \partial(\log D_{ij})/\partial P \quad (11)$$

where f_D and f_P are the component forces conductor a or on any subconductor of a, a', according as D and P are parameters locating conductor a with respect to the other $(n-1)$ conductors, or are parameters locating subconductor a' with respect to the other $(a'+\ldots+n')$ subconductors. In either the single-phase or the polyphase case, the total force $f=(f_D^2+f_P^2)^{1/2}$ can be determined in both magnitude and direction providing the derivatives indicated in the summations can be expressed as known functions of the dimensions of the conductors and the bus. Accordingly, we turn now to the development of equations for calculating these derivatives.

Equations for the Derivatives of the Geometric Mean Distances

By previously advanced theory[6,7] the geometric-mean-distance D_{12} between two arbitrarily located parallel-sided rectangular areas S_1 and S_2 as in Fig. 1 is

$$S_1S_2 \log D_{12} = -(25/12)S_1S_2 - (1/24)\sum_{i=1}^{4}\sum_{j=1}^{4}(-1)^{i+j} \times K(A_i,B_j) \quad (12)$$

wherein

$$K(A_i,B_j) = (A_i^4 - 6A_i^2B_j^2 + B_j^4)\log(A_i^2+B_j^2) + 4A_iB_j(B_j^2-A_i^2) + \tan^{-1}(B_j/A_i) - 2\pi A_iB_j \quad (13)$$

and

$$A_1 = |D+R+r|;\ A_2 = |D+R|;\ A_3 = |D|;\ A_4 = |D+R| \quad (14)$$

and

$$B_1 = |P+S+s|;\ B_2 = |P+S|;\ B_3 = |P|;\ B_4 = |P+S| \quad (15)$$

The parameter D in equation 14 and P in equation 15 may be positive, zero, or negative. If $r=R$, $s=S$, $D=-r$, and $P=-S$, the two areas S_1 and S_2 are identical and superimposed, and equation 12 yields the self-geometric-mean-distance of a rectangular area. If $r=R$, $s=S$, $P=-S$, and $D=D$, the two areas S_1 and S_2 are identical and symmetrically located a distance D apart, and equation 12 yields the corresponding mutual geometric mean distance as

$$S_1S_2\partial(\log D_{12})/\partial D = -(1/24)\sum_{i=1}^{4}\sum_{j=1}^{4}(-1)^{i+j}\partial K(A_i,B_j)/\partial A_i(dA_i/dD) \quad (16)$$

Correspondingly, equation 13 gives

$$\partial K(A_i,B_j)/\partial A_i = 4A_i(A_i^2-3B_j^2)\log(A_i^2+B_j^2) + 4B_j^2(B_j^2-3A_i^2)\tan^{-1}(B_j/A_i) - 3A_iB_j^2 - 2\pi B_j^3 \quad (17)$$

and equation 14 gives

$$dA_i/dD = d(D+\text{constant})/dD = \pm 1 \quad (18)$$

where + or − sign is to be chosen ac-

cording as in a particular instance the value of D is such that the quantity within the bars is positive or is negative. Finally, substituting equations 17 and 18 in equation 16 yields the desired equation

$$S_1S_2\partial(\log D_{12})/\partial D = -(1/24)\sum_{i=1}^{4}\sum_{j=1}^{4}(-1)^{i+j}[4A_i(A_i^2-3B_j^2)\log(A_i^2+B_j^2)^{1/2}+4B_j(B_j^2-3A_i^2)\tan^{-1}(B_j/A_i)+A_i^3-3A_iB_j^2-2B_j^3]dA_i/dD \quad (19)$$

If dA_i/dD is of the same sign for $i=1$ to 4, then

$$\sum_{i=1}^{4}\sum_{j=1}^{4}(-1)^{i+j}A_i^3dA_i/dD = 2\sum_{i=1}^{4}\sum_{j=1}^{4}(-1)^{i+j}B_j^3dA_i/dD=0 \quad (20)$$

and equation 19 reduces to

$$S_1S_2\partial(\log D_{12})/\partial D = -(1/24)\sum_{i=1}^{4}\sum_{j=1}^{4}(-1)^{i+j}[4A_i(A_i^2-3B_j^2)\log(A_i^2+B_j^2)^{1/2}+4B_j(B_j^2-3A_i^2)\tan^{-1}(B_j/A_i)-3A_iB_j^2]dA_i/dD \quad (21)$$

If

$dA_i/dD=1$ for $i=1$ to 4

then

$$3\sum_{i=1}^{4}\sum_{j=1}^{4}(-1)^{i+j}A_iB_j^2dA_i/dD=0$$

whence equation 21 reduces to

$$S_1S_2\partial(\log D_{12})/\partial D = -(1/24)\sum_{i=1}^{4}\sum_{j=1}^{4}(-1)^{i+j}U(A_i,B_j) \quad (22)$$

where

$$U(A_i,B_j)=4A_i(A_i^2-3B_j^2)\log(A_i^2+B_j^2)^{1/2}+4B_j(B_j^2-3A_i^2)\tan^{-1}(B_j/A_i) \quad (23)$$

By virtue of the identity $K(A_i,B_j)=K(B_j,A_i)$ to be obtained from equation 13 by interchanging A_i with B_j and the use of the trigonometric identity $\tan^{-1}(A_i/B_j)+\tan^{-1}(B_j/A_i)=\pi/2$, corresponding expressions for $S_1S_2\partial(\log D_{12})/\partial P$ follow from those for $S_1S_2\partial(\log D_{12})/\partial D$ through interchange of A_i and B_j and substitution of P for D. This analysis, easily effected, yields

$$S_1S_2\partial(\log D_{12})/\partial P = -(1/24)\sum_{i=1}^{4}\sum_{j=1}^{4}(-1)^{i+j}V(A_i,B_j) \quad (24)$$

wherein

$$V(A_i,B_j)=4B_j(B_j^2-3A_i^2)\log(A_i^2+B_j^2)^{1/2}+4A_i(A_i^2-3B_j^2)\tan^{-1}(A_i/B_j) \quad (25)$$

Equations 12–25 inclusive afford calculation of the derivatives occurring in the double summations defining f_D and f_P. For the case of two rectangular areas located as in Fig. 2, the specific equations are obtained as follows. For this case:

$$A_1=d+2c;\ A_2=d+c;\ A_3=d;\ A_4=d+c$$
$$B_1=b;\ B_2=0;\ B_3=b;\ B_4=0 \quad (26)$$

Substitution of equation 26 in equation 13 and therefrom in equation 12 yields

$$\begin{aligned}b^2c^2\log D_{12} = &-(25/12)/b^2c^2+\\ &(1/24)[6b^2(d+2c)^2-\\ &(d+2c)^4-b]\log[(d+2c)^2+b^2]-\\ &(1/12)[6b^2(d+c)^2-\\ &(d+c)^4-b^4]\log[(d+c)^2+b^2]+\\ &(1/24)(6b^2d^2-d^4-b^4)\log(d^2+b^2)+\\ &(1/24)(d+2c)^4\log(d+2c)^2-\\ &(1/12)(d+c)^4\log(d+c)^2+\\ &(1/24)(d)^4\log d^2+\\ &(b/3)(d+2c)^3\tan^{-1}b/(d+2c)-\\ &(b^3/3)(d+2c)\tan^{-1}b/(d+2c)+\\ &(2b/3)(d+c)\tan^{-1}b/(d+c)-\\ &(2b/3)(d+c)^3\tan^{-1}b/(d+c)-\\ &(1/3)b^3d\tan^{-1}(b/d)+\\ &(1/3)bd^3\tan^{-1}(b/d)\end{aligned} \quad (27)$$

Substitution of equation 26 in equation 23 and therefrom in equation 22 yields

$$\begin{aligned}b^2c^2\partial(\log D_{12})/\partial d = &+(1/24)[12b^2(d+2c)-4(d+2c)^3]\log[(d+2c)^2+b^2]-\\ &(1/12)[12b^2(d+c)-4(d+c)^3]\log[(d+c)^2+b^2]+\\ &(1/24)[12b^2d-4d^3]\log(d^2+b^2)+\\ &(1/24)[4(d+2c)^3]\log(d+2c)^2-\\ &(1/12)[4(d+c)^3]\log(d+c)^2+\\ &(1/24)[4d^3]\log d^2+\\ &b(d+2c)^2\tan^{-1}b/(d+2c)+\\ &(b^3/3)\tan^{-1}(d+2c)/b-\\ &2b(d+c)^2\tan^{-1}b/(d+c)-\\ &(2b^3/3)\tan^{-1}(d+c)/b+bd^2\\ &\tan^{-1}(b/d)+(b^3/3)\tan^{-1}(d/b)\end{aligned} \quad (28)$$

Simplified Equations

By well-established theory, the mutual electromagnetic force exerted between two long isolated nonpermeable conductors spaced D_{ij} centimeters between the parallel axes and carrying currents I_i and I_j abamperes, is

$$f_{ij}=2k_{ij}I_iI_j/D_{ij} \text{ dynes per cm of bus length} \quad (29)$$

Here k is a parameter, usually termed the electromagnetic space factor, of magnitude determined by the geometry and relative position of the cross sections of the two conductors. For identical conductor cross sections located as in Fig. 2, the electromagnetic factor is

$$\begin{aligned}k=D^2/(rs-RS)^2[&M(r,s)+M(R,S)+\\ &2M(R+T,T)+2M(t,S+T)-\\ &2M(R+T,S+T)-2M(T,T)]\end{aligned} \quad (30)$$

where $M(r,s)$ is defined by

$$\begin{aligned}M(r,s)/r^2=&2m\tan^{-1}m-\log(1+m^2)+\\ &n^2m^2/6(1+m^2)+n^4/90[1+\\ &(-1+3m^2)/(1+m^2)^3]+\ldots\end{aligned} \quad (31)$$

and $m=s/D$, $n=r/D$.

A form of $M(r,s)$, especially convenient to speedy, accurate numerical computation, is afforded by expanding the term of the right-hand member of equation 2 powers of m through use of

$$\tan^{-1}m=m-m^3/3+m^5/5-m^7/7+\ldots, \text{ for } m^2<1 \quad (32)$$

$$\tan^{-1}m=\pi/2-1/m+1/3m^3-1/5m^5+\ldots, \text{ for } m^2>1 \quad (33)$$

$$\log(1+m^2)=2m^2/(2+m^2)+2/3[m^2/(2+m^2)]^3+2/5[m^2/(2+m^2)]^5+\ldots, \text{ for } (1+m^2)>0 \quad (34)$$

and then combining use of equation 3 with equation 34 and a proper choice of equation 32 or 33. If $R=S=0$, the conductors are of full cross section and equation 30 reduces to

$$k=(D^2/r^2s^2)M(r,s) \quad (35)$$

If $r=3$ the conductors are of full-squa

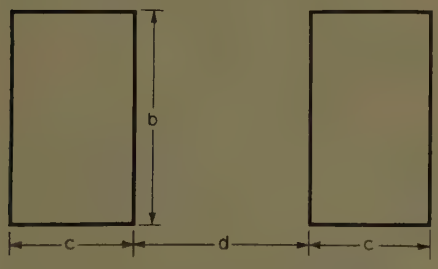

Fig. 2. Cross section of bus comprised of rectangular conductors

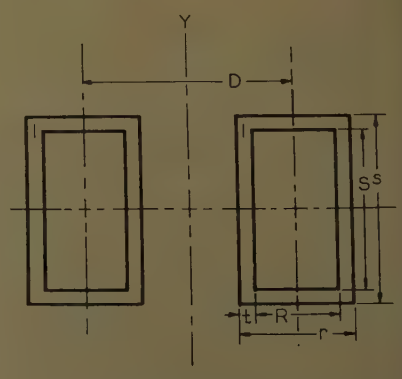

Fig. 3. Cross section of bus comprised tubular rectangular conductors

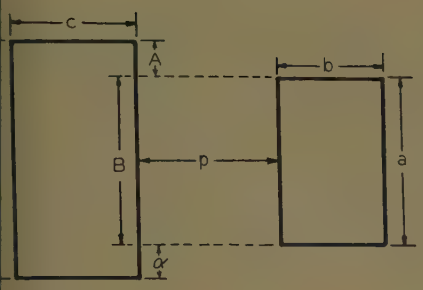

Fig. 4 (left). Two symmetrically located parallel-sided rectangular areas

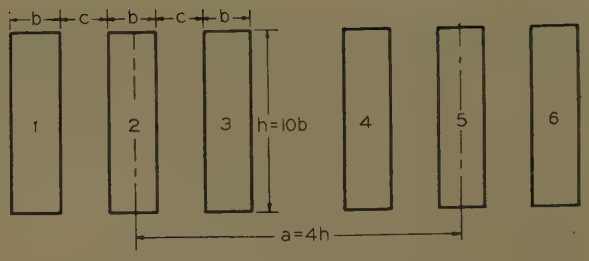

Fig. 5 (right). Cross section of triply divided conductor single-phase bus

oss section and equation 35 further duces to $k=(D^2/r^4)M(r,r)$ where, in pression of $M(r,r)$ by equation 31, $m=$ $=s/D=r/D$. As all terms comprising are dimensionless, the linear dimenons of the bus can be expressed in any esired arbitrary like unit of length.

pproximate Equations

If the width of each conductor or subonductor is small compared with its eight, as is often the case in practice, t is to be expected that a good approximation to the force acting on an individual onductor, and hence the total force on the us, can be obtained by letting the conductor width approach zero and computng the approximate force acting on the corresponding "line-segment" conductors. For a bus with cross section as in Fig. 2, equation 35 yields

$$k'_{ij}=\lim_{r\to 0}(D_{ij}^2/r^2s^2)M(r,s)=(D_{ij}^2/s^2)\lim_{r\to 0}M(r,s)/r^2 \quad (36)$$

Since $n=r/D$ approaches zero as r approaches zero, equation 31 gives

$$\lim_{r\to 0}M(r,s)/r^2=2m\tan^{-1}m-\log(1+m^2) \quad (37)$$

and substitution accordingly in equation 36 yields the corresponding expression for the electromagnetic space factor as

$$k'_{ij}=(D_{ij}^2/s^2)[2m\tan^{-1}m-\log(1+m^2)] \quad (38)$$

Accordingly, the mutual electromagnetic force between two line-segment conductors carrying currents I_i and I_j, as given by equations 29 and 38, is

$$f'_{ij}=2k'_{ij}I_iI_j/D_{ij} \text{ dynes per cm of bus length} \quad (39)$$

In conclusion, it is to be emphasized that in determining the value of the electromagnetic space factor k through use of equation 38 it is necessary that the cross sections of the conductors possess two principal axes of symmetry whose intersection fixes the "center" of the conductors and thus the distance between them—as is the case for all the bus configurations considered in this paper.

Check of Analysis by Use of Gray's Equation

In Rosa's paper,[8] Gray's corrected equation for the geometric mean distance of symmetrically located rectangles as in Fig. 4 is given as

$$\begin{aligned}abcd\log D=&1/4[(p+b+c)^2B^2-(p+b+c)^2/6-B^4/6]\log[(p+b+c)^2+B^2]-\\&1/4[(p+b)^2B^2-(p+b)^2/6-B^4/6]\log[(p+b)^2+B^2]-\\&1/4[(p+c)^2B^2-(p+c)^2/6-B^4/6]\log[(p+c)^2+B^2]+1/4[p^2B^2-p^2/6-B^4/6]\log(p^2+B^2)-(\text{the same series of terms with } B \text{ replaced by } A)+(B/3)(p+b+c)^3\tan^{-1}B/(p+b+c)+(B^3/3)(p+b+c)\tan^{-1}(p+b+c)/B-(B/3)(p+b)^3\tan^{-1}B/(p+b)-(B^3/3)(p+b)\tan^{-1}(p+b)/B-(B/3)(p+c)^3\tan^{-1}B(p+c)-(B^3/3)(p+c)\tan^{-1}(p+c)/B+(B/3)p^3\tan^{-1}B/p+(B^3/3)p\tan^{-1}p/B-(\text{the same series of terms with } B \text{ replaced by } A)-(B^2-A^2)/8[(p+b+c)^2-(p+b)^2-(p+c)^2+p^2]-(11/6)abcd \quad (40)\end{aligned}$$

where D is the geometric mean distance between the rectangles, p is the distance between rectangles, and $A=(d-a)/2$, $B=(d+a)/2$. For the case of two identical rectangles, as shown in Fig. 2, $p=d$, $b=c$, $a=b$, $c=c$, $d=b$, $A=0$, $B=b$; correspondingly, equation 40 yields

$$\begin{aligned}b^2c^2\log D=&(1/24)[6b^2(d+2c)^2-(d+2c)^4-b^4]\log[(d+2c)^2+b^2]-(1/12)[6b^2(d+c)^2-(d+c)^4-b^4]\log[(d+c)^2+b^2]+(1/24)[6b^2d^2-d^4-b^4]\log(d^2+b^2)+(1/24)(d+2c)^4\log(d+2c)^2-(1/12)(d+c)^4\log(d+c)^2+(1/24)d^4\log d^2+(b/3)(d+2c)^3\tan^{-1}b/(d+2c)+(b^3/3)(d+2c)\tan^{-1}(d+2c)/b-(2b/3)(d+c)^3\tan^{-1}b/(d+c)-(2b^3/3)(d+c)\tan^{-1}(d+c)/b+(b/3)d^3\tan^{-1}b/d+(b^3/3)d\tan^{-1}d/b-(25/12)b^2c^2 \quad (41)\end{aligned}$$

Confirmatively, this equation agrees with equation 27.

Differentiating the members of equation 41 with respect to d, gives

$$\begin{aligned}b^2c^2\partial(\log D)/\partial d=&(1/24)[12b^2(d+2c)-4(d+2c)^3]\log[(d+2c)^2+b^2]-(1/12)[12b^2(d+c)-4(d+c)^3]\log[(d+c)^2+b^2]+(1/24)[12b^2d-4d^3]\log(d^2+b^2)+(1/24)[4(d+2c)^3]\log(d+2c)^2-(1/12)[4(d+c)^3]\log(d+c)^2+(1/24)[4d^3]\log d^2+b(d+2c)^2\tan^{-1}b/(d+2c)+(b^3/3)\tan^{-1}(d+2c)/b-2b(d+c)^2\tan^{-1}(b/d+c)-(2b^3/3)\tan^{-1}(d+c)/b+bd^2\tan^{-1}(b/d)+(b^3/3)\tan^{-1}(d/b) \quad (42)\end{aligned}$$

Corroboratively, equation 42 agrees with equation 28. This agreement of equations 27 and 28 with, respectively, equations 41 and 42 provides confirmation of the correctness of the two general expressions and of the validity of the analysis underlying each of them.

Dimensional Units

In derivation of the basic quantities in the foregoing, convenience stems from taking all quantities in the absolute system: linear dimension in centimeters, current in abamperes, inductance in abhenrys per centimeter of bus length, energy in ergs per centimeter of bus length, and force in dynes per centimeter of bus length. As all terms in the expressions for the electromagnetic space factor k are dimensionless, the cross-sectional dimensions of the bus and conductor can be expressed in any convenient like unit of length. In particular, it is often convenient to express the bus dimensions in inches, the unit commonly used in American and British bus-conductor handbooks and/or sales manuals.

First Illustrative Example

Subconductor Currents

In illustration of application of the general theory derived in the foregoing consider analysis of the triply subdivided

conductor single-phase bus of Fig. 5. Each conductor is comprised of three identical subconductors. The bus dimensions are $b=c=1$ cm (centimeters), $h=10b=10$ cm, and $a=4h=40$ cm. This bus is that of the first illustrative example in reference 5. The rather lengthy calculations detailed therein[5] yield the currents as

$$I_1=-I_6=(35.11+j5.33)I;$$
$$I_2=-I_5=(18.75-j14.75)I;$$
$$I_3=-I_4=(46.14+j9.42)I \quad (43)$$

whereof $100I$ is the (normalized) phase current.

Determination of Electromagnetic Space Factors

The space factors of each subconductor with respect to the other five subconductors, as calculated from equations 30 and 31, are

$$k_{12}=k_{21}=k_{23}=k_{32}=k_{45}=k_{54}=k_{56}=k_{65}=0.4605$$
$$k_{13}=k_{31}=k_{46}=k_{64}=0.6365$$
$$k_{14}=k_{41}=k_{25}=k_{52}=k_{36}=k_{63}=0.9899$$
$$k_{15}=k_{51}=k_{26}=k_{62}=0.9903$$
$$k_{16}=k_{61}=0.9935$$
$$k_{24}=k_{42}=k_{35}=k_{53}=0.9896$$
$$k_{34}=k_{43}=0.9814$$

With all space factors thus in hand, determination of the forces exerted on each subconductor is easily effected.

Determination of Forces

Introducing in equation 29 the pertinent values of space factor, conductor currents, and conductor spacing yields the mutual force between two specified subconductors of the bus of Fig. 5. Thus, calculating accordingly for subconductor 1 gives

$$f_{12}=(339.3563-j192.4591)I^2 \text{ dynes/cm of bus length}$$
$$f_{13}=(449.5783+j183.5228)I^2$$
$$f_{14}=(-77.7022-j28.5419)I^2$$
$$f_{15}=(-34.7536+j19.7098)I^2$$
$$f_{16}=(-54.3863-j16.9024)I^2$$

The total force exerted on subconductor 1, as obtained by summing the five component forces, is

$$f_1=f_{12}+f_{13}+f_{14}+f_{15}+f_{16}=[672.0925-j34.6708)I^2 \text{ dynes/cm of bus length} \quad (44)$$

Similar procedure yields the force exerted subconductor 2. Thus

$$f_{23}=2k_{23}I_2I_3/D_{23}=(462.3742-j232.0644)I^2 \text{ dynes/cm of bus length}$$

$$f_{24}=2k_{24}I_2I_4/D_{24}=(-52.2960+j26.2472)I^2$$

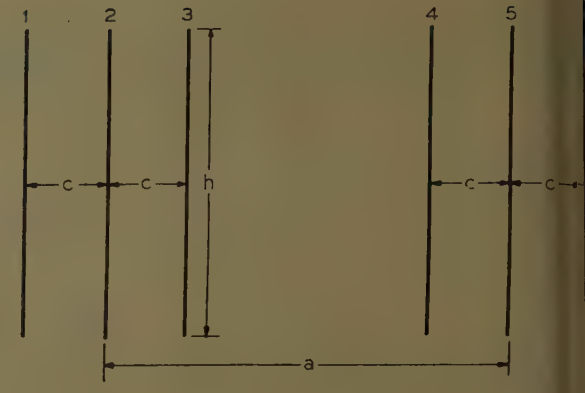

Fig. 6 Cross section of triply subdivided conductor single-phase line-segment bus

$$f_{25}=2k_{25}I_2I_5/D_{25}=(-6.6323+j27.3769)I^2$$

Noting that the forces exerted between two current-carrying elements are opposite in direction and equal in magnitude, and that by symmetry the values of currents and space factors for calculating f_{26} are the same as those for calculating f_{15}, yields

$$f_{21}=-f_{12}=(-339.3563+j192.4591)I^2 \text{ dynes/cm of bus length}$$

$$f_{26}=f_{15}=(-34.7536+j19.7098)I^2$$

Summing component values yields the total force exerted on subconductor 2 is

$$f_2=(29.3360+j33.7286)I^2 \text{ dynes/cm of bus length} \quad (45)$$

The component forces exerted on subconductors 3, 4, 5, and 6 are to be obtained in the same fashion. Proceeding accordingly gives the total forces exerted on these subconductors as

$$f_3=(-1203.1845-j1.1459)I^2 \text{ dynes/cm of bus length} \quad (46)$$

$$f_4=(1203.1845+1.1459)I^2 \quad (47)$$

$$f_5=(-29.3360-j33.7286)I^2 \quad (48)$$

$$f_6=(-672.0925+j34.6708)I^2 \quad (49)$$

It is of interest to note that f_1 and f_6 are of the same magnitude, but differ 180 degrees in angular phase. Such is also true of f_2 and f_5 and of f_3 and f_4. This expected contrasymmetry of forces provides a check on the accuracy calculation. Obviously in practice it can be utilized also to halve the actually needed calculation. Finally, the short-circuit forces on the two bus supports can be obtained by summing each set of forces. Thus, equations 44, 45, and 46 yield

$$f_1+f_2+f_3=(-501.7560-j2.0881)I^2 \text{ dynes/cm of bus length} \quad (50)$$

and equations 47, 48, and 49 yield

$$f_4+f_5+f_6=(501.7560+j2.0881)I^2 \text{ dynes/cm of bus length} \quad (51)$$

Equations 50 and 51 evidence that the horizontal forces exerted on the bus support are equal in magnitude and oppositely directed, as is to be expected from the symmetry of the bus about the horizontal plane through the axes of the subconductors.

Approximation by Line-Segment Conductors

A check on the accuracy of the values obtained in the previous section and insight as to the accuracy of final values and amount of reduction of numerical labor afforded by use of line-segment approximation stems from analysis of the bus of Fig. 6 by use of equations 38 and 39.

Thus, from equation 38 the space factors of each subconductor with respect to the other five subconductors are

$$k'_{12}=k'_{21}=k'_{23}=k'_{32}=k'_{45}=k'_{54}=k'_{56}=k'_{65}=0.458$$
$$k'_{13}=k'_{31}=k'_{46}=k'_{64}=0.6350$$
$$k'_{14}=k'_{41}=k'_{25}=k'_{52}=k'_{36}=k'_{63}=0.9898$$
$$k'_{15}=k'_{51}=k'_{26}=k'_{62}=0.9902$$
$$k'_{16}=k'_{61}=0.9934$$
$$k'_{42}=k'_{24}=k'_{35}=k'_{53}=0.9895$$
$$k'_{34}=k'_{43}=0.9812$$

Introducing in equation 39 the approximate values of space factor, conductor currents and conductor spacing and summing appropriately gives the total forces on the subconductors as

$$f'_1=-f'_6=(669.8058-j34.4301)I^2 \text{ dynes/cm of bus length} \quad (5$$

$$f'_2=-f'_5=(28.9188+j33.8575)I^2 \quad (5$$

$$f'_3=-f'_4=(-1200.4026-j1.5138)I^2 \quad (5$$

Finally, the short-circuit forces on the two bus supports are

$$f'_1+f'_2+f'_3=(-501.6780-j2.0594)I^2 \text{ dynes/cm of bus length} \quad (5$$

$$f'_4+f'_5+f'_6=(501.6780+j2.0594)I^2 \quad (5$$

Corroborative of the correctness of ca

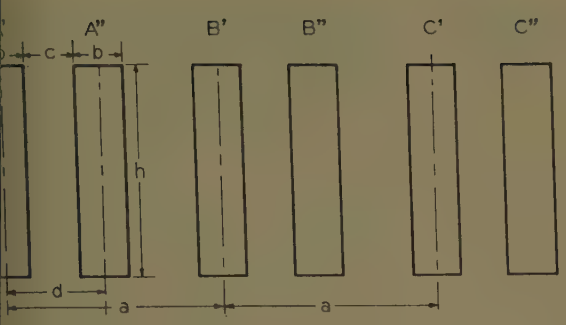

Fig. 7 (left). Cross section of doubly divided conductor 3-phase bus

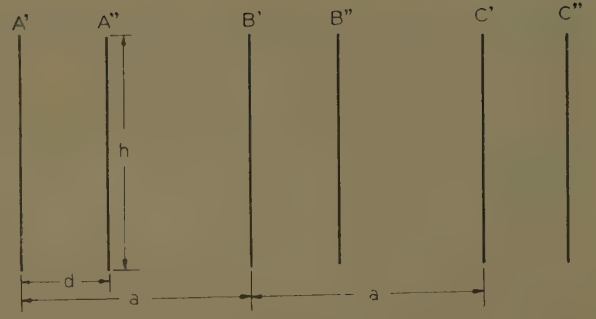

Fig. 8 (right). Cross section of "equivalent" rectangular 3-phase bus

ation, these two total forces are equal magnitude and oppositely directed.

mparison of Exact and Approximate Values

The short-circuit forces exerted on the pports, as stated in equations 55 and 56 r the bus of Fig. 6, are in excellent agreeent with the corresponding values of uations 50 and 51 for the bus of Fig. 5. his excellent agreement evidences that e width of the strap conductors has little fect on the magnitudes of the short-rcuit forces exerted on the bus supprts—in so long as this width is small y comparison with the height of the conuctors and the distances between conducrs. As such often occurs in practice, follows that the simpler calculation ased on line-segment approximation ill commonly suffice for design purposes.

Second Illustrative Example

In illustration of analysis pertinent to polyphase busses consider the doubly divided conductor 3-phase bus typified in Fig. 7. Each phase is comprised of two identical subconductors. The bus dimension are $a=6.67$ cm, $b=c=0.635$ cm, $d=1.27$ cm, $h=10.16$ cm. The currents in the subconductors, as determined in reference 5, are

$$I_{A'}=(0.5218-j0.0674)I;\quad I_{B'}=(-0.2967-j0.4389)I;\quad I_{C'}=(-0.2860+j0.4221)I \quad (57)$$

$$I_{A''}=(0.4782+j0.0674)I;\quad I_{B''}=(-0.2033-j0.4271)I;\quad I_{C''}=(-0.2140+j0.4439)I \quad (58)$$

Calculation as in the foregoing yields the forces exerted on the subconductor as

$$f_{A'}=(0.0306-j0.0271)I^2;\quad f_{B'}=(0.1312+j0.2052)I^2;\quad f_{C'}=(-0.1459-j0.1731)I^2 \quad (59)$$

$$f_{A''}=(-0.2094-j0.0591)I^2;\quad f_{B''}=(0.2235+j0.0025)I^2;\quad f_{C''}=(-0.0300+j0.0516)I^2 \quad (60)$$

The short-circuit forces exerted on the bus supports, as obtained by summing the forces acting on the two subconductors comprising each phase, are

$$f_A=f_{A'}+f_{A''}=(-0.1788-j0.0862)I^2 \text{ dynes/cm of bus length} \quad (61)$$

$$f_B=f_{B'}+f_{B''}=(0.3547+j0.2077)I^2 \quad (62)$$

$$f_C=f_{C'}+f_{C''}=(-0.1759-j0.1215)I^2 \quad (63)$$

In check of these values and to gain insight as to the degree of accuracy and amount of reduction of numerical work afforded by use of line-segment approximation, consider analysis of the bus of Fig. 8. Calculation as in the foregoing yields the short-circuit forces exerted on the bus supports of phases A, B, and C as

$$f'_A=f'_{A'}+f'_{A''}=(-0.1781-j0.0854)I^2 \text{ dynes/cm of bus length} \quad (64)$$

$$f'_B=f'_{B'}+f'_{B''}=(0.3535+j0.2068)I^2 \quad (65)$$

$$f'_C=f'_{C'}+f'_{C''}=(-0.1751-j0.1214)I^2 \quad (66)$$

A second procedure which provides approximate values of the total force acting on each bus support is to consider the two subconductors of one conductor as approximated by a single conductor with cross-sectional area equal to the total of the two conductors and carrying the total current of the two conductors, as indicated in Fig. 9.

The currents in conductors A, B, and C are $I_A=I_{A'}+I_{A''}=Ie^{j0}$, $I_B=I_{B'}+I_{B''}=Ie^{-j120}$ and $I_C=I_{C'}+I_{C''}=Ie^{j120}$. Substituting the appropriate values of space factors, conductor currents, and conductor spacings in equation 29 yields the mutual forces between any two specified conductors. Summing these gives the total forces exerted on conductors A, B, and C as

$$f_A=f_{AB}+f_{AC}=(-0.1933-j0.0952)I^2 \text{ dynes/cm of bus length} \quad (67)$$

$$f_B=f_{BA}+f_{BC}=(0.3732+j0.2149)I^2 \quad (68)$$

$$f_C=f_{CA}+f_{CB}=(-0.1790-j0.1197)I^2 \quad (69)$$

These values are in good agreement with the corresponding values of equations 61, 62 and 63. This agreement evidences the general validity and usefulness of this second approximate mode of calculation. Further, the numerical work required to obtain these values is yet much less than is required to obtain the "approximate" line-segment values of equations 64, 65 and 66 (which, in turn, were obtained by much less labor than the almost equal "exact" values).

Three-Phase Paired-Phase Arrangement

Fisher and Frank[11] show by detailed analysis and experimental investigation that the paired-phase arrangement of Fig. 10 is superior to more conventional arrangements (such as the interlaced bus Fig. 7), for transmitting low-voltage polyphase currents in the range of 1,000 amperes, at 600 volts or less. As this type of bus has come into very considerable use, it is of interest to compare the relative magnitudes of the forces acting on the

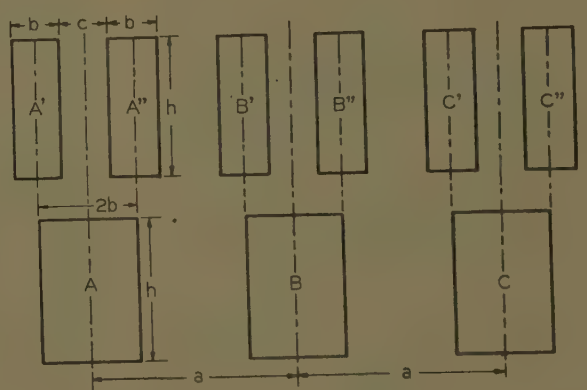

Fig. 9. Cross section of "equivalent" rectangular 3-phase bus

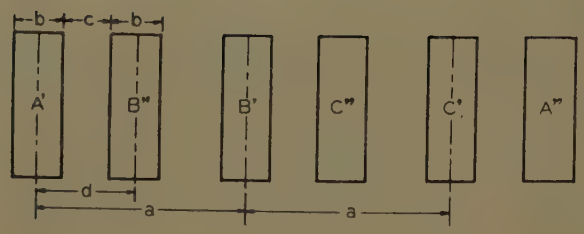

Fig. 10. Cross section of doubly divided conductor paired-phase 3-phase bus

supports of the typical 3-phase paired-phase bus of Fig. 10 with the corresponding values for the similarly rated interlaced bus of Fig. 7.

Calculation effects in the same manner as for the foregoing polyphase busses (the numerical details are given in reference 10) yields

$$I_{A'}=(0.4092+j0.2458)I;$$
$$I_{B'}=(-0.0358-j0.4410)I;$$
$$I_{C'}=(-0.3954+j0.1789)I \quad (70)$$

$$I_{A''}=(0.5908-j0.2458)I;$$
$$I_{B''}=(-0.4642-j0.4250)I;$$
$$I_{C''}=(-0.1046+j0.6871)I \quad (71)$$

It is to be noted that the currents in each closely spaced pair of subconductors (i.e., $A'-B''$, $B'-C''$, and $C'-A''$) are nearly equal and opposite; whence the external magnetic field produced by each pair of conductors is relatively weak—which fact accounts for the lower reactance voltage drops on a bus of this type, as compared with the corresponding values of an interlaced bus of the same current rating.

The effective force acting on each subconductor is

$$f_{A'}=(-0.0524-j0.1248)I^2;$$
$$f_{B'}=(0.1124+j0.2050)I^2;$$
$$f_{C'}=(0.0352-j0.2231)I^2 \quad (72)$$

$$f_{A''}=(-0.1836+j0.1206)I^2;$$
$$f_{B''}=(0.2579+j0.0442)I^2;$$
$$f_{C''}=(-0.1695-j0.0219)I^2 \quad (73)$$

and summing yields the force on the bus support of each pair as

$$f_{1s}=f_{A'}+f_{B''}=(0.2054-j0.0806)I^2 \text{ dynes/cm of bus length} \quad (74)$$

$$f_{2s}=f_{B'}+f_{C''}=(-0.0571+j0.1831)I^2 \quad (75)$$

$$f_{3s}=f_{C'}+f_{A''}=(-0.1484-j0.1025)I^2 \quad (76)$$

Comparison of the magnitudes of these forces with the corresponding values of equations 61, 62, and 63 for the interlaced bus of Fig. 7 reveals, as is to be expected, somewhat smaller forces on the paired-phase bus supports.

Finally, calculation ignoring the resistance of the conductors yields

$$f_{1s}=(0.1724-j0.1591)I^2 \text{ dynes/cm of bus length} \quad (77)$$

$$f_{2s}=(-0.0082+j0.3034)I^2 \quad (78)$$

$$f_{3s}=(-0.1642-j0.1443)I^2 \quad (79)$$

Comparison of the values of equations 74, 75, and 76 with corresponding values of equations 77, 78, and 79 evidences that the resistance of the conductors has an appreciable effect on the values of the forces (as is to be expected because of minimization of mutual reactance in virtue of the weak linking fields). However, the magnitudes of corresponding forces are yet in fair agreement. Accordingly, this example illustrates that in calculation of short-circuit forces, the resistance associated with the conductors can usually be ignored and calculation effected on the basis of inductive reactance alone, with a consequent considerable reduction of numerical labor. Primarily, this reduction occurs in the computation necessary to determination of the conductor currents.

Conclusion

1. General equations are derived for calculating the short-circuit forces associated with each subconductor, conductor, and bus support of a multiple-strap subdivided-conductor single-phase or polyphase bus.

2. Although use of these general equations is too time-consuming for common appreciation in practice, they afford both derivation of approximate equations convenient to use in practice and a means of ascertaining the degree of accuracy of the numerical values stemming from these approximate equations.

3. The short-circuit forces exerted on the bus supports of the triply divided bus of Fig. 5, as calculated from the general equations, are in excellent agreement with those calculated by the two approximate procedures. Such is also true for the doubly divided 3-phase bus of Fig. 7. These agreements evidence that ignoring the width of strap conductors has little effect on the calculated magnitudes of the short-circuit forces exerted on conductors and bus supports if the conductor width is small compared with the conductor height and major distances between conductors.

4. The magnitudes of the calculated associated forces are substantially the same for both phase sequences.[10] S evidences that either sequence can chosen in design calculation.

5. The magnitudes of the short-cir forces exerted on the bus supports of paired-phase bus of Fig. 10, calcula by ignoring the conductor resistance, in fair agreement with those calculated taking conductor resistance into consi ation. This degree of agreement dences that for most design purposes ductor resistance can usually be igno and calculation of short-circuit for effected on the basis of inductive rea ance alone, with a consequent consid able reduction in the numerical labor calculation.

References

1. Formulas for Calculating Short-Circ Forces Between Conductors of Structu Shape, Thomas James Higgins. *AIEE Tra tions*, vol. 62, Oct. 1943, pp. 659–63.

2. The Design of Bus-Bar Industrial Dis bution Systems: an Epitomization of Av able Data, T. J. Higgins. *Ibid.*, vol. 64, pp. 385–400; *discussion*, pp. 486–88.

3. Equations for the Inductance and Sho Circuit Forces of Busses Comprised of Doub Channel Conductors, C. M. Siegel, T. J. Higg *Ibid.*, pt. III (*Power Apparatus and Systems*), 71, Jan. 1952, pp. 522–31.

4. Enclosed Bus-Bar Electrical Distri tion Systems for Industrial Plants, E. Carlson. *Ibid.*, vol. 60, June 1941, pp. 297–3 *discussion* by O. R. Schurig, pp. 700–01; also latter's discussion of reference 3, pp. 530–31.

5. Equations for the Inductances and C rent Distribution of Multiple-Conduct Single-Phase and Polyphase Busses, T. H. C T. J. Higgins. *Ibid.*, pt. I (*Communication Electronics*), vol. 76, Nov. 1957, pp. 553–58.

6. Formulas for the Geometric Mean D tances of Rectangular Areas and of L Segments, T. J. Higgins. *Journal of Appl Physics*, New York, N. Y., vol. 14, 1943, pp. 18

7. Formulas for the Calculation of T Inductance of Linear Conductors of Str tural Shape, Thomas James Higgins. *AI Transactions*, vol. 62, Feb. 1943, pp. 53–57.

8. On the Geometric Mean Distances Rectangular Areas and the Calculation Self-Inductance, E. B. Rosa. *Bulletin*, Bureau Standards, Washington, D. C., vol. 3, 1907, p 42.

9. Equations for the Reactance a Current Distribution of Multiple-Str Single-Phase and Polyphase Busses, T. H. Ch *M.S. Thesis*, University of Wisconsin, Madis Wis., June 1953.

10. Equations for Short-Circuit Forces Multiple-Strap Single-Phase and Polyph Busses for Supplying Low-Frequency Indu tion Furnaces, T. H. Chin. *Ph.D. Thes* University of Wisconsin, June 1954.

11. Paired-Phase Bus Bars for Large Pol phase Currents, L. E. Fisher, R. L. Fran *AIEE Transactions*, vol. 62, Feb. 1943, pp. 71–77.

Discussion

Lawrence E. Fisher (General Electric Co pany, Plainville, Conn.): It is helpful learn that the more rigorous calculation the forces on bus bars is in close agreeme with the more simple calculations with defined limits.

take this opportunity to ask the au-
s if they have made any calculations or
ld like to make general comments on
forces to be expected on an interlaced
ase bus bar structure with 12 2- by
inch bus bars on 3/4-inch centers, for
nple, with the phase bars arranged
CAB'CABCABC.
ests appear to indicate that the forces,
cially on many of the inner bars, are
risingly low. Theoretically, since any
such as bar *B'* has about as many bars
e to it on the left as on the right side, it
ns reasonable to expect that the forces
ld be at least partially cancelled. The discusser should like to have the authors make comments on these points based on their previous studies.

T. H. Chin and **T. J. Higgins:** The authors express their appreciation of the complimentary comment by Mr. Fisher. They agree with his remark that it is to be expected that forces on the interior bars of the described arrangement ought be relatively low. It would not be difficult, though lengthy, to calculate approximately the actual forces on a bar in the arrangement cited, using theory set out in the paper, though the authors have not done so.

If such were done, the authors could expect to find relatively low forces for the reason he indicates. Namely, that these bars lie in a relatively weak field because of partial mutual cancellation, at a bar such as *B'*, of the "net" flux produced by the currents in the bars to the left and of that produced by the currents in the bars to the right. Also, it may well be that the actual current carried by such bars is reduced beyond those in the outer bars in the nonuniform distribution of currents that actually results in such an interlaced arrangement of numerous bars.

An Analysis of the Dynamics of an Electromechanical System

ROY HYINK
ASSOCIATE MEMBER AIEE

nopsis: This paper describes a method r the accurate computation of the dynamic erating characteristics of an electrome-anical system such as a relay or solenoid other electromagnetic device. This ethod is based upon the principle of con-rvation of energy and is particularly useful systems where energy is transformed from ne form to one or more other forms. While an a-c-operated contactor or relay will e used to demonstrate the method in this aper, the method is not restricted to this ype of device only, but can be applied to ny type of dynamic system. This type of pproach is one which is possible and prac-cal because digital computers can be used o do the calculations in a reasonable length f time.

IN MANY AREAS of design, the static characteristics of a system are used as basis of design because these character-stics can be calculated from the sketches r drawings from which the system is to e made. Many times the analysis of the lynamic operation of the system is de-ayed until actual models have been onstructed. Sometimes the model which will perform satisfactorily under slow-speed or static conditions will not pro-duce the proper performance when the system is operating under normal condi-tions. This paper will attempt to out-line a method of procedure which can be used to analyze the dynamic performance of an electromechanical system before any models have been constructed.

In the case of electromagnetic relays and contactors, this dynamic analysis has always appeared very difficult and time-consuming. Therefore, the study of dynamic operating conditions has been delayed until actual working models of the device have been built. In the past, engineers were not too concerned with the dynamic performance of electromagnetic relays and contactors because, in most applications, the operating times were not of importance in over-all system design, and the electrical and mechanical life requirements of such devices were not too severe. However, in recent years, engineers have been more and more concerned about such factors as operating time, mechanical life, electrical life of the contacts, and general shock resistance of the over-all device. Thus a need has arisen for methods of analysis of the dynamic operating conditions of relays and electromagnets.

The operation of any electromechanical system can be described by analyzing the energy relations which exist in the system. The total energy input to the system must equal the energy output, plus the losses within the system, plus the energy stored in the system. This is merely a restatement of the principle of conservation of energy, but it can become a powerful basic tool in the analysis of any electromechanical system. In a system such as an electromagnet which converts electric to mechanical energy, the energy input is electric, the energy output is the work done, the losses result in heating, and the stored energy is mechanical and magnetic. These energy relations for an a-c-operated electromagnet are shown in Fig. 1.

Paper 60-636, recommended by the AIEE Industrial Control Committee and approved by the AIEE Technical Operations Department for presentation at the AIEE Great Lakes District Meeting, Milwaukee, Wis., April 27–29, 1960. Manuscript submitted January 14, 1960; made available for printing March 7, 1960.

Roy Hyink is with Cutler-Hammer, Inc., Milwaukee, Wis.

Nomenclature

The symbols given here are those used within the main body of this paper.

e = instantaneous voltage applied to coil
E = rms value of the applied voltage ($e = \sqrt{2}\,E \sin \omega t$)
F_f = moving friction force
F_s = static friction force
F_L = force exerted by the load against which the magnet is working
F_M = force developed by the magnet
G_0 = total initial magnetic gap
G = magnetic gap at any time ($G = G_0 - X$)
i_c = instantaneous coil current
i_e = equivalent current representing eddy current and hysteresis losses
i_s = equivalent instantaneous secondary coil current
i = net instantaneous current producing a magnetic field ($i = i_c - i_e - i_s$)
I = rms value of coil current
Δi_c = increment of coil current during time, Δt
m = mass of moving parts
N = total turns on main coil
$\mathcal{P}$ = permeance of magnetic circuit
R_c = coil resistance
R_e = equivalent resistance of iron circuit to eddy current flow
R_t = equivalent resistance of all resistances coupled magnetically to main coil ($1/R_t = 1/R_e + 1/R_s$)
R_s = equivalent resistance of secondary coils
t = time
Δt = small fixed increment of time
Δt_f = final time increment for movement from last calculated gap to seal
V = velocity of moving magnet armature
ΔV = change of velocity occurring during time, Δt
W_c = total heat generated in coil before Δt interval
W_e = total electric energy put into system before Δt interval
W_f = total heat generated by friction before Δt interval
W_L = total work done on load before Δt interval
X = distance magnet armature has moved from original position

Fig. 1. Energy relations du the closure of an a-c elec magnet

ΔX = magnet armature movement during time Δt
Φ = total flux in a magnet
θ = value of ωt when magnet is energized

Discussion

It should be possible to set up a mathematical expression defining each quantity enclosed within a separate box as in Fig. 1. If it is possible to write mathematical expressions for these various quantities, then Fig. 1 can be converted into a mathematical equation. All of the expressions shown in the boxes in Fig. 1, with the exception of the energy stored in the magnetic field and the kinetic energy in the moving parts, are integral expressions. Therefore, these expressions must be evaluated from the time that the magnet was originally energized. If some point in time after the magnet has been energized but before it has reached the sealed position is called zero time, then the value of each one of these boxes at zero time can be represented by a symbol W with the proper subscript. After a time interval, Δt, following zero time, all of these values must be changed by an amount representing the energy contribution taking place during the time interval Δt. This energy summation can be accomplished with the following expressions.

Electric Energy Input

The electric energy input to this system can be represented by equation 1.

$$\text{Electric energy input} = \int_0^t e i_c dt \qquad (1)$$

It is possible to convert this integral equation into a difference expression by applying the trapezoid integration rule. Let the subscripts "0" and "t" on a quantity represent the instantaneous value at zero time and after some time interval, Δt. If Δi_c represents the change in coil current during this interval, it is possible to write equation 2.

$$\text{Electric energy input} = W_e + \frac{e_0 + e_t}{2}\left(i_{c0} + \frac{\Delta i_c}{2}\right)\Delta t \qquad (2)$$

Work Done (Energy Stored in Springs)

Assume that the loading of this magnet or the force that opposes this magnet upon moving from open to closed position is shown by the solid line in Fig. 2. This curve represents the force versus displacement characteristics of a group of springs. In this case three springs are shown, but the shape of this curve is not important as long as it can be defined in a manner similar to that shown in Fig. 2. The area under this curve represents the energy stored in the spring system when the magnet is in the sealed position. This work can be expressed mathematically by the integral expression which is shown as equation 3:

$$\text{Work done (energy stored in springs)} = \int_0^x F_L dx \qquad (3)$$

Let the additional subscripts "0" and "t" represent the value of F_L at the beginning and end of some interval of time. Then if the trapezoid integration rule is applied to this expression, the following difference expression can be stated:

$$\text{Work done (energy stored in springs)} = W_L + \left(\frac{F_{L0} + F_{LT}}{2}\right)\Delta X \qquad (4)$$

where ΔX equals the distance the magnet moves during time, Δt.

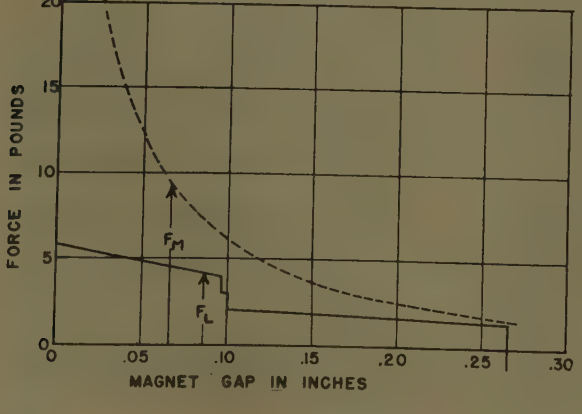

Fig. 2. Curve of spring loading on the magnet versus gap (solid) and curve of average force developed by the magnet versus gap if the magnet closes slowly (dashed)

Energy Loss in Coil

The energy loss in the coil is elect energy which is converted to heat as t coil current flows through the coil resi ance. The rate at which this heat produced is, of course, the coil curre squared times the resistance of the c Therefore, it is possible to write the follo ing expression for the energy loss in t coil:

$$\text{Energy loss in coil} = \int_0^t i_c^2 R_c dt \qquad (5)$$

In this case it is assumed that the c resistance will remain constant, but, course, the coil current will vary duri some interval of time. Consider the valu of this expression for some interval time, Δt. If it is assumed that the co current varies linearly during this tim interval, it is possible to write the follow ing expression for the energy loss in t coil:

$$\text{Energy loss in coil} = W_c + \int_0^{\Delta t}\left(i_{c0} + \frac{\Delta i_c}{\Delta t}\,t\right)R_c dt \qquad (6)$$

If the indicated integration is per formed, the following difference expressio results:

$$\text{Energy loss in coil} = W_c + R_c\left(i_{c0}^2 + i_{c0}\Delta i_c + \frac{(\Delta i_c)^2}{3}\right)\Delta t \qquad (7)$$

Energy Loss in Magnetically Coupled Circuits

In any electromagnet there are energy losses in circuits which are coupled to th coil circuit only through mutual induct ance. In an a-c electromagnet these ar losses such as the hysteresis and eddy cur rent losses in the iron of the magnet and the energy loss due to current flowing in any secondary coil on the electromagne such as a shading coil. Since these losse result in heating of the magnet and are primarily ohmic in nature, they can be represented by equivalent resistances in parallel with the coil circuit. In the case of a secondary coil, the equivalent resist ance would be the turns ratio of the main coil turns divided by the secondary coil turns squared times the secondary resist ance. In the case of eddy current and hysteresis losses, an equivalent resistance value can be derived from the core-loss data published by suppliers of electrical steel. These equivalent resistance values

be combined into one equivalent stance value which is defined as R_t. e only voltage appearing in the second- circuit is that part of the applied tage which is not dropped across the resistance. For the purposes of this per, it will be assumed that all second- circuits are coupled 100% with the mary coil. While this is not strictly e, in any other case it is possible to ad- t the values of R_e and R_s so that this umption can be made without serious or. It is now possible to set up an egral expression for the energy loss in gnetically coupled circuits as shown in uation 8.

ergy loss in magnetically coupled circuits

$$= \int_0^t \frac{1}{R_t}(e - i_c R_c)^2 dt \quad (8)$$

If the time interval Δt is assumed and e trapezoid rule for integration is used, e following difference expression re- lts:

nergy loss in magnetically coupled circuits

$$= W_t + \frac{\Delta t}{R_t}\left[\left(\frac{e_0+e_t}{2}\right)^2 - (e_0+e_t)\left(i_{c0}+\frac{\Delta i_c}{2}\right)R_c + \left(i_{c0}^2 + i_{c0}\Delta i_c + \left(\frac{\Delta i_c}{2}\right)^2\right)R_c^2\right] \quad (9)$$

Energy Loss Due to Friction

The total energy generated by friction an be expressed as the product of the riction force times the distance through hich it is effective. After the incre- ental movement, ΔX, this quantity an be represented as shown in equation 0.

Energy loss due to friction $= W_f + F_f|\Delta X|$ (10)

Energy Stored in Magnetic Field

The energy stored in a magnetic field can be expressed by the following integral equation:

Energy stored in magnetic field

$$= \int_0^{N\Phi} i\, d(N\Phi) \quad (11)$$

Since most of the energy in an open a-c electromagnet is stored in the air gap, it is possible to assume a linear relation between flux and current. The total flux in any magnet at any time will be equal to the permeance of that magnet multiplied by the equivalent magnetizing ampere-turns. Now it is possible to rewrite this expression for the energy in the magnetic field as follows:

Energy stored in magnetic field $= \frac{1}{2}(Ni)^2\mathcal{P}$ (12)

Note that the current in this expression is not the coil current, but is the net instantaneous current producing the magnetic field. When the losses in magnetically coupled circuits were considered, it was implied that there were currents flowing in these circuits. These currents can be converted into equivalent coil currents and subtracted from the coil current to yield the net magnetizing current. The net magnetizing current thus obtained is used in this expression. The magnitude of these currents can be calculated by the expressions shown in equations 14 and 15.

$$i = i_c - i_e - i_s \quad (13)$$

$$i_e = \frac{e - i_c R_c}{R_e} \quad (14)$$

$$i_s = \frac{e - i_c R_c}{R_s} \quad (15)$$

Energy in Moving Parts (Kinetic Energy)

The kinetic energy of the electromechanical system at any time can be represented by equation 16. If the motion of the device is along a straight line, this expression can be evaluated directly. If the motion of the electromagnet is along an arc of a circle, it is necessary to convert the moment of inertia of the device to equivalent mass and the angular velocity to an equivalent velocity before evaluating with this expression. For the purpose of this paper, it is enough to say that the kinetic energy can be expressed by an expression of the type shown in equation 16.

Energy stored in moving parts (kinetic energy) $= \frac{1}{2}mv^2$ (16)

One more expression is required before the expressions developed to this point can be used for the dynamic analysis of an a-c magnet. That expression is for the force developed by the magnet at any particular time. This force will be a function of the magnetic gap and the net magnetizing current flowing at the time being considered. The force developed by an electromagnet can be expressed as equation 17.

$$F_M = -\frac{1}{2}(Ni)^2\frac{d\mathcal{P}}{dG} \quad (17)$$

By proper analysis of the expressions given thus far, it should be possible to compute the dynamic operation of an a-c-operated electromagnet. As these various expressions are examined, the task of computing the operation of the magnet appears to be quite ambitious, and indeed it would be were it not for the aid of digital computers in this type of computation. With the digital computer, it is only necessary to program the computation for one time interval, Δt, and repeat this computation again and again until the magnet has finally reached a sealed position.

If the energy stored in the magnetic field and the pull developed by the electromagnet are to be evaluated, it is necessary to derive an expression for the permeance of the electromagnet as a function of gap. A method of setting up this expression is shown in Appendix I. There are other ways to set up the expression for permeance versus gap such as field mapping or electrical measurements on actual sample magnets, but the primary purpose of this paper would not be served by going into such details.

Method of Solution

Assume that a sinusoidally varying voltage is applied to the coil so that $e = 1.414E \sin \omega t$. Assume that θ is the value of ωt at the instant the voltage is applied. Therefore, in equation 2 e_0 is established as $1.414E \sin \theta$ and e_t can be calculated knowing Δt. At the instant the circuit is closed, the net current i_0 is zero. Also assume that i_{c0} is zero. This is not strictly true but it leads to negligible error. Δi_c is not known. All the W terms are zero at this instant. Since the current is zero at the first instant, there will be no force developed by the magnet and it is assumed that the magnet will develop zero force during the entire first interval of time Δt. Since the magnet develops no force, there will be no work done during this interval. Upon examining equation 7, it can be seen that all quantities in this equation are known except Δi_c. Likewise, all quantities in equation 9 are known except for Δi_c. Since there is no magnetic force developed, there will be no motion. Thus the energy loss due to friction during this interval will be zero and the value of expression 10 is known. The kinetic energy of the moving parts will be zero after the time interval Δt because there is no motion. After the time interval, Δt, the energy stored in the magnetic field will be as shown in equation 12 except that i will be replaced by $i_0 + \Delta i_c$. (In order to simplify the calculation, the assumption has been made that $\Delta i = \Delta i_c$ for calculation of the stored magnetic energy only.)

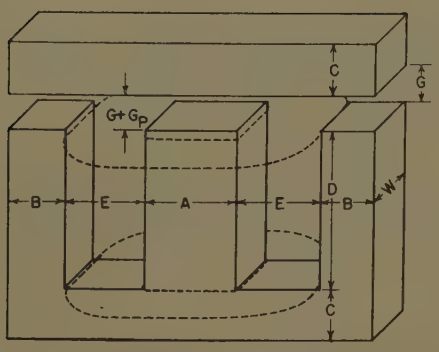

Fig. 3. Outline of magnet used for the example

Dashed line is coil outline
G_p is gap at center leg when G=0

Thus, if the mathematical equation represented by Fig. 1 is written, the only unknown quantity will be Δi_c. This equation can be calculated for Δi_c. Knowing Δi_c, the energy contribution for this interval due to each one of these, expressions can be evaluated. Now the value of each expression shown in Fig. 1 is known after a time interval, Δt. The complete expression for the evaluation of Δi_c is given in Appendix II.

As the force developed by the magnet increases and exceeds the friction force, the magnet will start to move. The net force producing motion at any time is given by equation 18 or 19.

$$ma = F_M - F_L \pm F_f \quad \text{if} \quad |F_M - F_L| > F_s \quad \text{and} \quad v = 0 \qquad (18)$$

$$ma = 0 \quad \text{if} \quad |F_M - F_L| \leq F_s \quad \text{and} \quad v = 0 \qquad (19)$$

In this equation the friction force is plus or minus, depending upon the velocity at that particular time. The assumption is made that the acceleration remains constant for a time interval, Δt. Then the change in velocity during that time interval will be shown in equation 20.

$$\Delta V = a(\Delta t) \qquad (20)$$

The displacement during that time interval will be shown in equation 21 or in 22.

$$\Delta X = \frac{1}{2} a(\Delta t)^2 + V_0(\Delta t) \qquad (21)$$

$$\Delta X = \left(V_0 + \frac{\Delta V}{2}\right)(\Delta t) \qquad (22)$$

Thus, after solving for Δi_c, all of the expressions in Fig. 1 can be evaluated at the end of any time interval, Δt. In the case of the kinetic energy and the energy of the magnetic field, the total energy after the time interval, Δt, can be calculated directly. For all other expressions, the energy contribution during the time interval, Δt, can be evaluated and added to the total energy represented by this term from initial energization until the time interval under consideration, W. This process is then repeated for as many Δt time intervals as desired.

The method of calculating permeance shown in Appendix I does not yield good results for magnetic gaps less than about 0.020 inch. Therefore this procedure is varied slightly at small gaps in the following manner. When a gap becomes le than some predetermined limit, the sumption is made that the acceleratio will remain constant at the least c culated value until the magnet is seale Therefore, if one knows the acceleratio during this last interval and the velocit for the beginning of the interval, equatio 21 can be used to calculate the final i terval, Δt_f. This final Δt_f is added the time previously accumulated to gi the total closing time.

The details of how each expression evaluated on a digital computer and th order in which they are calculated w not be discussed here, as these facto will vary with the type of computer use This method of analysis has been used c a *LGP-30* digital computer (Royal McB Company) with success.

Discussion of Results

This method of computation of dynam operating conditions of an a-c magnet suc as shown in Fig. 3 has produced som very good results. Fig. 4 shows some ca culated curves for the magnet discussed i Appendix II, together with some curve actually measured on the same magne The loading on this magnet was as show in Fig. 2. The velocity of this magne was measured by using a model *6V3* linear motion velocity transducer manu facturer by Control Components Com pany, Brookline, Mass. This is essen tially an air core transformer with a rod

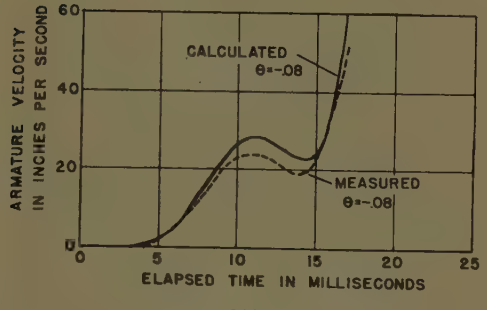

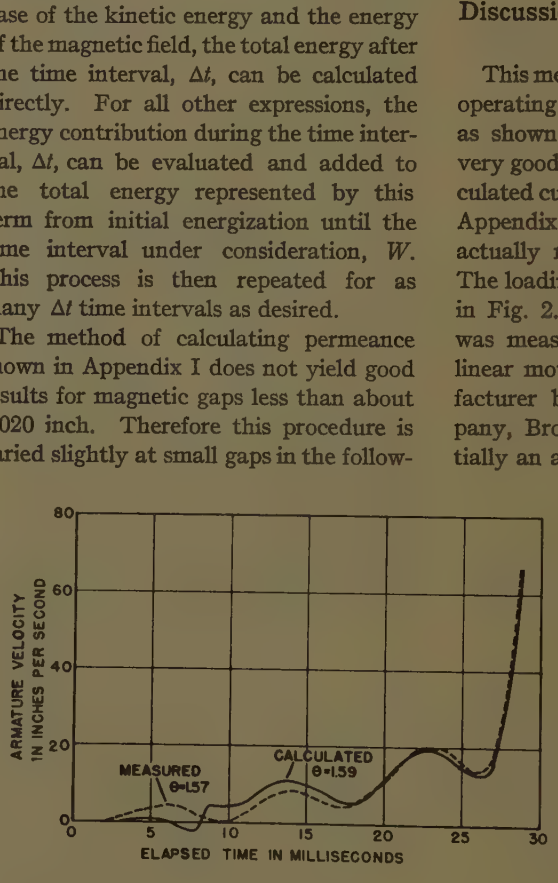

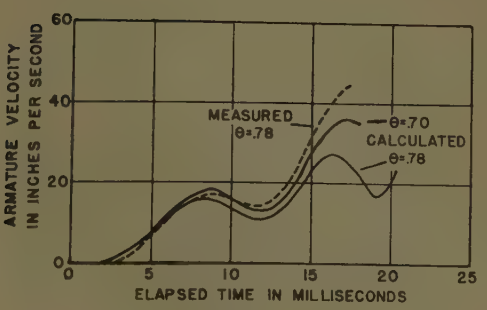

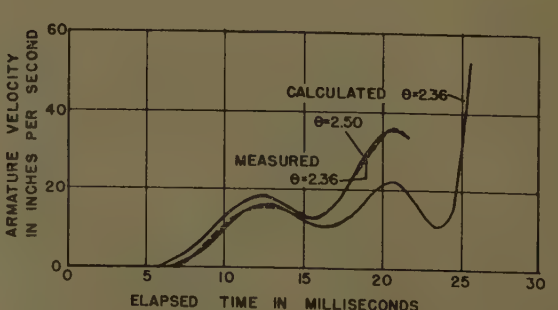

Fig. 4. Calculated and measured velocity versus time

CURVES

A—$\theta \approx 0$
B—$\theta \approx \pi/4$
C—$\theta \approx \pi/2$
D—$\theta \approx 3\pi/4$

ped permanent magnet as a core. The e of the transducer was attached to the gnet armature. The transducer out- voltage, which is proportional to nature velocity, was displayed on an illoscope. At the same time, through e use of an electronic switch, the coil tage was also displayed on the oscillo- pe. The value of θ was varied by ergizing the magnet coil with a syn- ronous switch. The value of θ for the ur curves shown was established by amining the oscilloscope record of e applied voltage. An attempt was ade to establish θ at 0, $\pi/4$, $\pi/2$, $3\pi/4$.

The closing velocity curve of an a-c agnet can vary considerably depending the value of θ. Figs. 4(A) and 4(D) ch show two calculated curves for values θ differing by only small amounts. The curacy with which θ was determined r the measured curve was ± 0.1 radian best. There was also some chattering bounce of the contacts energizing the il. This bounce is not considered in is analysis.

This analysis of an a-c magnet was ade with the assumption that the iron as infinite permeability. It can be own that this will lead to small errors if he flux density is less than 85,000 lines er square inch and if the total air-gap ength is more than 1% of the iron length. f this analysis is applied to a d-c electro- agnet, the flux versus ampere-turn haracteristics of the iron must be in- luded because generally the flux density n d-c magnets reaches higher levels than t does in a-c magnets.[1]

Appendix I

The permeance of a magnetic field in air an be estimated by a method described in eference 2. For the example used in this paper, a magnet as shown in Fig. 3 is used. The letter symbols used for dimensions are ndicated on Fig. 3 except for two dimen- sions, H and K. Let K represent the dis- tance from the bottom of the coil slot to the top of the copper winding (neglecting the insulation on top of the coil). Let H repre- sent the actual height of the copper winding measured in the same direction as dimen- sion D. By applying the methods referred to previously, it is possible to write the fol- lowing expressions:

$$\mathcal{P}_c=\mu\left[\frac{AW}{G+G_p}+0.52A+1.04W+0.48\times(G+G_p)+\frac{2A}{\pi}\ln\left(\frac{C+\frac{D}{2}}{G+G_p}+1\right)+\frac{C}{2}+\frac{D}{4}\right] \quad (23)$$

$$\mathcal{P}_o=\mu\left[\frac{BW}{G}+0.52B+0.78W+0.39G+\frac{0.64C(2E+A)}{C+D+G}+\frac{2B+W}{\pi}\times\ln\left(\frac{C+\frac{D}{2}}{G}+1\right)+\frac{C}{2}+\frac{D}{4}\right] \quad (24)$$

$$\mathcal{P}_L=\mu\left[\left(\frac{2W}{E}+1.04+\frac{4}{\pi}\ln\left(\frac{A}{E}+1\right)\right)\times\left(\frac{H}{3}+D-K\right)+0.52W+0.31E\right] \quad (25)$$

$$\mathcal{P}_T=\frac{2\mathcal{P}_0\mathcal{P}_c}{2\mathcal{P}_0+\mathcal{P}_c}+\mathcal{P}_L \quad (26)$$

where

$\mathcal{P}_c$ = permeance of air gap at center pole
$\mathcal{P}_0$ = permeance of air gap at each outer pole
$\mathcal{P}_L$ = leakage permeance
$\mathcal{P}_T$ = total magnet permeance

It is now possible to calculate the average force developed by this magnet when the magnet is held at any particular fixed gap. Under this condition the current equals

$$I=\frac{E}{\sqrt{R_c^2+\omega^2N^4\mathcal{P}_T^2}} \quad (27)$$

The average force can be calculated with equation obtained from reference 2.

$$F_M=4.43(NI)^2\frac{d\mathcal{P}_T}{dG}\text{ pounds} \quad (28)$$

For the example used in this paper, the following dimensional values are assumed:

$A=0.672$ inch
$B=0.400$ inch
$C=0.375$ inch
$D=1.125$ inches
$E=0.577$ inch
$H=0.934$ inch
$K=1.014$ inches
$W=0.622$ inch
$G_p=0.008$ inch
$N=2{,}200$ turns
$R_{coil}=99$ ohms
$\omega=377$
$E=230$ volts rms
$\bar{\mu}=3.19\times10^{-8}$ webers per ampere-turn–inch
$m=0.337/(8.86\times386)$ joules per inch/inch per second^2
$\Delta t=0.0002$ second

If the force developed at each gap is plotted against the gap, the curve shown by the broken line in Fig. 2 results.

Appendix II

In order to solve this problem it is necessary to write the proper equation which is expressed as a diagram in Fig. 1. Since the body of this paper describes the transition from an integral expression to a finite difference expression for each term, this equation is expressed below in finite difference form:

$$W_e+\frac{e_0+e_t}{2}\left(i_{c0}+\frac{\Delta i_c}{2}\right)\Delta t=W_L+\frac{F_{L0}+F_{LT}}{2}\Delta X+W_c+R_c\left(i_{c0}^2+i_{c0}\Delta i_c+\frac{\Delta i_c^2}{3}\right)\Delta t+W_t+\frac{\Delta t}{R_t}\left[\left(\frac{e_0+e_t}{2}\right)^2-(e_0+e_t)\times\left(i_{c0}+\frac{\Delta i_c}{2}\right)R_c+\left(i_{c0}^2+i_{c0}\Delta i_c+\left(\frac{\Delta i_c}{2}\right)^2\right)R_c^2\right]+W_f+F_f|\Delta X|+\frac{1}{2}N^2(i_0^2+2i_0\Delta i_c+\Delta i_c^2)\mathcal{P}_{Te}+\frac{1}{2}mV_t^2 \quad (29)$$

where

$i_0=i_{c0}-i_{e0}-i_{s0}$

After ΔX has been found by the use of equations 18–21, this equation can be solved for Δi_c.

$$(\Delta i_c)^2\left[R_c\frac{\Delta t}{3}+\frac{R_c^2}{R_t}\frac{\Delta t}{4}+\frac{N^2}{2}\mathcal{P}_{Tt}\right]+(\Delta i_c)\left[-\left(\frac{e_0+e_t}{2}\right)\left(\frac{\Delta t}{2}\right)+R_ci_{c0}\Delta t-(e_0+e_t)\frac{R_c}{R_t}\left(\frac{\Delta t}{2}\right)+\frac{R_c^2}{R_t}i_{c0}\Delta t+N^2i_0\mathcal{P}_{Tt}\right]+\left[-W_e-\frac{e_0+e_t}{2}i_{c0}\Delta t+W_L+\frac{F_{L0}+F_{LT}}{2}\Delta X+W_c+R_ci_{c0}^2\Delta t+W_t+\left(\frac{e_0+e_t}{2}\right)^2\frac{\Delta t}{R_t}-(e_0+e_t)\frac{R_c}{R_t}i_{c0}\Delta t+\frac{R_c^2}{R_t}i_{c0}^2\Delta t+W_f+F_f|\Delta X|+\frac{N^2}{2}i_0^2\mathcal{P}_{Tt}+\frac{1}{2}mVt^2\right]=0 \quad (30)$$

This is a quadratic equation in Δi_c which can be solved with the quadratic formula. There is a problem as to which sign to use for the radical in the quadratic formula. The following criterion was established because it works well in the actual problem:

If $i_{co}\geq 0$

$$\Delta i_c=\frac{-b+\sqrt{b^2-4ac}}{2a}$$

If $i_{co}<0$

$$\Delta i_c=\frac{-b-\sqrt{b^2-4ac}}{2a}$$

References

1. The Analytical Design and Evaluation of Electromagnets, J. Kelly, J. E. Wallace. *AIEE Transactions*, pt. I (*Communication and Electronics*), vol. 75, 1956 (Jan. 1957 section), pp. 675–80.

2. Electro-Magnetic Devices (book), Herbert C. Roters. John Wiley & Sons, Inc., New York, N. Y., 1941, chap. V, pp. 196–200, 423.

Design of Servo Compensation Based on the Root Locus Approach

E. R. ROSS
STUDENT MEMBER AIEE

T. C. WARREN
STUDENT MEMBER AIEE

G. J. THALER
MEMBER AIEE

IN GENERAL, the system function of a linear feedback control system may be symbolized by

$$\frac{\theta_C}{\theta_R}(s)=\frac{G(s)}{1+GH(s)} \qquad (1)$$

where

$\theta_C(s)$ = the Laplace transform of the output
$\theta_R(s)$ = the Laplace transform of the input
$G(s)$ = the forward transfer function
$GH(s)$ = the loop transfer function

Furthermore the characteristic equation of the closed-loop system may be defined by

$$1+GH(s)=0 \qquad (2)$$

and the roots of the characteristic equation may be evaluated by the usual root locus plot of the loop transfer function.

In the usual design, the steady-state error is limited by specifying a minimum gain, which is usually designed as K_p, K_v, K_a, etc., depending upon the number of integrations in the loop transfer function. With such a gain specification, the locations of the roots of the uncompensated system are usually not satisfactory, and compensation must be used. The designer can usually interpret his specifications in terms of a desired location for a pair of complex conjugate roots which should dominate the system response characteristics. This paper presents a method for computing the poles and zeros of a compensator which will force roots to exist at the designated locations with the specified open-loop gain. The method is exact, it may be applied for either a cascaded compensator or a compensator in a feedback loop, and it yields numerical answers for the pole and zero locations in a few minutes.

Paper 60-779, recommended by the AIEE Feedback Control Systems Committee and approved by the AIEE Technical Operations Department for presentation at the AIEE Summer General Meeting, Atlantic City, N. J., June 19–24, 1960. Manuscript submitted November 2, 1959; made available for printing March 28, 1960.

E. R. Ross, Lt., Royal Canadian Navy, is with the Department of National Defense (Navy), Ottawa, Ont., Canada. T. C. Warren, Lt., United States Navy, is stationed on the *USS Helena*. G. J. Thaler is with the United States Naval Postgraduate School, Monterey, Calif.

Basic Theory

Assume that a designer is given a feedback control system with loop transfer function $GH(s)$, such that the poles and zeros of $GH(s)$ are known and the gain constant has been adjusted to satisfy minimum gain requirements, and given also the s-plane co-ordinates for a desired pair of complex roots which are to be realized by compensation without altering steady-state accuracy. The solution to this problem may be considered in two parts, first, the root locus must be altered so that some segment of the root locus passes through the designated root points, and second, the design must force the roots to lie at the selected points. In general, the first of these requirements may be satisfied by a multiplicity of compensators; an infinite number of pole-zero combinations can force the root locus to pass through the designated root point. When the gain requirement is added, however, the number of possible solutions is restricted. If it is possible to make the root locus pass through the selected point with a single-pole single-zero compensator, then only one such compensator can be found which also satisfies the gain requirement. If several sections are to be used the solution is not unique, but for identical cascaded sections certain restrictions may be determined as will be shown.

Derivation of the equations for the compensator design is readily accomplished, as may be explained with the aid of Fig. 1. The root location, r, is specified as are the poles and zeros of $GH(s)$, which are not shown in Fig. 1, and the gain (K_p, K_v, K_a) is also known. The point r is not on the root locus of the uncompensated system, therefore the phase at this point is not $180n$ degrees, but some other angle which may be computed by substituting the s co-ordinates of the root point into $GH(s)$, or by use of the spirule. The angle which a compensator must provide to make r lie on the root locus is readily determined by subtraction, and is designated in Fig. 1 as the angle ϕ. In like manner the root locus gain at $s=r$ may be evaluated from $GH(s)$

$$G \triangleq \left|\frac{r^n(r+P_1)(r+P_2)\dots}{(r+z_1)(r+z_2)\dots}\right|$$

This gain value, G, may also be evaluated analytically or by using a spirule. The vector ratio contributed by the compensator is

$$g=\left|\frac{a}{b}\right|$$

when the compensator is a single-zero single-pole filter, and a and b are the distances from the zero and pole to r, as defined by Fig. 1. The root locus gain of the compensated system at point r is G/g.

To satisfy steady-state requirements it is necessary that

$$K=\frac{G\alpha}{g} \qquad (8)$$

where

K = gain constant of the uncompensated system
$\alpha=z/p$ for the compensator (see Fig. 1)

From these relationships, and Fig. 1,

$$\alpha=\frac{z}{P}=\frac{z}{z+c}=\frac{gK}{G}=\frac{aK}{bG} \qquad (8)$$

$$\frac{z}{a}=\frac{K(z+c)}{bG}=\frac{\sin(\lambda-\phi)}{\sin\delta} \qquad (8)$$

$$\frac{z+c}{b}=\frac{\sin\lambda}{\sin\delta} \qquad (8)$$

and by manipulation

$$z=\frac{hK}{G}\frac{\sin\lambda}{\sin\theta} \qquad (8)$$

$$z+c=P=\frac{h\sin\lambda}{\sin(\theta-\phi)} \qquad (10)$$

where

$$\lambda=\cot^{-1}\left(\cot\phi-\frac{K}{G}\csc\phi\right)$$

$$\theta=\pi+\phi-\delta-\lambda$$

Equations 9 and 10 give the locations of the required zero and pole. Note that k, K, G, ϕ, and δ are effectively given by

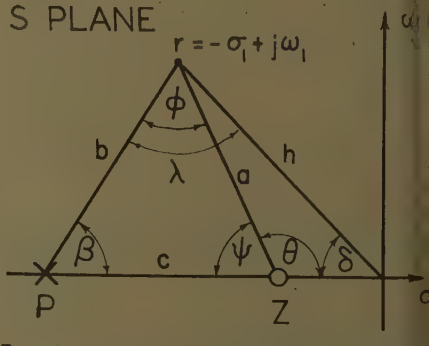

Fig. 1. s-plane diagram for the derivation of equations

pecifications, and λ and θ are readily uted.

r a double-section lead compensator ly the same approach may be used erive the equations and the result

$$\sqrt{\frac{K}{G}}\frac{\sin\lambda_2}{\sin\theta_2} \tag{11}$$

$$=P=\frac{h\sin\lambda_2}{\sin(\theta_2-\phi_2)} \tag{12}$$

re

$$\cot^{-1}\left(\cot\phi_2-\sqrt{\frac{K}{G}}\csc\phi_2\right)$$

$$\pi+\phi_2-\delta-\lambda_2$$

$$\phi/2$$

the subscript 2 is used to designate t the zero and pole are repeated.

or a larger number of identical sec- ns the equations are

$$h\sqrt[n]{\frac{K}{G}}\frac{\sin\lambda_n}{\sin\theta_n} \tag{13}$$

$$=\frac{h\sin\lambda_n}{\sin(\theta_n-\phi_n)} \tag{14}$$

ere

$$=\cot^{-1}\left(\cot\phi_n-\sqrt[n]{\frac{K}{G}}\csc\phi_n\right)$$

$$=180°+\phi_n-\delta-\lambda_n$$

$$=\phi/n$$

For a phase-lag compensator the pole is oser to the origin than the zero, and the gle ϕ becomes negative. The equa- ons for this case are the same as for the se of phase lead, it is only necessary to e the proper sign with ϕ.

When the gain is not restricted the mpensator pole and zero may be laced at any locations which satisfy the equirement for the angle ϕ. The sim- lest approach in this case is to select ne of the points (perhaps the zero) rbitrarily, then lay off the angle ϕ with a protractor to locate the other point (pole).

Root Relocation Zones

When there are no restrictions on the ocations of the compensator pole and ero, and no gain restriction, a root may e located at any point in the s-plane by se of a single-pole single-zero compensa- or, see Appendix I. The addition of estrictions on gain, and on the location of compensator poles and zeros places limita- ions on the regions in the s-plane where roots can be located with a single-pole single-zero compensator. For any given system it is easy to subdivide the s-plane into root relocation zones. One set of dividing lines are the root loci themselves, which are loci of $180N$ degrees ($N=-1, -3, -5 \ldots$). A second set of dividing lines are the phase angle loci for $2n\pi$ ($n=0, 1, 2, 3 \ldots$). The areas bounded by these lines may be labeled lag areas and lead areas. Lag areas are 0 to 180 degrees; 360 to 540 degrees; 720 to 900 degrees; etc. Lead areas are 180 to 360 degrees; 540 to 720 degrees; 900 to 1,080 degrees, etc. The type of compensation required to reshape a root locus through a selected point is normally designated by the type area in which the selected point lies. This is true whether there are restrictions on gain, etc., or not. If there is no restriction on gain or on pole-zero location, then a root may be relocated at any point in the designated zone with a single-pole single-zero compensator. When the gain restriction is added, and the compensator pole and zero are restricted to the negiatve real axis, then a single-pole single-zero compensator can relocate a root only in a limited subarea of each relocation zone. The dividing lines on the s-plane which define the limits for single-section compensators may be determined very simply by drawing pseudo-root loci according to the following rules:

To find the dividing line for a single-section lead compensator draw the root loci for a pole-zero configuration which consists of all of the zeros of the original open-loop function (but none of the poles) plus an additional zero at the origin, plus a pole located at each root of the uncompensated system. The pseudo-root loci obtained from this pole-zero configuration subdivide the original lead areas into an area for single lead section compensation and an area for multiple lead section compensation.

To find the dividing line for a single-section lag compensator draw the root loci for a pole-zero configuration, which consists of all of the poles (but none of the zeros) of the original open-loop function plus an additional pole at the origin plus a zero located at each root of the mpensated system. The pseudo-root loci obtained in this fashion subdivide the original lag areas into a single lag section area and a multiple lag section area. Proof that these rules are valid is given in Appendix II.

The root relocation zones defined in this fashion permit the designer to select the desired root location, determine the type of compensation required, and determine whether one or more sections of compensator are required. (The pseudo-root loci define an absolute limit on single-section compensation. If a root relocation point is selected too near this line in the single-section zone, the resulting pole-zero ratio may not be practical.) If the selected root relocation point is in a multiple section zone, the designer may decide to use several identical sections, or may obtain several nonidentical section by repeated application of single-section design.

The Design Procedure

1. Draw the root locus of the uncompensated system, and locate the roots using the specified K.
2. Construct the root relocation zones.
3. Select the point at which a root is to be relocated.
4. Determine ϕ and G at the selected point.
5. Apply equations 9 and 10 if a single-section compensator is needed, or equations 11 and 12 for two identical sections, or equations 13 and 14 for n number of sections.

If several nonidentical sections are desired, step 5 is altered as is shown later.

Applications of the Design Procedure

Single Lead Section Compensation

Consider the second-order type 2 system defined by

$$G(s)=\frac{400}{s^2} \tag{15}$$

The original root locus is shown in Fig. 2, with roots at $\mp j$ 20. The entire left-half plane is the lead area, the right-half plane is the lag area. Addition of the pseudo-root loci subdivides these areas into single lead, single lag, multiple lead, and multiple lag zones. It is desired to relocate the roots at $-15\mp j$ 22.5, and by inspection this can be done with a single lead section. The computations are as follows:

The root locus phase at the point is $\phi_1=248°$ from which $\phi=68°$.

$\delta=56°$

$G=(27)(27)$

$h=27$

$\frac{K}{G}=\frac{400}{729}=0.548$

$\lambda=\cot^{-1}(\cot 68°-0.548\csc 68°)=100.7°$

$\theta=180+68-56-100.7=91.3°$

Note that $\theta>\phi$ which checks the requirement for a single lead section. Using equations 9 and 10

$$z=\frac{hK\sin\lambda}{G\sin\theta}=14.5$$

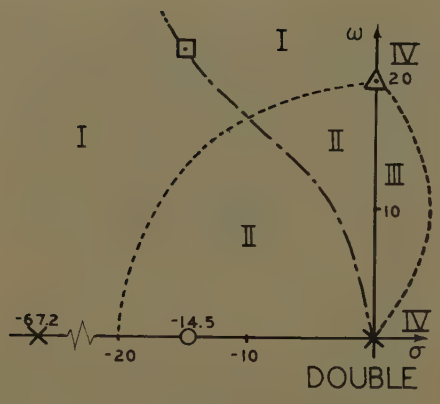

Fig. 2. $KG(s)=\frac{400}{s^2}$, **compensated to give** $KG(s)=\frac{1830(s+14.5)}{s^2(s+67.2)}$, **with constant** K_a

△ = Original root, ⊡ = Final root, — Original root locus, — — — Final root locus, ... Limit lines. I. Single-section lead area. II. Multiple-section lead area. III. Single-section lag area. IV. Multiple-section lag area. These symbols are used in all remaining figures

$$P=\frac{h\sin\lambda}{\sin(\theta-\phi)}=67.2$$

Therefore, the compensated system transfer function is

$$KG(s)=\frac{1830\,(s+14.5)}{s^2(s+67.2)} \qquad (16)$$

The root loci for the compensated system are also shown in Fig. 2.

Consider the second-order type 1 transfer function

$$G(s)=\frac{100}{s(s+5)} \qquad (17)$$

The roots of the closed-loop system are at $-2.5\mp j\,9.2$, and it is desired to relocate the roots at $-14.14\mp j\,14.14$. The root relocation zones are sketched as shown in Fig. 3, and it is seen that the desired root location is in a single lead section zone. The following values are readily computed.

$\phi=78°$ $\qquad h=20$
$\delta=45°$ $\qquad \lambda=94.9$
$G=340$ $\qquad \theta=118.1$
$K/G=0.295$

Applying equations 9 and 10

$z=-6.67$ $\qquad P=31.0$

The compensated transfer function is

$$G(s)=\frac{454(s+6.67)}{s(s+5)(s+31.0)} \qquad (18)$$

and the compensated root locus is shown in Fig. 3.

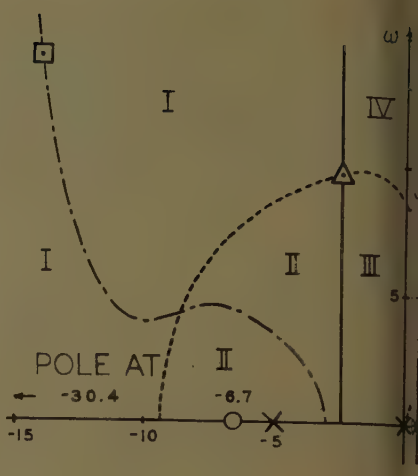

Fig. 3. $KG(s)=\frac{100}{s(s+5)}$ **compensated constant** K_v **to give** $KG(s)=\frac{454(s+6.$
$s(s+5)(s+36$

Compensation with Two Lead Sections

Consider the third-order type 1 system defined by

$$G(s)=\frac{420}{s(s+1)(s+15)} \qquad (19)$$

The original root locus is shown in Fig. 4 and the system is unstable. It is desired to relocate the roots at point B, and construction of the root relocation zones shows that multiple lead sections are required. Computing values at point B,

$\phi=117°$ $\qquad K/G=0.1375$
$\delta=59\frac{1}{2}°$ $\qquad h=14.62$

Assuming two lead sections,

$\phi_2=58\frac{1}{2}°$
$\lambda_2=79.9$
$\theta_2=99.1°$

Since $\theta_2>\phi_2$ two sections are enou
Then $\sqrt{K/G}=0.371$ and using equati
11 and 12

$$z=\frac{h\sqrt{K/G}\sin\lambda_2}{\sin\theta_2}=5.4$$

$$P=\frac{h\sin\lambda_2}{\sin(\theta_2-\phi_2)}=22.1$$

From which the compensated trans
function is

$$G(s)=\frac{6950(s+5.4)^2}{s(s+1)(s+15)(s+22.1)^2}$$

The compensated root locus is shown
Fig. 5. Insertion of the two identi
sections introduces a pair of comp
conjugate roots as shown.

A root may be located at point B
Fig. 4 using two nonidentical lead s

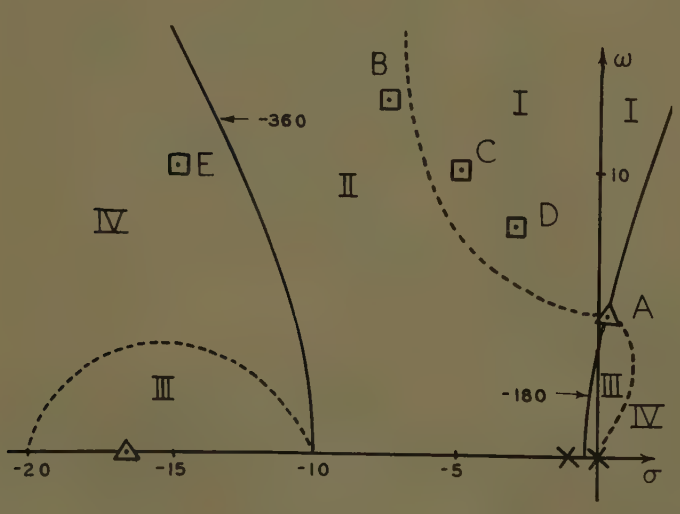

Fig. 4. Root locus and limit lines for the system $KG(s)=\frac{420}{s(s+1)(s+15)}$

B, C, D, E—Root locations referred to in text

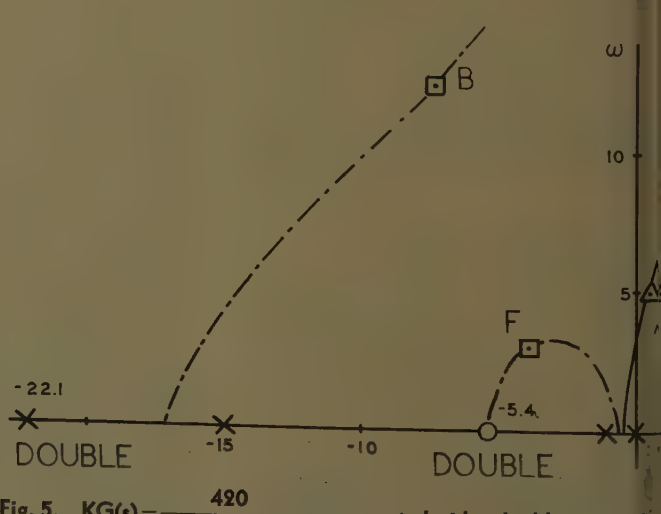

Fig. 5. $KG(s)=\frac{420}{s(s+1)(s+15)}$ **compensated with a double section le**
compensator for constant K_v **to give** $KG(s)=\frac{6950(s+5.4)^2}{s(s+1)(s+15)(s+22.1}$
F = introduced root

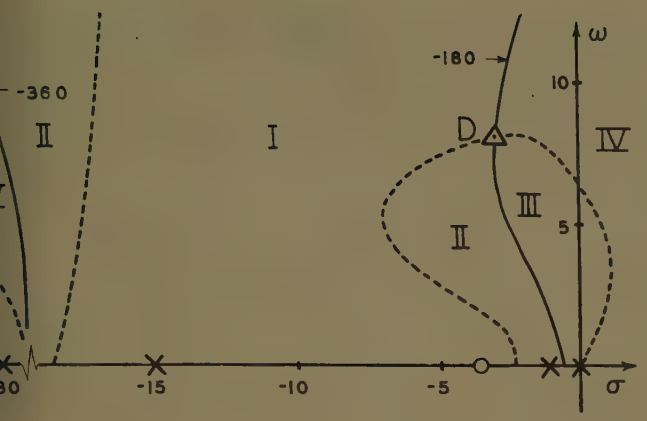

6. Root locus and root relocation zones for first step of successive ingle-section lead compensators $KG(s)=\frac{3570(s+3.54)}{s(s+1)(s+15)(s+30.1)}$

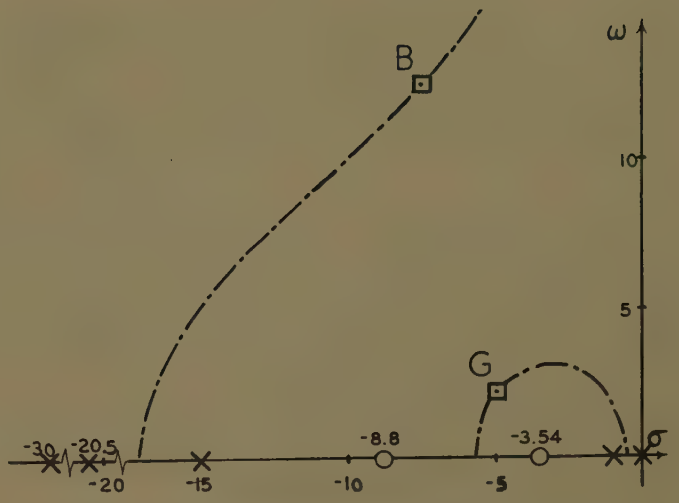

Fig. 7. Final root locus of $KG(s)=\frac{8300(s+3.54)(s+8.8)}{s(s+1)(s+15)(s+20.5)(s+30.1)}$
G = introduced root

ns by simply repeating the single-sec- n design procedure with judicious oice of an intermediate root location. point D in the single-lead section zone hosen as the point at which the root is be located in the first step, then at int D

=70°	$K/G=0.417$
69°	$\lambda=94.5°$
=8.55	$\theta=86.48°$

en using equations 9 and 10, $z=3.54$ d $p=30.1$.

The transfer function for the partially mpensated system is

$$s)=\frac{3570(s+3.54)}{s(s+1)(s+15)(s+30.1)} \qquad (21)$$

ne root loci are shown in Fig. 6 with root location zones added to show that point now lies in a single lead zone. At oint B, using equation 21

=40°	$\lambda=76.8°$
=59°	$\theta=84°$
$/G=0.615$	$h=14.6$

gain using equations 9 and 10, $z=8.8$ nd $p=20.5$.

The compensated root loci are shown in ig. 7. Note that there is little difference etween the introduced roots in Fig. 7 nd those in Fig. 5.

INGLE LAG SECTION COMPENSATION

Consider the high-gain-type zero trans- r function

$$(s)=\frac{3.72\times10^6}{(s+5)(s+15)(s+25)(s+35)} \qquad (22)$$

he root loci for the system are shown in ig. 8. The high gain places complex oots in the right-half plane, and construc- ion of the root relocation zones indicates hat compensation without reducing K_p equires multiple lead sections, or a single ag section. It is decided to use the single lag section relocating the roots at $-5\mp j$ 7. Using the usual computations

$\phi=-21.7°$
$h=8.7$
$K/G=69.0$
$\delta=54.7°$
$G=5.40\times10^4$
$\theta=103.7°$

$$\lambda=\cot^{-1}[\cot(-21.3°)-69.0\csc(-21.3°)]$$
$$=\cot^{-1}\left[(-2.54)-(69.0)\left(-\frac{1}{0.3665}\right)\right]$$
$$=\cot^{-1}[-2.54+188]=\cot^{-1}185.46$$
$$=0.31°$$

From which $z=3.28$, $p=0.0492$.

The compensated transfer function becomes

$$G(s)=\frac{6.45\times10^4(s+3.28)}{(s+0.0492)(s+5)(s+15)(s+25)(s+35)} \qquad (23)$$

USE OF TWO LEAD SECTIONS INSTEAD OF FOUR LAG SECTIONS

Consider the transfer function of equation 19, and the root location zones of Fig. 4. It is desired to place complex roots at point E, $(s=-15\mp j\ 10)$. This point lies in a multiple lag zone, and upon checking it is found that four identical lag sections are required if lag compensation is used On the other hand, if a lead compensator is desired to place a root at C $(s=-5\mp j\ 10)$ and root relocation zones are drawn as in Fig. 9, it is seen that point E now falls within a single lead zone.

The compensator required to place the root at C is

$$G_c(s)=\frac{s+2.71}{s+73}$$

which is not a desirable attenuation ratio, but the compensator required to make the final relocation at E is

$$G_c=\frac{s+14.8}{s+40.3}$$

so the compensated transfer function is

$$G(s)=\frac{31{,}800(s+2.71)(s+14.8)}{s(s+1)(s+15)(s+40.3)(s+73)} \qquad (24)$$

and the composite compensator is satisfactory. The final root locus is shown in Fig. 9.

Conclusions

An analytic method has been developed for obtaining the required compensator parameters to permit arbitrary location of the closed-loop roots for feedback control systems for arbitrarily designated gain. The method is aided by the definition of root relocation zones which provide a visual guide in the application of the

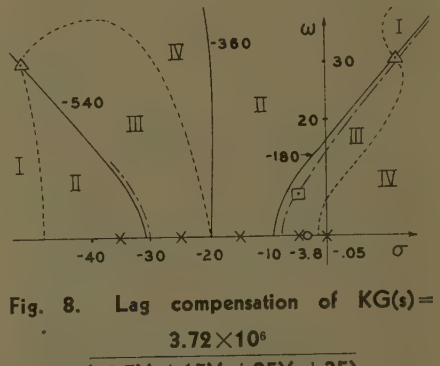

Fig. 8. Lag compensation of $KG(s)=\frac{3.72\times10^6}{(s+5)(s+15)(s+25)(s+35)}$ with constant K_p to give $KG(s)=\frac{6\times10^4(s+3.8)}{(s+5)(s+15)(s+25)(s+35)(s+0.05)}$

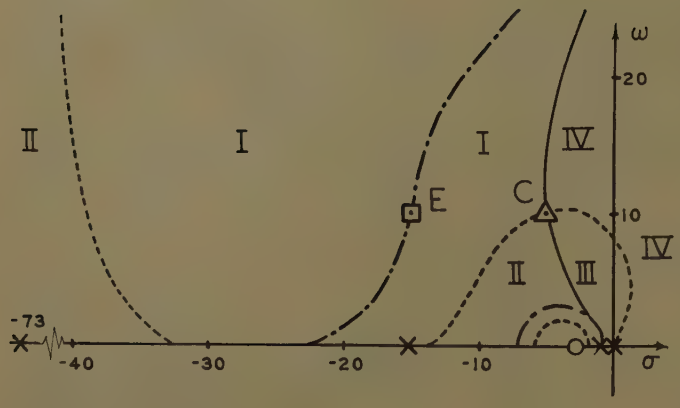

Fig. 9. First-step compensation and final root locus for relocation to point E; original system

$$KG(s)=\frac{420}{s(s+1)(s+15)}$$

First step compensated system: $KG(s)=\frac{11700(s+2.71)}{s(s+1)(s+15)(s+73)}$

Final system: $KG(s)=\frac{31800(s+2.71)(s+14.8)}{s(s+1)(s+15)(s+40.3)(s+73)}$

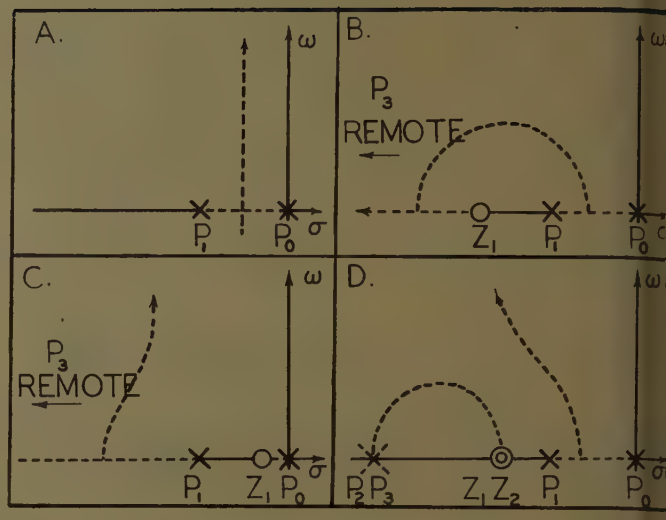

Fig. 10. Effect of compensators on root loci on the s-plane

A—Two-pole root locus
B—Locus with lead compensator with remote pole
C—Effect of moving zero inside P_1
D—Effect of double-section phase lead compensator

method. The method is flexible, fast, and accurate.

Appendix I

When there are no restrictions on gain, or on pole and zero locations, a single-pole single-zero compensator can normally reshape the root locus to pass through any selected point on the s-plane. This can be illustrated with a simple two-pole root locus as shown in Fig. 10(A). Using a single lead section the root locus may be made to pass through any selected point to the left of the uncompensated root locus as may be seen from Fig. 10(B), in which the pole of the lead section is assumed to be far out on the negative real axis. In this case the original root locus is bent into a closed curve, and if the location of the zero is shifted on the real axis, then the radius of the root-locus curve changes, and the locus may be passed through any selected point. If the zero is moved to the right of P_1 a real root is introduced near the origin, but the complex roots remain to the left of the original root locus as shown by Fig. 10(C). Moving the pole of the compensator merely provides a multiplicity of loci through any selected point, but these loci are still restricted to the designated area. In like manner when a single-section lag compensator is used, the complex roots are restricted to the right of the original root locus, and it is possible that the equations may specify a pole in the right-half plane. Thus, for a simple two-pole system, the complex roots can be relocated at any point on the s-plane by a single-section compensator providing there are no restrictions on the gain or the real axis locations of the compensator pole and zero.

When additional restrictions are considered, multiple-section compensators may be required. At least two additional roots are introduced by such compensators. Fig. 10(D) illustrates the case of a double lead section used with the two-pole system. From Fig. 10(D) it is seen that the introduced roots may be complex, and it is not immediately obvious which of the two segments of root locus will pass through an arbitrarily specified point.

Appendix II

Introducing the restriction that the compensation must locate a root at the designated point with a specified value of gain (K_p, K_v, K_a) so as to limit the error, it is immediately apparent that the root relocation zones require more detailed definition. The basic lead and lag areas are not changed, but the simultaneous restrictions of a single-section compensator and a specified gain can be satisfied only in a subsection of the designated area. From Fig. 1 it can be seen that for a phase lead compensator, as ϕ increases the compensator pole moves out on the negative real axis, approaching infinity. In the limit, $\phi=\theta$ for the pole located at infinity. Thus, when using a single-section phase lead compensator the phase angle requirement is

$$0<\phi<\theta \qquad (25)$$

which may also be seen from equation 1
The maximum displacement of the ro
from its uncompensated location, for
specified gain and using a single lead se
tion, is a locus of points defined for th
compensator pole at infinity and th
zero swept along the negative real axi
The equations which must be satisfied a

$$\cot\lambda=\cot\phi-\frac{K}{G}\csc\phi \qquad (2$$

$$\theta=180^\circ-\delta-\lambda+\phi \qquad (2$$

$$\theta=\phi \qquad (2$$

In like manner, a limit line is defined fo
a single-section phase lag compensato
except that the limit is defined for th
zero at infinity and the pole swept alon
axis. Equations 26 and 27 apply, but th
restriction on θ is

$$\theta\geqq 0 \qquad (2$$

These limit lines may be computed poin
by point using the equations but it
more convenient to introduce a fictitiou
pole-zero configuration and plot pseud
root loci which are identically the desire
limit lines for root location by a singl
section compensator.

To show that the pseudo-root locu
does coincide with the single-section lim
lines, consider the general open-loop tran
fer function

$$KG(s)=\frac{KY_1(s)}{Y_2(s)} \qquad (3$$

The characteristic equation of the corr
sponding closed loop is

$$1+KG(s)=0 \text{ or } Y_2(s)+KY_1(s)=0 \qquad (3$$

Let the system be compensated by

ase lead compensator such that the
npensator pole is allowed to approach
nus infinity. This is equivalent to the
roduction of a zero. The limiting
en-loop transfer function for the com-
nsated system is

$$G_1(s)=\frac{K_1(s+z_1)Y_1(s)}{Y_2(s)} \quad (32)$$

ere the value of K_1 is not specified.
e characteristic equation of the corre-
onding closed loop is

$$1+K_1G_1(s)=0 \text{ or } Y_2(s)+K_1(s+z_1)Y_1(s)=0 \quad (33)$$

z_1 is swept along the negative real axis
th K_1 continuously adjusted to keep the
gain (K_p, K_v, K_a) constant, the roots of the characteristic equation are swept along a locus which is a limit line for a single-section lead compensator.

There exists on open-loop transfer function for which the root loci (here called pseudo-root loci) are identically the limit lines for the compensated system. This open-loop transfer function is

$$K_2G_2(s)=\frac{K_2sY_1(s)}{Y_2(s)+KY_1(s)} \quad (34)$$

where the value of K_2 is not specified. That this is the correct transfer function may be seen from the characteristic equation

$$Y_2(s)+KY_1(s)+K_2sY_1(s)=0 \quad (35)$$

since equations 33 and 35 are identical if we define $K_2=K_1$ and $K=K_1z$. By a similar manipulation the proof may be extended to the phase lag case.

References

1. Control-System Dynamics (book), Walter R. Evans. McGraw-Hill Book Company, Inc., New York, N. Y., 1954.

2. Synthesis of Feedback Control System by Phase-Angle Loci, Yaohan Chu. *AIEE Transactions*, pt. II (*Applications and Industry*), vol. 71, Nov. 1952, pp. 330–39.

3. Servomechanism Analysis (book), George J. Thaler, Robert G. Brown. McGraw-Hill Book Company, Inc., first edition, 1953.

Discussion

. R. Evans (Aeronutronic, Newport
each, Calif): The authors are to be
mmended not only for the original work
t for the condensation no doubt required
submit it in this paper. The purpose of
is discussion is largely to insert a few
eps which other readers may find helpful.
In equation 5 the gain K based on G in
uation 3 is greater than K_p, K_v, or K_a by
e factor, $p_2p_2 \ldots /z_1z_2 \ldots$. In equation
for example $K_v=420/15$.
In equation 10 divide s/a from equa-
on 7 by $(s+c)/b$ from equation 8 as the
st step in developing the equation for
mbda.
Consider the general lead network mak-
g the open loop function in Appendix II

$$K_1G_1(s)=\frac{KY_1(s)}{KY_2(s)}\,\frac{(1+T_1s)}{(1+T_2s)} \quad (36)$$

Setting this function equal to -1, clearing the denominator, and regrouping gives

$$[K_1Y_1(s)+Y_2(s)]\,[1+T_2s]+(T_1-T_2)s\,KY_1(s)=0 \quad (37)$$

For $T_1-T_2=0$, the roots must be $-1/T_2$ and the zeros of the uncompensated function given in equation 31. For T_1-T_2 infinite, the roots must be the origin and the zeros of $Y_1(s)$.

Denoting the uncompensated roots as r_1, r_2 etc., equation 2 can be rewritten as

$$\frac{(T_1-T_2)s\,KY_1(s)}{[K'(1-s/r_1)(1-s/r_2)\ldots][1+T_2s]}=-1 \quad (38)$$

The root locus of equation 38 with (T_1-T_2) is the limit of the single lead network for T_2 constant. Making T_2 zero rather than small can be shown to eliminate a phase lag at a typical root r_1 so that the locus has maximum change in directio from its original path.

E. R. Ross, T. C. Warren, and G. J. Thaler: We wish to thank Mr. Evans for his interest, and for the clarification of some important points. It should also be noted that the techniques developed in this paper can be extended and amplified. Some extensions[1] have already been investigated. It is possible to construct limit lines for two identical sections. It is also possible to construct loci of constant $x=z/p$ within the single-section zone. The additional labor involved is not excessive, but the advantage gained is not enough to make these techniques attractive.

Reference

1. Compensation of Servomechanisms Using Root Relocation Zone Concepts, Oscar E. Sanden, Jr. *Master's Thesis*, U. S. Naval Postgraduate School, Monterey, Calif., 1960.

Aircraft Storage Batteries

WALTER J. HAMER
MEMBER AIEE

LEAD-ACID, nickel-cadmium, and silver-zinc storage batteries have been used, or have been proposed for use, in commercial and military aircraft. Each one of these electrochemical systems has characteristics that recommend it for service in aircraft. Lead-acid batteries, dating from the double-chamber Mark 1–7 series, have been used for a long time in such service and are well adapted to the conventional electric circuits used in airplanes. Nickel-cadmium batteries may be "hermetically" sealed, an obviously desirable characteristic, and exhibit good outputs over a wide range of discharge rates. Silver-zinc batteries give high electrical output per unit weight and volume, a most desirable characteristic for aircraft where weight and volume are at a premium. Recently, a fourth system, the silver-cadmium battery, has been proposed but insufficient data are presently available to predict its over-all performance.

In present-day aircraft where nominal 24-volt d-c electric systems are the most common, 24-volt batteries are used. This necessitates the use of 12 cells in lead-acid, 19–20 cells in nickel-cadmium, and 14 cells in silver-zinc batteries. The individual cells are insulated from each other by glass, plastic, rubber linings, or other insulating material, and the cell terminals are connected by high-current-carrying intercell connectors. Lead is used for the intercell connectors for lead-acid batteries and nickel-plated copper is invariably used for the alkaline nickel-cadmium and silver-zinc batteries. A quick-disconnect receptacle is mounted on the side near the top of the battery and is used with a high-current-carrying lead to the bus bar of the aircraft electric circuit.

Individual lead-acid cells are housed in molded composition cases enclosed in aluminum containers covered with an acid-resistant plastic or bituminous material. The intercell connectors for lead-acid batteries are covered with a rubberized sealing compound. The vents of

Paper 60-849, recommended by the AIEE Chemical Industry Committee and approved by the AIEE Technical Operations Department for presentation at the AIEE Summer General Meeting, Atlantic City, N. J., June 19–24, 1960. Manuscript submitted March 22, 1960; made available for printing June 3, 1960.

Walter J. Hamer is with the National Bureau of Standards, Washington, D. C.

Table I. Specifications for Aircraft Storage Batteries

Characteristic	Battery: Lead-Acid (1)	Lead-Acid (2)	Nickel-Cadmium (1)	Nickel-Cadmium (2)	Silver-Zinc (1)	Silver-Zinc (2)	Silver-Zinc (3)
A—Capacity Determinations							
Weight, pounds	55	80	55	80	30	55	75
Height*	8 3/4	10 1/4	8 3/4	10 1/4	7 3/4	8 3/4	10 1/4
Length*	9 15/16	9 15/16	9 15/16	9 15/16	7 5/8	9 15/16	9 15/16
Width*	7 11/16	9 11/16	7 11/16	9 11/16	7 3/4	7 11/16	9 11/16
Volume†	0.387	0.570	0.387	0.570	0.265	0.387	0.570
Volts	24	24	24	24	24	24	24
No. of cells	12	12	19–20	19–20	17	17	17
Capacity, ampere-hours	20	34	20	34	30	50	75
Rates, amperes‡							
(a)	10	17	10	17	15	25	37.5
(b)	18.2	30	18.2	30	27	45	68
(c)	125	200	150	240	150	480	1,350§
Cutoffs, volts	19.2	19.2	19.2	19.2	18.2	18.2	18.2
	18.0	18.0	18.0	18.0	16.8	16.8	16.8
	14.4	14.4	14.4	14.4	13.3	13.3	11.9§
Charge rates							
Initial‖	8 (85%)	13 (85%)	8 (90%)	14 (90%)	12 (90%)	22 (90%)	34 (90%)
Finish‖	3 (55%)	5 (55%)	2 (40%)	3 (40%)	2 (17%)	4 (17%)	6 (17%)
Total	140±2%	140±2%	130±2%	130±2%	107±3%	107±3%	107±3%
B—Automatic Program (Cycles)							
Discharge, amperes, 1 hour	18.2	30	18.2	30	27	45	68
Charge, 2 hours‖	8 (85%)	13 (85%)	8 (90%)	14 (90%)	12 (90%)	22 (90%)	34 (90%)
Finish charge, 2 hours‖	3 (40%)	5 (40%)	2 (25%)	3 (25%)	2 (15%)	4 (15%)	6 (15%)
Total	122±5%	122±5%	115±5%	115±5%	115±3%	105±3%	105±3
Stand, hours							
After charge	1	1			1	1	1
After discharge			3	3	6	6	6
Cycles per day	4	4	3	3	2	2	2

* Maximum in inches.
† Maximum in cubic feet.
‡ (a) Also called the 2-hour rate.
(b) Also called the 1-hour rate.
(c) Also called the 5-minute rate at 80 F and the 3-minute rate at 0 F (for the silver-zinc battery the 4-minute rate at 0 F).
§ Intermittent.
‖ Plus or minus 5%.

each cell are supplied with special vent caps that permit escape of gas and prevent leakage of electrolyte. They are designed to operate in various positions. Nickel-cadmium cells are housed in plastic, steel, or nylon cases enclosed in steel or cast-aluminum containers. Nickel-cadmium batteries are of two types, vented and sealed. In the vented types free electrolyte is generally used; in the sealed types restricted electrolyte is used. The term "restricted electrolyte" applies when the electrolyte is largely confined in the battery separators; the term "free electrolyte" is used for an excess of electrolyte, i.e., when the electrolyte is not confined to the separators and extends above the upper edges of the plates. The sealed types are provided with a pressure-relief valve to release excessive gas pressure. Even when hermetically sealed they exhibit a slight release of gas. The vented types are provided with Bunsen seals. Silver-zinc cells are housed in plastic or nylon cases enclosed in a plastic-covered steel, fiber glass, or magnesium-alloy container. They are not sealed but retain electrolyte owing to the use of a Bunsen valve or a standpipe type of vent.

Since every pound added to a plane increases the take-off distance, weight of the batteries is of major concern. Thinner plates, closer spacings, and lighter materials are used in their construction. Lead-acid batteries use thin low antimony-lead grids or lead-plated grids with highly expanded active material, microporous-rubber or plastic separators, and in some cases glass-mat retainers. Sintered plates are used in nickel-cadmium batteries and are enclosed, as a rule, in nylon envelopes or retainers. Electroformed plates and cellulosic separators or envelopes are generally used in the construction of silver-zinc batteries. Sulfuric acid having a specific gravity of 1.280 is used in the lead-acid batteries, while the nickel-cadmium and silver-zinc batteries utilize an electrolyte of 30–35% potassium hydroxide.

A common standard size of aircraft battery is a cube, 10 inches on a side, weighing less than 80 pounds, with a nominal capacity of at least 34 ampere-hours at the 2-hour rate. Smaller sizes are also available. Lead-acid, nickel-cadmium, and silver-zinc batteries have all been made in sizes approximating the standard size, and therefore, when weight and space are considered, are interchangeable in aircraft. Specifications for these three types of aircraft batteries are listed in Table I. Two standard typ are available for both lead-acid and nick cadmium batteries and three standa types are available in silver-zinc batteri The charging and discharging rates f capacity determinations and for aut matic cycling are given, respectively, parts A and B of Table I.

Batteries in aircraft must survive seve environmental conditions. Tests of t batteries, therefore, must be both ele trical and physical. The batteries mu withstand abrupt temperature change changes in altitude, changes in fligh attitude, wide ranges in humidity, acce eration, vibration, shock, and even fungu growth. To compound the problems, th electric systems associated with th batteries in aircraft are also subjected t similar changes in environment. Sinc service conditions for batteries may b ideal under one environment but poo under another, any changes in the assoc ated electric circuit may be acute in re gard to the proper maintenance of th battery. This is especially true in regar to the charging of the batteries. Becaus of these severe conditions in aircraft serv ice, the laboratory testing of aircraf batteries becomes a difficult problem Even so, since one would hardly take of with a battery about which little o nothing is known, a realistic test of battery type is essential.

In this paper a testing program fo aircraft batteries is outlined which i based on three premises: (1) that the pro gram gives realistic data on the main characteristics of the batteries; (2) tha relative and meaningful data betwee samples are obtained; and (3) that al batteries, regardless of type, are to be used under identical conditions, i.e., with identical electric circuits for identical pur poses. The last premise may not be a very realistic one from the standpoint o the design and characteristics of the battery, but is a realistic one if economy in aircraft design and interchangeability of battery types are prerequisites.

In setting up a standard test procedure for aircraft batteries, cognizance must be taken of (1) the electric circuit used in aircraft, (2) the use to which the battery may be put, and (3) the speed with which the battery may be expected to be diverted from one application to another. Power in an aircraft is supplied by generators. At the main bus a voltage of 28 or 28.5 volts is maintained. The batteries float or are charged directly on this constant-potential bus. Because of the high power available in aircraft relative to battery capacity there is little tendency for the bus-bar voltage to fall as a result

the heavy currents at the beginning of a arge, and the batteries are, therefore, arged at constant potential. In this y the batteries are kept in readiness for ergency use. Generators with voltage gulators normally set at 27.7 volts con- tute a major portion of the electric rcuit. When a generator fails, a most likely occurrence, the battery is called on to supply power for the operation of ectric equipment such as radio, radar, d lighting. The battery also serves as source of stand-by power for the opera- on of retractable landing gear and in ilitary craft for the operation of gun rrets and bomb bays. Accordingly, en, except for their use as stabilizers in e electric circuits which requires little ergy, the batteries are called upon for ry little service during flight. Their e should, therefore, be long unless the atteries are mechanically defective ragile, for example) or are adversely fected by float charge. Under these nditions the testing of batteries under oat charge at constant potential may ffice for a battery evaluation.

On the ground, however, the battery ay be called upon for engine starting. t is this most severe requirement that overns aircraft battery design. An "air- raft start" may involve the starting of ll engines or the starting of one engine nd the auxiliary equipment which in turn tarts the other engines. In any case, the urrents required for engine starting may ange from 200 to 400 amperes, depending n the ambient temperature, and for jet ngines may be as high as 1,000 or 2,000 mperes. The batteries thus must be apable of sustaining high rates of dis- harge. After an aircraft start, the attery should be capable of being brought ack to full charge within a few minutes o that the full capacity of the battery ay be available for other applications. When the battery is fully discharged, as ay result from an emergency use or a flame-out," the battery should be ca- able of being brought back to a state of ull charge within a short time, preferably ne hour. In short, an aircraft battery hould be capable of being adapted to arious applications with speed, even from fully discharged state. Furthermore, hese characteristics should not be criti- ally dependent on ambient temperature r on the heat generated in the battery.

As a result of these service require- ents the testing of aircraft batteries on loat charge at constant potential does not uffice. The tests must include discharges t various rates and temperatures and tudies of the effect of repeated charges on he batteries. Since the bus bar in air-

Table II. Cycle Programs for Lead-Acid, Nickel-Cadmium, and Silver-Zinc Aircraft Batteries

Cycles	Type of Charge	Discharge Rates		
		Lead-Acid	Nickel-Cadmium	Silver-Zinc
1–3	CC*	2-hr	2-hr	2-hr
4	CC	5-min	5-min	5-min
5	CC	1-hr	1-hr	1-hr
6	CC	3-min (0 F)	3-min (0 F)	4-min (0 F)
7	CC	2-hr	2-hr	2-hr
8	CP† (4 hrs)	2-hr	2-hr	2-hr
9–22	CC	1-hr‡	1-hr‡	1-hr‡
23	CC			2-hr
24	CC			5-min
25	CC			5-min
26	CP (4 hrs)			2-hr
23–28	CC	1-hr‡	1-hr‡	
29	CC	2-hr	2-hr	
30	CC	5-min	5-min	
31	CC	5-min	5-min	
32	CC	5-min	5-min	
27–33	CC			1-hr‡
33	CC	2-hr	2-hr	1-hr‡
34	CP (4 hrs)	2-hr	2-hr	2-hr (CC charge)
35	CC (stand)			2-hr
36	CC			2-hr
35–60	CC	1-hr‡	1-hr‡	
37–50	CC			1-hr‡
51	CC			2-hr
52	CP (4 hrs)			2-hr
53–59	CC			1-hr‡
60	CC			2-hr
61	CC	2-hr	2-hr	
62	CC (stand)	2-hr	2-hr	
63	CC	2-hr	2-hr	
64	CP (4 hrs)	2-hr	2-hr	
65–90	CC	1-hr‡	1-hr‡	
91	CC	2-hr	2-hr	
92	CP (4(hrs)	2-hr	2-hr	
93–99	CC	1-hr‡	1-hr‡	
100	CC	2-hr	2-hr	
Total time (approximate)		40–42 days	47–49 days	39–41 days

* Constant current.
† Constant potential: 28.5 volts for lead-acid and nickel-cadmium, 28 volts for silver-zinc.
‡ Automatic cycling.

Table III. Outputs of Lead-Acid, Nickel-Cadmium, and Silver-Zinc Aircraft Batteries at 80 F and at the 2-Hour Rate (17 Amperes)

Type	Weight, Pounds	Volume, Cubic Feet	Capacity, Ampere-Hours	CC Voltage	Watt-Hours Per Pound	Cycles
Lead-Acid (12 Cells) OCV = 25.6 – 25.8 Volts						
1	80.0	0.58	35.2	23.4	10.3	100
2	55.0	0.40	23.4	23.8	10.0	46
3	76.4	0.58	37.9	23.3	11.6	100
4	51.3	0.39	21.5	23.6	9.9	0*
5	78.5	0.57	36.8	23.4	11.0	100
6	80.0	0.57	38.4	23.4	11.2	100
Nickel-Cadmium (19–20 Cells) OCV = 25.5 – 26.5 Volts						
1	76.0	0.53	39.3	23.2	12.1	100
2	54.0	0.48	21.0	23.2	10.0	50
3	80.0	0.57	37.4	24.9	11.6	74
4	77.0	0.57	37.7	24.9	12.2	42
5	78.0	0.57	40.3	24.6	12.7	50
6	80.0	0.57	43.8	24.5	13.3	100
7	70.0	0.48	35.6	24.6	12.5	322†
Silver-Zinc (14 Cells) OCV = 26.0 – 26.2 Volts						
1	34.0	0.26	43.1	21.1	26.8	35
2	25.5	0.26	40.0	21.3	33.4	25
3	75.0	0.56	110.8	21.4	31.7	30
4	76.0	0.57	76.6	21.4	21.6	25
5	76.0	0.57	65.0	21.1	18.1	25
6	55.0	0.38	55.4	21.3	21.5	10
7	66.9	0.57	157.0	21.5	50.5	43

* Gave 100 cycles but below requirement throughout cycle life.
† With free electrolyte.

craft is at constant potential, it may appear obvious that charging should be done at constant potential. However, the constant-current method of charging is a well-established method of charging batteries where the internal condition of the cells is not known and offers an opportunity to test the effects of overcharging on battery performance. Accordingly, a more complete evaluation of the over-all

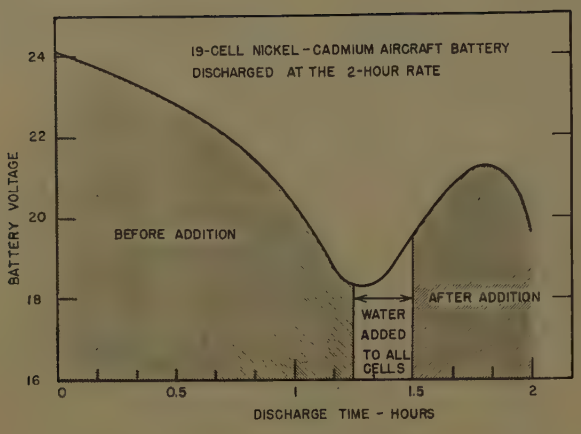

Fig. 1. Effect of water addition on the discharge of nickel-cadmium batteries

characteristics of a battery is afforded by a combination of constant-current and constant-potential charging, and the following standard procedure includes both.

Cycling of Aircraft Batteries

A standard test procedure for testing aircraft batteries is outlined in Table II. It consists of subjecting the batteries to cycles of charge–discharge at constant current with constant-potential charging interspersed at intervals. The total time of the cycle program ranges from 39 to 49 consecutive days. Lead-acid and nickel-cadmium batteries are subjected to at least 100 cycles whereas silver-zinc batteries are subjected to 60 cycles. The total outputs are comparable, however. Two distinct types of discharges are made during the cycling: those made automatically and those made to determine capacity at the rates listed, respectively, in parts A and B of Table I. The automatic discharges are made across a known resistor and the electric circuit is so adjusted that the integrated current drain equals the rated drain. For the capacity discharges the current is maintained constant using a carbon pile and the time required to reach the cutoff voltage, listed in part A of Table I, is accurately determined. Automatic charging is also done across a known resistor whereas charging prior to a capacity determination is accurately controlled at constant current.

In referring to Table I, it may be noted that lead-acid batteries are cycled four times a day, nickel-cadmium batteries three times a day, and silver-zinc batteries twice a day, with the stand times between cycles being different in each case. This becomes necessary because of the differences in the heat produced in the three types of batteries during the charging and discharging processes. The internal resistance of aircraft batteries has been materially reduced in recent years and so they accept a charge, especially a constant-potential charge, more readily. Since the heat capacity of aircraft batteries is low, the heat released during the charging produces an exaggerated change in temperature. Cooling in airplanes is advisable, and if provided, the differences in the permissible cycles per day become inconsequential.

Various makes of lead-acid, nickel-cadmium, and silver-zinc batteries were subjected to the cycle program as outlined in Table II. These results are brought together for the 2-hour rate in Table III. The data show the marked advantage of the silver-zinc batteries, at least regarding output per unit weight and volume. On the average, lead-acid batteries give 10 watt-hours per pound, nickel-cadmium 12, and silver-zinc 29.1. The spread between the results obtained with the silver-zinc batteries is more marked than with the other types. A comment is needed on the cycle life listed in the last column. These data represent the total number of cycles for which the battery gave capacities above 80% of rated capacity and are minimum values. Lead-acid battery no. 4 is listed as giving no cycles. Actually, this battery gave more than 100 cycles but the capacity was below rated capacity from the start; its cycle life is, therefore, listed as zero. However, the battery performed well and was merely misrated in capacity. After the batteries reached 80% of rated capacity they tended to decay in capacity rapidly. Nickel-cadmium batteries may be restored by short-circuiting and overcharging whereby the total number of cycles is increased somewhat.

The data of Table III also show another significant fact. The first six nickel-cadmium batteries were made with restricted electrolyte and were sealed whereas battery no. 7 was vented and contained free electrolyte. It will be noted that battery no. 7 gave at least 300 cycles of operation while the others gave 100 cycles or less. In this connection it should be emphasized that for military planes a service-free battery is a major aim. This means one that will need no addition of water or electrolyte during its life or in any other way, other than the need for charging, require attention. Battery no. 7 had water added during the cycle tests; the other nickel-cadmium batteries did not. This fact explains in part why battery no. 7 gave so many more cycles than the others. Sealed nickel-cadmium batteries tend to go dry during use and their output thus is limited. In Fig. 1 data are shown for a 19-cell sealed nickel-cadmium battery which had lost an appreciable amount of water during cycling. Water was quickly added during one chosen discharge, and the capacity of the battery is seen to be increased.

In Table IV the effect of temperature on the three types of aircraft batteries

Table IV. Outputs of Lead-Acid, Nickel-Cadmium, and Silver-Zinc Aircraft Batteries at 0 F and High Rates

Type	Rate, Amperes	Watt-Hours Per Pound: 80 F	Watt-Hours Per Pound: 0 F	Per Cent
Lead-Acid				
1	200	4.1	2.6	63
2	117	4.6	2.9	63
3	200	4.8	2.5	52
4	125	4.5	2.8	62
5	200	4.2	2.5	60
6	200	4.9	2.8	57
Nickel-Cadmium				
1	240	7.0	3.0	43
2	150	6.3	3.1	49
3	180	8.4	3.1	37
4	180	8.6	3.1	36
5	180	8.7	3.1	36
6	180	8.9	3.2	36
7	180	9.1	7.1	78*
Silver-Zinc				
1	300	14.5	10.3	72
2	300	22.0	18.7	85
3	400	15.0	13.0	87
4	180	17.1	16.3	95
5	180	17.6	16.5	94
6	300	11.6	0	0

* With free electrolyte.

Table V. Retention of Charge at 80 F Per Cent

Type No.*	Lead-Acid	Nickel-Cadmium	Silver-Zi
1	91	90	89
2	98	78	85
3	100	78	67
4	90	96	88
5	96	79	91
6	96	91	73
7	84	90	80
8	45		66
9	96		145
10	100		0
11			60
12			95

* Numbers do not refer to the same batteries list in Tables III and IV.

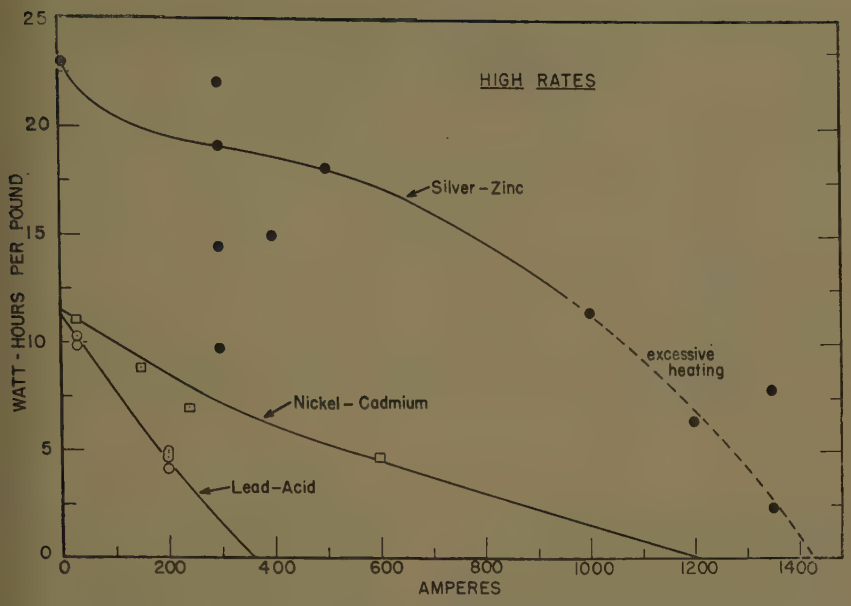

g. 2. Comparison of outputs of lead-acid, nickel-cadmium, and silver-zinc batteries as a function of current

Table VI. Data on Batteries Whose Characteristics Are Shown in Figs. 4–15

Type	Weight, Pounds	Volume, Cubic Feet	Capacity, Ampere-Hours
A—Batteries of Nearly Identical Weight and Volume			
Lead-acid	77.1	0.63	36*
Nickel-cadmium	78.3	0.59	36*
Silver-zinc	72.9	0.57	72*
B—Batteries of Nearly Equal Ampere-Hour Capacity†			
Lead-acid	78.6	0.57	38
Nickel-cadmium	81.8	0.57	47
Silver-zinc	33.8	0.26	42

* Nominal rated capacities were 34, 34, and 75 ampere-hours, respectively.
† Nominal rated capacities were 34 ampere-hours.

own. In these tests the batteries were ought to 0 F (degrees Fahrenheit) ior to the discharges. The ampere ain is not exactly comparable but the ta suffice to illustrate the temperature fects. It should be noted again that nted and sealed nickel-cadmium batter- s respond differently: vented cells per- rm better at the lower temperature than sealed cells. The data given for the ver-zinc batteries include effects of cuperation. These batteries show a op in working voltage below normal cut- f in the early stages of the discharge and en recuperate in voltage as the batteries arm. If recuperation were ignored the rcentage of the 80 F output would be ss than 30%. Effect of temperature on e charging characteristics of these three pes of batteries is discussed later.

Data on the retention of charge, after a 14-day stand on open circuit, for various batteries are listed in Table V. In general, all types exhibit about the same retention of charge: 90 to 100%. However, some makes have exhibited poor retention of charge. These have been defective in other regards and their poor retention of charge has been indicative of faulty construction.

In Fig. 2 data on the outputs of the three types as a function of current drain are presented. This figure shows the high rates sustained by the silver-zinc battery. Above 1,000 amperes, these batteries must be removed from the circuit prior to attainment of normal cutoff voltages owing to excessive heating. However, in practice the need for high-current drains is only intermittent, such as

Fig. 3 (below). High-rate discharge of silver-zinc battery

Fig. 4 (right). 400-ampere discharges of lead-acid (A), nickel-cadmium (B), and silver-zinc (C) batteries

A—At 80 F
B—At 0 F

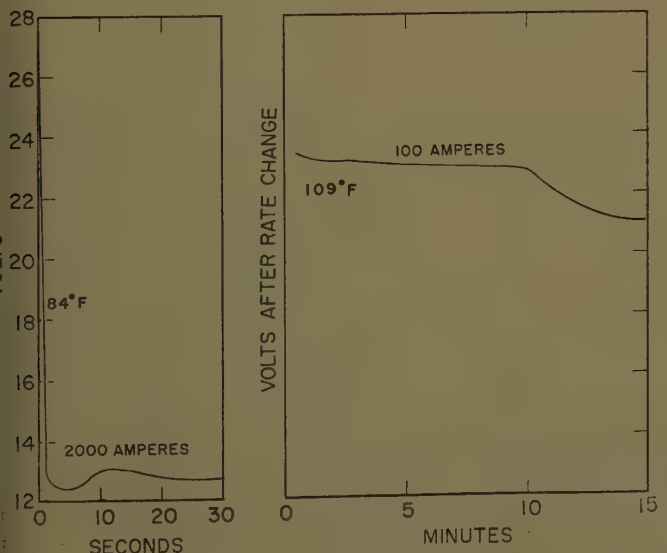

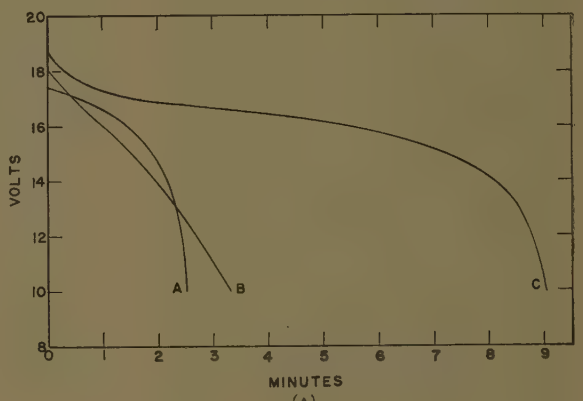

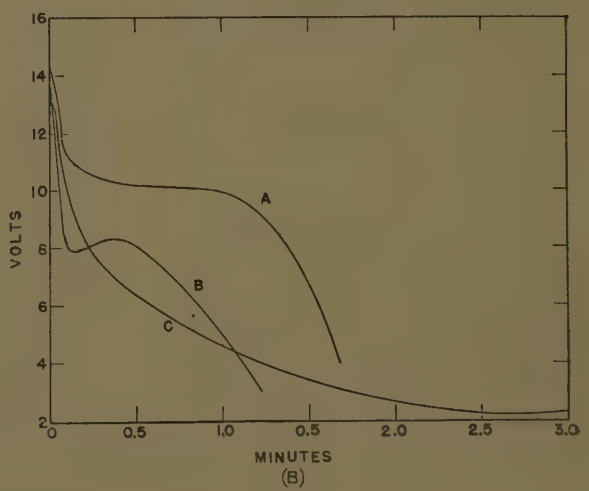

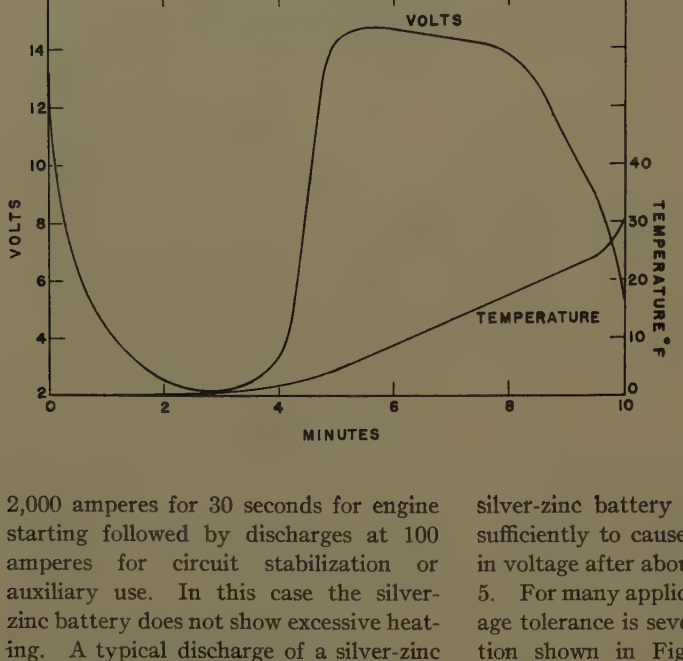

Fig. 5. Effect of internal warming on silver-zinc battery at 0 F

2,000 amperes for 30 seconds for engine starting followed by discharges at 100 amperes for circuit stabilization or auxiliary use. In this case the silver-zinc battery does not show excessive heating. A typical discharge of a silver-zinc battery under these conditions is given in Fig. 3.

Discharge Characteristics of Aircraft Batteries

In the foregoing section some data obtained during the cycling of lead-acid, nickel-cadmium, and silver-zinc batteries were presented. These data referred mostly to outputs obtained under specified cycle conditions. Additional data on these three types of batteries are presented in this section and include some data at −20 F. For this discussion, batteries of nearly equal weight and volume were chosen. These batteries may, therefore, be interchangeable in aircraft where space and weight are the dominant issues. Specifically, the three batteries discussed had the weight, volume, and ampere-hour capacity (at the 2-hour rate) as given in part A of Table VI.

Fig. 4(A) shows the output given by the fully charged lead-acid (*A*), nickel-cadmium (*B*), and silver-zinc (*C*) batteries at 80 F and for a 400-ampere discharge. (*A, B, and C are used in all figures to represent, respectively, the lead-acid, sealed nickel-cadmium, and silver-zinc batteries.*) This figure shows the advantage of the silver-zinc battery. The difference between the lead-acid and nickel-cadmium batteries is not appreciable. The situation is quite different, however, at 0 F as shown in Fig. 4(B). The silver-zinc battery now gives less output than either the lead-acid or nickel-cadmium battery and the lead-acid battery now gives somewhat more output than the nickel-cadmium battery. However, as stated in the previous section, the silver-zinc battery warms on discharges sufficiently to cause a large recuperation in voltage after about 3 minutes; see Fig. 5. For many applications, however, voltage tolerance is severe, and the recuperation shown in Fig. 5 then cannot be effectively used.

Data obtained on the three battery types at the somewhat lower rate of 180 amperes, at 80 F, 0 F, and −20 F are given in Fig. 6. At 80 F, the silver-zinc battery again shows higher output than the other two and the nickel-cadmium battery now shows higher output than the lead-acid battery. At 0 F, Fig. 6 (B), the silver-zinc battery shows only slightly more output than the other two; here again the silver-zinc battery shows voltage recuperation owing to internal heating and if this recuperation is taken into account its output exceeds that obtained for the other two types of batteries. At −20 F, Fig. 6(C), only the lead-acid battery has a usable output; the behavior of the other two is erratic. Again the silver-zinc battery shows voltage recovery but somewhat erratically.

Performance of the batteries at a moderate drain of 50 amperes at 80 F and 0 F is shown in Fig. 7. At 80 F, Fig. 7(A), the silver-zinc battery gives nearly twice the output of the other two. At 0 F, Fig. 7(B), lead-acid and nickel-cadmium batteries behave almost identically whereas the silver-zinc battery shows quite markedly the voltage recovery discussed previously. Initially this battery drops in voltage at a fast rate but recovers to give nearly four times the output of the other two types. For applications requiring power for only 10 or 20 minutes, however, this recovery is of no advantage. One must decide in any application whether it is electrical quantity, electric energy, or voltage constancy that is the more significant.

Finally, the traits of the three types of batteries at low-current drains, as may be

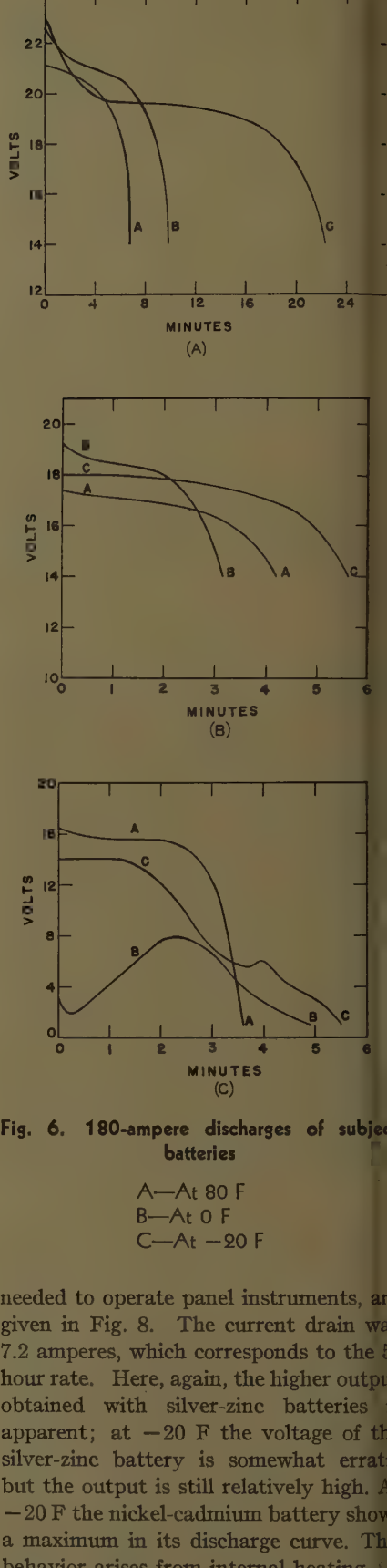

Fig. 6. 180-ampere discharges of subje batteries

A—At 80 F
B—At 0 F
C—At −20 F

needed to operate panel instruments, a given in Fig. 8. The current drain wa 7.2 amperes, which corresponds to the hour rate. Here, again, the higher outpu obtained with silver-zinc batteries apparent; at −20 F the voltage of th silver-zinc battery is somewhat errat but the output is still relatively high. −20 F the nickel-cadmium battery show a maximum in its discharge curve. Th behavior arises from internal heating.

The foregoing characteristics referr to batteries of nearly equal weight a volume. However, the ampere-hour c pacity differed markedly. While th lead-acid and nickel-cadmium batteri had nominal capacities of 34 amper

7. 50-am-
discharges
subject bat-
teries

—At 80 F
—At 0 F

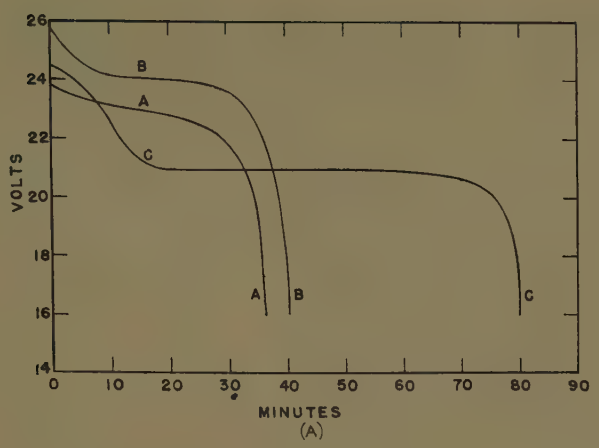

(A)

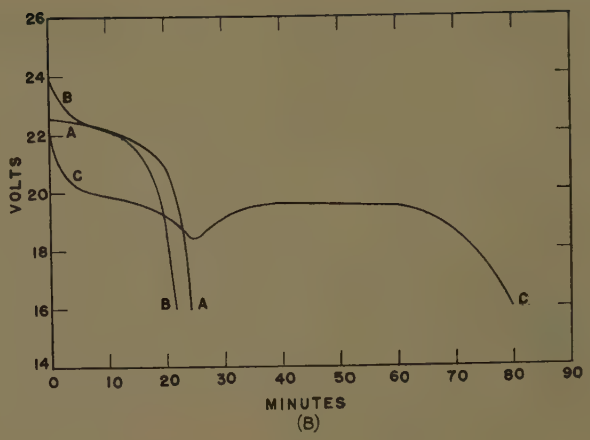

(B)

urs, the silver-zinc battery had a minal ampere-hour capacity of 75. is difference was reflected in the dis-arge curves. In Figs. 9–12 compari-ns are given of batteries of the same minal ampere-hour capacity (data on e weight and volume of the batteries e given in part B of Table VI). In each ure the temperature change which sued during the discharge is shown for ch type. The silver-zinc and nickel-dmium batteries show about the same te of temperature rise and a greater rise an that shown by lead-acid batteries at w currents (2- and 1-hour rates) while r high currents (5- and 3-minute rates) ere is not much difference between the types. These figures show that although nearly the same ampere-hour capacity is obtained between types the watt-hours differ, with the silver-zinc system giving the least. Figs. 9 and 10 also show the initial large drop in working voltage for the silver-zinc types. At 0 F the silver-zinc battery, in this comparison, shows poor output but if a short stand period of one minute (Fig. 12) is taken during the discharge, the output is materially improved because of internal heating.

Charge Characteristics of Aircraft Batteries

A study of the charging characteristics of aircraft batteries shows some important factors which are pertinent to their use on airplanes. Since, in practice, batteries are charged at constant potential on planes, the charging of batteries under these conditions was especially studied. Constant-potential charging curves for the three battery types are shown in Figs. 13, 14, and 15 for 120 F, 80 F, 0 F, and −20 F. A constant potential of 28 volts was used for the first two temperatures, 28.5 volts for 0 F, and 29 volts for −20 F. In each figure the ampere-hour output of the previous discharge is given as well as the ampere-hour input received by the battery within 4 hours. The percentage of charge received by the battery within this specified time is also listed.

Fig. 13(A) shows some very important traits of the three batteries. It may be seen that the silver-zinc battery accepts a high initial inrush of current. The current then drops so rapidly that the battery, although only initially 67% discharged (49.7 amp-hours/75 amp-hours = 0.67), is only recharged 103% within 4 hours. Since, on the average, silver-zinc batteries should be given 107% of previous outputs (see part A, Table I) to be fully charged, the battery was not fully charged. Of course, a longer time could be used to effect a full charge. If the potential for constant-potential charging were raised, the initial inrush of current would be greater and could seriously overload the generator. The charging curves for the lead-acid and nickel-cadmium batteries are normal during the

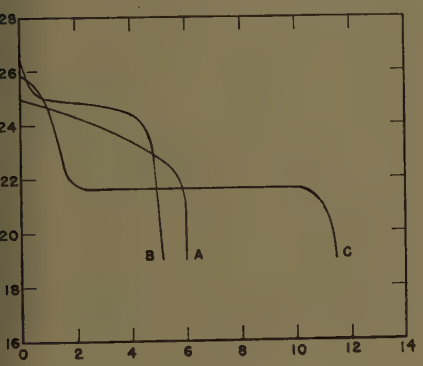

(A)

Fig. 8. 7.2-ampere discharges of subject batteries

A—At 80 F
B—At 0 F
C—At −20 F

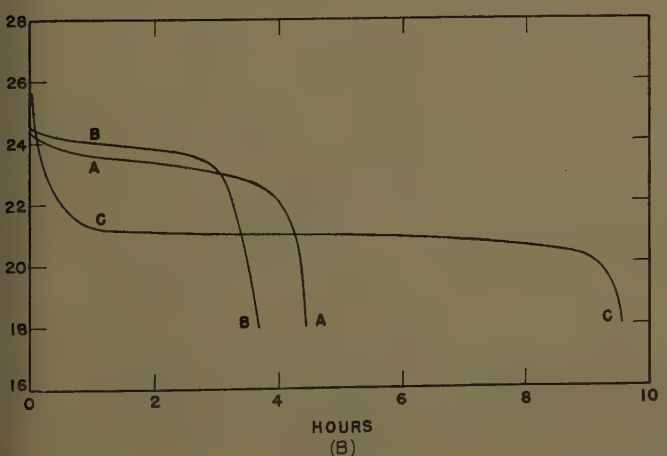

(B)

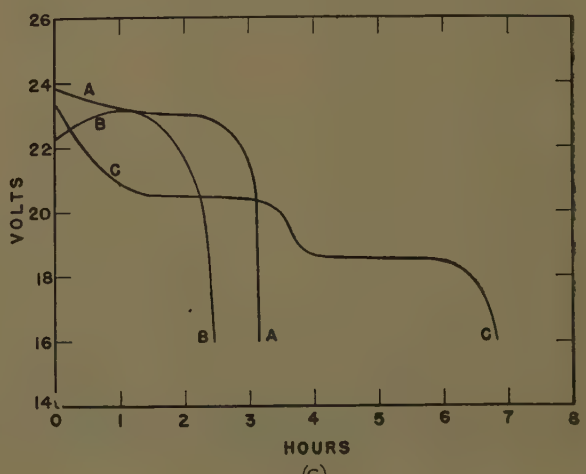

(C)

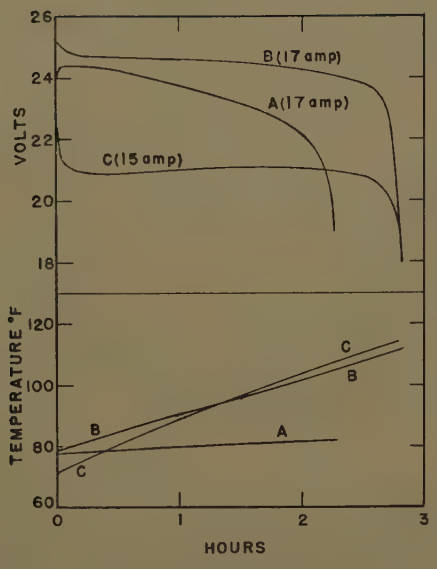

Fig. 9. Two-hour rate discharges of subject batteries at 80 F

early stages of the charge. However, at a certain point the rise in temperature in nickel-cadmium batteries decreases the internal resistance of the battery sufficiently to more than offset the increasing counter electromotive force and the charging current begins to rise. As the charging current rises, so does the temperature leading to the phenomenon known as "vicious cycling": as the current rises so does the temperature and as the temperature rises so does the current until the battery "burns up." In the case shown in Fig. 13(A) a temperature of 155 F was attained within $3\frac{1}{2}$ hours. If the charging were continued the current acceptance and the temperature would both rise. To prevent this in practice nickel-cadmium batteries are supplied with thermostats that limit the charging when 135 F is reached. A description of a typical thermostat is given later.

Similar data for 80 F are given in Fig. 13(B). Here, again, the initial high inrush of current is found for silver-zinc batteries. Again at 28 volts the silver-zinc battery does not receive sufficient charge within 4 hours; the amount received is 93%. Considerably longer charging times would be required for full charge since the charging current becomes quite low at the end of 4 hours. In this case, the nickel-cadmium battery shows no tendency to go into the vicious cycle. In Fig. 14 data are given on batteries that had been cooled to 0 F. The initial high inrush of current still persists for the silver-zinc battery. The charging curves are normal but the three batteries received less than 65% of charge in 4 hours even with the charging voltage raised to 28.5 volts. In this case all batteries were essentially in a fully discharged state at the start of the charging. The nickel-cadmium and silver-zinc batteries accept charge better than the lead-acid battery at 0 F, but there is some indication that over longer charging periods the lead-acid battery would accept comparable charges.

Fig. 15 shows charging characteristics of the three batteries at −20 F. The charging curves are similar to those obtained at 0 F but, even with the charging voltage raised to 29 volts, it is not feasible effectively to charge any of the batteries at −20 F. The nickel-cadmium battery received only 50% of charge and the other two types received much less. Of course, a higher charge would be received by the batteries if the charging time were extended; this would be impractical, however.

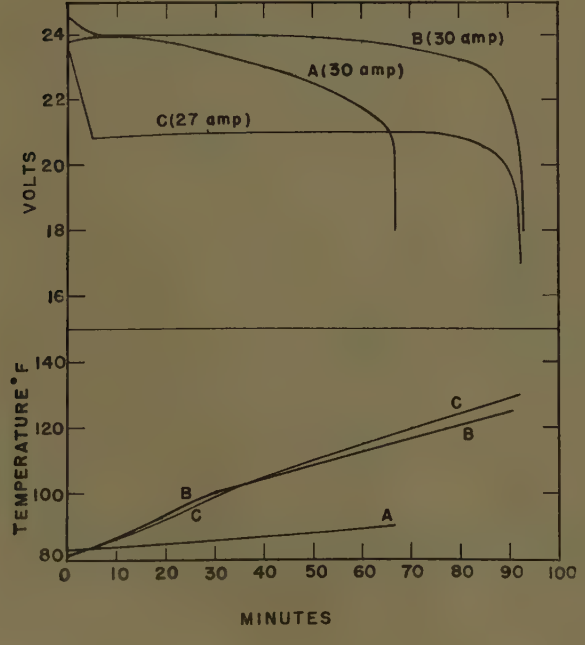

Fig. 10 (left). One-hour rate discharges of subject batteries at 80 F

Fig. 12 (right). Three-minute rate discharges of subject batteries at 0 F

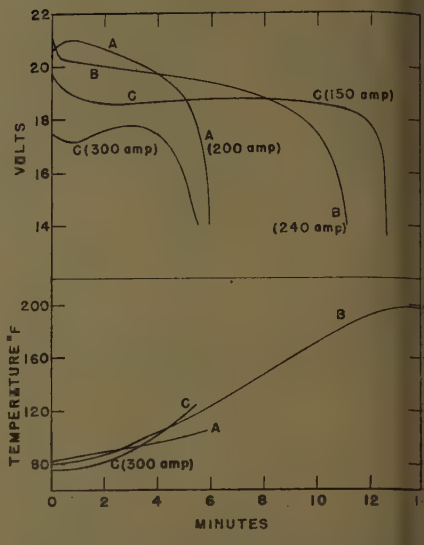

Fig. 11. Five-minute rate discharges . . subject batteries at 80 F

The above charging characteristic become more pronounced when th battery is more fully discharged at th start of the charge since more heat then generated during the charging proc ess. The effects are less than when th batteries are on float charge. On cyclin at constant potential the batteries ten to decline in capacity.

A diagram of a typical thermostat used to limit the charging when batter temperature becomes too high is show in Fig. 16. The positive terminal of th battery is joined to a current coil (*CC*) housed in the battery and thence to th main battery contactor (*BC*) and on t the aircraft bus. A second lead runs fro the positive battery terminal through thermostat (*BT*) built in the battery t the field of the main battery contacto through a single-throw double-pole switc (*STDP*). The thermostat is set to ope

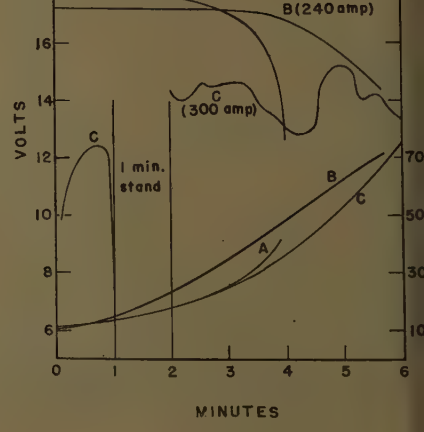

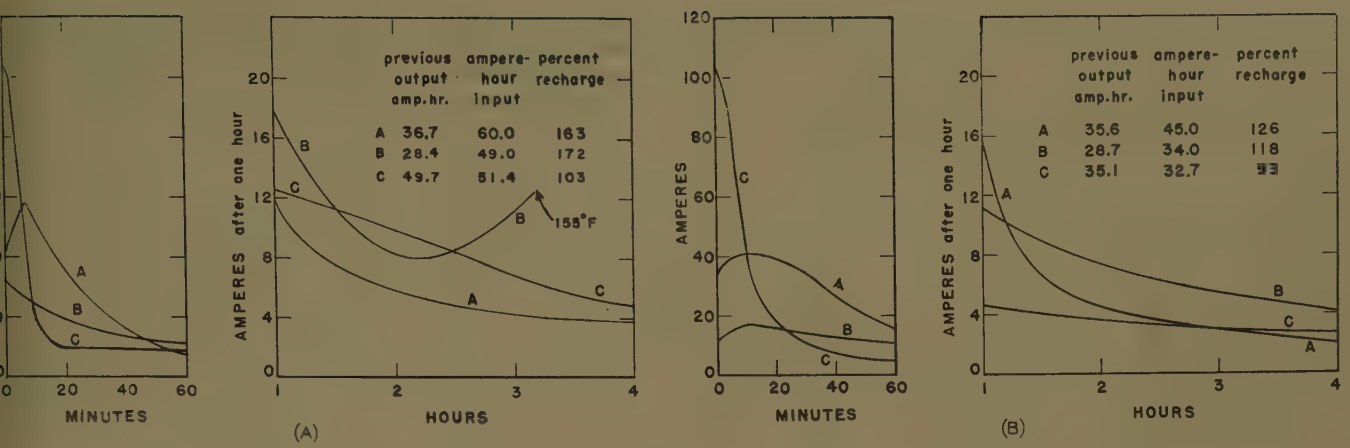

Fig. 13. Constant-potential charging (28 volts) of subject batteries

A—At 120 F
B—At 80 F

135 F. A polarized relay (*PR*) is alleled with the thermostat. A third d from the positive battery terminal s through a voltage coil (*VC*) and the gle-throw double-pole switch to the erator side from the main battery con- tor. The polarized relay is activated the voltage and current coils. When attery is on charge the main battery ntactor and thermostat are closed and polarized relay open. If the charg- voltage becomes too high and the ttery temperature reaches 135 F the rmostat opens, resulting in the open- of the battery contactor. The ttery is now off charge. If the bus tage drops so that battery power is quired the polarized relay closes ereby the main battery contactor is sed when the bus voltage is 0.3 volt ow battery voltage. The current nding will hold the polarized relay sed as long as a minimum of 4 amperes flowing from the battery. Restoration bus voltage will open the polarized relay and the main battery contactor if the battery is still hot. The thermostat will close when the battery temperature has dropped to 125 F and the original normal circuits will be re-established. The thermostat is generally welded to the outside of one cell of the battery and the other parts of the control are housed in a case mounted in the battery container near the quick-disconnect receptacle.

The above system may also be used to provide self-heating of batteries at low temperatures, especially silver-zinc types. A lead is connected to the negative terminal through a second thermostat (*HT*) that will open at any temperature above 0 F. A lead from this thermostat goes to a heater (*H*) of about 4-ohm resistance and thence to the bus side of a single-throw double-pole switch. The heater is best placed at the bottom of the battery case. Closing the battery switch will permit about 100 watts to heat the battery internally if the temperature of the battery is initially below 0 F. The output at the higher temperature more than offsets the energy utilized to heat the battery.

Physical Tests of Aircraft Batteries

Physical tests of aircraft batteries should include tests of the effects of (1) altitude, (2) operating position, (3) mechanical shock, (4) thermal shock, (5) vibration, (6) operation temperature, and (7) electrolyte level on battery performance, as well as tests of (8) gas tightness of cells, (9) sealing compound, (10) insulation, (11) intercell connectors, and (12) vent caps. Space will not permit a complete discussion of all these; suffice it to say that most aircraft batteries meet the physical requirements. Brief descriptions of the physical tests follow.

Altitude

A fully charged battery at 80 F is placed in an altitude chamber at sea level and

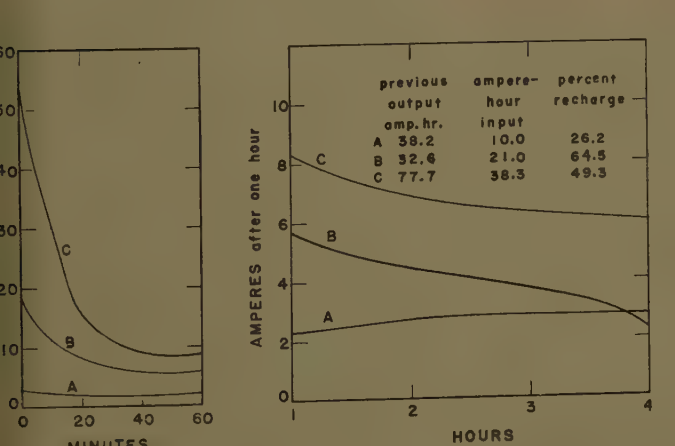

g. 14. Constant-potential charging (28.5 volts) of subject batteries at 0 F

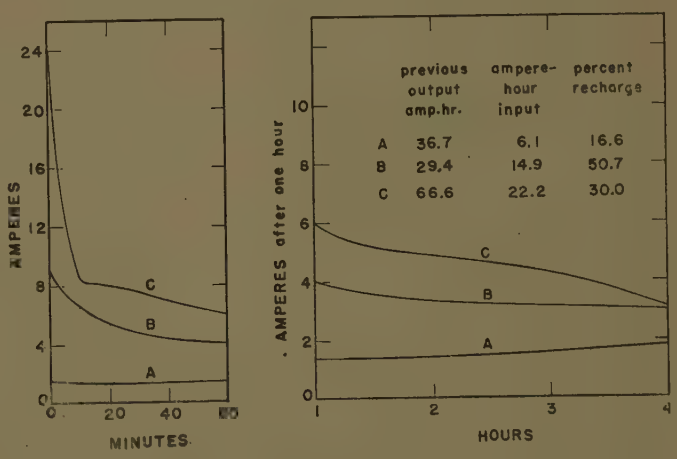

Fig. 15. Constant-potential charging (29 volts) of subject batteries at −20 F

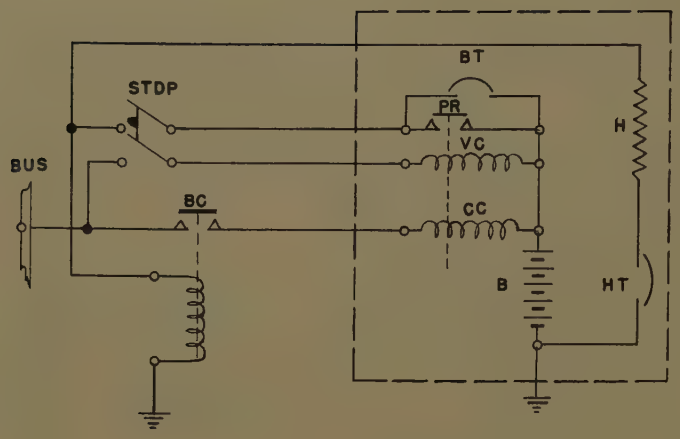

Fig. 16. Overtemperature and heating circuits for aircraft batteries

discharged at the 3-minute rate to normal cutoff voltage (see part A of Table I for 3-minute rates and cutoff voltages). The temperature of the chamber and battery is then reduced to 14 F (−10 degrees centigrade) and the discharged battery is charged at a constant potential of 28 volts for 2.3 hours as the air pressure is reduced to an altitude corresponding to 50,000 feet above sea level. The pressure change is accomplished within 15 minutes. During the last 5 minutes of charge the pressure is restored to sea level. The battery is then discharged at the 3-minute rate to the normal cutoff voltage. This procedure is repeated twice with the third discharge being made at 80 F. During the charging at reduced pressure the battery is inspected for electrolyte flooding or boiling. No flooding or boiling of electrolyte is acceptable and altitude changes should have no adverse effect on capacity. Most aircraft batteries meet these requirements. The silver-zinc batteries show their usual response to constant-potential charges.

Operating Position

A fully charged battery at 80 F is discharged at the 5-minute rate (Table I) to the normal cutoff voltage. After 2 minutes of discharge the battery is inverted without interrupting the discharge and after two additional minutes of discharge the battery is restored to its normal operating position. Voltage readings are taken 5 seconds before and after each change in position. The battery is expected to deliver its full rated capacity under these conditions and the voltage variation during changes in position is not expected to exceed 0.5 volt. Also, no leakage of electrolyte should occur. In general, aircraft batteries meet these requirements except for the voltage variation where voltage changes as much as 0.8 volt have been observed. These changes do not affect capacity, however.

Mechanical Shock

A battery is submitted to an average acceleration of 35 *g* acting between 10 and 20 milliseconds and then tested for shock in the direction of the three major axes. The shock in the vertical axis is in the direction which tends to eject cells from the battery container. The battery is mounted in the carrier in such a way that the force acceleration is transmitted to the hold-down bar in the normal manner. Battery voltages are recorded by a graphic meter during the shock test. No battery fractures or voltage fluctuations are acceptable.

Thermal Shock

A fully charged battery is discharged at 80 F at the 2-hour rate to the normal cutoff voltage (see part A of Table I for 2-hour rates and cutoff voltages). It is then recharged and placed immediately in an ambient temperature of 185 F and after 4 hours transferred to an ambient temperature of −40 F and kept there for 4 hours. The battery is then returned to 185 F and the procedure of cooling and heating repeated twice. The battery is then warmed from −40 F to 80 F and a discharge made again at the 2-hour rate. During this test the battery is expected to show no fractures and little or no loss in capacity.

Vibration

A fully charged battery is mounted on a vibrator in the upright position; for lead-acid batteries the vent caps are in place. The battery is bolted to the vibrator table with long bolts attached to the hold-down straps on the cover as in an actual aircraft installation. Vibration is applied with the frequency cycling between 10 and 500 cps (cycles per second) in 15-minute cycles with an acceleration of 5 *g*. A total of four 15-minute cycle vibration are made and during each frequency is varied from a minimum o cps to a maximum of 500 cps and bac 10 cps. One 30-second discharge is m at the 1-hour rate during each cycle. general no voltage variations are no but resonance points, usually in battery cover, appear at points erally above 100 cps. Therefore, battery is further vibrated for 30 minu at each of the frequencies for which re nance is observed. No adverse effe owing to vibration are observed in bet constructed batteries.

Operation Temperature

This test is designed to ascertain if battery has a tendency to go into "vicious cycle." A fully charged batte is heated in an ambient temperature 120 F for 6 hours, followed by a charge at the 1-hour rate. No decre in capacity is permissible. The batte is then fully charged and placed in ambient temperature of 140 F for 7 hou and then discharged at the 5-minute ra to cutoff voltage and immediately charg at a constant potential of 30 volts for hours. Measurements are made of t current and temperature rise during t constant-potential charge. The lat test is then repeated.

Electrolyte Level

This test is applied mainly to lead-ac batteries with nonspill vent caps. T electrolyte level is adjusted until it is 1 inch above the baffle after the batte has been completely discharged at t 2-hour rate. The battery is then charged at a rate 20% higher than t normal rate until the total charge is 150 of rated capacity. Spraying and loss electrolyte are looked for and the batte then discharged at the 1-hour rate. loss in capacity should be observed and spraying or loss of electrolyte. The sam test may be applied to silver-zinc batteri and to vented nickel-cadmium batteri For sealed nickel-cadmium batteries t electrolyte level is tested as described connection with Fig. 1.

Gas Tightness of Cells

A fully charged battery at 80 F is su jected to 5 pounds per square inch for minutes by air passing through the filli hole in the cell cover. This test is n used, as a rule, for sealed nickel-cadmiu batteries.

Sealing Compound (When Applicabl

A fully charged battery is placed in ambient temperature of 200 F for 6 hou

removed and immediately tilted 90 es and kept in that position for 5 tes. No flow of sealing compound s of electrolyte should result.

LATION

current-carrying parts are ex- d to be capable of withstanding a tial of 2,500 volts (rms) at commer- requency for 1 minute between the nt-carrying parts and the con- r. This test is also known as a di- ic test.

RCELL CONNECTORS

is test is designed to test the ability e intercell connectors to conduct high nts. A fully discharged battery is ged at a constant potential of 28 volts hours or until the battery tempera- reaches 120 F, whichever occurs first. ermination of the charge the battery aced in a constant-temperature oven 20 F for 2 hours and then discharged 20 F at a rate equal to 200% of the est specified rate (see part A of Table or 1 minute. No failure of the cur- carrying parts should occur.

T CAPS

his test is applied specifically to lead- cells. Valves are required to close ween 42 and 48 degrees when the back pressure of the gas passing through the valve is equal to 1 cm Hg (centimeters of mercury). When the valve is closed and under a static pressure of 1 cm Hg it is required to open at an angle not greater than 38 degrees and not less than 32 degrees. Under a static pressure of 50 cm Hg the valve is required to open when in the vertical position. These requirements simulate requirements of jet planes. They are also required to withstand immersion in sulfuric acid of specific gravity of 1.300 for 10 days at 200 F in the vertical position and to meet the mechanical shock, thermal shock, and vibration tests previously outlined.

Summary

In the foregoing, some characteristics of lead-acid, nickel-cadmium, and silver-zinc aircraft batteries were presented. Many advantages of each system were emphasized and certain disadvantages mentioned. The latter suggest areas where more research is needed. Efforts are needed to improve cycle life (especially under constant-potential charging), charge retention, charge acceptance, and low-temperature performance. With increased use of jet planes, missiles, and space vehicles where high temperatures are involved, batteries must be designed to withstand unusually high temperatures. As one example, since batteries are cut out of a charging circuit at 135 F or higher, it is obvious that batteries would be totally ineffective in an environment where the ambient temperature is 135 F or higher. The batteries would then receive no charge. At present, reserve batteries, activated at the time of use, offer a solution to this severe environmental condition for auxiliary but not for prime power. More research is needed to find ways to increase hydrogen overvoltage on lead, cadmium, and zinc whereby the gassing of batteries would become less severe. More studies of oxygen overvoltage are also needed.

References

1. D. C. Power Systems for Aircraft (book), R. H. Kaufman, H. J. Finison. John Wiley & Sons, Inc., New York, N. Y., 1952.

2. Storage Batteries (book), G. W. Vinal. John Wiley & Sons, Inc., fourth edition, 1955.

3. Aircraft Batteries and Their Behavior on Constant-Potential Charge, G. A. Earwicker. *Proceedings*, Institution of Electrical Engineers, London, England, vol. 103, pt. A, supplement no. 1, 1956, p. 180.

4. A Review of the State of the Art and Future Trends in Electrochemical Battery Systems. I. The More Common Systems, W. J. Hamer. *Proceedings*, Seminar on Advanced Energy Sources and Conversion Techniques, *No. AD209301*, Armed Services Technical Informa, tion Agency, Washington, D. C. (*No. P.B. 151461* Office of Technical Services, U. S. Department of Commerce), vol. 1, Nov. 1958.

Analyzing the Transient Response of a Nonlinear Servosystem by the Phase-Plane Method

W. A. STEIN
MEMBER AIEE

IS COMMON practice in college ervomechanism laboratories to build imple "linear" servomechanism system n which the student can determine frequency and transient response. is simple system is generally composed of an error detector, electronic amplifier, and 2-phase servomotor as illustrated in Fig. 1. The student is immediately disturbed to discover that both the frequency and transient responses depend on the magnitude of the input signal. This is, of course, contrary to linear theory. The only conclusion that can be reached is that the apparently linear system just is not linear due to the characteristics of the 2-phase motor. In a previous publication it was shown why the M_p and resonant frequency of the frequency response characteristics varied with the magnitude of the input signal.[1] It is the purpose of this paper to show how the nonlinear characteristics of the 2-phase motor influences the transient response of the system. This analysis is best carried out by means of the phase-plane method.

er 60-863, recommended by the AIEE Feed- k Control Systems Committee and approved he AIEE Technical Operations Department for sentation at the AIEE Summer General Meet- Atlantic City, N. J., June 19–24, 1960. Manu- pt submitted February 18, 1959; made avail- for printing May 4, 1960.

A. Stein (deceased), was with the United States val Postgraduate School, Monterey, Calif.

author wished to acknowledge the assistance he Office of Naval Research in obtaining special ipment for this project.

Motor Characteristics From Dynamometer Tests

In this analysis the speed versus torque curves of the 2-phase motor must be known in both the first and fourth quad-

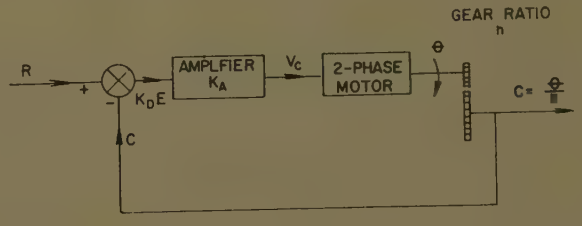

Fig. 1. Block diagram of simple servomechanism

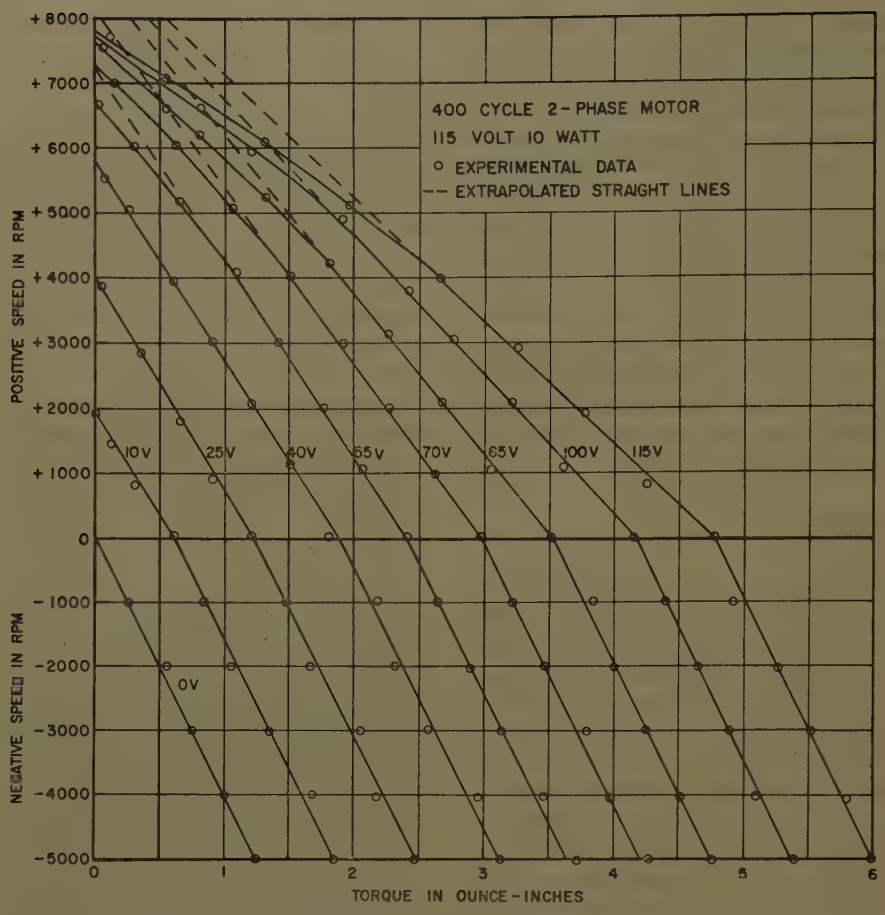

Fig. 2. Speed-torque curve of 2-phase servomotor experimentally obtained by special dynamometer

rants for different values of voltage on the control winding, V_c. This requires a special dynamometer capable of measuring both motor and braking torques of these motors.[2]

Fig. 2 shows the speed-torque curve experimentally obtained on the special dynamometer for a small 10-watt motor. A characteristic of such a dynamometer is that in the motor range, the dynamometer indicates the output torque; hence, the viscous friction torque of the motor and load must be added to obt the developed torque. In the brak zone the dynamometer reads the dev oped torque directly. This is a fine poi as the viscous friction torque is only small percentage of the output torq in a good ball-bearing motor and t error introduced by neglecting this probably less than the inaccuracies int duced by heating effects.

The general conclusions reached fr the speed-torque curves of Fig. 2, wh hold not only for this particular 10-w motor but also for some half dozen 2-ph instrument servomotors, which the auth has also tested, are listed.

1. The stalled torque is proportional the voltage on the control winding

$$T_{\text{stalled}} = A V_c$$

where A is the constant of proportionalit

2. Within the normal range of operat below 50% rated speed, the curves essentially straight lines. For the low speed portion the family of curves is giv by the equation

$$T = A V_c - \left|\frac{\partial T}{\partial \omega}\right| \omega$$

The $\partial T/\partial \omega$ term is the reciprocal of the sl of the speed-torque curve and is commo referred to as the motor damping ra Note that although the curves are rep sented by straight lines, these lines are parallel but have different slopes $1/\partial T$ which are functions of the control windi voltage V_c.

3. In the braking range the torque-sp characteristics are straight parallel lines

Derivation of Isocline Equations

The developed torque of the mot can be expressed in the same form as equ tion 2 which was derived for the outp torque. In all the ball-bearing moto

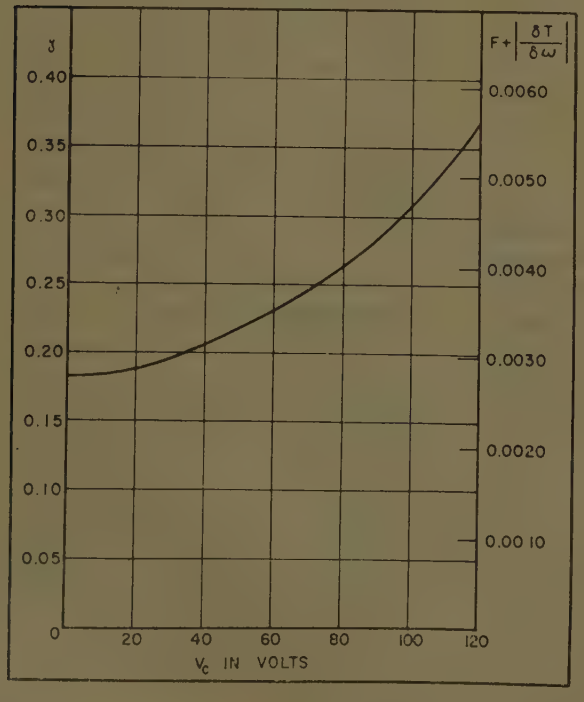

Fig. 3 (left). Plot of damping ratio ζ and $F+|\partial T/\partial \omega|$ versus control field voltage V_c

Fig. 4 (right). Locating a point on the phase trajectory by Lienard's construction

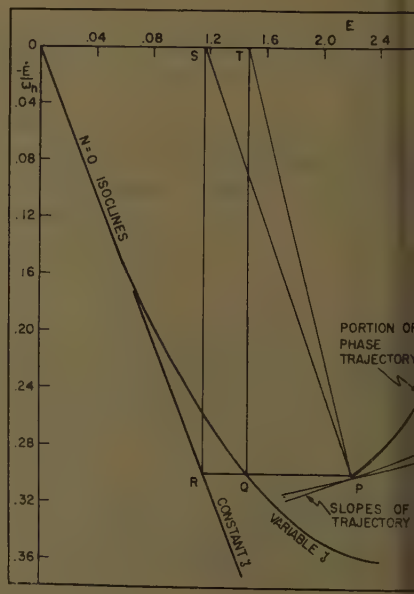

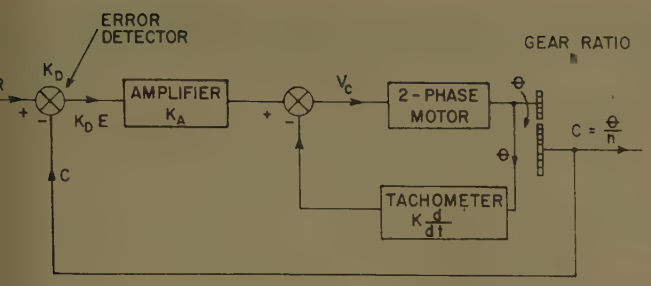

Fig. 5. Block diagram of servomechanism with tachometer feedback

ted the friction torque at maximum eed was about 1 or 2% of the full load rque and had little effect on $\partial T/\partial\omega$; nce, the error introduced by using uation 2 instead of the developed rque is very small.

Assume that all the developed torque used in accelerating the inertia load and ercoming the viscous friction of the otor and load.

$$= J\ddot{\theta}+F\dot{\theta} \tag{3}$$

s the error is defined as

$$=(R-C)K_D \tag{4}$$

d the controlled variable C is related to e motor output θ by

$$=\frac{\theta}{n} \tag{5}$$

here n is the gear ratio. The 2nd order fferential equation describing the sys-m is therefore

$$+\left(F+\left|\frac{\partial T}{\partial\omega}\right|\right)\dot{E}+\frac{AK_DK_A}{Jn}E=0 \tag{6}$$

he control winding voltage V_c was liminated by recognizing that in the mple system

$$_c=K_AE \tag{7}$$

he equation of the isoclines can be de-ermined by substituting $d\dot{E}/dt$ for $\ddot{E}$ and dividing each term of the equation by either $\dot{E}$ or its equivalent dE/dt

$$\dot{E}=\frac{-AK_AK_DE}{JN+\left(F+\left|\frac{\partial T}{\partial\omega}\right|\right)n} \tag{8}$$

The N of equation 8 is defined as being the slope of the phase trajectory, $N \equiv d\dot{E}/dE$.

It is immediately apparent that the isoclines are not straight lines as $\partial T/\partial\omega$ is a function of V_c which in turn is proportional to the error signal E.

The general form for the differential equation of a linear 2nd order servomechanism with a step input is

$$\ddot{E}+2\zeta\omega_n\dot{E}+\omega_n^2E=0 \tag{9}$$

By comparing equation 6 with equation 9, several valuable relationships are derived:

$$\omega_n=\frac{AK_DK_A}{Jn} \tag{10}$$

$$\zeta=1/2\sqrt{\frac{n}{AK_DK_AJ}}\left(F+\left|\frac{\partial T}{\partial\omega}\right|\right) \tag{11}$$

The $\partial T/\partial\omega$ is evaluated in ounce-inches per radian per second from the reciprocal of the slopes of the dynamometer curves of Fig. 2. It will be observed in Fig. 3 that the $F + |\partial T/\partial\omega|$ is a function of the control field voltage V_c. The natural frequency ω_n of the system is then independent of V_c, but the damping ratio ζ of this nonlinear system will fluctuate during the transient response. When the voltage on the control field is large, $\partial T/\partial\omega$ will also be large. As seen from equation 11 the system becomes less damped as it comes into correspondence. The isocline equation 6 can be put into the more useful general form of equation 12.

$$\dot{E}=\frac{-\omega_n^2E}{N+2\zeta\omega_n} \tag{12}$$

Since ζ is not a constant the isoclines will not be straight lines.

Obtaining the Phase Trajectories

The variation of $\partial T/\partial\omega$ in the first quadrant of the speed-torque curves was plotted in Fig. 3; however, it will be observed that in the fourth quadrant or braking range the curves are all straight parallel lines and $\partial T/\partial\omega$ is a constant. This is a property of all the 2-phase motors tested by the author and also was observed by independent researchers.[3-4] In drawing the isoclines special caution must be used. In quadrants II and IV of the phase plane, the values of $\partial T/\partial\omega$ must be those measured in the first quadrant of the speed-torque curves; whereas, in the I and III quadrants of the phase plane, the value of $\partial T/\partial\omega$ is invariant and is obtained from the fourth quadrant of the speed-torque curves. This means that in the I and III quadrants the isoclines will be straight radial lines originating from the origin. This is explained in detail in Appendix I.

$$\frac{dy}{dx}=\frac{-f(y)-x}{y} \tag{13}$$

where $f(y)$ represents a function of y. Equation 9 can be manipulated into a form which satisfies this requirement.

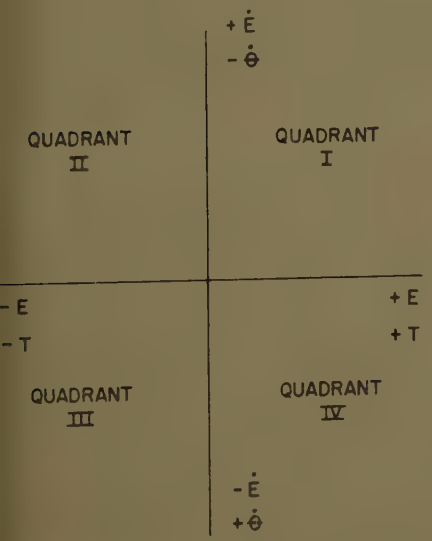

Fig. 6 (left). The phase-plane axes with numbered quadrants

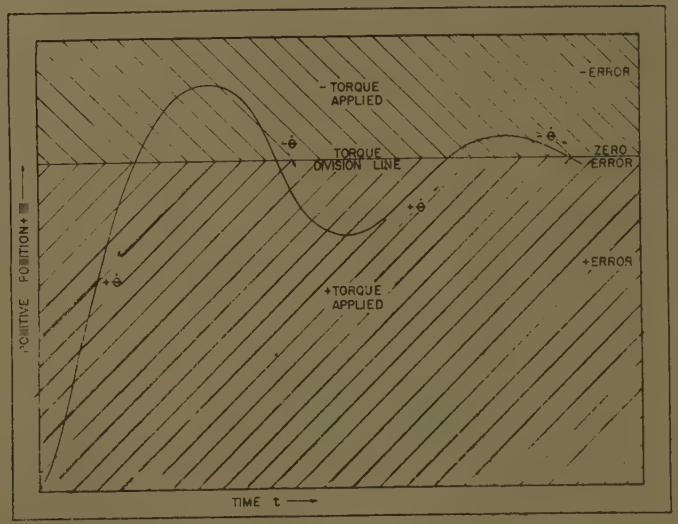

Fig. 7 (right). Sketch of transient response with regions of positive and negative torque, and positive and negative speed indicated

$$\frac{d\left(\frac{\dot{E}}{\omega_n}\right)}{dE}=\frac{-2\zeta\left(\frac{\dot{E}}{\omega_n}\right)-E}{\frac{\dot{E}}{\omega_n}} \qquad (14)$$

Lienard's construction is a relatively simple graphical method for determining the slope of the phase trajectory at any point P in the $\dot{E}/\omega_n$ versus E plane; see Fig. 4. The numerator of the general form is set equal to zero and the resulting equation is plotted on the phase plane.

$$E=-2\zeta\frac{\dot{E}}{\omega_n} \qquad (15)$$

To determine the slope of the phase trajectory at any point P, a horizontal line is drawn from P to this curve thus locating Q at the intersection. A vertical line projected to the E-axis determines the point T. The slope of the phase trajectory at the point P is perpendicular to the line TP. It will be observed that the curve obtained by setting the numerator of equation 14 equal to zero is simply the $N = 0$ isocline of equation 12. In Fig. 4 are plotted two $N = 0$ isoclines: the first is for the actual physical system where ζ is a function of V_c which in turn varies directly as E and the second is for a constant ζ of 0.185 which is the approximate value of ζ at small values of V_c. The stabilizing effect of the variable ζ becomes apparent from Lienard's construction as seen from the two possible slope lines of the phase trajectory at point P. The slope obtained for the variable ζ isocline is not as steep as that for the constant ζ isocline and as a result the phase trajectory of the actual physical system will tend to home into the origin faster than if the ζ remained constant.

It will be noted that the entire phase trajectory can be constructed using Lienard's construction. This method will not, however, be as accurate as that obtained by the isocline method. It must be realized that the Lienard construction line used to draw the phase trajectory in the I and III quadrants of the phase plane are straight lines as the value of ζ remains constant within these quadrants.

Compensation by Tachometer Feedback

Servomechanisms are quite often compensated by means of tachometer feedback as shown in Fig. 5. For the tachometer compensated system equations 2, 3, 4, and 5 are still valid. The control winding voltage is then changed to

$$V_c=K_AK_DE-K_t\dot{\theta} \qquad (16)$$

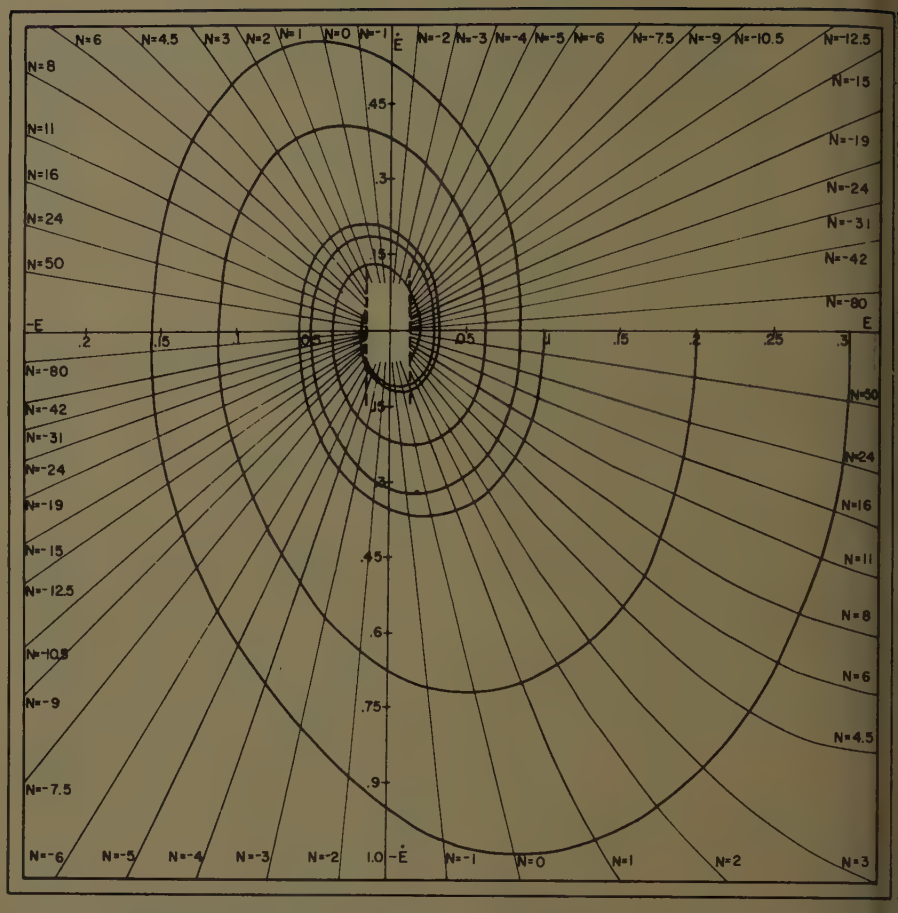

Fig. 8. Normalized phase-plane trajectories for step inputs of 0.1, 0.2, and 0.3 radian

The tachometer feedback system which is still a 2nd order system can be analyzed by the phase-plane method, the equation of the isoclines being of the same form as equation 12.

$$\dot{E}=\frac{-\omega_n^2E}{N+2\zeta\omega_n} \qquad (12)$$

The tachometer feedback has no effect on the natural frequency and equation 1 still holds. The damping ratio ζ is, however, affected and becomes

$$\zeta=1/2\sqrt{\frac{n}{AK_DK_AJ}}\left(F+\left|\frac{\partial T}{\partial\omega}\right|+AK_t\right) \qquad (17)$$

Thus the damping ratio of the compensated system can be increased by adding tachometer feedback. The analysis of the tachometer compensated system proceeds in similar fashion as that of the simple system. The effect of combining the AK_t with the nonlinear $\partial T/\partial\omega$ is to decrease the influence of the motor and more nearly linearize the system.

Conclusion

In conclusion it is observed that the nonlinearity of the 2-phase motor influences the transient response of a simple servomechanism changing the per-cent overshoot, frequency of oscillation and number of oscillations before coming into correspondence. The phase-plane analysis of this paper is extremely useful in giving one a better insight into this unusual behavior.

Appendix I

Construction of Isoclines

In Fig. 6 the phase-plane axes are shown and the quadrants are numbered through IV. In this figure the $+\dot{E}$ axis is labeled $-\dot{\theta}$ and the $-\dot{E}$ axis is labeled $+\dot{\theta}$. This can be best reasoned through as follows:

$$E\leftrightharpoons K_K(R-C)\leftrightharpoons K_D\left(R-\frac{\theta}{n}\right) \qquad (18$$

Since for a step input, R is a constant $\dot{E}$ is proportional to $-\dot{\theta}$, the speed of the motor in the opposite direction from the positive applied torque. The torque in the simple servo system of Fig. 1 is proportional to the error signal and the horizontal axes can be labeled $+T$ and $-T$.

As seen in Fig. 6 the speed and torque in quadrants II and IV of the phase plane

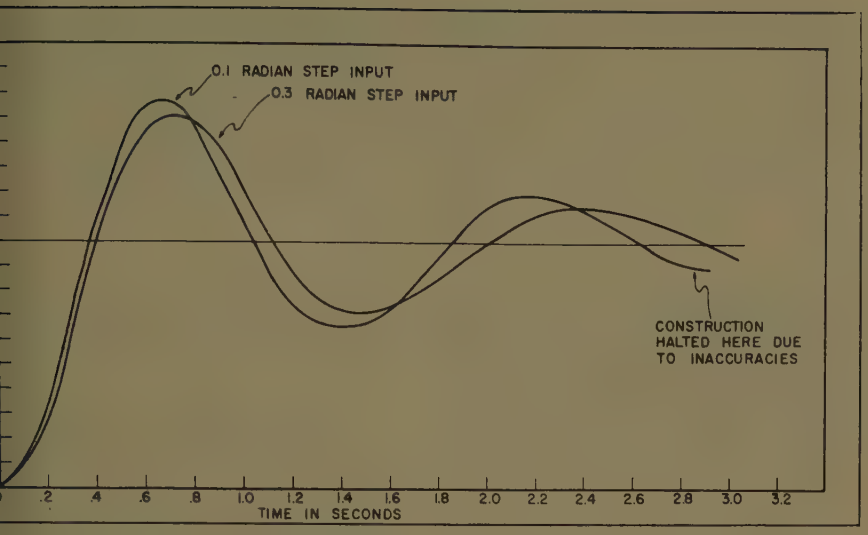

Fig. 9. Transient responses for step function inputs of 0.1 and 0.3 radian

of the same algebraic sign and the $/\partial\omega$ obtained from the first quadrant the speed-torque curve must be used. quadrants I and III the speed and que have algebraic signs and the con- nt value of $\partial T/\partial\omega$ determined from fourth quadrant of the speed-torque ve must be used.

Fig. 7 shows the transient response to tep input with the regions of positive l negative torque, and positive and gative speed indicated.

ase Trajectories and Transient Response

To check the validity of this analysis e 10-watt motor was built into a ser- mechanism whose parameters were

(amplifier gain) = 25 volts/volt
(error detector gain) = 18 volts/radian
gear ratio) = 500
(motor torque constant) = 0.0413 ounce-inch/volt
(total inertia) = 0.60 ounce-inch^2

e natural frequency of this system was lculated to be 4.9 radians per second. g. 8 is a small reproduction of the orig- l phase plane, with many of the iso- clines omitted in order not to obscure the drawing. The method employed in constructing the phase trajectories on the isoclines is presented in Appendix II. Phase trajectories for step inputs of 0.1, 0.2 and 0.3 radian are shown in Fig. 8. By numerical methods[5] the transient responses of two of these phase trajectories are calculated and plotted in normalized form in Fig. 9.

The parameters of this system were purposely chosen to produce a small ζ in the working voltage range as illustrated in Fig. 3. As a result this system is probably more lively than a properly designed system should be. The theory holds regardless of the relative damping of the servo and since a lively servo more effectively emphasizes the results of a variable ζ, it was chosen for this example.

There is an operating threshold of about 7 volts on the 2-phase motor; that is, if the control field voltage drops below 7 volts, the motor does not develop sufficient torque to keep it running. This 7 volts is equivalent to about 0.015 radian of error and is drawn in as two vertical lines in Fig. 8.

The usual transient behavior of this simple system is immediately observed.

1. The percentage overshoot is greater for the small step inputs

2. When there is a small step input the system is faster with higher frequencies of oscillation

3. The frequency of oscillations in a transient response becomes greater as time increases. Since the error signal decreases as correspondence is approached, the damping ratio ζ is decreased; and the frequency of oscillation

$$\omega = \omega_n \sqrt{1-\zeta 2}$$

over part of the cycle becomes larger. During the other portion of the cycle ζ does not vary; hence, ω also remains invariant

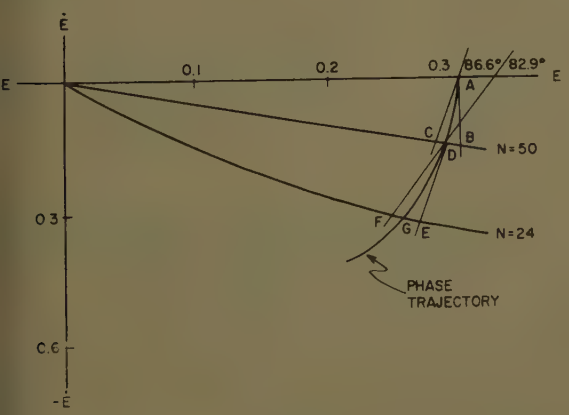

Fig. 10. Method used in constructing phase trajectories

Lienard's Construction

Another very effective method of showing the influence of the ζ varying with the magnitude of the control field voltage V_c is Lienard's construction. In order to employ this method the differential equation describing the physical system must be capable of being converted into a general form.

Appendix II

Construction of Phase Trajectories

The phase trajectory was constructed with respect to the isoclines by one of the accepted methods; however, to make this article more complete it will be briefly outlined in this appendix. For a step input of 0.3 radian, the phase trajectory starts at point A on the positive E axis at 0.3 radian. From point A of Fig. 10, two lines are constructed; one a vertical line and the other making an angle of 86.6 degrees with the positive E axis, since $\tan^{-1} 50/3 = \tan^{-1} 16.7 = 86.6°$. The 50 is the value of N assigned to the next isocline and the 3 is the scale ratio. Point D is then located midway between points B and C. From points D are constructed two lines making angles of 86.6° and 82.9° with the positive E axis. The point G is then located on the $N=24$ isocline midway between points E and F. The initial part of the phase trajectory is then drawn in with a French curve between the points A, D, and G.

References

1. Evaluating the Effect of Nonlinearity in a 2-Phase Servomotor, W. A. Stein, G. J. Thaler. *AIEE Transactions*, pt. II (*Applications and Industry*), vol. 73, 1954 (Jan. 1955 section), pp. 518–21.

2. A Special Dynamometer for Testing Small Motors, S. H. Van Wambeck, W. A. Stein.

Electrical Engineering, vol. 71, no. 6, June 1952, pp. 549–51.

3. Basic Feedback Control System Design (book), G. J. Savant. McGraw-Hill Book Company, Inc., New York, N. Y., 1958, p. 278.

4. The Effect of Non-Sinusoidal Impressed Voltages on A. C. Servo Motors, C. W. Busey, W. R. Bartow. *Master Thesis*, U. S. Naval Postgraduate School, Monterey, Calif., 1955.

5. Control System Synthesis (book), J. G. Truxal. McGraw-Hill Book Company, Inc., 1955, pp. 625–30.

6. Etude Des Oscillations Entretenues, A. Lienard. *Revue Générale de l'Electricité*, Paris, France, vol. 23, 1928, pp. 946–54.

7. Introduction to Non-linear Mechanics (book), N. Minorsky. J. W. Edwards, Ann Arbor, Mich., 1947, pp. 106–15.

8. Nonlinear Vibrations (book), J. J. Stoke Interscience Publishers, Inc., New York, N. Y 1950.

9. Ordinary Nonlinear Differential Equ tions (book), N. W. Mc Lachlan. Clarendon Pres Oxford, England, 1950 and 1956.

10. Analysis and Control of Nonlinea Systems (book), M. M. Ku. The Ronald Pre Company, New York, N. Y., 1958.

Discussion

H. Chestnut (General Electric Company, Schenectady, N. Y.): Mr. W. A. Stein in this paper has served to bring out a number of important points in connection with servosystems. First, that many simple control systems are not really linear and that the phase-plane method provides a useful tool to obtain a more exact solution for such problems. Second, the response obtained for some such nonlinear systems with different input amplitudes, as for example Fig. 5, may not differ too significantly in the over-all performance obtained. Although, as pointed out by the author, the peak overshoots and the frequency of oscillation are not independent of input amplitude predicted from linear performance, the curves do reflect the fact that in nondimensionalized form the results are not strongly amplitude sensitive.

G. J. Thaler: I wish to thank Mr. Chestnut for emphasizing those points which are of particular interest to the design engineer. It is important that the engineer should realize that many control systems are not linear, and it is equally important to reali that the nonlinear effect may be significa in a given application and therefore neg gible.

It is also important to understand t mechanism and effects of the nonlinearit in as much detail as possible, since suc understanding leads to the logical use of e gineering judgment in design. I feel su Dr. Stein wished to point out that the u of phase-plane analysis, where applicabl leads to such understanding, and as a resu he shows that the nonlinear effects of t 2-phase motor are readily swamped o by addition of linear tachometer feedback

Sampled-Data Control Systems with Two Digital Processing Units

J. C. HUNG
ASSOCIATE MEMBER AIEE

Synopsis: This paper presents the theory and procedure for designing sampled-data control systems of the rippleless type having a digital processing unit in the forward line and another digital processing unit in the feedback loop to respond optimally to inputs as well as to neutralize the disturbance. Two examples using the proposed design procedure are given, and their root loci are plotted and discussed.

RECENT LITERATURE has been concerned with the theory and the design procedure for sampled-data control systems utilizing a digital processing unit in the forward line to achieve the desired input-output performance.[1–8] The effect of disturbances for systems having unity feedback has also been mentioned.[3] Nevertheless, so far as extant literature is concerned, little has been mentioned of systems having two digital processing units, one in the forward line and the other in the feedback loop, to achieve both a deadbeat input-output function and the neutralization of disturbances.

It will be shown that by using two digital processing units the input-output function and the disturbance-output function can be implemented independently. The design criterion for the disturbance-output function is that the effect of the disturbance upon the output subsides to zero completely, either at the sampling instants only, or ripple-free, depending on the designer's specification, in the least number of sampling periods. The required mathematical form for the input-output transfer function has been discussed by Bergen and Ragazzini, and wi be included for completeness.[2] Th technique described can be used for re ular design. In the following the inpu and disturbances are assumed to be d scribable as finite powers of t.

Referring to Fig. 1, the notation used this paper is as follows:

$C(z)$ = pulsed system output in response input signal
$R(z)$ = pulsed input function
$K(z)$ = pulsed input-output function = $C(z)$ $R(z)$
$C'(z)$ = pulsed system output in response disturbance
$U(z)$ = pulsed disturbance function
$J(z)$ = pulsed disturbance-output function $C'(z)/U(z)$
$G_1(s)$ = Laplace transform of plant transf function
$H(s)$ = Laplace transform of hold circuit
$G(z)$ = pulsed transfer function of plant-hol combination = $G_1H(z)$
$D_1(z)$, $D_2(z)$ = pulsed transfer functions digital processing units
$E(z)$ = pulsed error function in response input function = $R(z) - C(z)$
$E_1(z)$ = pulsed input of $D_1(z)$ in response input signal
$E_1'(z)$ = pulsed input of $D_1(z)$ in response disturbance
$E_2(z)$ = pulsed commanding signal in sponse to input signal
$E_2'(z)$ = pulsed commanding signal in sponse to disturbance

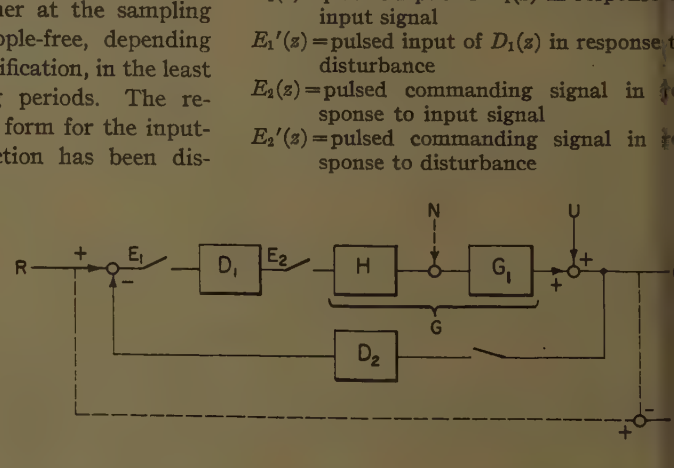

Fig. 1. Sampled-data system with two digital processing units

Paper 60-867, recommended by the AIEE Feedback Control Systems Committee and approved by the AIEE Technical Operations Department for presentation at the AIEE Summer General Meeting, Atlantic City, N. J., June 19–24, 1960. Manuscript submitted November 1, 1959; made available for printing June 1, 1960.

J. C. Hung is with the Department of Electrical Engineering, New York University, New York, N. Y.

The author wishes to express his gratitude to Dean J. R. Ragazzini and Professor S. S. L. Chang of New York University for their devoted guidance and reviewing of the manuscript. This research was supported by the United States Air Force under Contract *AF 49(638)–586* monitored by the Office of Scientific Research, Air Research and Development Command, Washington 25, D. C.

ferring to Fig. 1, the basic relations een the variables and the components eadily shown to be as follows:

$$=\frac{C(z)}{R(z)}=\frac{D_1(z)G(z)}{1+D_1(z)D_2(z)G(z)} \quad (1)$$

$$=\frac{C'(z)}{U(z)}=\frac{1}{1+D_1(z)D_2(z)G(z)}$$

$$=1-D_2(z)K(z)=\frac{K(z)}{D_1(z)G(z)} \quad (2)$$

$$=\frac{R(z)-C(z)}{R(z)}=1-K(z) \quad (3)$$

$$)=\frac{K(z)}{D_1(z)G(z)}=\frac{1}{1+D_1(z)D_2(z)G(z)}=J(z) \quad (4)$$

$$)=\frac{K(z)}{G(z)}=\frac{D_1(z)}{1+D_1(z)D_2(z)G(z)} \quad (5)$$

$$z)=\frac{D_2(z)}{1+D_1(z)D_2(z)G(z)}=J(z)D_2(z) \quad (6)$$

$$z)=\frac{D_1(z)D_2(z)}{1+D_1(z)D_2(z)G(z)}=\frac{K(z)D_2(z)}{G(z)} \quad (7)$$

$$z)=\frac{K(z)}{J(z)G(z)} \quad (8)$$

$$z)=\frac{1-J(z)}{K(z)} \quad (9)$$

$$)=NG_1(z) \quad (10)$$

strictions on Mathematical Forms

The mathematical form of the plant- d transfer function is

$$)=\frac{z^{-m}(p_0+p_1z^{-1}+\ldots+pz_a{}^{-a})}{q_0+q_1z^{-1}+\ldots+q_bz^{-b}} \quad (11)$$

ere the factor z^{-m} represents the plant nsfer lag. The constant q_0 assures that output of the plant does not depend the future of the input.

The restrictions on the pulsed input- tput function $K(z)$ are mentioned later.[2] st, $K(z)$ must contain in its numerator plant transfer lag factor z^{-m}. cond, $K(z)$ must contain as its zeros the zeros of $G(z)$ which are outside or the unit-circle of z-plane. Third, for system having no steady-state input- tput error during the sampling in- nts in response to an input function

$$z)=\frac{A(z)}{(1-z^{-1})^m} \quad (12)$$

ere $A(z)$ does not contain $(1-z^{-1})$ as a tor, the error function, equation 3, must ve the factor $(1-z^{-1})^m$ as its zero so as cancel the same factor in the de- minator of $R(z)$, that is

$$\frac{z)}{z)}=1-K(z)=(1-z^{-1})^mF(z) \quad (13)$$

Equation 13 is equivalent to the following m conditions

$$\lim_{z\to 1} K(z)=1$$

$$\lim_{z\to 1} K'(z)=0$$

$$\vdots$$

$$\lim_{z\to 1} K^{(m-1)}(z)=0 \quad (14)$$

where all the derivatives are taken with respect to z^{-1}. These m equations can be solved for m constants resulting in a $K(z)$ for minimal prototype response. If the criterion other than the shortest settling time is desired more than m constants should be determined.

The disturbance may be expressed in the form

$$U(z)=\frac{B(z)}{(1-z^{-1})^n} \quad (15)$$

where $B(z)$ has no $(1-z^{-1})$ factors. Equation 15 includes deterministic type of disturbances describable as finite powers of t. This form of disturbance is a practical and reasonable one. In the case of regulator design, it includes the practical cases such as leakage of flow control, load change of speed control, and shift of static characteristic of the plant.

The first restriction on the pulsed disturbance-output function $J(z)$ comes from the criterion that the disturbance must be neutralized.

In order to have zero steady-state disturbance effect at the sampling instants, the disturbance-output function, equation 2, must contain as its zero the factor $(1-z^{-1})^n$. That is

$$J(z)=\frac{C'(z)}{U(z)}=1-D_2(z)K(z)=(1-z^{-1})^nV(z) \quad (16)$$

Equation 15 is equivalent to the following n conditions:

$$\lim_{z\to 1} J(z)=0$$

$$\lim_{z\to 1} J'(z)=0$$

$$\vdots$$

$$\lim_{z\to 1} J^{(n-1)}(z)=0 \quad (17)$$

where all derivatives are taken with respect to z^{-1}. These n equations can be solved for n constants, resulting in a $J(z)$, which gives a fastest subsidence of disturbance effect. The second restriction on $J(z)$ can be seen readily from equation 8, which can be written in the form

$$J(z)=\frac{K(z)}{D_1(z)G(z)} \quad (18)$$

In order to avoid the pole-zero cancellation outsider or on the unit-circle, $J(z)$ must contain as its zeros all the unstable poles of $G(z)$.

It is of interest to note that Bertram's condition that $1-K(z)$ must contain as its zeros all the undesirable poles of $G(z)$ can be removed by using a digital unit in the feedback loop.[7] The latter method has the advantage that the polynomial $K(z)$ can be made shorter giving a shorter settling time.

The procedure is as follows: After $K(z)$ is obtained by the method indicated in equation 14, obtain $D_2(z)$ from the equation

$$1-D_2(z)K(z)=Q(z)$$

where $Q(z)$ is a finite polynomial containing all the undesirable poles of $G(z)$; and obtain $D_1(z)$ from the equation

$$D_1(z)=\frac{K(z)}{G(z)[1-D_2(z)K(z)]}$$

Additional Restrictions on Ripple-free Systems

The additional requirement for implementing a ripple-free input-output function is that quantity E_2 be the quotient of a finite polynomial in z^{-1} and the factor $(1-z^{-1})^q$, where $q\leqq h+1$, and h is the order of hold. This means that first, the function $K(z)$ must contain as its zeros, all the zeros of $G(z)$; and second, the pole order m of $R(z)$, as defined in equation 12, cannot be greater than the number of integrations in the plant $G_1(s)$ by more than $h+1$. The latter is because of the fact that an hth order hold cannot produce a smooth output if the input is of order greater than $h+1$. If the number of plant integrations is less than $m-(h+1)$ then additional integrations must be inserted between the hold and the plant.

A similar requirement exists for implementing a ripple-free disturbance-output function. Since $J(z)$ is designed to be a finite polynomial in z^{-1}, which, from quantity E_2, requires that $K(z)D_2(z)$ also be a finite polynomial. To insure that the system is ripple-free, the additional requirement is that $E'(z)/U(z)$ be the quotient of a finite polynomial and the factor $(1-z^{-1})^p$, where $p\leqq h+1$, and h is the order of hold. This condition is satisfied when, from equation 7, $K(z)$ contains as its zeros all the zeros of $G(z)$; and when the pole order n of $U(z)$, as defined in equation 15, is not greater than the number of plant integration by more than $h+1$.

The system is ripple-free for both input-output and disturbance-output functions if it is ripple-free for either one having a higher pole order.

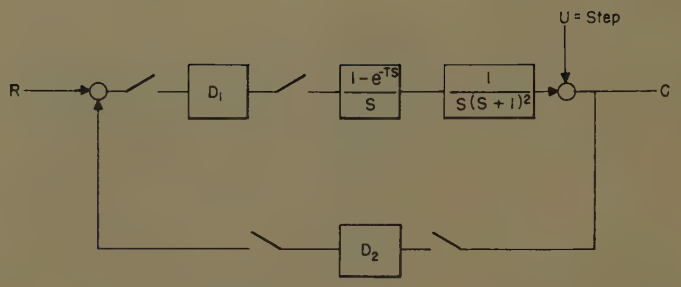

Fig. 2. Sampled-data system for example I

Design Procedure

The desired performance includes: first that the disturbance effect dies off rapidly, and second, that the input-output performance has a zero steady-state error. The design procedure is as follows:

Find the function $K(z)$ satisfying the aforementioned requirements for the desired input-output performance.[2] Thus

$$K(z)=z^{-m}W(z)M(z) \tag{19}$$

where $W(z)$ contains all the zeros outside of the unit-circle of $G(z)$, and $M(z)$ has no zeros outside of the unit-circle.

To have the fast subsidence of disturbance effect at the sampling instants it is desired that $J(z)$ be as short a polynomial in z^{-1} as possible.

$$J(z)=1-D_2(z)K(z) \tag{2}$$

The shortest $J(z)$ is obtained by letting $D_2(z)$ contain as its denominator for factor $M(z)$, that is,

$$D_2(z)=\frac{b_0+b_1z^{-1}+\ldots+b_{n-1}z^{-n-1}}{M(z)} \tag{20}$$

where all the b's will be determined later. Equation 2 then becomes

$$J(z)=1-\frac{b_0+b_1z^{-1}+\ldots+b_{n-1}z^{-n-1}}{M(z)}\times z^{-m}W(z)M(z)$$
$$=1-(b_0+b_1z^{-1}+\ldots+b_{n-1}z^{-n-1})z^{-m}W(z) \tag{21}$$

As mentioned before, $J(z)$ must satisfy the n conditions formulated in equation 16. These n conditions determine the n constants $b_0, b_1, \ldots,$ and b_{n-1}.

If a ripple-free performance is desired the conditions stated in the previous paragraph must be included.

If the staleness factor is used in $K(z)$ it must be contained as a zero in $D_2(z)$.

That is, if

$$K(z)=\frac{z^{-m}W(z)M(z)}{(1-Cz^{-1})^q} \tag{22}$$

where $(1-Cz^{-1})^q$ is the staleness factor, then

$$D_2(z)=\frac{(b_0+b_1z^{-1}+\ldots+b_{n-1}z^{-n-1})(1-Cz^{-1})^q}{M(z)} \tag{23}$$

and

$$J(z)=1-D_2(z)K(z)$$
$$=1-(b_0+b_1z^{-1}+\ldots+b_{n-1}z^{-n-1})z^{-m}W(z) \tag{24}$$

Equation 24 is the same as equation 21 but the two digital processing units $D_2(z)$ are different.

Obtain the digital processing unit pulsed transfer function $D_1(z)$ from the equation

$$D_1(z)=\frac{K(z)}{J(z)G(z)} \tag{8}$$

It is worth noting that the disturbance function $U(z)$ used throughout the previous discussion is for the disturbance affecting the system at the output point as shown in Fig. 1. If the disturbance is applied at another point of the system, however, the design procedure is the same, provided that a modified disturbance function is used. For example, a disturbance $N(s)$ may appear between the hold and the plant Fig. 1. This disturbance can be represented by an equivalent disturbance at the output as

$$U(s)=N(s)G_1(s) \tag{25}$$

resulting in a pulsed disturbance function

$$U(z)=NG_1(z) \tag{26}$$

An example will be given to illustrate this aspect.

The equations 19, 21, 22, and 24 show that $K(z)$ and $J(z)$ can be implemented independently, but both of them are restricted by the nature of the plant.

Example I

In Fig. 2, $D_1(z)$ and $D_2(z)$ are to be determined to give a performance having zero steady-state input-output error and zero steady-state disturbance effect at the sampling instants. The disturbance is assumed to be a unit step. Using pulsed functions, one has

$$G(z)=\frac{z^{-1}(1+2.34z^{-1})(1+0.16z^{-1})}{(1-z^{-1})(1-0.368z^{-1})^2}$$

$$U(z)=\frac{1}{1-z^{-1}}$$

CASE A

If the input signal is also a unit step, then

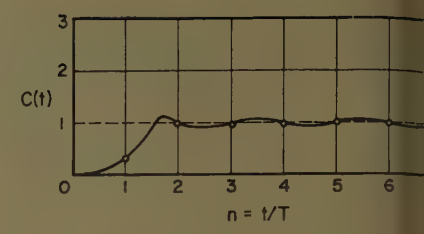

Fig. 3. Output of example I-A in respon to unit step input

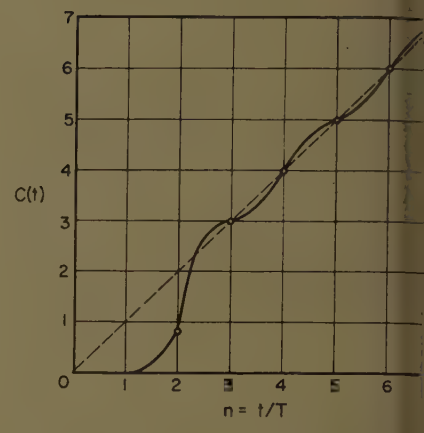

Fig. 4. Output of example I-B in response unit ramp input

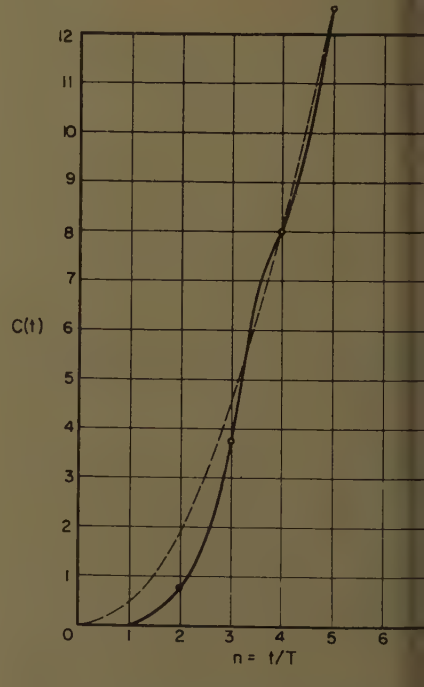

Fig. 5. Output of example I-C in respon to constant acceleration input

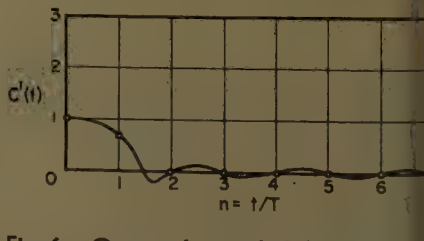

Fig. 6. Output of example I-A, B, and C response to step-type disturbance u(t)

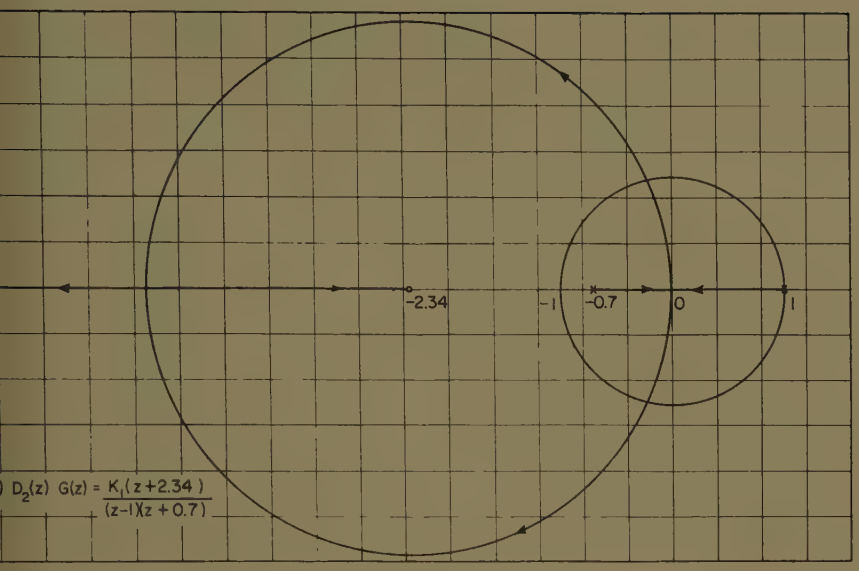

Fig. 7. Root-locus plot for example I

$=\frac{1}{1-z^{-1}}$

ind $K(z)$, let

$)=z^{-1}(1+2.34z^{-1})a_0$

lying the condition $K(1)=1$, gives a_0
3, so

$)=0.3z^{-1}(1+2.34z^{-1})$

$z)=\frac{b_0}{0.3}$

$)=b_0z^{-1}(1+2.34z^{-1})$

lying the condition $J(1)=0$, gives $b_0=$
so that

$)=(1-z^{-1})(1+0.7z^{-1})$

e digital units are

$z)=1$

$z)=\frac{0.3(1-0.368z^{-1})^2}{(1+0.7z^{-1})(1+0.16z^{-1})}$

e respective output response of the
ut signal and the disturbance are

$)=0.3z^{-1}+z^{-2}+z^{-3}+\ldots$

$z)=1+0.7z^{-1}$

SE B

If the input signal is a unit ramp,
en

$z)=\frac{z^{-1}}{(1-z^{-1})^2}$

find $K(z)$, let

$z)=z^{-1}(1+2.34z^{-1})(a_0+a_1z^{-1})$

plying the conditions $K(1)=1$, and $K'(1)=0$, gives $a_0=0.805$, and $a_1=-0.506$, and gives

$K(z)=z^{-1}(1+2.34z^{-1})(0.805-0.506z^{-1})$

Let

$D_2(z)=\frac{b_0}{0.805-0.506z^{-1}}$

then

$J(z)=1-b_0z^{-1}(1+2.34z^{-1})$

Applying the condition $J(1)=0$, gives again $b_0=0.3$, and again gives

$J(z)=(1-z^{-1})(1+0.7z^{-1})$

The two digital processing units are

$D_2(z)=\frac{0.372}{1-0.629z^{-1}}$

$D_1(z)=\frac{0.805(1-0\ 629z^{-1})(1-0.368z^{-1})^2}{(1+0.7z^{-1})(1+0.16z^{-1})}$

The respective output responses of the input signal and disturbance are

$C(z)=0.805z^{-2}+3z^{-3}+4z^{-4}\ldots$

$C'(z)=1+0.7z^{-1}$

CASE C

If the input signal is of the constant acceleration type, then

$R(z)=\frac{z^{-1}(1+z^{-1})}{2(1-z^{-1})^3}$

Following the same procedure,

$K(z)=1.47z^{-1}(1+2.34z^{-1})\times(1-1.24z^{-1}+0.477z^{-2})$

$J(z)=(1-z^{-1})(1+0.7z^{-1})$

$D_2(z)=\frac{0.204}{1-1.24z^{-1}+0.477z^{-2}}$

$D_1(z)=\frac{1.47(1-1.24z^{-1}+0.477z^{-2})(1-0.368z^{-1})^2}{(1+0.7z^{-1})(1+0.16z^{-1})}$

$C(z)=0.735z^{-2}+3.746z^{-3}+8z^{-4}+12.5z^{-5}+\ldots$

$C'(z)=1+0.7z^{-1}$

The responses for these systems are shown in Figs. 3, 4, 5, and 6. It can be seen that the three input-output functions obtained are exactly the same as those obtained for unity feedback systems using Bergen and Ragazzini's procedure.[2] Since the disturbances for the three systems are the same, the same $J(z)$ function was obtained. This shows the independence of implementing the $K(z)$ and $J(z)$ functions. It is also interesting to note that if the input signal and the disturbance are of the same order, then $D_2(z)$ results in unity, a unity feedback system!

It is of interest to note that

$$K(z)=\frac{1}{D_2(z)}\,\frac{D_1(z)D_2(z)G(z)}{1+D_1(z)D_2(z)G(z)}$$

and that, in this example, the poles of $K(z)$ are the zeros of $D_2(z)$, which are fixed and the zeros of $1+D_1(z)D_2(z)G(z)$ which are given by the root locus of $1+D_1(z)D_2(z)G(z)$ shown in Fig. 7. The root loci of all these systems are identical but the zeros of $D_2(z)$ are all at the origin of the z-plane and differ in number, there being none for case A, one for case B, and two for case C. In all cases the two roots contributed by $1+D_1(z)D_2(z)G(z)$ are at the origin.

It is further observed that the pole-zero cancellations effected in the open loop pulsed transfer functions differ. They are as follows:

A. Step input system
$z=0.368,\ 0.368,\ -0.16$

B. Ramp input system
$z=0.368,\ 0.368,\ -0.16,\ 0.629$

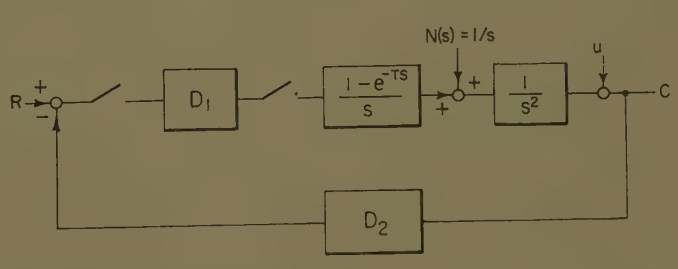

Fig. 8. Sample-data system for example II

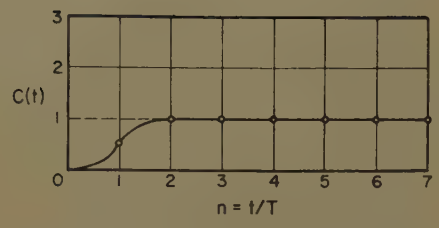

Fig. 9. Output of example II-A in response to unit step input

C. Constant acceleration input system
$z=0.368,\ 0.368,\ -0.16,\ 0.62\pm j0.304$

Example II

The system shown in Fig. 8 is to be implemented to give a ripple-free input-output performance and a ripple-free neutralization of disturbance effect. The disturbance is of the step type, which appears at the point between the hold and the plant. The Laplace transform of the disturbance function is

$$N(s)=\frac{1}{s}$$

The equivalent disturbance at the output end is

$$U(s)=N(s)G_1(s)=\frac{1}{s^3}$$

whose pulsed function is

$$U(z)=\frac{z^{-1}(1+z^{-1})}{2(1-z^{-1})^3}$$

The pulsed plant-hold transfer function is

$$G(z)=\frac{z^{-1}(1+z^{-1})}{2(1-z^{-1})^2}$$

CASE A

If the input is a unit step, then

$$R(z)=\frac{1}{1-z^{-1}}$$

Let

$$K(z)=z^{-1}(1+z^{-1})a_0$$

Applying the condition $K(1)=1$, gives $a_0=0.5$, so that

$$K(z)=0.5z^{-1}(1+z^{-1})$$

Let

$$D_2(z)=\frac{b_0+b_1z^{-1}+b_2z^{-2}}{0.5}$$

then

$$J(z)=1-(b_0+b_1z^{-1}+b_2z^{-2})z(1+z^{-1})$$

Applying the conditions $J(1)=0$, $J'(1)-0$ and $J''(1)=0$, gives $b_0=2.125$, $b_1=-2.5$, and $b_2=0.875$, therefore

$$J(z)=(1-z^{-1})^3(1+0.875z^{-1})$$

The digital processing units are

$$D_2(z)=4.25-5z^{-1}+1.75z^{-2}$$

$$D_1(z)=\frac{1}{(1-z^{-1})(1+0.875z^{-1})}$$

The respective output responses of the input signal and the disturbance are

$$C(z)=0.5z^{-1}+z^{-2}+z^{-3}+\ldots$$

$$C'(z)=z^{-1}+1.875z^{-2}+0.875z^{-3}$$

CASE B

If the input is a unit ramp, then

$$R(z)=\frac{z^{-1}}{(1-z^{-1})^2}$$

Let

$$K(z)=z^{-1}(1+z^{-1})(a_0+a_1z^{-1})$$

Applying the condition $K(1)=1$, and $K'(1)=0$, gives $a_0=1.25$, and $a_1=-0.75$, therefore

$$K(z)=z^{-1}(1+z^{-1})(1.25-0.75z^{-1})$$

Let

$$D_2(z)=\frac{b_0+b_1z^{-1}+b_2z^{-2}}{1.25-0.75z^{-1}}$$

then

$$J(z)=1-(b_0+b_1z^{-1}+b_2z^{-2})z^{-1}(1+z^{-1})$$

Applying the conditions required for $J(z)$ gives the same constants as before, thus

$$J(z)=(1-z^{-1})^3(1+0.875z^{-1})$$

The two digital units are

$$D_2(z)=\frac{1.7-2z^{-1}+0.7z^{-2}}{1-0.6z^{-1}}$$

$$D_1(z)=\frac{2.5(1-0.6z^{-1})}{(1-z^{-1})(1+0.875z^{-1})}$$

The respective output responses of the input signal and the disturbance are

$$C(z)=1.25z^{-2}+3z^{-3}+4z^{-4}+\ldots$$

$$C'(z)=z^{-1}+1.875z^{-2}+0.875z^{-3}$$

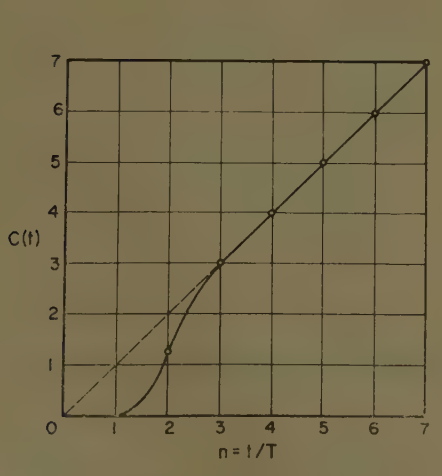

Fig. 10. Output of example II-B in response to unit ramp input

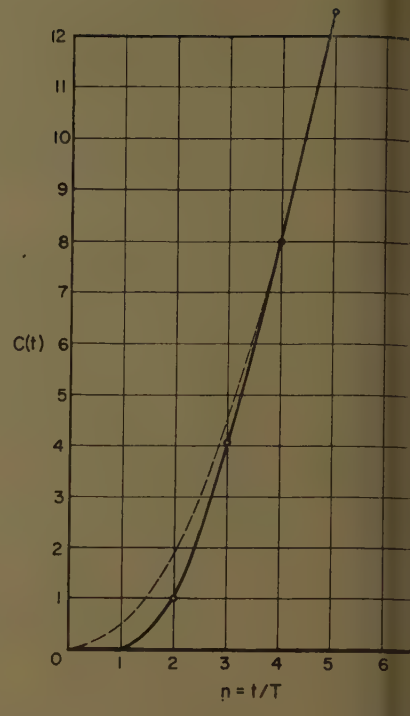

Fig. 11. Output of example II-C in respo to constant acceleration input

CASE C

If the input is constant acceleratio then

$$R(z)=\frac{z^{-1}(1+z^{-1})}{2(1-z^{-1})^3}$$

Following the same procedure,

$$K(z)=2.125z^{-1}(1+z^{-1})(1-1.18z^{-1}+0.411z$$

$$J(z)=(1-z^{-1})^3(1+0.875z^{-1})$$

$$D_2(z)=1$$

$$D_1(z)=\frac{4.25(1-1.18z^{-1}+0.411z^{-2})}{(1-z^{-1})(1+0.875z^{-1})}$$

$$C(z)=1.0625z^{-2}+4.0625z^{-3}+8z^{-4}+12.5z^{-5}+\ldots$$

$$C'(z)=z^{-1}+1.875z^{-2}+0.875z^{-3}.$$

The responses are shown in Figs. 9, 11, and 12. And the root loci of the three systems, which are the same, plotted as shown in Fig. 13. It is interesting to note that all the root loci through the $z=0$ point. The number poles of $K(z)$ at the origin differs for t

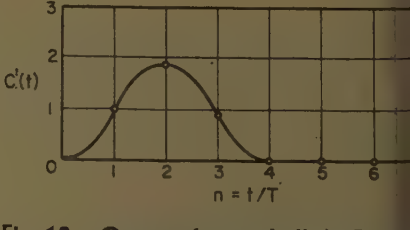

Fig. 12. Output of example II-A, B, and in response to step type disturbance n(t)

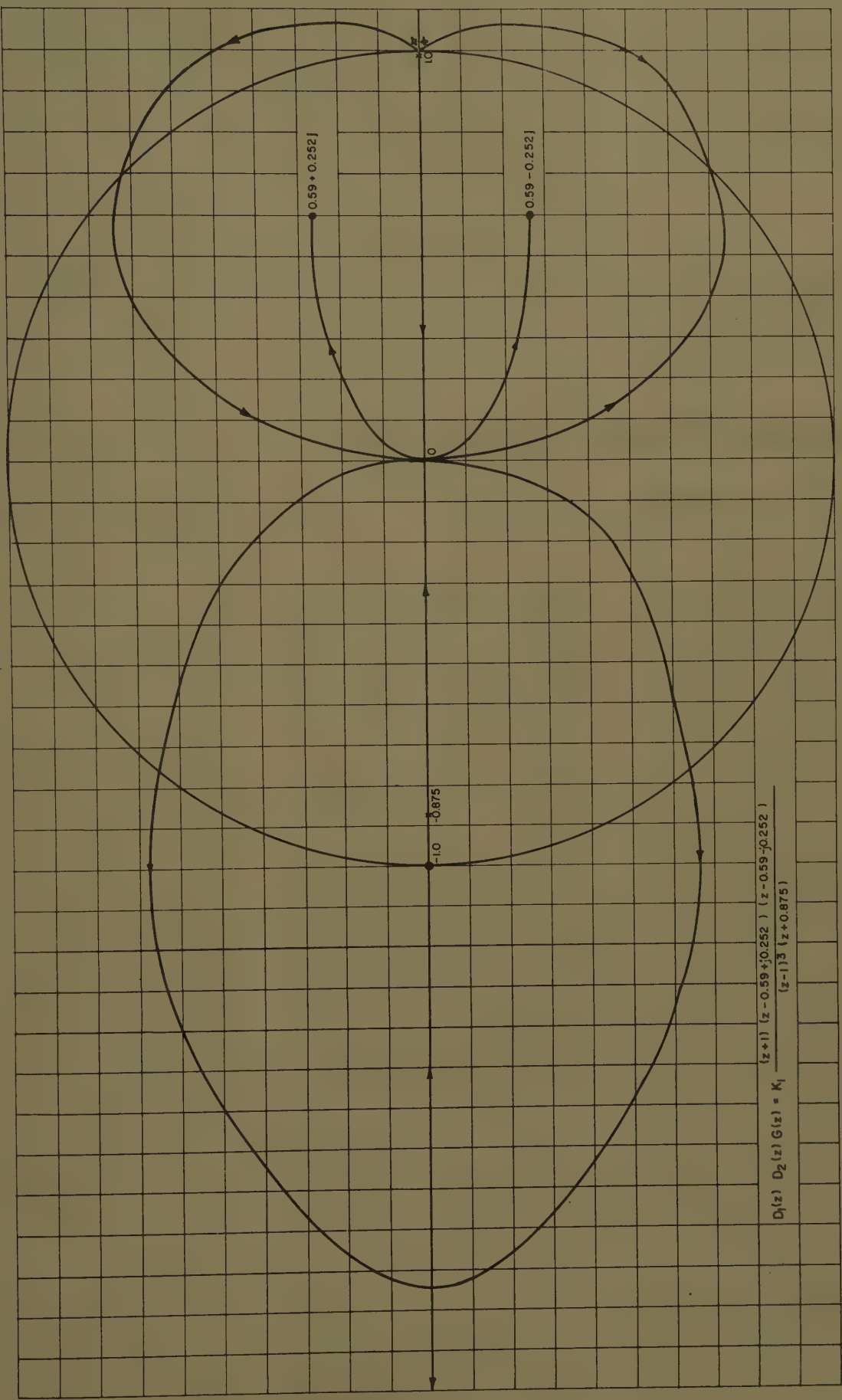

Fig. 13. Root-locus plot for example II

three cases, there being two for case A, three for case B, and four for case C. This is caused by there being two, one, and no poles of $D_2(z)$ respectively at the origin. In terms of root loci, one may say that a deadbeat system is the one which is so implemented such that its root loci are forced to pass through the origin, and its operating point is chosen at the origin.

Conclusion

The procedure of implementing two digital processing units to neutralize the effect of simple disturbance of a deadbeat system has been presented. By simple disturbance is meant a disturbance of step, ramp, or constant acceleration type. The neutralization can be realized for disturbances affecting the system any place except the input point. A ripple-free system for both input-output and disturbance-output performance can be obtained simultaneously.

References

1. The Analysis of Sampled-Data System, J. R. Ragazzini, L. A. Zadeh. *AIEE Transactions*, pt. II (*Applications and Industry*), vol. 71, Nov. 1952, pp. 225–34.

2. Sampled-Data Processing Techniques for Feedback Control Systems, A. R. Bergen, J. R. Ragazzini. *Ibid.*, vol. 73, Nov. 1954, pp. 47.

3. Sampled-Data Control Systems (bo J. R. Ragazzini, G. F. Franklin. McGraw Book Company, Inc., New York, N. Y., 1958

4. Optimum Design Technique for Feedb Control Systems (book), S. S. L. Chang. Graw-Hill Book Company, Inc. (to be publish

5. The Design of Sampled-Data Feedb Systems, G. V. Lago, J. G. Truxal. *AIEE T actions*, pt. II (*Applications and Industry*), vol Nov. 1954, pp. 247–53.

6. Extension of Continuous-Data Sys Design Technique to Sampled-Data Con Systems, G. W. Johnson, D. P. Lindorff, C. Nordling. *Ibid.*, vol. 74, Sept. 1955, pp. 252–6

7. Factors in the Design of Digital C trollers for Sampled-Data Feedback Syst J. E. Bertram. *Ibid.*, vol. 75, July 1956, pp. 151

8. Sampled-Data Control Systems (bo E. I. Jury. John Wiley & Sons, Inc., New Y N. Y. 1958.

A Constant-Voltage Battery Charger

C. H. LEET
MEMBER AIEE

W. ZUG
ASSOCIATE MEMBER AIEE

THE USE OF BATTERIES in control centers, such as are found in sub- and central stations, is well established. With this application goes the need for a battery charger which will maintain the battery in a fully charged state. It must also carry any fixed load and be capable of recharging the battery when required by battery and circuit conditions.

Under normal operating conditions, the battery charger, battery, and load are connected in parallel. The charger, up to the limit of its capacity, furnishes the steady connected load, and the current taken by the battery at float voltage. With the charger maintaining a voltage across the battery a few hundredths of a volt per cell in excess of open-circuit voltage, the battery will accept sufficient current to offset internal losses (self-discharge). In this fully charged condition, the battery is said to be floated. The battery furnishes all system load currents in excess of charger capacity, such as momentary currents for circuit breaker closing, tripping, etc. In the event of an a-c power failure in the station, the charger cannot supply direct current and the battery takes over to carry the load. The battery is discharged to a degree depending on the duration of the outage, d-c loads, and the battery capacity. After a-c supply has been restored following a power failure, or when the d-c load has decreased to within the charger rating, the battery has to be recharged. During the recharge, the charger must also carry the normal connected load.

Requirements of a Float Charger

In order to float the battery and thus keep it fully charged, the charger should exhibit a constant-voltage characteristic with changing load conditions and a-c supply voltage fluctuations. This constant-voltage characteristic is also one of the requirements to obtain maximum life of the battery. Because of the low incremental impedance of the charger required for the constant-voltage characteristic, current limiting provisions have to be made to limit the charger current to a safe value when the battery voltage is l i.e., when recharging a battery after a-c power failure. A means of adjust the output voltage of the charger is quired since periodic equalizing char are usually recommended by batt manufacturers.

Types of Chargers

There are two main groups of charg the rotating type and the static recti type. The diverter-pole charger is of rotating type and it meets the afo mentioned electrical requirements. Ho ever, wear and maintenance, down ti and noise which are typical for rotat equipment have encouraged the devel ment of static chargers. Ordinary sta equipment eliminates the disadvanta of the rotating machines in respect to w and noise but does not meet the electri requirements inherently as do rotat chargers. Sensitivity to a-c supply vo age fluctuations has been an importa factor in preventing the static recti charger from being widely used. Furth more the range from zero to about 1 of the charger output current rati where it is most important for the life

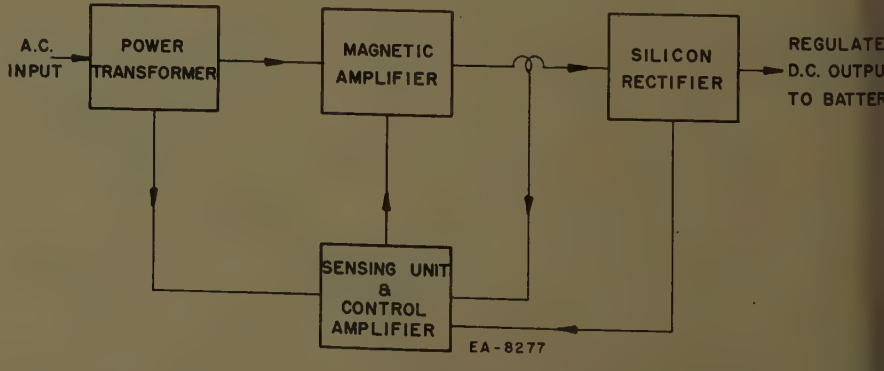

Fig. 1. UR rectifier block diagram

Paper 60-895, recommended by the AIEE Chemical Industry Committee and approved by the AIEE Technical Operations Department for presentation at the AIEE Summer General Meeting, Atlantic City, N. J., June 19–24, 1960. Manuscript submitted March 24, 1960; made available for printing May 17, 1960.

C. H. Leet is with The Electric Storage Battery Company, Philadelphia, Pa., and W. Zug is with The Electric Products Company, Cleveland, Ohio.

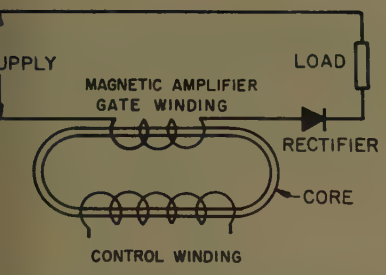

2. Self-saturating magnetic amplifier

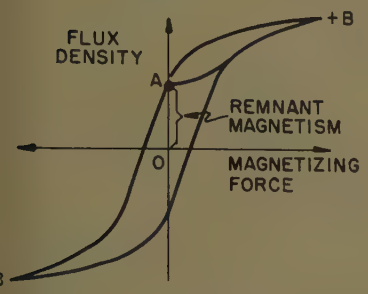

Fig. 3. Hysteresis loop

battery to hold constant voltage, is included in the closely regulated e.

UR Rectifier

o overcome the deficiencies of both rotating charger and the rectifier ger as stated above, the Utility Recti- charger-type "UR" was developed. charger uses the latest advances in it technique in connection with ponents such as silicon rectifiers that no detectable aging and theoretically nited life, and magnetic amplifiers have high efficiency and long life parable to a transformer. All ad- ages of the rotating charger are re- ed or actually improved. The ger is relatively insensitive to a-c ly voltage fluctuations, will regulate tant voltage from zero to full load, limit the output current to a safe e for charger and battery, can easily djusted for output voltage, retains ruggedness of a machine, and actually roves over-all conversion efficiency. UR charger eliminates all the obvious dvantages of a rotating element, such ear, maintenance, and noise.

ory of Operation

UR Rectifier Block Diagram

Fig. 1, only the components essential he operation of the charger are shown. essential components for the opera- and auxiliary devices such as switches. s, alarm relay, etc., are omitted. The tion of the components shown in the ram is as follows:

Power Transformer

The power transformer serves a double purpose. First of all it serves as a matching transformer to match the available a-c line voltage to the battery charging voltage requirements. Taps on the high-voltage winding facilitiate the matching of the a-c line voltage available at the charger installation to the transformer. In using the voltage tap closest to the nominal value of the a-c supply voltage, the average value around which the voltage fluctuates, the maximum benefit from the regulating capability of the charger will be obtained and at the same time will result in the best possible efficiency and power factor.

The transformer also serves as an isolating transformer. Usually the a-c supply is grounded in one-phase center tap, or star point. The transformer, however, isolates the battery circuit from the a-c supply circuit and the battery circuit can be operated grounded or ungrounded.

Magnetic Amplifier

The magnetic amplifier can be viewed as a valve which, as signalled by the sensing unit with a control amplifier, allows more or less current to pass through the rectifiers to the battery. The magnetic amplifier is of the self-saturating type in a modified saturable reactor circuit.

The reactor consists of a core on which one a-c winding also known as load or gate winding, and one or more control windings are placed. Fig. 2 shows a simple self-saturating circuit.

If we assume that the magnetic amplifier gate winding is connected to an a-c supply without rectifier or load in series, and with no signal applied to the control winding, then the assembly will behave like a simple reactor or a transformer in no load condition. A voltage is being induced which will impede the flow of current and only magnetizing current will flow. According to the equation $e = d\phi/dt$, however, a change of magnetic flux must take place to induce a voltage. If therefore, for some reason the magnetic flux reaches saturation, then no change in flux will take place, no voltage will be induced, and the current flow will no longer be impeded. Saturation of the core can be obtained by several means, such as high a-c voltage on the gate winding, a d-c control signal, or by self-saturation. Fig. 3 shows a typical hysteresis loop of a silectron core obtained by driving a core to positive saturation and then reversing the magnetizing force to negative saturation. This is also the loop obtained when applying full rated a-c voltage to the gate winding. If we now place a rectifier diode in series with the gate winding, then the magnetizing current will be blocked in the negative direction by the diode preventing a demagnetization of the core during the negative half-cycle. Neglecting leakage currents, the core will retain a remnant magnetism from O to A. At the next positive half cycle the flux will start its excursion at point A rather than at point $-B$ and the core will saturate quickly. This mode of operation is known as self-saturation. After saturation, the current is limited only by the load resistance. It is now possible to reset the point A on the left flank of the hysteresis loop to anywhere between $+B$ and $-B$ by means of the d-c control winding. When A is reset to $-B$ then no saturation will take place and the output will be magnetizing current only. Any output between minimum and maximum can be obtained in using the proper reset point as adjusted by means of the control winding.

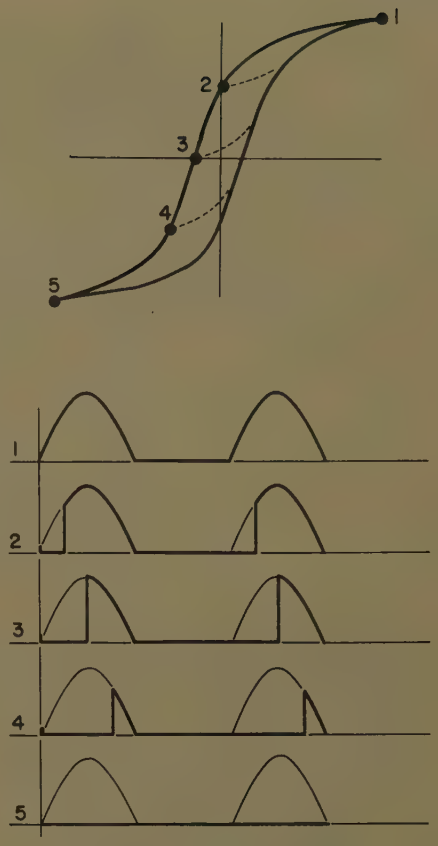

Fig. 4. Output waveshape

Fig. 4 shows the output current waveshape, or voltage, appearing across the load for various reset points.

The half-wave magnetic amplifier is commercially impractical because of the voltage induced in the control winding by transformer action before the core is saturated, and because of the low average

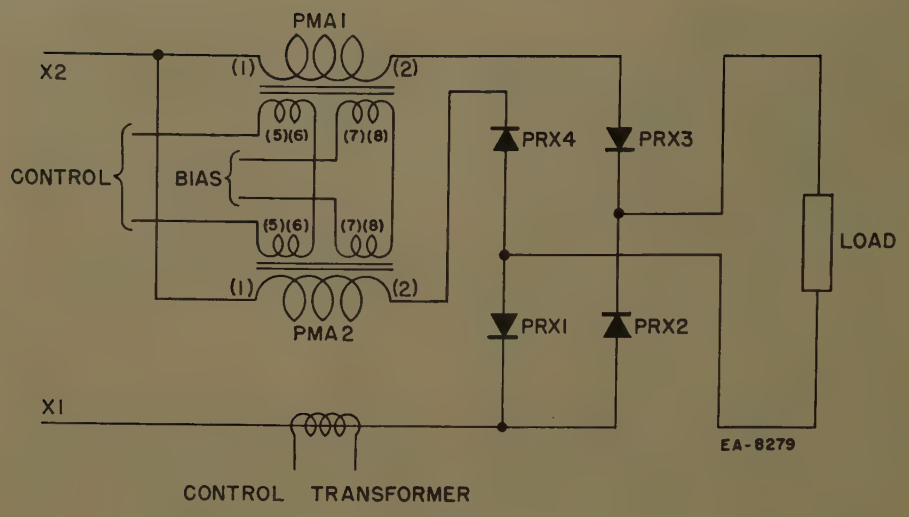

Fig. 5. Rectifier bridge circuit

output, unequal loading of transformer, and a-c line. For this reason a full-wave arrangement is used in which the voltages induced in the control windings oppose each other during alternate half-cycles and cancel each other. From among the various possible circuits, the bridge circuit was chosen since it imposes the lowest blocking voltage upon the rectifier diodes and because of its transient behavior. This circuit is shown in Fig. 5.

The control power being used is very small and consists essentially only of the d-c magnetizing force. The control winding likewise is very small and requires only a fraction of the copper used in the gate winding. This is in contrast with simple saturable reactors which operate on an equal ampere-turn principle between gate and control winding and where the copper required for the control winding is approximately equal to the gate copper requirement.

The core material being used is grain-oriented silicon steel which permits high flux densities with very little magnetizing force requirements. The core is tape wound and cut (C-core) so that the coils can be inserted easily without using special winding techniques. The core halves have lapped butt joints for a minimum air gap. The resulting magnetic amplifier assembly is of the smallest size presently possible for power reactors.

Fig. 6 shows a typical transfer or control characteristic of the self-saturating magnetic amplifier described. It can be noted that with zero control applied, some output exists. To obtain minimum output a negative control signal has to be applied and for maximum output a positive signal has to be applied. This seems to require a reversible control signal. However, in using a separate control winding, normally called a bias winding, the characteristic can be shifted to any position required. Fig. 7 shows an arrangement being used in the utility rectifier where bias is adjusted for minimum output and the control can now be undirectional. Power ratios between control and output of 1:5,000 are easily obtained.

Rectifier

The rectifier network is of the full-wave bridge type and serves a double purpose: first, to rectify the a-c power for charging the battery, and second, to serve as diodes for the self-saturated magnetic amplifiers.

The diodes are silicon rectifiers which are not subject to aging as is selenium. They can be used at ambient temperatures up to 150 degrees, have much lower leakage current and lower forward voltage drop than selenium. Over-all efficiency of the diode can be as high as 99%. The silicon diodes are mounted on heat dissipating fins of proper size to limit the junction temperature of the diode to a safe value. Protection against surge and short-circuit currents is obtained by properly co-ordinated and extremely fast acting current-limiting silver quartz sand fuses. This fast action is required because of the small thermal capacity of the diode junction. Circuit breakers alone, without current-limiting fuses, are not fast enough to afford complete protection of the diodes.

Sensing Unit and Control Amplifier

The sensing unit consists of several sections:

voltage sensing network
current sensing network
control amplifier

Voltage Sensing Network

Fig. 8 shows the principal components used for voltage sensing. These components are $P1$, $P2$, $R1$ comprising one of the bridge, $R2$ another leg, and R the third leg. The fourth leg, $R3$ immaterial and necessary only to sup the voltage reference diode $D11$ (Ze diode) with sufficient operating curr $P1$ and $P2$ are potentiometers to ad float and equalizing voltage separat When switch ECT is closed, equali voltage can be adjusted with $P2$ and v ECT open, float voltage can be adjus by means of $P1$. When $P1$ and $P2$ adjusted, only ECT needs to be opene closed to change from equalizing volt to float voltage or vice versa. The uses a timer which opens ECT after preset time period to return the char from equalizing to float voltage. heart of the sensing unit is the volt reference or Zener diode. This di exhibits a voltage drop which is essenti independent of changes in current flow in the reverse breakdown or Zener reg and therefore it is also independent changes in supply voltage V. A port of the sensing voltage is compared w the constant reference voltage and differences exist, corrective measures taken by the control amplifier which turn controls the main stage magne amplifier. This correcting principle known as closed-loop regulator or feedb control. As long as the unit is operat in the voltage controlled range, the brid network will be balanced except for small error voltage necessary to drive control amplifier (preamplifier).

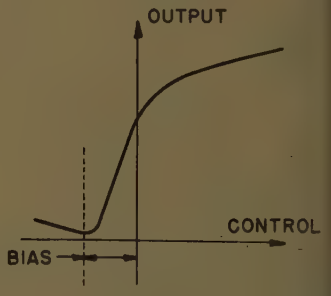

Fig. 6. Magnetic amplifier characteris with zero control signal

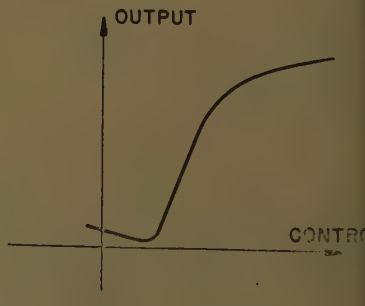

Fig. 7. Magnetic amplifier characteristic w negative control signal

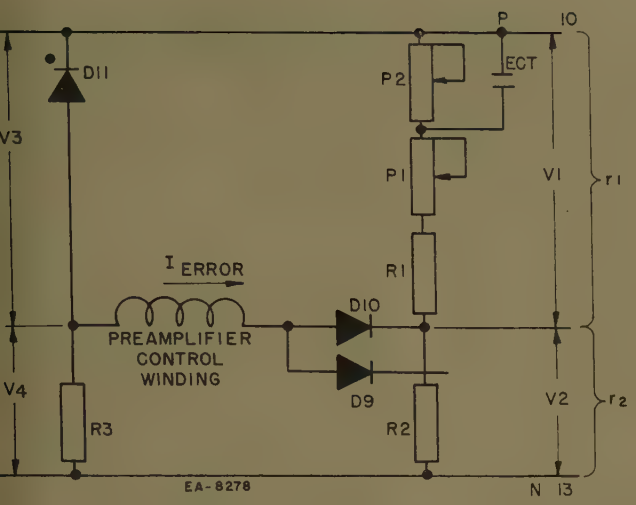

Fig. 8. Voltage sensing network

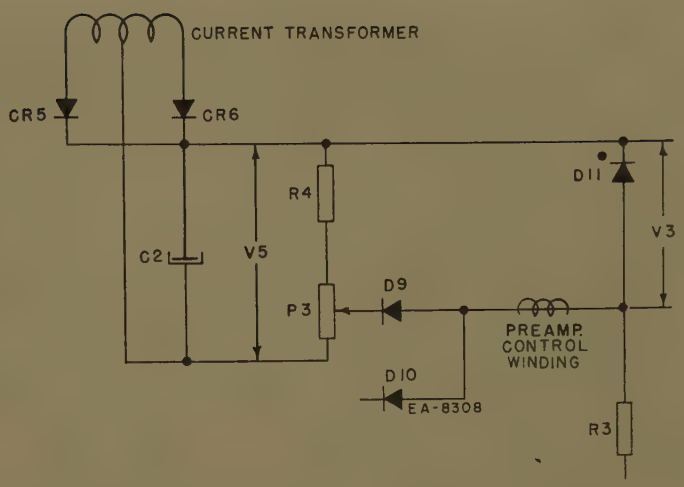

Fig. 9. Current sensing network

ıe bridge is balanced when

$$V2 = V3 : V4 \qquad (1)$$

ıe ratio of $V1 : V2$ is equal to the ratio 2 whereby $r1$ equals $R1+P1+P2$ $r2$ equals $R2$. $V3$ has a constant e and $V4$ is the difference between V $V3$. $V2$ is also the difference between ıd $V1$. The bridge ratio can now be essed as follows:

$$\frac{V1}{1} = \frac{r2}{r1} \text{ or } \frac{V}{V1} - 1 = \frac{r2}{r1} \text{ or } V1 = \frac{V}{1+\frac{r2}{r1}} \qquad (2)$$

is evident then that $V1$ changes with ıange of supply or sensing voltage V e $V3$ the reference voltage remains stant. The difference between $V1$ and or error voltage is

$$_{or} = V1 - V3 = \frac{V}{1+\frac{r2}{r1}} - V3 \qquad (3)$$

he resistance $r1$ is composed of $R1-$ and $P2$. If we now assume that the r voltage can be neglected since it is than 1% of the sensing voltage we manipulate the equation for error ıge and obtain

$$+P1+P2 = \frac{V3 \times R2}{V - V3} \qquad (4)$$

ince $V3$ and $R2$ are constant, a change ither $P1$ or $P2$ will result in a change he sensing voltage V. An easy means voltage adjustment is thereby avail-

rent Sensing Network

ig. 9 shows the principal components he current sensing network, used to t the current output to a safe value. current transformer measures the ent flowing in the a-c line of the power ifier bridge. Control rectifiers $CR5$ $CR6$ rectify the transformer output in a full-wave center-tap arrangement and supply the network $R4$ and $P3$. $C2$ serves as a filter capacitor. The voltage drop across $R4$ and $P3$ is therefore directly proportional to the main current measured by the current transformer. This voltage is compared with $V3$, the reference voltage, and if this voltage as preset by $P3$ is larger than $V3$, a current will flow in the preamplifier control winding to take corrective action, that is, to limit the current at the preset value. The reason for diodes $D9$ and $D10$ is now also evident. They are simply a means of selection between current and voltage control. If the current sensing voltage $V5$ is of a larger value than the voltage sensing voltage $V1$, then the unit will be operating on current control. $D9$ will conduct the preamplifier control current while $D10$ will be reverse biased and prevent interference from the voltage sensing network.

Conversely if the voltage sensing voltage is larger than the current sensing voltage, $D10$ will conduct the preamplifier control current. The diode $D9$ will then be reverse biased to prevent interference from the current sensing network.

Control Amplifier

The control amplifier serves to amplify the error signal obtained from the current or voltage sensing networks to a level necessary to drive the power magnetic amplifier to cutoff or saturation. The mode of operation of the control amplifier is the same as explained for the power magnetic amplifier, only the construction and core material used is different. The core is a tape wound torroidal core exhibiting a square loop hysteresis characteristic. Since this core has no air gap and a very sma'l leakage field, a high amplification factor is obtained. The schematic diagram for the control amplifier is essentially a duplicate of the power magnetic amplifier, and only the control characteristic is different as shown in F'g. 10.

Because of the high residual flux density (remnant magnetism) in the self-saturating mode of operation of the core material used, the output is practically maximum with no control current applied to the control amplifier control winding. An increase in control current results in a decrease of output current. Because of this, no bias winding is required for the control amplifier in this application. Feedback control systems, especially with high gain amplifiers, tend to be unstable, therefore an antihunt provision has to be made to stabilize the circuit. The second control winding on the control amplifier is used as an antihunt winding and will effectively suppress sustained oscillations.

The complete antihunt network consists of capacitor $C3$ (Fig. 11), resistor $R5$, and the antihunt winding on the torroid. Due to the capacitor, the winding will get a signal only during transient conditions. The polarity of the winding is such that it opposes any change in the output of the rectifier charger.

Circuit Function

If we consider a steady-state condition on a 60-cell utility rectifier at half-rated current, battery float voltage, and nominal a-c supply voltage, then typical values of control currents and error voltage would be as follows:

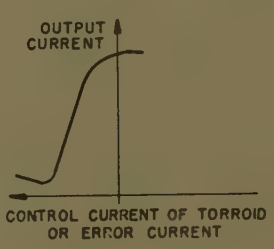

Fig. 10. Control amplifier characteristic

error voltage: 0.1V, i.e., $V1$ is 0.1 volt larger than $V3$
error current: 0.5 milliampere (ma), i.e. current in the control amplifier control winding
control current: 60 ma, i.e. the output current of the control amplifier which is the control current of the power magnetic amplifier
load current: 6 ampere, i.e. the current into the battery or load, controlled by the power magnetic amplifier
battery voltage: 129 volts
a-c supply voltage: 230 volts

As long as the a-c input and d-c output conditions of the rectifier remain unchanged, the values of error voltage, current, and control current would not change either. However, if a change in input, output, or a combination of input and output conditions occurs, then their steady-state values of control and error voltage and current will change also.

If we assume either a supply voltage decrease, a load current increase, or a combination of supply voltage decrease and load current increase, then the rectifier would be incapable of supplying load current demand if the steady-state values in the error and control circuit remain unchanged. In that situation the battery would supply the additional load current requirement and the battery voltage would drop.

At this point, the feedback regulator comes into action. Actually the voltage starts to drop and a transient period begins. According to equation 3, a drop in the battery voltage, which is the sensing voltage V, will result in a decrease of the error voltage V_{error}. This decrease in error voltage will naturally cause a decrease in error current. Referring to Fig. 8 it can be seen that I error is the control current of the control amplifier. According to the control amplifier control characteristic as shown in Fig. 10, a control current decrease results in an increase of the control amplifier output current. Since the output current of the control amplifier is the control current of the power magnetic amplifier, a reference to Fig. 7 will show that the increase in control current will also increase the output current. When the output current has increased enough to compensate for, or to supply the original increase in current demand, a new steady-state condition will arise which could have the following typical circuit conditions.

error voltage	0.07 volt
error current	0.35 ma
control current	80 ma
load current	10 amperes
battery voltage	128.8 volts

The actual voltage decrease from the first steady-state condition is only 0.2 volt, and this is due to the high amplification factors in the control amplifier as well as in the power magnetic amplif

Conversely now if we assume eithe supply voltage increase, a load current crease, or a combination of both, then rectifier would supply more current th actually needed. Here then, the batt would take on the excessive output c rent and the battery voltage would ri The feedback regulator comes again i action and the opposite of the previou described transient condition takes pla As soon as the voltage rises the error vo age increases, which increases the er current, resulting in a decrease of cont current. This brings about a decrease output current until a new, balanced co dition exists. Again only a very minu change in the battery voltage is necessa to compensate for a change in inp and/or output conditions. These volta changes are well within the voltage regu ting accuracy of the regulator.

The action of this regulator is cont uous stepless, and therefore keeps t battery voltage under close regulation all times, as long as power is available.

Surge Voltage and Voltage Spike Effects

In the average substation and cent station where the UR charger is installe

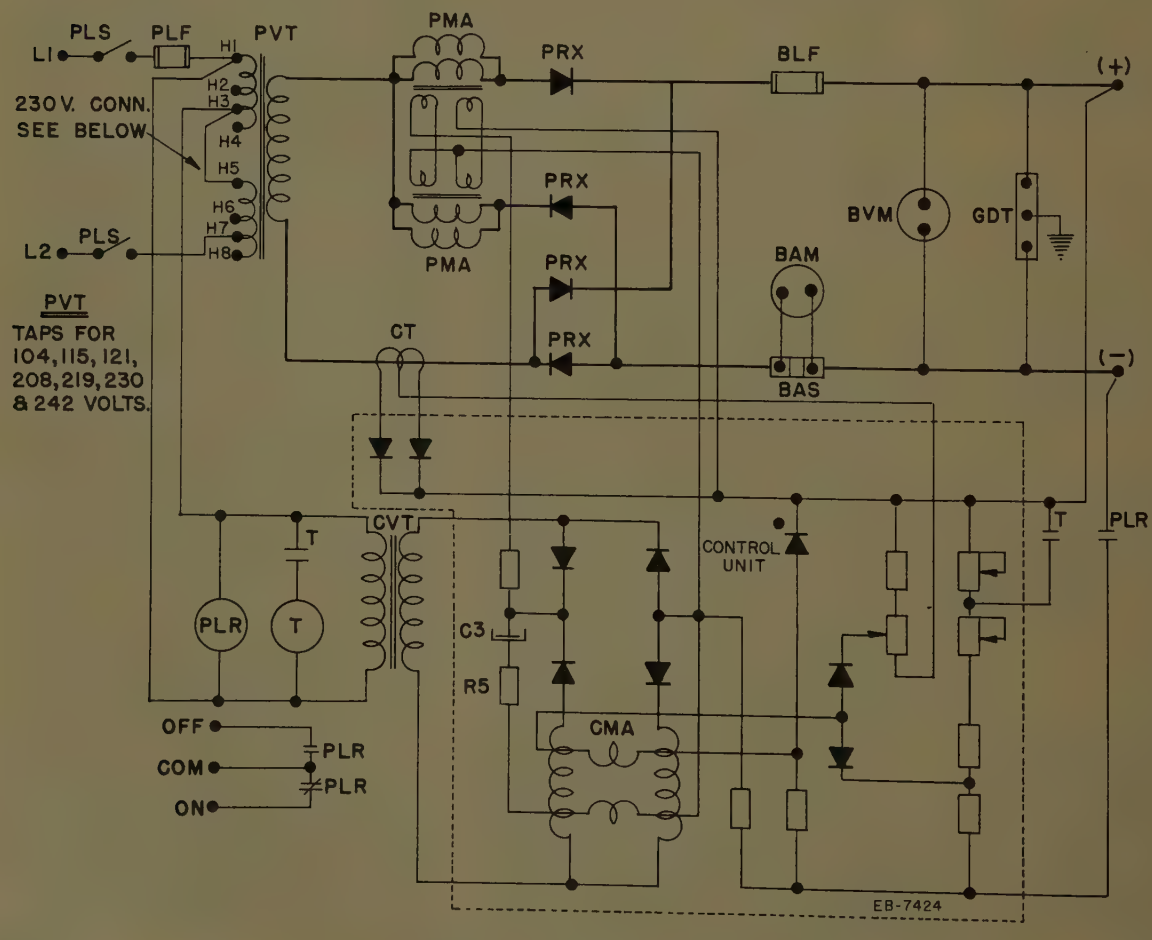

Fig. 11. Sing phase schema diagram

BAM = Battery meter
BAS = Battery meter shunt
BLF = Battery fuse
BVM = Battery vo meter
CMA = Control a plifier
CT = Current tra former
CVT = Control transformer
PLF = Power fuse
PLR = Power rela relay
PLS = Power ala switch
PMA = Power ma netic amplifier
PRX = Power rec fier silicon
PVT = Power vo age transformer
T = Timer
GDT = Ground d tection equipme (lights, voltmeter, relay) optional

e voltages or voltage spikes occur. se may come from the a-c supply, sformer leakage reactance etc., or may come from the d-c load when ly inductive circuits are switched. age spikes coming from the a-c supply a value up to 600 volts have been de- ed on the low-voltage side of the power sformer at the input of the rectifier ge. Voltage spikes in excess of 1,000 s caused by switching inductive loads also quite common. Although the er behind them is usually very low, it fficient to start the Zener breakdown a silicon diode and destroy the junc- . To prevent damage to the silicon ction, a surge voltage suppressor is re- ed. As long as voltage spikes are ted by the suppressor, in their voltage d-up, to values below the breakdown age of the diode, no breakdown will e place. Capacitors and nonlinear stors (thyrite) are usually used for purpose.

Capacitors can be used effectively if the ge voltages are of a short duration, resenting a frequency in the order of cycles, and of low power. Longer ation and higher power surges will re- re very large capacitors. These may ten the surges into a low-voltage long- ation transient, which is not neces- ily safe. Capacitors in connection with er circuit elements may lead to oscilla- n and other surge voltage conditions. nlinear resistors exhibit a decreasing istance characteristic with increased tage impressed across them. Thus en a voltage spike appears across such nonlinear resistor, its resistance de- ases and the resulting surge current ins the power off the surge voltage, pre- nting a dangerous voltage build-up. ese resistors, unfortunately, have an erent current drain causing a power s which is considerable in the range ere they exhibit their most nonlinear aracteristic.

Since the UR charger must always be nnected to a battery and the battery haves as an extremely large capacitance, was decided to utilize this battery prop- ty for surge voltage suppression. eference literature ascribes a capacitance fect equal to several hundred farads to a ttery.[1] This capacitance effect is suffi- ent to limit even higher power, long uration surges to a safe value and does not use additional power loss, i.e., beyond e current normally required to float the ttery. In the bridge-type rectifier ed, one surge voltage protecting element sufficient to give protection against volt- e spikes if connected directly across e bridge output, regardless of whether

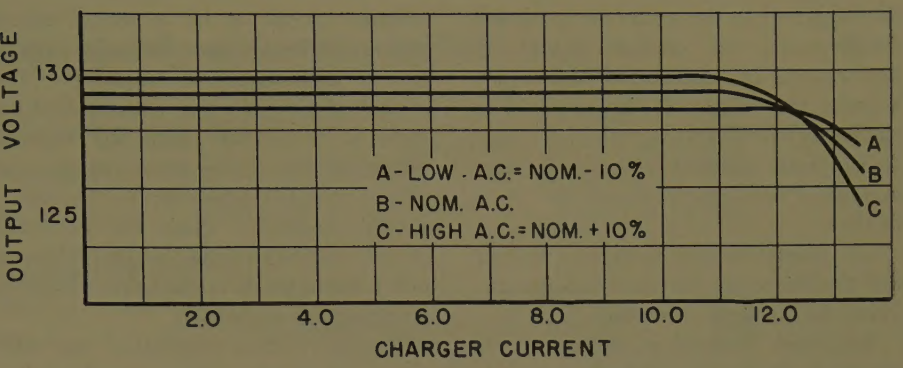

Fig. 12. Charger voltage regulation

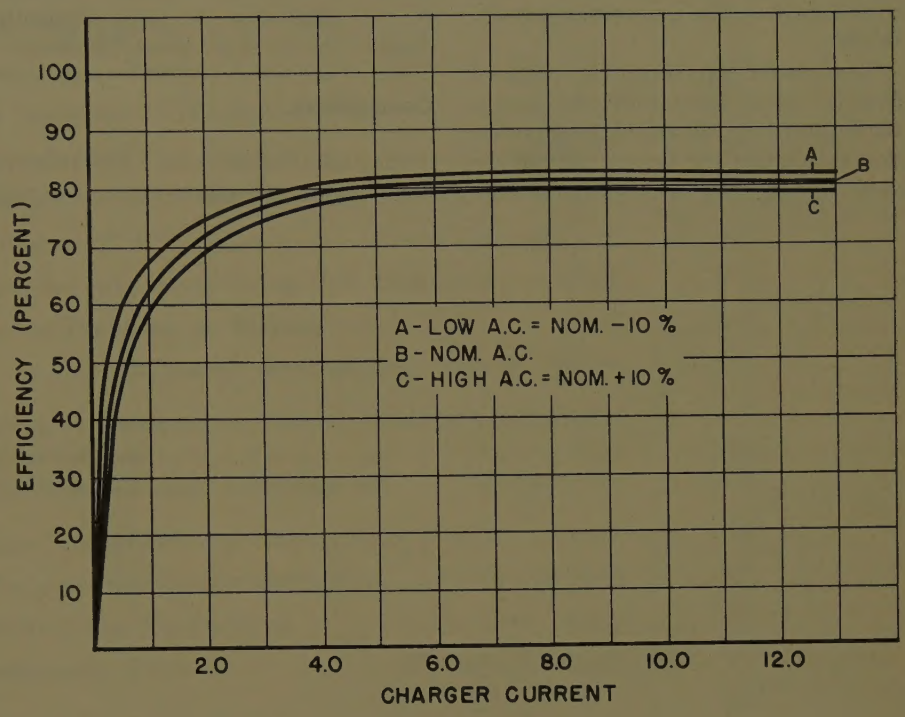

Fig. 13. Charger efficiency

the voltage surges are coming from the a-c side or from the d-c side of the bridge. To retain the protection of the battery against a-c and d-c voltage surges, it is imperative that these two points be observed very closely:

1. The impedance of the connecting leads between battery and charger be kept to an absolute minimum. Otherwise a voltage build up may take place in the lead impedance on extremely short duration spikes before they can be drained off by the battery. Leads should be twisted together, runs should be as short as possible, and sharp bends be avoided.
2. Load leads should be connected directly to the battery terminals and not to the charger. Connecting the charger to a d-c bus and the battery to the same bus should be avoided as this practice can easily lead to a voltage build-up which can be dangerous.

Features

One of the features of the type UR rectifier as mentioned before is its capability to regulate the voltage down to zero load. This is accomplished by means of a special magnetic amplifier design which keeps the magnetizing current below the current drawn by the voltage sensing network and therefore regulation down to zero load is possible. It is important however, to keep in mind that the battery has to be connected to the charger output in order to obtain regulation to zero load. The magnetic amplifier is subjected only to the difference between a-c voltage and battery voltage as long as the battery is connected. If the battery were to be removed, the magnetic amplifier gate winding would be subjected to the full a-c voltage which is several times the normal gate voltage, the magnetizing current would increase tremendously and regulation would be limited. This, however, is of little consequence since the voltage regulation accuracy is primarily of importance for the life of the battery and is main-

tained as long as the battery is connected. Furthermore, the charger should not be operated, i.e., energized by a-c supply, without the battery in the circuit since the battery acts as a very effective means to suppress transient voltages or surge voltages which could endanger the silicon diodes.

The charger affords protection to itself and the battery in the case of a fault, providing full back-up protection.

Sustained overload is limited by the current-limit circuit and back-up protection is provided by the inverse time element of a dual element fuse or by thermal trip elements in the transformer primary circuit.

Short-circuit protection is obtained from fast-acting current-limiting fuses in the d-c output circuit and back-up protection from either the fast element of the dual element fuse in the transformer primary circuit or by a second set of current-limiting fuses between transformer and magnetic amplifiers. The characteristic of the current-limiting fuses is co-ordinate with the thermal characteristics of the silicon diodes and affords complete protection for any short-circuit condition. There are no other circuit elements (circuit breakers) known today which would operate fast enough to give adequate protection.

Typical voltage regulation and efficiency curves are shown in Figs. 12 and13. The voltage regulation curve shows also the influence of the current limit circuit. Fig. 11 illustrates the basic schematic diagram for the single phase UR charger.

Conclusions

The UR charger meets the requirements for an ideal sub- and central-station battery charger. It can maintain batte charge voltage within plus or minus 1 with an a-c voltage variation of plus minus 10% from zero to rated outp current. Being a completely static d vice, it has no moving elements to wea create noise, and require maintenanc The use of ample safety factors throug out insure extremely long, trouble-free li A switch is provided to enable the manu operator give the battery an equali charge. Optional devices include equalize charge timer, ground detecti lights or relays, charge failure indicato a-c failure alarm, and operation on 50-60-cycle a-c power from a wide range standard voltages.

Reference

1. Battery Impedance: Farads, Millioh Microhenrys, E. Wilihnganz, Peter Rohn *AIEE Transactions*, pt. II (*Applications and dustry*), vol. 78, Sept. 1959, pp. 259–62.

Power Apparatus and Systems—August 1960

Conference Papers Open for Discussion

The conference papers listed below have been accepted for AIEE Transactions and are now open for written discussion until October 27. Duplicate double-spaced typewritten copies for each discussion should be sent to Edward C. Day, Assistant Secretary for Technical Papers, American Institute of Electrical Engineers, 33 West 39th Street, New York 18, N.Y., on or before October 27.

Preprints may be purchased at 50¢ each to members; $1.00 each to nonmembers if accompanied by remittance or coupons. Please order by number and send remittance to:

AIEE Order Department
33 West 39th Street
New York 18, N. Y.

60-637 Studies of Electrodynamic Forces Occurring at Electrical Contacts.....Snowdon

60-639 New Contactorless Precision D-C Hoist Has Wide Speed Range and Torque Control.....Hansen, Karlson, Mierendorf

AIEE PUBLICATIONS

	Member Prices	Nonmember Prices: Basic Prices*†	Nonmember Prices: Extra Postage for Foreign Subscription
Electrical Engineering			
Official monthly publication containing articles of broad interest, technical papers, digests, and news sections: Institute Activities, Current Interest, New Products, Industrial Notes, and Trade Literature. Automatically sent to all members and enrolled students in consideration of payment of dues. (Members may not reduce the amount of their dues payment by reason of nonsubscription.) Additional subscriptions are available at the nonmember rates.		annually $12* Single copies $1.50*	$1.00
Bimonthly Publications			
Containing all officially approved technical papers collated with discussion (if any) in three broad fields of subject matter as follows:	annually	annually	
Communication and Electronics	$5.00	$8.00*	$0.75
Applications and Industry	$5.00	$8.00*	$0.75
Power Apparatus and Systems	$5.00	$8.00*	$0.75
Each member may subscribe to any one, two, or all three bimonthly publications at the rate of $5.00 each per year. A second subscription to any or all of the bimonthly publications may be obtained at the nonmember rate of $8.00 each per year.			
Single copies may be obtained when available.	$1.50 each	$1.50* each	
AIEE Transactions			
An annual volume in three parts containing all officially approved technical papers with discussions corresponding to six issues of the bimonthly publication of the same name bound in cloth with a stiff cover.	annually	annually	
Part I Communication and Electronics	$4.00	$8.00*	$0.75
Part II Applications and Industry	$4.00	$8.00*	$0.75
Part III Power Apparatus and Systems	$4.00	$8.00*	$0.75
Annual subscription to all three parts (beginning with vol. 77 for 1958).	$10.00	$20.00*	$2.25
Annual subscription to any two parts.		$15.00*	$1.50
AIEE Standards			
Listing of Standards, test codes, and reports with prices furnished on request.			
Special Publications			
Committee reports on special subjects, bibliographies, surveys, and papers and discussions of some specialized technical conferences, as announced in ELECTRICAL ENGINEERING.			

*Discount 25% of basic nonmember prices to college and public libraries. Publishers and subscription agencies 15% of basic nonmember prices. For available discounts on Standards and special publications, obtain price lists from Order Department at Headquarters.

†Foreign prices payable New York exchange

Send all orders to:

Order Department
American Institute of Electrical Engineers
33 West 39th Street, New York 18, N. Y.